Interrogating the energy conservation of *Clostridium ljungdahlii* by genetic manipulation and bench-scale fermentation

Dissertation

der Mathematisch-Naturwissenschaftlichen Fakultät

der Eberhard Karls Universität Tübingen

zur Erlangung des Grades eines

Doktors der Naturwissenschaften

(Dr. rer. nat.)

vorgelegt von

Christian-Marco Klask

aus Essen

Tübingen

2021

Gedruckt mit Genehmigung der Mathematisch-Naturwissenschaftlichen Fakultät der Eberhard Karls Universität Tübingen.

Tag der mündlichen Qualifikation:	10.11.2021
Dekan:	Prof. Dr. Thilo Stehle
1. Berichterstatter/-in:	Prof. Dr. Largus T. Angenent
2. Berichterstatter/-in:	Prof. Dr. Karl Forchhammer

This dissertation is dedicated to the pursuit of a greener and more sustainable world, where humans and nature can co-exist in harmony and progress, prosperity, and justice are still attainable for everyone.

Acknowledgements

First, I would like to acknowledge my advisor, Prof. Lars Angenent, for accepting me to his lab and providing me with guidance and independence in my research interests throughout my PhD. I thank Lars for his constant commitment to communication, individual meetings, and my development into a highly reflective scientist. Especially, in the development process of building my own bioreactor system Lars advice was outstanding and always a great help. The lessons he taught me about bioreactor work and excellent project management are certainly lessons I will remember in my future career as a scientist. I would also like to give special thanks to Lars for all the flexibility he offered me in my research projects when ideas changed over time and goals had to be redefined.

Second, I would like to thank Dr. Bastian Molitor for his constant supervision and helpful advice in my molecular and genetic work. Bastian's office door was always open for questions, and I especially enjoyed the intense conversations on molecular biology topics in the countless face-to—face meetings. With Bastian's help, I was able to discover new research interests in genetics for myself once again. I also appreciated a lot the time we shared together on international conferences, where he kindly introduced me to other scientists. Finally, I would like to thank Lars and Bastian for editing and proofreading my written reports, manuscripts, and presentation slides.

Third, I would like to express sincere gratitude to my two further committee members Prof. Karl Forchhammer and Prof. Ralf Takors for their time as examiner to evaluate and review my research. I thank Prof. Forchhammer and his lab member Dr. Björn Watzer for his support with questions about Cyanophycin and the microbial nitrate reduction. I would like to thank Prof. Angenent, Prof. Forchhammer, Prof. Takors, Dr. Molitor for their participation in my oral defense and reviewing my research.

Next, I would like to thank all lab members of the Environmental Biotechnology Group. Since I joined Prof. Angenent's lab in 2017 as one of the first lab members, I have been involved in the overall setup and development of the group. I saw the lab growing and evolving into a community of helpful, inspiring, and brilliant scientists, colleagues, and friends. While I appreciate everyone in the lab, Christian Fink, Akanksha Mishra, and Isabella Casini deserve special recognition. Especially in my first years as a PhD student in a new city, a new environment, and a brand-new lab, they have filled my daily life with joy, success, and fun at and after work. In the most difficult and triumphant moments of this PhD, I loved the timeless, understanding, and motivating evening conversations with Christian Fink, who have become an amazing friend of mine. Furthermore, I would also like to thank Dr. Sebastian Beblawy and Dr. Pengfei Xia for their kind advice in the lab, their help with difficult research questions, and their motivation to believe in me during challenging times. I also would like to

acknowledge and thank Nicolai Kliem-Kuster for his countless support and helping hand in my bioreactor project. In addition, I would like to thank Benedikt Jäger, who did an internship in our lab under my supervision. I am thankful for all his help with the qPCR experiments and being patient and a great learner. In addition, there are many other people from the lab who I would like to acknowledge. I thank Caroline Schlaiß, Sarah Schulz, Patrick Schweizer, Nils Rohbohm, Liam Fritzstevens, Ramiro Blasco Gómez, Ginés Cano, Richard Hegner, Ulrike Benhain, Kim Rennhack, Julia Schumacher, Pengfei Xia, and Joe Usack for all the great times during and after work. I am grateful for the last 4 years I have spent in such a great lab and for all the friendships that have been formed during that time and I am sure will last for a long time to come.

Furthermore, I acknowledge funding from the Alexander von Humboldt Foundation in the framework of the Alexander von Humboldt Professorship, which was awarded to Prof. Angenent. This financial support enabled a great environment for independent research, success, and development of young scientists.

I also owe tremendous thanks to my family, who guided me through my last years, always supported me, and often reminded me to take breaks and have fun apart from the lab. I thank my parents Angelika Becker-Klask and Manfred Klask, who helped me through every major decision and moment in my life. I thank my two brothers Frederik and Marius for all the great fun and moments of understanding and appreciation for my research, whenever we met. And finally, my deepest love and gratitude goes to my friend Jana Senger, who always did her best to keep me sane and happy during stressful moments; she knew exactly when to encourage me to keep going and when to hold me back so I could recover from a stressful time.

TABLE OF CONTENTS

LIST OF ABBREVIATIONS

AA	amino acid
acetyl-CoA	acetyl coenzyme A
ADP	adenosine diphosphate
ATP	adenosine triphosphate
bp	base pair(s)
C1	one-carbon
CGP	cyanophycin
CO	carbon monoxide
CO_2	carbon dioxide
CODH	carbon monoxide dehydrogenase
CODH/ACS	carbon monoxide dehydrogenase/acetyl-CoA synthase
CoFeSP	corrinoid iron-sulfur protein
CRISPR	Clustered Regularly Interspaced Short Palindromic Repeats
C-source	carbon source
E_0'	standard reduction potential
EMP	Embden–Meyerhof–Parnas
Fd	ferredoxin
FDH	formate dehydrogenase
Fd_{ox}	ferredoxin (oxidized)
Fd_{red}	ferredoxin (reduced)
FeS-cluster	iron-sulfur cluster
Fld	flavodoxins
FMN	flavin mononucleotide
H^+	proton
H_2	hydrogen
HDR	homology-directed repair
HRT	hydraulic retention time
kDa	kilo Dalton
MBS	Multi-Bioreactor-System

MES	2-(N-morpholino)ethanesulfonic acid
Na^+	sodium ion
$NAD^+ + H^+$	nicotinamide adenine dinucleotide (oxidized)
NADH	nicotinamide adenine dinucleotide (reduced)
$NADP^+ + H^+$	nicotinamide adenine dinucleotide phosphate (oxidized)
NADPH	nicotinamide adenine dinucleotide phosphate (reduced)
Nfn	NADH/NADPH transhydrogenase
NHEJ	non-homologous end-joining
Nqr	Na^+-translocating NADH:ubiquinone oxidoreductases
N-source	nitrogen source
O_2	oxygen
OD_{600}	optical density at 600 nm
ori	origin of replication
PAM	protospacer adjacent motif
PBS	phosphate buffered saline
PMF	proton motif force
rcf	relative centrifugal force
RNF complex	*Rhodobacter* nitrogen fixation like complex
RCM	rich clostridial medium
rpm	revolutions per minutes
RT	room temperature
syngas	synthesis gas
TE	transcription efficiency
THF	tetrahydrofolate
TMH	transmembrane helices
TSP	(trimethylsilyl)-tetradeutero sodium propionate
WLP	Wood-Ljungdahl pathway
WT	wild type
ΔG‘	Gibbs free energy

SUMMARY

Acetogenic bacteria have great potential for the use in modern industries to convert gaseous substrates, such as carbon monoxide (CO), carbon dioxide (CO_2), and hydrogen (H_2) into valuable biochemicals. Gas fermentation with acetogenic bacteria provides an alternative route with a reduced CO_2 footprint when compared to existing petrochemical-based production processes. The main products of the acetogenic gas fermentation are acetate and ethanol, with the latter being a drop-in biofuel. Commercial gas fermentation plants with acetogenic bacteria are operated by the company Lanzatech, which underlines the industrial relevance of this technology. Although acetogenic bacteria are promising biocatalysts, their general metabolism is suffering from energy limitations. The main currency of the energy metabolism of a bacterial cell is ATP. The ATP is required for cell growth and for many metabolic pathways, such as those that can be used to produce valuable and industrial relevant products. All known acetogenic bacteria use the Wood-Ljungdahl pathway (WLP) to fix carbon. However, the WLP has no net ATP gain. One mole of ATP is invested to fix CO_2, while one mole of ATP is regenerated through dephosphorylation of acetyl phosphate to acetate. The only way an acetogenic bacterium can acquire surplus ATP during autotrophy is based on membrane complexes such as the Rhodobacter Nitrogen Fixation-like complex (RNF complex). This complex generates a proton or sodium ion gradient across the bacterial membrane, which is then used by an ATPase to generate ATP. However, the ATP gain of this chemiosmotic mechanism is low. For instance, the acetogenic bacterium *Clostridium ljungdahlii* can generate a maximum of 0.63 ATP/mol H_2 when growing with H_2 and CO_2. This small amount of ATP is just enough to enable growth and a functional metabolism. On the one hand, the low ATP gain is an advantage for biofuel production because electrons are predominantly used for the product rather than for biomass. On the other hand, the energy limitation in acetogenic bacteria is one of the highest burdens to overcome, and still limits the production of high-value and ATP-demanding fermentation products, which are required for a broad application of the acetogenic gas fermentation in industry. Therefore, more research with these microbes is highly required.

This dissertation investigates the RNF complex of the acetogenic bacterium *C. ljungdahlii* and its impact on autotrophic energy metabolism. A CRISPR-Cas12a technique was developed and used for the genetic manipulation of genes that are associated with the RNF complex and the energy metabolism. A full deletion of all RNF complex genes was achieved in *C. ljungdahlii* for the first time and confirmed the essential role of this complex for autotrophy. Furthermore, the manipulation of the gene *rseC*, which has a potential role in the transcriptional control of the RNF-complex gene expression, unraveled a novel and unknown factor for a functional RNF complex in *C. ljungdahlii*. In

addition, this dissertation focuses on nitrate metabolism of *C. ljungdahlii*, which was recently characterized in detail. Nitrate reduction in *C. ljungdahlii* is tightly connected to energy metabolism. The mechanism behind this is not understood yet. However, when *C. ljungdahlii* co-utilizes nitrate and CO_2, more ATP is generated and available for its metabolism. The potential use of this increased ATP pool is addressed with the implementation of a pathway to produce the biopolymer cyanophycin. Cyanophycin mainly consists of the amino acids arginine and aspartate and might be a suitable precursor for the feed and food industry. In addition, new insights were made by studying the nitrate reduction of *C. ljungdahlii* in self-built bioreactors. Bioreactor experiments with acetogenic bacteria are essential to investigate the microbial behavior under controlled conditions (*e.g.,* pH-control, continuous gassing, continuous medium feed). Experimental data from bioreactor experiments are one critical step for the upscaling process of gas fermentation of acetogenic bacteria, and therefore a key factor to show the applicability of this technology.

ZUSAMMENFASSUNG

Acetogene Bakterien haben ein großes Potenzial für den Einsatz in einer modernen und nachhaltig-orientierten Industrie, um gasförmige Substrate wie Kohlenmonoxid (CO), Kohlendioxid (CO_2) und Wasserstoff (H_2) in wertvolle Biochemikalien umzuwandeln. Die Gasfermentation mit acetogenen Bakterien hat nur einen geringen oder sogar negativen CO_2-Fußabdruck und bietet damit eine interessante Alternative zu bestehenden petro-chemischen Produktionswegen. Die Hauptprodukte der acetogenen Gasfermentation sind Acetat und Ethanol, wobei letzteres direkt als Biokraftstoff verwendet werden kann. Kommerzielle Gasfermentationsanlagen mit acetogenen Bakterien werden bereits von der Firma Lanzatech betrieben, was die industrielle Relevanz dieser Technologie unterstreicht. Obwohl acetogene Bakterien als vielversprechende Biokatalysatoren gelten, ist ihr Energiestoffwechsel jedoch stark limitiert. Die Hauptwährung des Energiestoffwechsels innerhalb einer Bakterienzelle ist ATP. Dieses ATP wird für das Zellwachstum und für viele weitere Stoffwechselwege benötigt, z.B. auch für solche die zur Herstellung wertvoller und industriell relevanter Produkte genutzt werden. Alle bekannten acetogenen Bakterien nutzen den *Wood-Ljungdahl pathway* (WLP) zur Fixierung von Kohlenstoff. Der WLP hat jedoch keinen Netto-ATP-Gewinn. Ein Mol ATP wird investiert, um CO_2 zu fixieren, während ein Mol ATP durch die Dephosphorylierung von Acetylphosphat zu Acetat regeneriert wird. Die einzige Möglichkeit, wie ein acetogenes Bakterium unter autotrophen Bedingungen zusätzliches ATP erzeugen kann, basiert auf Membrankomplexen wie dem *Rhodobacter Nitrogen Fixation-like complex* (RNF-Komplex). Dieser Komplex erzeugt einen Protonen- oder Natriumionengradienten über die Bakterienmembran, der dann von einer ATPase zur Erzeugung von ATP genutzt wird. Der ATP-Gewinn dieses chemiosmotischen Mechanismus ist jedoch ebenfalls gering. So kann das acetogene Bakterium *Clostridium ljungdahlii* beim Wachstum mit H_2 und CO_2 maximal 0.63 ATP/mol H_2 erzeugen. Diese geringe Menge an ATP reicht gerade aus, um Wachstum und einen funktionierenden Grundstoffwechsel zu ermöglichen. Einerseits ist der geringe ATP-Gewinn ein Vorteil für die mikrobielle Biokraftstoffproduktion, da die Elektronen überwiegend für das Produkt und nicht für die Biomasse verwendet werden. Andererseits ist die Energiebeschränkung bei acetogenen Bakterien eine der größten Hürden, die es zu überwinden gilt, da diese maßgeblich die Produktion hochwertiger und ATP-fordernder Fermentationsprodukte einschränkt. Diese sind aber für eine breite Anwendung der Gasfermentation mit acetogenen Bakterien in der Industrie erforderlich, wodurch weitere Forschung mit diesen Mikroben notwendig ist.

In dieser Dissertation wird der RNF-Komplex des acetogenen Bakteriums *C. ljungdahlii* und sein Einfluss auf den autotrophen Energiestoffwechsel untersucht. Für die genetische Manipulation von

Genen, die mit dem RNF-Komplex und dem Energiestoffwechsel assoziiert sind, wurde eine CRISPR-Cas12a-Plasmid-Technik entwickelt und eingesetzt. Hiermit wurde erstmals eine vollständige Deletion der gesamten RNF-Komplex-Gene in *C. ljungdahlii* erreicht, welche die essenzielle Rolle dieses Komplexes für die Autotrophie bestätigte. Darüber hinaus konnte durch die Manipulation des Gens *rseC*, welches eine entscheidene Rolle in der transkriptionellen Kontrolle der RNF-Komplex-Genexpression spielt, ein neuer und bisher unbekannter Faktor für einen funktionellen RNF-Komplex in *C. ljungdahlii* aufgedeckt werden. Zudem liegt ein weiterer Fokus dieser Dissertation auf dem Nitrat-Stoffwechsel von *C. ljungdahlii*. Dieser wurde erst kürzlich beschrieben und ist auf noch nicht vollständig aufgeklärter Weise eng mit dem Energiestoffwechsel verbunden. Wenn Nitrat zusammen mit CO_2 verwertet wird, entsteht zusätzliches ATP für den Metabolismus. Die potenzielle Nutzung dieses erhöhten ATP-Pools wird mit der Implementierung eines Stoffwechselwegs zur Produktion des Biopolymers Cyanophycin in dieser Dissertation angesprochen. Cyanophycin besteht hauptsächlich aus den Aminosäuren Arginin und Aspartat und könnte ein interessantes Vorstufenprodukt für die Lebensmittel- und Futtermittelindustrie sein. Des Weiteren wurden neue Erkenntnisse durch die Untersuchung der Nitratreduktion in selbstgebauten Bioreaktoren gewonnen. Bioreaktorexperimente mit acetogenen Bakterien sind essenziell, um das mikrobielle Verhalten unter kontrollierten Bedingungen, wie z.B. pH-Kontrolle, kontinuierliche Begasung oder kontinuierliche Mediumzufuhr, zu untersuchen. Experimentelle Daten aus Bioreaktoren sind ein wesentlicher Schritt für den Skalierungsprozess der Gasfermentation von acetogenen Bakterien und damit ein Schlüsselfaktor für die Anwendbarkeit dieser Technologie.

LIST OF PUBLICATIONS

a) Published journal articles

Klask, C.-M., Kliem-Kuster, N., Molitor, B., and Angenent, L.T. (2020). Nitrate feed improves growth and ethanol production of *Clostridium ljungdahlii* with CO_2 and H_2, but results in stochastic inhibition events. Frontiers in Microbiology, 11, 724.

Xia, P.F., Casini, I., Schulz, S., Klask, C.M., Angenent, L.T., and Molitor, B. (2020). Reprogramming Acetogenic Bacteria with CRISPR-Targeted Base Editing *via* Deamination. ACS Synthetic Biology, 9(8), 2162-2171.

b) Submitted manuscript

Klask, C.M., Jäger, B., Angenent L. T. , and Molitor, B. Genetic evidence reveals the indispensable role of the *rsec gene for autotrophy* and the importance of a functional electron balance for nitrate reduction in *Clostridium ljungdahlii*. Submitted to mBio, 02.08.2021. Pre-print available: https://doi.org/10.1101/2021.08.03.455012.

c) Preliminary manuscript

Klask, C.M., Ernst, M., Lemke, S., Angenent, L.T., and Molitor, B. Production of Cyanophycin in recombinant strains of *Clostridium ljungdahlii*.

CHAPTER 1
INTRODUCTION

1.1. Motivation and objectives

In the 21st century, our modern society is facing the urgent need to incorporate sustainable technologies into traditional industrial processes to decrease global carbon dioxide (CO_2) emissions and their far-reaching consequences such as global warming. Moreover, the growing living standard of millions of people engenders the huge amount of waste materials generated by industries and the combined activity of many individuals. At the same time, increasing CO_2 emissions, which are mainly driven by the overuse of fossil fuels, have become a critical issue and an undoubtful burden for future generations. For 2021, it is assumed that global CO_2 emissions will increase by 5% to a total of 33 billion tons mainly driven by a strong rebound in demand for coal in electricity generation (IEA, 2021). This would be the second-largest increase in history and at the same time reverse the decline of CO_2 emissions due to the impact of the Covid-19 pandemic. Consequently, new technologies need to be developed by re-thinking and re-innovating existing manufacturing routes (*e.g.,* by integrating technologies, which rely on renewable resources and renewable energy) to produce future materials, food, and fuels with as little CO_2 emissions as possible or with a negative carbon footprint. Modern biotechnology provides several technologies to counteract most of these anthropogenic global problems. Even more, this can be achieved in a way that industry can gain from it in their long-time strategy of becoming more sustainable. One of these technologies encompasses the idea of "waste-gas to biofuel". In short, C1 gases, such as carbon monoxide (CO), and CO_2, together with H_2 are used as a feedstock for gas fermentation of microbes, which convert the gaseous substrate into bio-based fuels with a reduced CO_2-footprint (Dürre, 2017; Takors *et al.*, 2018). Synthesis gas (syngas), consisting of a mixture of CO, CO_2, and H_2. It can be derived from mixing pure gases or from industrial, agricultural, or municipal wastes, and provides another suitable universal and inexpensive feedstock for microbes (Bengelsdorf and Dürre, 2017; Takors *et al.*, 2018). In addition, syngas can be produced from gasification of coal, liquid hydrocarbons, or biomass under oxygen-limiting conditions while its composition is varying based on the source material (Sutton *et al.*, 2001; Latif *et al.*, 2014). Syngas derived from gasified biomass or certain steel mill waste gas streams is already clean enough or may need only a little cleaning before feeding into a syngas fermentation system (Abubackar *et al.*, 2011; Liew *et al.*, 2016). In case of petrochemical waste materials (*e.g.,* plastic waste), the produced syngas mixture will often require more intense cleaning before a certain purity is reached to be clean enough

for a gas fermentation, which makes this process relative costly and still economically unfeasible (Lopez et al., 2018).

One promising and well-studied groups of microbes, which can utilize syngas, are acetogenic bacteria (acetogens). These obligate anaerobic microbes can naturally convert C1 gases, such as CO alone, CO_2 and H_2, or gas mixtures of these (e.g., syngas) into the main fermentation products acetate and ethanol (Drake *et al.*, 2008). However, other short chain fatty acids or their corresponding alcohols (*e.g.,* butyrate and butanol) are also produced by some species (Henstra *et al.*, 2007; Phillips *et al.*, 2015). Especially, the produced alcohols attract industrial interest (Dürre, 2017). A lot of research was performed during the past years to expand the syngas fermentation product range (Molitor *et al.*, 2017; Humphreys and Minton, 2018). The central aim of these studies was to genetically change the metabolism to produce higher value alcohols, esters, or medium-/long chain carboxylic acids. Today, the company LanzaTech is the commercially most successful industrial player in the field of syngas fermentation. Pilot and commercial demonstrations of LanzaTech showed that ethanol and 2,3-butanediol can be produced at industrial scale by syngas fermentation with the acetogen *Clostridium autoethanogenum*. Production of butanol, propanol, and acetone is already available at lab scale (Köpke *et al.*, 2016; Liew *et al.*, 2016). Nevertheless, the biotechnological production of higher value carbon products *via* syngas fermentation is still limited. One of the main reasons is due to the inefficient energy conversion of acetogenic bacteria (Bertsch and Müller, 2015). Elucidating the acetogenic energy metabolism is, therefore, one of the biggest hurdles to overcome for an efficient microbial conversion and economic syngas fermentation process (Molitor *et al.*, 2017; Katsyv and Müller, 2020). *Clostridium ljungdahlii* is another prominent acetogen, which is closely related to *C. autoethanogenum* (>98% genetic identity), the genome is fully sequences (Köpke *et al.*, 2010), and it is known to be one of the best studied acetogens for its metabolism (Tanner *et al.*, 1993; Tanner and Laopaiboon, 1997; Schuchmann and Müller, 2014; Mohammadi *et al.*, 2016).

All known acetogens use the Wood-Ljungdahl pathway (WLP) to grow autotrophically with C1 gases (Katsyv and Müller, 2020). However, the WLP is a non-ATP generating pathway (Schuchmann and Müller, 2014). One mole of ATP is invested for fixation of one mole of CO_2, while one mole of ATP is regenerated by the dephosphorylation of acetyl-phosphate into acetate (Wood *et al.*, 1986; Ljungdahl, 2009). The production of ethanol does not directly contribute to the formation of any ATP. Instead, it plays an important function for the regeneration of reducing equivalents, such as NAD(P)H or ferredoxin (Fd). In *C. ljungdahlii* the only way to generate ATP for its anabolism, is based on the *Rhodobacter nitrogen fixation-like* (RNF) complex activity (Schmehl *et al.*, 1993; Tremblay *et al.*, 2012; Schuchmann and Müller, 2014). The RNF complex in *C. ljungdahlii* catalyzes the oxidation of Fd^{2-} and the subsequent reduction of NADH while protons (H^+) are translocated over the membrane (Tremblay

et al., 2012). The generated proton motif force (PMF) can then be used to synthesize ATP *via* a membrane bound F_1F_O ATPase (Biegel *et al.*, 2011). Therefore, the RNF complex plays a key role in the energy conversion in acetogens (Schuchmann and Müller, 2014). The number of available studies in the literature that investigate the RNF complex of acetogens is limited or the conclusions lack further experimental support (Katsyv and Müller, 2020). Especially the regulation of the RNF complex-encoding genes is not understood and remains elusive. Consequently, a better understanding of the RNF complex and its genetics is an essential prerequisite to increase the biotechnological potential of acetogens.

In this dissertation, I discuss the important role of the RNF complex in *C. ljungdahlii* and its impact on the energy metabolism. I developed a CRISPR-Cas12a system for precise gene deletion in the genome of *C. ljungdahlii*. With this genetic tool, I targeted genes, which are associated with the RNF complex or supposedly responsible for its regulation. Furthermore, I designed and built a multi-bioreactor system for multiple gas fermentation experiments with *C. ljungdahlii* under continuous and pH-controlled conditions. With this work, I focused on the nitrate reduction in *C. ljungdahlii*. It was recently shown that nitrate reduction in *C. ljungdahlii* is connected to the energy metabolism and provided a 2.8-fold increased ATP level in cells growing in nitrate containing medium with H_2 and CO_2 (Emerson *et al.*, 2019). This is a considerable increase in the amount of available ATP in the metabolism of an acetogen, which usually suffers from energy limitations (Schuchmann and Müller, 2014). It was reported that the wild type (WT) of *C. ljungdahlii* converted the extra energy from nitrate reduction into enhanced biomass levels. However, the mechanism how nitrate reduction is linked to the energy metabolism remained unclear (Emerson *et al.*, 2019). Since the RNF complex is most-likely the only respiratory enzyme in *C. ljungdahlii* the question arised if and how electrons are shifted from this complex into the nitrate reduction pathway (Tremblay *et al.*, 2012; Katsyv and Müller, 2020). The main objectives of this work were: 1) Investigation of the RNF complex and its essential role for the autotrophy by genetic manipulation; 2) Interrogation of the energy metabolism with nitrate as external electron acceptor; 3) Re-direction of the energy flux into value-added biochemicals.

1.2. Organization and summary of chapters

Chapter 2 provides a literature review, which gives a detailed background about *C. ljungdahlii* and its metabolism as representative for acetogens. Particular emphasis is placed on: 1) the autotrophic metabolism; 2) the principle of acetogenic energy conversion; 3) the biochemistry of the RNF complex; and 4) the nitrate metabolism. In addition, previous genetic work on acetogens using genetic tools, such as CRISPR/Cas techniques, are highlighted. The last section of the literature review summarizes the recently investigated nitrate reduction in *C. ljungdahlii* and its impact on the energy metabolism.

Chapter 3 describes the gas fermentation of *C. ljungdahlii* in nitrate-containing medium using a self-built Multi-Bioreactor-System. I demonstrated successfully that simultaneous gas fermentation with H_2 and CO_2 of *C. ljungdahlii* WT under continuous conditions was possible in up to six bioreactors at a scale of 1 L. Using the Multi-Bioreactor-System, I investigated the nitrate reduction of *C. ljungdahlii* under pH-controlled conditions and compared this to growth with ammonium, which is the standard nitrogen source (N-source) in the cultivation medium. I found that growth with nitrate was also enhanced in bioreactors as previously reported for bottle experiments (Emerson *et al.*, 2019). In contrast to the findings of Emerson *et al.* (2019), I showed that ethanol production is possible and even enhanced in continuous bioreactors with pH control when nitrate is provided to cells of *C. ljungdahlii*. However, the cultivation was accompanied by growth inhibition events that appeared during the cultivation and led to a metabolic crash. These inhibition events appeared at different timepoints for each bioreactor that contained medium with nitrate but not for those that contained medium with ammonium. I explained this by a sensitive pH-buffering effect that resulted from the interplay between undissociated acetic acid production through acetogenesis on the one hand and ammonium production through nitrate reduction on the other hand. The results of Chapter 3 gave clear evidence for the importance to cultivate acetogens, such as *C. ljungdahlii*, under pH-controlled conditions. By limiting the physiological characterization of acetogens to bottle experiments, the impact of changes in the metabolism (*e.g.,* due to the feedstock or a genetic modification) might remain unclear and have a different character in bioreactor experiments, which are, therefore, a critical step in upscaling.

Chapter 4 is about a novel CRISPR/Cas9 technique to perform genetic manipulation on a one-nucleotide resolution (base-editing) in the genome of *C. ljungdahlii*. A deactivated version of the Cas9 nuclease was generated and fused with an activation-induced cytidine deaminase. With this genetic tool it was possible to install premature STOP codons into genes, which are responsible for the acetate and ethanol production in *C. ljungdahlii*. The genetic work and strain engineering was conducted by the post-doctoral researcher Peng-Fei Xia. My contribution to this work was the establishment of a suitable method for the cultivation of the recombinant strains under autotrophic and heterotrophic conditions. I performed several preliminary cultivation experiments with *C. ljungdahlii* WT and concluded on following parameters as best growth conditions for a physiological characterization, which provide a high data quality: For heterotrophic conditions, I found that cultures of *C. ljungdahlii* that grow in 100 mL medium, which is filled in 240-mL bottles showed stable growth, provided enough culture volume for subsequent analyses (*e.g.,* pH, acetate, ethanol), and generated data with less variance in triplicates. For autotrophic conditions, I concluded that best growth and cultivation conditions are achieved in 100 mL medium in 1000-mL bottles, which were pressurized with H_2 and CO_2. The high medium/headspace ratio provided a sufficient amount of gaseous substrate for the

microbes and enabled stable autotrophic growth. All generated strains of the work presented in Chapter 4 were physiologically characterized with the developed cultivation method. I grew two recombinant strains of *C. ljungdahlii* under heterotrophic conditions, and found that the ability to produce ethanol was significantly restricted through the insertion of a STOP codon within the *adhE1* and *adhE2* genes. Under heterotrophic conditions, the encoding enzymes AdhE1/2 usually convert acetyl-CoA to ethanol *via* acetaldehyde as an intermediate. Furthermore, the results described in Chapter 4 showed that the base-editing tool was successfully used to manipulate the *aor1/2* genes, which are responsible for the autotrophic alcohol production. In addition, an *in-silico* analysis revealed the capability of the developed base editing across the genome of *C. ljungdahlii* and found editable sites in 99.83% (4177 out of 4184) of all genes, which proofed the applicability of this tool for future genetic engineering work in *C. ljungdahlii*.

Chapter 5 deals with the genetic manipulation of RNF-complex associated genes and the impact of their deletion on autotrophy and the nitrate metabolism. For this work, I have generated a CRISPR/Cas12a system to enable precise gene deletion in the genome of *C. ljungdahlii*. I successfully conducted gene deletion of the full RNF-complex encoding gene cluster *rnfCDGEAB*, the putative RNF-complex regulator gene *rseC*, and a gene cluster encoding for a nitrate reductase. Furthermore, I generated plasmid-based complementation and overexpression strains of each gene or gene cluster target. I used the bottle cultivation method developed in Chapter 4 for a detailed physiological characterization of the metabolism and nitrate reduction in each strain during autotrophy and heterotrophy. I found that the deletion of either *rnfCDGEAB* or *rseC* led to a complete loss of autotrophy. These non-growing cells were also unable to reduce nitrate as indicator for metabolic activity. In contrast, growth and nitrate reduction was still possible for both mutants during heterotrophy, but growth was notably reduced for the *rnfCDGEAB* deletion strain. The deletion of the nitrate reductase gene cluster resulted in a loss of nitrate reduction, but the recombinant strain was still able to grow autotrophically. The successful complementation experiments and restore of the autotrophy and nitrate reduction showed that the conducted gene deletion was, indeed, responsible for the phenotype. The loss of autotrophy by the deletion of the *rnfCDGEAB* gene cluster was expected because of previous studies that were performed with the acetogen *A. woodii* (Westphal *et al.*, 2018). On the contrary, the *rseC* gene deletion that I had conducted is the first one reported in literature and revealed the relevance of this protein for the autotrophy of *C. ljungdahlii*. With qPCR-based gene expression experiments, I could reveal that the restriction in autotrophy in the *rseC* deletion strain was due to a significant repression of the RNF-complex encoding genes. I discussed the potential role and function of the *rseC* gene or its encoded protein, and how it might interact with the RNF complex on a transcriptional level. Furthermore, I concluded the work presented in Chapter 5 with an *in-silico*

research section to evaluate the distribution and location of putative *rseC* genes in the genomes of other prominent acetogens. I found indications that the *rseC* is part of the genome in most of the investigated acetogens, but that *rseC* is only located directly upstream of the RNF-complex gene cluster, when the RNF/ATPase system is using H^+-ions for energy conservation. Through protein structure prediction tools, I identified that the amino acid sequence of *rseC* likely encodes for two transmembrane helices. I concluded my work with the hypothesis that *rseC* is a positive transcriptional regulatory for the *rnfCDGEAB* gene expression during autotrophy but not during heterotrophy.

Chapter 6 provides work in which the heterologous production of cyanophycin in recombinant strains of *C. ljungdahlii* was studied. Cyanophycin is an intracellular biopolymer consisting of a poly-L-aspartic acid backbone with arginine side chains. It serves as carbon and nitrogen storage polymer in various microbes such as cyanobacteria. Its synthesis is catalyzed by the single key enzyme CphA, which is encoded by the gene *cphA* and requires two mole of ATP per polymerization cycle. Thus, the synthesis is highly ATP dependent. Acetogens, such as *C. ljungdahlii*, have a limited energy metabolism during autotrophy. In contrast, *C. ljungdahlii* gains more ATP for the metabolism during nitrate reduction. In the wild-type strain, this additional ATP is used to form more biomass. Therefore, the highly ATP-dependent cyanophycin synthesis is an ideal and relatively simple pathway to investigate whether the accelerated energy conversion during nitrate reduction can be re-directed into a valuable bioproduct. Cloning of two *cphA* genes and transformation of *E. coli* and *C. ljungdahlii* with respective plasmids was successful. While an *E. coli* strain that overexpresses the *cphA* gene from the cyanobacterium *Anabaena* sp., led to high accumulation of cyanophycin, no detectable cyanophycin was accumulated in any tested *C. ljungdahlii* strain. I performed a bioreactor experiment with an optimized medium to gain sufficient amounts of biomass of the recombinant *C. ljungdahlii* strains. The biomass was then used for a subsequent chemical purification of cyanophycin and further biochemical analyses. Several detection methods (*e.g.*, microscopy, SDS-PAGE, NMR analyses) were applied, but could only confirm the cyanophycin accumulation in the *E. coli* strain. I discussed several explanations why the cyanophycin synthesis was not present in *C. ljungdahlii*. I conclude this chapter with recommendations for future experiments and molecular work required to finally enable the cyanophycin synthesis also in *C. ljungdahlii.*

Chapter 7 provides a closing summary and an overall discussion about the findings of each chapter and their impact on the energy metabolism of *C. ljungdahlii*. Primary emphasis is put on conclusions and further interpretation of the essential role of the RNF complex. In addition, recommendations for future work are made and discussed.

CHAPTER 2

BACKGROUND AND LITERATURE REVIEW

2.1. Acetogens

Acetogens are a group of obligate anaerobic bacteria that are attracting industrial interest due to their ability to convert waste gases, such as CO, CO_2, and H_2, into valuable chemical products (Mohammadi *et al.*, 2011; Latif *et al.*, 2014). Main fermentation products are acetate and often ethanol, while some strains can also produce minor amounts of 2,3-butandiol, butanol, and lactate (Ragsdale and Pierce, 2008). Over 100 acetogenic species from 22 genera were isolated and characterized in the past decades with the most representatives in the genera *Clostridium* and *Acetobacterium* (Drake *et al.*, 2008). The central pathway that is used by acetogens is the reductive acetyl-CoA pathway, which is also known as Wood-Ljungdahl pathway (WLP) in which CO_2 is fixed for the metabolism (Ljungdhal, 1986; Wood, 1991; Drake *et al.*, 2008). The WLP is the only known pathway that combines energy conservation and carbon utilization. It is discussed to be the most efficient pathway of CO_2 fixation that exists (Schuchmann and Müller, 2014), and is most-likely the oldest microbial pathway for generation of ATP and biomass that has evolved in a primeval world (Drake *et al.*, 2008; Martin *et al.*, 2014).

2.2. *Clostridium ljungdahlii* – A model microbe for acetogenesis

The rod-shaped, motile, and non-pathogenic bacterium *Clostridium ljungdahlii* was isolated in 1987 and named after Lars G. Ljungdahl for his outstanding achievements in the discovery of the WLP (Tanner *et al.*, 1993). The full genome was sequenced in 2010 and comprises 4,630,065 bp, which makes it one of the largest clostridial genomes that is known in the literature (Köpke *et al.*, 2010). In the group of acetogens, *C. ljungdahlii* is one of the most widely studied members for its autotrophic growth (Schuchmann and Müller, 2014; Katsyv and Müller, 2020). Acetate and ethanol are the main fermentation products. Butyrate and butanol are not produced by the wild type (WT), because the corresponding genes are not present in the genome. In addition, *C. ljungdahlii* can produce minor amounts of lactate and 2,3-butanediol (Tanner *et al.*, 1993; Köpke *et al.*, 2010). Today, there are more than 100 studies available in which this bacterium was investigated directly or indirectly (PubMed search 05/2021).

2.2.1. Heterotrophic growth

C. ljungdahlii can use various sugars, such as fructose, arabinose, ribose, or glucose (only after adaption), as well as different carbonic acids, purines, and some amino acids (Tanner and Laopaiboon, 1997; Huhnke *et al.*, 2010; Köpke *et al.*, 2010) for heterotrophic growth. The genome encodes the full set of genes for gluconeogenesis (to glucose-6-phosphate) and for the Embden–Meyerhof–Parnas (EMP) pathway. However, the key enzymes of the Entner-Doudoroff pathway are not present, but *C. ljungdahlii* may utilize D-gluconate *via* 6-phosphogluconate to D-ribulose-6-phosphate, which is then used for the pentose-phosphate pathway (Köpke *et al.*, 2010). Glycine can be also fermented as an intermediate *via* the clostridial purine degradation pathway, which yields acetate and ATP (Dürre and Andreesen, 1983).

2.2.2. Autotrophic growth

C. ljungdahlii uses the WLP for autotropic growth with CO, CO_2, and H_2 (Tanner and Laopaiboon, 1997). This pathway consists of two separated branches to fix CO_2 for the central metabolism. In the methyl branch, a formate dehydrogenase reduces CO_2 to formate, which is then activated with tetrahydrofolate (THF) *via* a synthetase under the hydrolysis of one mole ATP (Ljungdhal, 1986; Ragsdale and Pierce, 2008). The resulting formyl-THF is further converted *via* methenyl-THF and methylene-THF to methyl-THF while consuming two H^+-ions and splitting off water (Ragsdale and Pierce, 2008; Schuchmann and Müller, 2014). In the final step of the methyl branch, the yielded methyl group is linked to a corrinoid iron-sulfur protein (CoFeSP) by a methyltransferase, and is transferred to a subunit of the carbon monoxide dehydrogenase/acetyl-CoA synthase (CODH/ACS). The required carbonyl group is supplied by a second CO_2 molecule, which is reduced to CO in the carbonyl branch *via* CODH activity of the same enzyme (Ragsdale and Pierce, 2008). CO can enter the pathway at this stage to provide the carbonyl group directly. The released acetyl coenzyme A (acetyl-CoA) is then converted into acetate by a phosphotransacetylase and an acetate kinase while one mole of ATP is synthesized by substrate-level phosphorylation. The CoA-group is recycled at this point. Since the generated ATP is directly re-used in the methyl branch, the WLP remains being a non-ATP generating pathway, which explains why acetogens are highly depended on a chemiosmotic mechanism for ATP synthesis during autotrophy (Ljungdhal, 1986; Wood, 1991; Schuchmann and Müller, 2014).

2.3. Energy conversation and electron bifurcation

C. ljungdahlii and other acetogens use substrate-level phosphorylation during glycolysis of sugars, which yields in acetate as fermentation product *via* phosphotransacetylase/acetate kinase activity and up to four moles of ATP (Schuchmann and Müller, 2014). The two resulting molecules of CO_2 that are released during glycolysis are shuttled to the WLP and being reduced by reducing equivalents into

another molecule of acetate. For instance, hexoses can be completely converted into 3 molecules of acetate without the release of any CO_2. In this process, additional ATP is gained, which gives acetogenic bacteria a growth advantage compared to other microbes without a WLP in certain environmental niches. During autotrophic growth, the reduction of two molecules of CO_2 with H_2 as sole electron donor is an exergonic reaction ($\Delta G' = -40$ kJ per mole H_2 at physiological conditions). However, this is only for the overall stoichemetry, and single reactions in the WLP can be more exergonic but also endergonic (Schuchmann and Müller, 2014). Overall, there are only a few exergonic reactions with redox potentials that are high enough to drive a chemiosmotic process to generate an ion gradient for a subsequent ATP generation. In this context, the reduction of CO_2 into CO, with a redox potential of -520 mV, is the largest thermodynamic barrier to overcome for acetogens, while the redox potential of the H^+/H_2 couple is only -414 mV (Thauer *et al.*, 1977). There are three electron carriers known in the WLP: 1) NADH; 2) NADPH; and 3) ferredoxin. However, only the latter one can reach a physiological redox potential that ranges from -450 mV to -500 mV (Fuchs, 2011; Buckel and Thauer, 2018). For acetogens the redox potential of the H^+/H_2 couple was postulated to be close to -320 mV under physiological conditions (Poehlein *et al.*, 2012). The exact redox potentials of the Fd_{ox}/Fd_{red} and CO_2/CO couples are still unknown (Schuchmann and Müller, 2014). The key to how acetogens overcome the energy barrier of electron transfer from H^+/H_2 towards Fd_{ox}/Fd_{red} is by flavin-based electron bifurcation (**Figure 1**) (Buckel and Thauer, 2013; 2018).

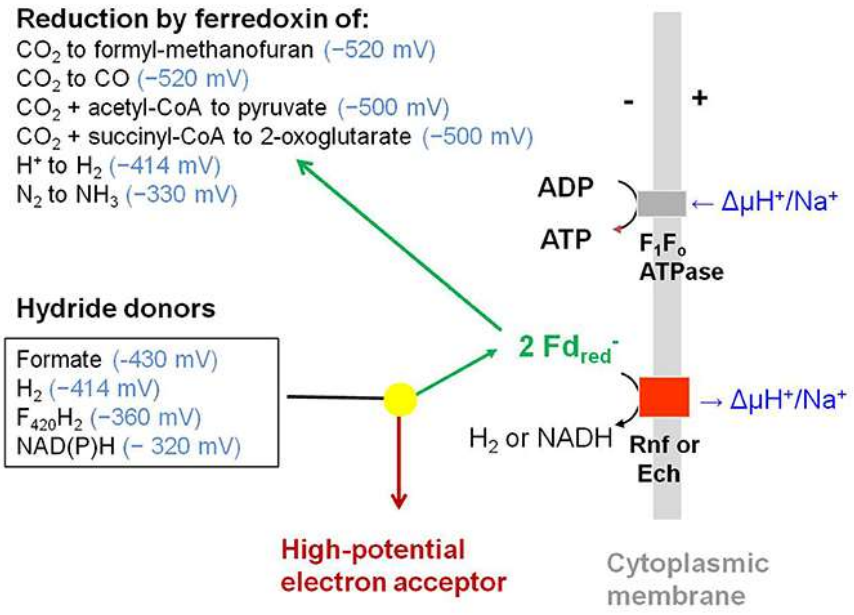

Figure 1 Electron-bifurcation based on flavoenzyme complexes and Fd re-oxidation reactions (Buckel and Thauer, 2018). Described are putative electron donors, acceptors, and their corresponding reduction potential. Fd has a general reduction potential (E_0') of -420 mV. However, this can be lower (-500 mV) *in vivo*. Electron-bifurcation may proceed backwards (confurcation) in case of H^+-ions, NAD(P)+, or pyruvate function as high-potential electron donors.

For this mechanism, a hybrid electron pair, such as NAD(P)H, H_2, $F_{420}H_2$, or formate is split into one electron with a more negative potential and in one electron with a more positive potential compared to the donor electron pair (**Figure 2**). This enables microbes to reduce Fd or flavodoxin (Fld) *via* low potential electrons (Buckel and Thauer, 2018). So far, more than ten different flavin-bifurcation enzymes were characterized in bacteria, which couple endergonic to exergonic reactions (Buckel and Thauer, 2018).

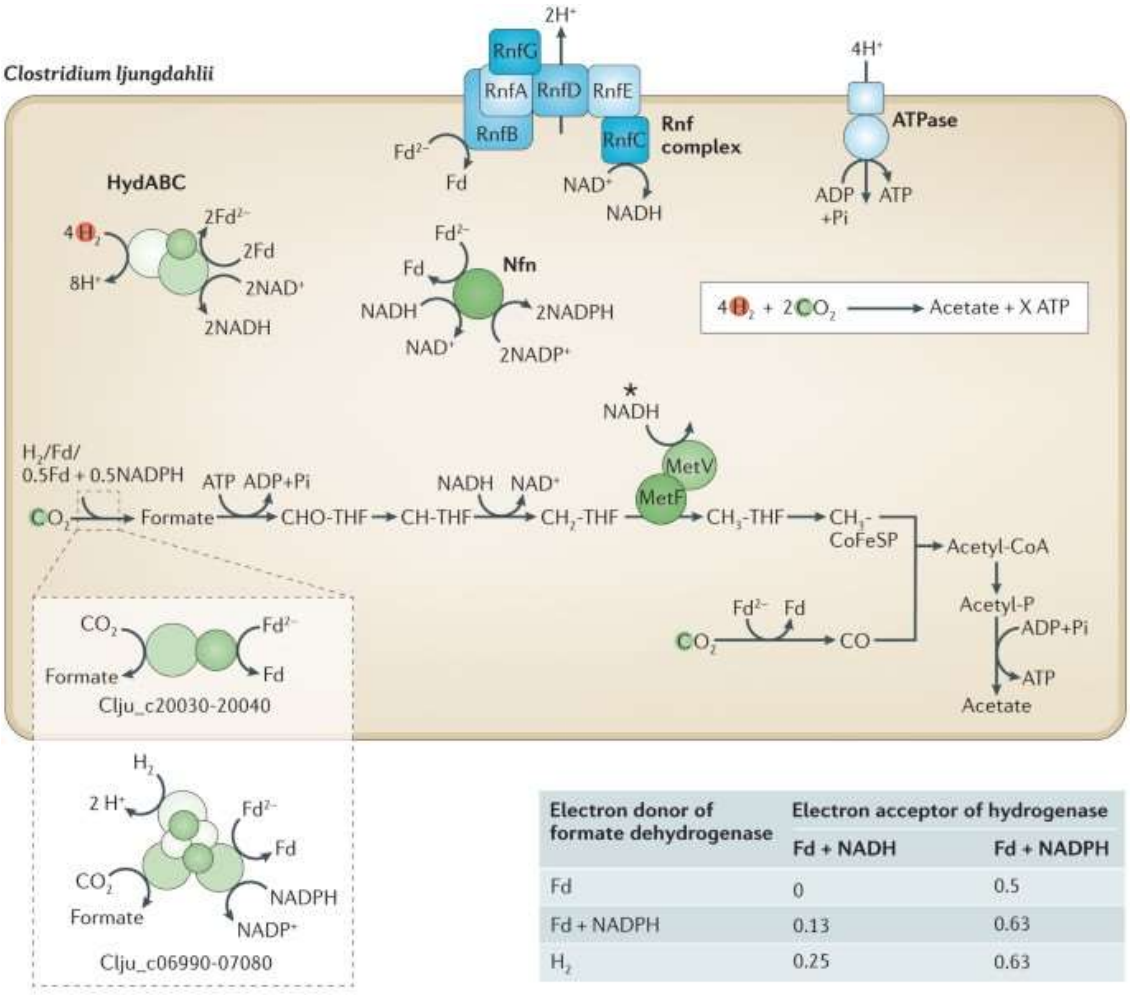

Electron donor of formate dehydrogenase	Electron acceptor of hydrogenase	
	Fd + NADH	Fd + NADPH
Fd	0	0.5
Fd + NADPH	0.13	0.63
H_2	0.25	0.63

Figure 2 Model of the autotrophic metabolism and enzymes involved in the energy conversation of *C. ljungdahlii* (Schuchmann and Müller, 2014). *C. ljungdahlii* uses the WLP to fix carbon under autotrophic conditions. The energy metabolism requires several enzymes, including electron-bifurcating reactions, to maintain and regenerate reducing equivalents. The RNF complex generates a H^+-gradient *via* oxidation of Fd^{2-} (Fd_{red}) and reduction of NAD^+. Subsequently, an ATPase is generating ATP driven by the H^+-gradient. A detailed description of the WLP and electron-bifurcation is found in the literature (Drake et al., 2008; Schuchmann and Müller, 2014; Buckel and Thauer, 2018).

Obviously, flavin-based electron-bifurcating enzymes are also present in the metabolism of *C. ljungdahlii*. The genome of *C. ljungdahlii* contains genes for four [FeFe] hydrogenases and one [NiFe] hydrogenase (Blaut and Gottschalk, 1984; Köpke *et al.*, 2010). Two of the [FeFe] hydrogenases have most likely a bifurcating character. One of them distributes electrons from H_2 towards Fd and NAD^+

(HydABC, CLJU_c14720–14700), and the other one forms a complex with a formate dehydrogenase (FDH) and distributes the electrons between CO_2 reduction, Fd_{ox}, and $NADP^+$ (Formiat-H_2-lyase/HytABCDE, CLJU_c06990-07080). Transcriptomic data showed that the remaining three hydrogenases are not part of acetogenesis (Köpke *et al.*, 2010; Tan *et al.*, 2013). There are three gene clusters for FDHs found in the genome. Besides the FDH, which is forming the bifurcating complex with the hydrogenase, a second FDH (CLJU_c20030–20040) might receive electrons from Fd_{red}. A selenocysteine-containing FDH is encoded by the third gene (CLJU_c08930) (Schuchmann and Müller, 2014). The last notable enzyme that has a putative electron bifurcating character is the NADH/NADPH transhydrogenase (Nfn, CLJU_c37240) (Köpke *et al.*, 2010). This enzyme might use Fd_{red} to oxidize NADH and subsequently reduce $NADP^+$ into NADPH. A homologous protein with a similar mechanism was also found in cells of *Clostridium kluyveri* (Wang *et al.*, 2010).

2.4. RNF complex – The key enzyme for energy conservation in *C. ljungdahlii*

C. ljungdahlii lacks the genetic constitution to synthesize any functional cytochromes or quinones for generation of a chemiosmotic gradient to drive an ATPase for generation of ATP (Köpke *et al.*, 2010). The only alternative route left to generate the gradient is mediated by the transmembrane located *Rhodobacter nitrogen fixation*-like complex (RNF complex). The RNF complex was first characterized to play an essential role in the nitrogen fixation pathway of *Rhodobacter capsulatus* (Schmehl *et al.*, 1993). The photosynthetic apparatus of this bacterium generates an electrochemical ion potential, which is used by the membrane located RNF complex to reduce Fd for a subsequent electron transfer to the dinitrogenase reductase in the cytoplasm (Schmehl *et al.*, 1993). Schmehl *et al.* (1993) concluded that the RNF complex is a novel electron-transfer system sharing high sequence similarities to Na^+-translocating NADH:ubiquinone oxidoreductases (Nqr) (Kumagai *et al.*, 1997). Later, it was suggested that the oxidation of Fd_{red} is coupled to the reduction of NAD^+ at the RNF complex in *R. capsulatus* (Müller *et al.*, 2008). Today, it is known that RNF genes are found in various microbes, such as chemolithotrophs, photolithotrophs, and chemoorganoheterotrophs, which are living in mesophilic or even thermophilic habitats (Biegel *et al.*, 2011; Katsyv and Müller, 2020; Kuhns *et al.*, 2020). A common feature of all RNF complexes is the generation of the chemiosmotic gradient either based on Na^+-ions or H^+-ions, which are then used either by an Na^+-dependent or H^+-dependent ATPase (Biegel *et al.*, 2011; Schuchmann and Müller, 2014; Katsyv and Müller, 2020). The presence of RNF-complex encoding genes (*rnf* genes) is considerably higher in facultative anaerobic/strict anaerobic species (>150 species) compared to only a few strict aerobic species, most being intracellular symbionts (Biegel *et al.*, 2011). This indicates the important role of the RNF complex in the anaerobic world. *Rnf* genes are commonly clustered in operons consisting of 6-7 genes (Biegel *et al.*, 2011). Their organization alternates but can be subdivided into three major groups: 1) *rnfABCDGE*;

2) *rnfCDGEAB*; and 3) *rnfBCDGEA*. The cluster of *R. capsulatus* (group 1) was first described to consist of five genes (Schmehl *et al.*, 1993), but later being corrected to encompass seven genes (*rnfABCDGEH)* (Jouanneau *et al.*, 1998). The role of the *rnfH* gene is still unknown and is lacking in most known *rnf* operons (Biegel *et al.*, 2011). Besides *R. capsulatus*, an *rnf* homolog operon (*rsxABCDGE*) was identified in *Escherichia coli* (Koo *et al.*, 2003), *Pseudomonas stutzeri*, and *Azotobacter vinelandii* (Curatti *et al.*, 2005). The second group of *rnf* clusters (*rnfCDGEAB*) is distributed among *Clostridium* species (Brüggemann *et al.*, 2003; Seedorf *et al.*, 2008; Biegel *et al.*, 2011). In addition, this group was also identified in *Acetobacterium woodii* (Biegel *et al.*, 2009). The third group of the cluster (*rnfBCDGEA*) is associated with some *Bacterioides* or *Chlorobium* species. More detailed information and tables with more representatives is available in a detailed review about the biochemistry, evolution, and the physiological role of the RNF complex in prokaryotes (Biegel *et al.*, 2011).

Beside the RNF complex, a similar membrane-bound protein complex exists, which is associated with the energy conservation in some thermophilic acetogens (Biegel *et al.*, 2011; Schoelmerich and Müller, 2019). This complex is called Ech complex and transfers electrons from reduced Fd across the membrane to protons which yields molecular H_2 (Schuchmann and Müller, 2014). An Ech complex was found instead of an RNF complex in the thermophilic acetogens *Thermoanaerobacter kivui* and *Moorella thermoacetica* (Pierce *et al.*, 2008; Schuchmann and Müller, 2014; Schoelmerich and Müller, 2020). Therefore, it is assumed that acetogens contain either an RNF or an Ech complex for their energy conservation. A recent review grouped all known acetogens into RNF- or Ech-acetogens and describes in detail the bioenergetic energy conservation mechanisms (Katsyv and Müller, 2020). However, for this dissertation, the following sections will only focus on the RNF complex since an Ech complex does not exist in *C. ljungdahlii*.

2.4.1. RNF gene regulation

Even though RNF complexes are known for many acetogens, only little is known about their transcriptional and translational regulation. For *C. ljungdahlii*, a small 417 bp putative regulator gene (*rseC*, CLJU_c11350) is located directly upstream of the *rnfCDGEAB* gene cluster (Köpke *et al.*, 2010). It was shown that *rseC* is upregulated under autotrophic conditions such as reported for the *rnf* genes (**Figure 3**) (Held, 2013; Nagarajan *et al.*, 2013; Al-Bassam *et al.*, 2018). Furthermore, a recent study revealed that *rseC* expression and translation follows tightly the profile of the gene *rnfC* (**Figure 3B and 3C**) (Al-Bassam *et al.*, 2018). Thus, it is assumed that *rseC* plays an important role for autotrophy but only a minor role for heterotrophy in *C. ljungdahlii*. Transcription start sites (TSS) and putative terminator hairpin structures were identified for *rseC* and the *rnfCDGEAB* gene cluster, which indicates that *rseC* is expressed as an individual transcript (**Figure 3A**) (Held, 2013; Al-Bassam *et al.*, 2018).

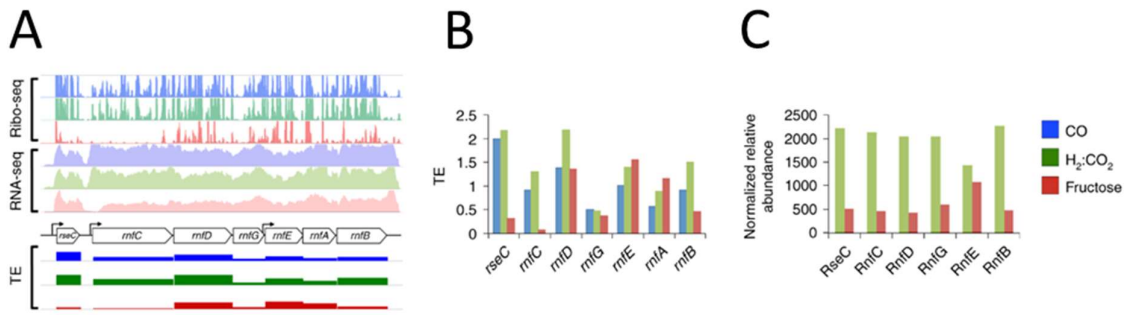

Figure 3 Transcriptional and translational regulation of the *rnf* genes at their putative regulator gene *rseC* under autotrophic and heterotrophic conditions in *C. ljungdahlii* (Al-Bassam *et al.*, 2018). The *rnf* genes and *rseC* undergo a high transcriptional and translational upregulation. The *rseC* gene follows tightly the profiles of *rnfC*. This indicates a strong association between *rseC* and the *rnfCDGEAB* gene cluster, which is not understood yet. Transcription start sites (TSS) were identified for *rseC* and *rnfCDGEAB* indicating that two individual transcripts exist. Another TSS was detected between *rnfG* and *rnfE* with an unknown function. (A) Transcription and translation of the RNF complex using RNA-sequencing (RNA-seq) and ribosome profiling (Ribo-seq) methods; (B) Transcription efficiency (TE) profiles of each individual gene under autotrophic and heterotrophic conditions; (C) translation profiles corresponding to each individual gene under both conditions.

Interestingly, the *rnfCDGEAB* possesses a second TSS between *rnfG* and *rnfE*. This could be an indicator for a further internal transcriptional control, which is not understood yet (Al-Bassam *et al.*, 2018). Besides the evidence that *rseC* is associated with the RNF complex in *C. ljungdahlii*, further detailed insights in the regulation of the RNF complex or distribution of *rseC* genes are missing. Interestingly, the *rseC* gene was already described as important factor in regulation of the oxidative stress response in *E. coli* mediated by SoxR and the *rsxABCDGE* genes, which share homology to the *rnf* genes in *R. capsulatus* (Koo *et al.*, 2003). Here, the *rseC* gene is organized in the *rseABC* operon, but located separately from the *rsxABCDGE* genes (De Las Peñas *et al.*, 1997; Koo *et al.*, 2003). For *E.* coli, it is assumed that the RseC protein is responsible to mediate the reduction of SoxR by repressing its own regulator gene *soxS* (Koo *et al.*, 2003).

2.4.2. Biochemistry of the RNF complex

For a long time, the purification of RNF complexes from acetogens remained challenging and was in most cases limited to the purification and characterization of RNF-complex subunits (Kumagai *et al.*, 1997; Backiel *et al.*, 2008; Biegel *et al.*, 2011; Suharti *et al.*, 2014). All attempts to purify the RNF complex of *C. ljungdahlii* and *A. woodii* had failed or suffered to some extent from instability of the complex as reported for *Clostridium tetanomorphum* and *Fusobacterium nucleatum* (Kim *et al.*, 2004; Boiangiu *et al.*, 2005; Kuhns *et al.*, 2020). In addition, a first complete topology of the RNF complex in *Vibrio cholera* could be completed based on experimental data for every RNF-complex subunit (Hreha *et al.*, 2015). However, this was a predicted model and experimental crystallography data of the purified enzyme are still necessary to unravel the exact structure and composition of the entire complex. Finally, the breakthrough in the purification of a full and intact RNF complex was achieved

recently with the thermophilic bacterium *Thermotoga maritima* (Kuhns *et al.*, 2020). For the first time it was possible to reconstitute the function and ion transport of a purified RNF complex together with a purified ATPase and liposomes *in vitro*. This was the missing experimental data proofing that the RNF complex is indeed a respiratory enzyme complex, which is translocating Na^+-ions and forms the respiratory system in *T. maritima* together with an Na^+-dependent F_1F_O ATPase (Kuhns *et al.*, 2020).

2.4.3. RNF subunits and their prosperities

The RNF complex most likely consists of monomer subunits (**Table 1**). This is deduced from experiments in which the molecular mass of the complete RNF complex of *A. woodii* was 186 kDa, which is most likely the sum of all subunit masses (Biegel *et al.*, 2011). A final proof for the oligomerization state of the RNF complex of *A. woodii* is still missing but results of other studies support this assumption (Backiel *et al.*, 2008; Suharti *et al.*, 2014; Hreha *et al.*, 2015). Furthermore, the recent experimental data from the first purified RNF complex of *T. maritima* further agree on this hypothesis (Kuhns *et al.*, 2020). Interestingly, native PAGE experiments with the RNF complex of *T. maritima* also showed protein sizes of ≈290 kDa (monomer-based RNF complex ≈150 kDa), which indicated a potential dimer structure of the RNF complex or individual subunits. However, further experimental data will be required to elucidate the oligomerization state (Kuhns *et al.*, 2020). Biegel *et al.* (2011) provide a detailed overview of all RNF-complex subunits and their characteristics in *A. woodii* (**Table 1**). The subunit RnfC is a soluble protein with a molecular mass of 48.7 kDa, which binds to the membrane of the cell in *A. woodii* and in *V. cholera* (Biegel *et al.*, 2009; Hreha *et al.*, 2015). Cysteine motifs (C-XX-C-XX-C-XXX-C-P) were found in the amino acid sequence of RnfC being typical indicators for 4Fe4S clusters (Schmehl *et al.*, 1993; Hreha *et al.*, 2015). FeS-clusters with UV/vis-absorbance peaks at 419 nm and 330 nm were identified in RnfC subunits from *E. coli*, which expressed the *rnfC* gene of *R. capsulatus* from a plasmid (Jouanneau *et al.*, 1998). Besides the FeS-clusters, flavins were also suggested to be part of RnfC (Kumagai *et al.*, 1997), and corresponding FMN (flavin mononucleotide) sites are present in the amino acid sequence (Yagi, 1993; Yagi *et al.*, 1993; Kumagai *et al.*, 1997). However, experimental proof is still missing. Furthermore, conserved residues, which share high similarities to NADH binding sites, were associated with RnfC, which indicates a possible binding site for NADH (Biegel *et al.*, 2011; Hreha *et al.*, 2015). RnfD is a membrane-integral protein with 6-9 transmembrane helices and a molecular mass of 35 kDa (Biegel *et al.*, 2011). UV/vis spectroscopy of RnfD from *V. chlorea* revealed a flavin binding site, however, its biological function is not fully understood yet (Backiel *et al.*, 2008). For *V. cholera*, RnfD is likely to play a critical role in the Na^+-uptake (Hreha *et al.*, 2015).

Table 1 Subunits of the RNF complex and their prosperities in *A. woodii* (Biegel *et al.*, 2011). It is likely that the RNF complex of *C. ljungdahlii* shares similarities to the RNF complex of *A. woodii*. However, the RNF complex of *A. woodii* is Na^+-dependent (Westphal *et al.*, 2018) and the RNF complex of *C. ljungdalii* is H^+-dependent instead (Tremblay *et al.*, 2012). The recent experimental data from the purification of the RNF complex of *T. maritima* (Kuhns *et al.*, 2020) are not considered. FMN, flavin mononucleotide; FeS, iron-sulfur; and TMH, transmembrane helices.

	Subunit					
	RnfC	**RnfD**	**RnfG**	**RnfE**	**RnfA**	**RnfB**
Size (bp)	1332	960	624	591	588	1002
Mass (kDa)	48.7	35	22.8	21.6	21.4	36.6
Predicted localization	Soluble	Membrane integral	Membrane associated	Membrane integral	Membrane integral	Membrane associated
TMH[a]	0	6-9	1	6	6	1-2
Experimental localization	Membrane	Membrane	Membrane	Membrane	Membrane	Membrane
Cofactors predicted	FeS, Flavin	FMN	FMN	-	-	FeS
Cofactors experimentally found	FeS[b]	FMN[c]	FMN[c]	-	-	FeS[b]

[a] TMH, number of transmembrane helices deduced from the amino acid sequence.
[b] Experimental data come from *R. capsulatus* (Jouanneau *et al.*, 1998).
[c] Experimental data come from *V. cholerae* (Backiel *et al.*, 2008).

The membrane protein RnfG in *A. woodii* has a size of 22.8 kDa and possesses 30 hydrophobic amino acids on its N-terminus (Biegel *et al.*, 2009). A possible interaction with flavin is also predicted for this subunit (Backiel *et al.*, 2008). The experimental data gained from the purification of the RNF complex of *T. maritima* showed that RnfD and RnfG, indeed, possess covalently bound flavins (Kuhns *et al.*, 2020). RnfE is also a membrane-integral protein with a molecular mass of 21.6 kDa. Its biochemical characterization is still incomplete (Biegel *et al.*, 2011). RnfB is a protein with a molecular mass of 36.6 kDa and 30 hydrophobic amino acids at its N-terminus, indicating a membrane anchoring feature (Jouanneau *et al.*, 1998). In addition, it contains cysteine motives for six 4Fe4S clusters (Biegel *et al.*, 2011). Interestingly, cells of *R. capsulatus* showed a 4-fold decreased amount of RnfB when they were exposed to iron limiting conditions (Jouanneau *et al.*, 1998). Overall, further experimental data derived from other microbes are still required for a more detailed biochemical characterization of RNF complexes and their corresponding subunits (Katsyv and Müller, 2020; Kuhns *et al.*, 2020).

2.5. RNF complex of *C. ljungdahlii*

The genome of *C. ljungdahlii* contains a *rnfCDGEAB* gene cluster (CLJU_c11360–410), and therefore belongs to the second group of *rnf* operons that is representative for *Clostridia* (Köpke *et al.*, 2010; Biegel *et al.*, 2011). So far, all attempts to purify the RNF complex of *C. ljungdahlii*, which is highly required to give experimental evidence for the composition and biochemistry of each subunit, have failed (Kuhns *et al.*, 2020). However, first predictions can be made based on the available genome

sequence data and knowledge gained from work with other microbes (Köpke *et al.*, 2010). In *C. ljungdahlii,* the subunits RnfA, RnfD, and RnfE are predicted to be integral membrane proteins due to their amino acid sequence domains (Köpke *et al.*, 2010; Biegel *et al.*, 2011). In contrast, RnfC and RnfB are missing these protein domains, which indicates their membrane association or soluble character (Köpke *et al.*, 2010). Based on the assumptions of Biegel *et al.* (2011) and the investigations of the RNF complex from *R. capsulatus* (Kumagai *et al.*, 1997; Jouanneau *et al.*, 1998; Hreha *et al.*, 2015), the RnfB and the RnfG subunits of *C. ljungdahlii* are most likely membrane anchored. Both protein sequences contain a stretch of 30 hydrophobic amino acids at the N-terminus in *A. woodii*, which could form one or two transmembrane helices (Biegel *et al.*, 2009; Biegel *et al.*, 2011). Typical ferredoxine domains with 4Fe4S cluster are present in RnfC and RnfB (Köpke *et al.*, 2010). The RNF complex of *C. ljungdahlii* is H^+-dependent, which was experimentally shown with a protonophore and ionophore treatment *in vivo*, respectively (Tremblay *et al.*, 2012). However, this finding was already predicted since only typical genes for a H^+-dependent, but not for a Na^+-dependent, F_1F_O ATPases are present in the genome of *C. ljungdahlii* (Köpke *et al.*, 2010).

To date, there is only a single study available in literature, which focused on the RNF complex of *C. ljungdahlii* (Tremblay *et al.*, 2012). The authors have reported a partial disruption of the *rnfA* and *rnfB* gene by single crossover integration, which led to a complete loss of autotrophy. However, the same *rnf* mutant was still able to grow with fructose, but showed reduced growth rate (reduction by ~30%). This was in coincidence with the predicted essential role of the RNF complex for the energy conservation in acetogens (Tremblay *et al.*, 2012; Schuchmann and Müller, 2014). For the remaining heterotrophy, it was assumed that glycolysis serves enough ATP for growth of the *rnf* mutant. Although, autotrophy of the *rnf* mutant was restored after 95 h cultivation with H_2 and CO_2. It was found that the reconstitution of the wild-type genotype was responsible for this observation. Any attempts to generate a plasmid that harbours the *rnfA* and *rnfB* gene for a complementation experiment failed (Tremblay *et al.*, 2012). Therefore, it was postulated that the expression of both genes is most likely toxic for *E. coli.* Tremblay *et al.* (2012) also tested the impact of the *rnf* mutation on the ability to fix nitrogen in an ammonium-free medium that contained nitrogen as sole nitrogen source during growth with fructose (Tremblay *et al.*, 2012). In this experiment, only the wild type was able to grow, and thus nitrogen fixation in the *rnf* mutant was abolished. These findings are consistent with similar findings for *rnf* gene mutants of *R. capsulatus* (Schmehl *et al.*, 1993; Jouanneau *et al.*, 1998).

2.6. Further genetic work on *rnf* genes

Besides the single RNF study available for *C. ljungdahlii* and the work performed with *R. capsulatus*, only three other studies are available for which *rnf* genes were manipulated successfully (Hess *et al.*, 2016; Lo *et al.*, 2017; Westphal *et al.*, 2018). First, in *Bacteroides fragilis* all Na^+-dependent ferredoxin:NAD-oxidoreductase activity was lost in the absence of *rnf* genes (Hess *et al.*, 2016). Second, an *rnf* mutant of the non-acetogen *Clostridium thermocellum* (restricted to heterotrophic growth) showed decreased ethanol production, which indicated the important role of NADH regeneration *via* the RNF complex (Lo *et al.*, 2017). Third. the most recent study investigated the deletion of the entire *rnfCDGEAB* operon in *A. woodii* (Westphal *et al.*, 2018). In consistence with the findings for the *rnf* mutant of *C. ljungdahlii*, the *rnf* mutant of *A. woodii* completely lost its ability to grow with H_2 and CO_2, but was still able to grow with fructose. Interestingly, acetogenesis under autotrophic conditions was strongly reduced in the *rnf* mutant (down to 20%, compared to the wild type), but still possible in resting cells (Westphal *et al.*, 2018). Subsequently, the authors compared ATP synthesis between the mutant and the wild type and confirmed that only the wild type but not the *rnf* mutant was able to synthesize ATP under autotrophic conditions. In conclusion, these findings showed that the RNF complex is the only respiratory enzyme in *A. woodii*, and most likely also in all other acetogens that contain *rnf* genes (Schuchmann and Müller, 2014; Westphal *et al.*, 2018; Katsyv and Müller, 2020). Despite the genetic attempts to delete *rnf* genes, overexpression of these genes was only investigated in *C. thermocellum* (Lo *et al.*, 2017). This overexpression mutant showed increased RNF-complex activity under heterotrophic conditions. A higher ethanol production, which was initially expected by the authors, did not occur. It was assumed that more RNF-complex activity would result in a larger pool of NADH, which would than increase the alcohol dehydrogenases activity, and consequently lead to higher ethanol concentrations. Interestingly, an additional hydrogenase maturation gene deletion (*ΔhydG*) in the the *rnf*-gene overexpression mutant, finally increased the ethanol production by 30% (Lo *et al.*, 2017). Deletion of the *hydG* gene and the *ech* gene (coding for a NiFe-hydrogenase) were previously shown to completely cease H_2 evolution in the non-acetogenic *C. thermocellum* (Biswas *et al.*, 2015). Indeed, *C. ljungdahlii* also possesses the *hydG* and a putative gene for a NiFe-hydrogenase, but the NiFe-hydrogenase does not seem to play a role in the acetogenesis based on transcriptomic data (Köpke *et al.*, 2010; Tan *et al.*, 2013). The small number of studies dealing with *rnf* genes and limited experimental data available, indicates the strong need for further genetic work to understand the RNF complex and its genetics in detail.

2.7. Metabolic engineering in *C. ljungdahlii* and related acetogens

In the last years, much effort was performed to generate recombinant strains of *C. ljungdahlii* and closely related acetogens with the aim to increase the metabolic production range and rate (Bengelsdorf *et al.*, 2013; Liew *et al.*, 2013; Humphreys and Minton, 2018). For *C. ljungdahlii*, minor amounts of butanol (Köpke *et al.*, 2010), butyrate (Ueki *et al.*, 2014), acetone (Banerjee *et al.*, 2014), mevalonic acid (Diner *et al.*, 2018), and 3-hydroxybutyric acid (3HB) (Woolston *et al.*, 2018) were produced by introducing heterologous biosynthesis pathways. Unfortunately, the generation of recombinant strains of acetogens is still time consuming and limited to a small number of genetic tools, genetic markers, and inefficient transformation rates (Molitor *et al.*, 2016a). Nevertheless, new genetic approaches were introduced throughout the last decade, including the implementation of a lactose-inducible promotor system (Hartman *et al.*, 2011; Banerjee *et al.*, 2014), an anhydrotetracycline-inducible promoter system (Girbal *et al.*, 2003; Dong *et al.*, 2012; Nagaraju *et al.*, 2016b; Woolston *et al.*, 2018), phage serine integrase-mediated site-specific genome engineering (Huang *et al.*, 2019), a temperature sensitive origin of replication (pWV01ts) (Molitor *et al.*, 2016a), anaerobic fluorescence marker genes (Molitor *et al.*, 2016a; Streett *et al.*, 2019; Flaiz *et al.*, 2021), and an optimized transformation protocol (Molitor *et al.*, 2016a). In addition, methods for the CRISPR/Cas technology were developed and used for precise gene deletion (Huang *et al.*, 2016; Nagaraju *et al.*, 2016b; Shin *et al.*, 2019; Zhao *et al.*, 2019) or gene regulation by CRISPR interference (CRISPRi) (Woolston *et al.*, 2018; Zhao *et al.*, 2019; Fackler *et al.*, 2021). However, the CRISPR/Cas technology for acetogens is still evolving quickly and more tools are developed. Nevertheless, the use of this technique in acetogens is often suffering from low transformation efficiency, inefficient DNA repair of the host cells, or toxicity caused by the expressed Cas protein (Huang *et al.*, 2016; Nagaraju *et al.*, 2016b; Zhao *et al.*, 2019). Furthermore, successful genetic work on other acetogens was carried out with the ClosTron tool (Heap *et al.*, 2007; Heap *et al.*, 2010). This method uses bacterial group II introns in combination with a resistance marker to inactivate a desired gene in the genome. In the optimized version, this method allows the recycle of resistance markers, which is important due to the limited number of marker genes available for clostridia. Another genetic tool for marker-less modifications of clostridial genomes was introduced later on by using the event of multiple allelic crossover exchanges (Al-Hinai *et al.*, 2012). Here, two homologous regions recombine with up- and downstream regions of the desired genes introduce a resistance marker at a gene position. Subsequently, another crossover event recovers the marker gene and excises the DNA at the target position. This method was further developed in a patent by the company LanzaTech (Walker and Köpke, 2015).

The modular plasmid system pMTL80000 (**Figure 4**) is the most frequently used shuttle-vector system to transfer DNA into various clostridial species, such as *C. ljungdahlii*, and was used in several studies (Heap *et al.*, 2009; Humphreys and Minton, 2018).

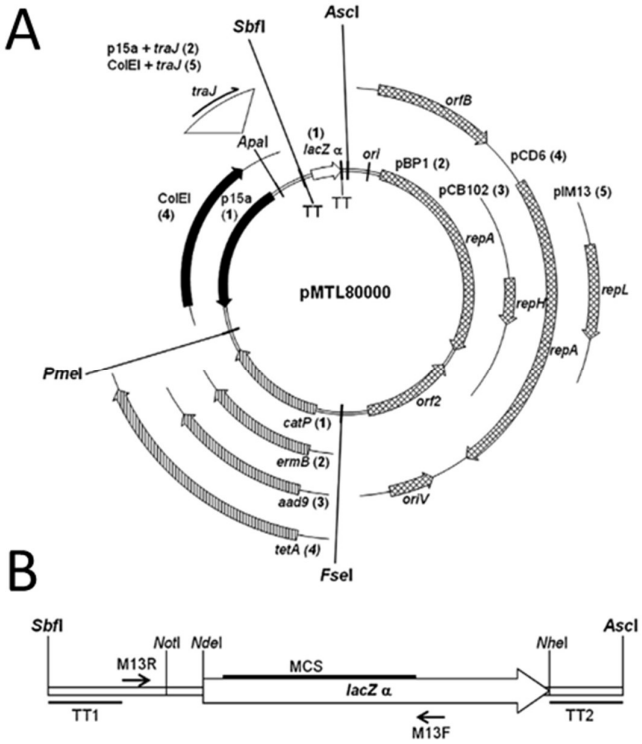

Figure 4 The modular shuttle-vector system pMTL80000 as suitable platform for genetic work on Clostridia (Heap et al., 2009). (A) The four modules can be combined in different combinations to generate a desired plasmid sequence with unique features by using rare eight-cutting restriction enzymes. Two different Gram-negative origin of replication (*ori*) types enables the cloning and assembly in *E. coli*. Subsequently, the Gram-positive *ori*(s) enable a sufficient plasmid replication in clostridial cells; (B) The multiple cloning site (MCS) module is used for the insertion of genes and is flanked by two terminator sequences (TT1 and TT2). Further information and a detailed description of each module and feature can be derived from http://www.clostron.com/pMTL80000.php.

The pMTL80000 system is commercially available (http://www.clostron.com/pMTL80000) and encompasses four modules. Each has exchangeable components (by rare eight-cutting restriction enzymes), which enables quick construction of plasmids with different functions. The four modules are (**Figure 4A**): 1) origin of replication for Gram-positive bacteria (pBP1, pCB102, pCD6, and pIM13); 2) origin of replication for Gram-negative bacteria (ColE1, p15a) with an optional transfer gene for conjugation (*traJ*); 3) resistance marker genes (*catP* for chloramphenicol, *ermB* for erythromycin, *tetA* for tetracycline, and *aad9* for spectinomyin); and 4) a multiple cloning site (MCS) (**Figure 4B**) with the option to add the *catP* reporter gene, a spacer, or one of the two clostridia promoters P_{fdx} or P_{thl}, respectively. The pMTL80000 system is optimized for cloning in *E. coli* before transferring the generated plasmids into the host of interest (Heap *et al.*, 2009).

2.8. CRISPR in *C. ljungdahlii*

The first appearance of the CRISPR/Cas technique in context with *C. ljungdahlii* was published by Huang *et al.* (2016). The authors reported about precise gene deletion with a high efficiency rate with the Cas9 nuclease. They targeted the four genes: 1) *pta (*CLJU_c12770, encoding for the phosphotransacetylase*);* 2) *adhE (*CLJU_c16510*,* encoding a bifunctional aldehyde/alcohol dehydrogenase); 3) *ctf* (CLJU_c39430*,* encoding for an acyl-CoA transferase*),* and (4) *pyrE* (CLJU_c35860*,* encoding for an orotate phosphoribosyl transferase). Electroporation was used for transformation. First screening of the mutants revealed that there was most likely a mix of the desired mutant and the WT in the liquid medium, which was applied for regeneration of the cells (Huang *et al.*, 2016). However, plating of some cell suspension with a subsequent isolation and screening of single colonies overcame this problem and several single mutant colonies were isolated. In the same year, the CRISPR/Cas technique was also developed for the closely related strain *C. autoethanogenum* (Nagaraju *et al.*, 2016b). Beside similar gene targets compared to the study with *C. ljungdahlii* (Huang *et al.*, 2016), it was found that the uncontrolled expression of the *cas9* gene was responsible for a poor efficiency of the CRISPR system. To address this problem, the authors tested different tetracycline-inducible promoters that were constructed in a small gene library (Nagaraju *et al.*, 2016a). The initial efficiency of CRISPR gene editing was improved by 50% by using an inducible system. Furthermore, the authors suggested to use inducible promoters for future work to minimize possible off-target activity of the Cas9 nuclease in the cell. This is consistence with the findings of a study in which a CRISPRi system was implemented for *C. ljungdahlii* (Woolston *et al.*, 2018). Even under non-inducing conditions, the *dcas9* gene, which is controlled by the lactose-inducible promoter, enabled the transcriptional repression of the target gene in the genome of *C. ljungdahlii*. The authors assumed that a single dCas9 protein synthesized in the cell is already enough to generate the desired phenotype. The high sensitivity of CRISPRi systems is known to be also one of the main disadvantages of this technique, since only constitutive downregulation of genes might be possible (Larson *et al.*, 2013). Furthermore, Woolston *et al.* (2018) showed that multiplexing sgRNAs enabled a simultaneous downregulation of several genes in their *C. ljungdahlii* mutants. Multiplexing can be a powerful tool to characterize and understand metabolic pathways by applying simultaneous downregulation on various pathway steps (Larson *et al.*, 2013; Woolston *et al.*, 2018).

Despite the implementation of plasmid-based CRISPR systems in *C. ljungdahlii*, others investigated the genome of *C. ljungdahlii* and the closely-related *C. autoethanogenum* using single-molecule sequencing technologies (Roberts *et al.*, 2013) to identify evidence for potential native CRISPR system (Brown *et al.*, 2014). Interestingly, *C. autoethanogenum* possesses an active native CRISPR system while *C. ljungdahlii* does not.

2.9. Cas12a - an alternative CRISPR nuclease

The discovery of the CRISPR/Cas system and its first demonstration *in vitro*, revolutionized the genome editing world (Jinek *et al.*, 2012). In December 2018, the work of Jinek *et al.* (2012) had already been cited more than 6000 times, which indicates the tremendous impact on the scientific world and the exponential progress made with CRISPR techniques (Lino *et al.*, 2018). The most known and best understood CRISPR technique is CRISPR/Cas9, which was reviewed in detail throughout the past years (Doudna and Charpentier, 2014; Sander and Joung, 2014; Sternberg and Doudna, 2015; Dominguez *et al.*, 2016). In short, the Cas9 of the CRISPR system is an RNA-guided endonuclease, which cleaves DNA (double strand break) at a specific position with a very high accuracy. The single-guide RNA (sgRNA) for Cas9 consists of two RNA elements: (1) a chimeric crRNA; and (2) a tracerRNA. The Cas9 performs a double strand break at the position at which the sgRNA binds to a targeted DNA. In addition, the target genomic site requires a short protospacer adjacent motif (PAM) located at the 3' end of the DNA site. The PAM sequence of Cas9 is NGG (Sander and Joung, 2014). Since the design of sgRNA is easy and cheap, several genomic targets can be addressed by using the same plasmid-based CRISPR/Cas9 system. In comparison, standard gene deletion methods are time consuming and costly or limited to available selective marker as described above.

During the past years, numerous alternative CRISPR/Cas systems were discovered, which made a classification of the different systems indispensable (Koonin *et al.*, 2017). In general, all known CRISPR/Cas system are divided into two classes. Class 1 comprises CRISPR/Cas systems with multi-subunit effector complexes, while Class 2 defines CRISPR/Cas systems with single-protein effector modules (Koonin *et al.*, 2017). Within these two classes several further types and subtypes of the Cas proteins are distinguished, which gives a hint for the immense diversity in CRISPR-system evolution (Koonin *et al.*, 2017). A detailed description of all CRISPR/Cas system would go beyond the scope of this dissertation but can be found in literature by several reviews from the past years (Makarova *et al.*, 2011; Nakade *et al.*, 2017; Hille *et al.*, 2018; Koonin and Makarova, 2019; Pickar-Oliver and Gersbach, 2019). Therefore, the following section will only focus on the CRISPR/Cas12a (former CRISPR/Cpf1) system, which has recently become one of the most promising alternative CRISPR systems available for genetic engineering compared to CRISPR/Cas9 system (**Figure 5**).

The functionality of the CRISPR/Cas12 system was first discovered in 2015 (Zetsche *et al.*, 2015). However, CRISPR/Cas12 was already assumed to be a new type V variant of Class 2 CRISPR system found in several microbial genomes before (Schunder *et al.*, 2013; Vestergaard *et al.*, 2014; Makarova *et al.*, 2015). The PAM sequence for Cas12a was examined by cloning the *Fncas12a* gene encoding for the Cas12a from *Francisella novicida* (FnCas12a) into *E. coli*, and screening for interference against a

PAM plasmid library (Zetsche *et al.*, 2015). It was found that in contrast to Cas9, which requires a 3'-located G-rich PAM sequence (NGG), FnCas12a uses the 5'-located T-rich PAM sequence TTN instead (Zetsche *et al.*, 2015). Later, the PAM sequence TTTN was identified to be preferred by other Cas12a nucleases, such as isolated from *Lachnospiraceae sp.* (LbCas12a) or *Acidaminococcus sp.* (AsCas12a) (Zetsche *et al.*, 2015; Yamano *et al.*, 2016). The use of T-rich PAM sequences is from particular interest because it extends the potential target sites in A/T-rich genomes (Zetsche *et al.*, 2015). Furthermore, Cas12a is guided by a single crRNA with no need of a tracrRNA, which is indispensable for Cas9. The short crRNA for FnCas12a encompasses a 19-nucleotide repeat and a 23-25 protospacer sequence (total of 42-44 nucleotides), while the typical sgRNA length for the Cas9 is around 100 nucleotides (Jinek *et al.*, 2012; Zetsche *et al.*, 2015).

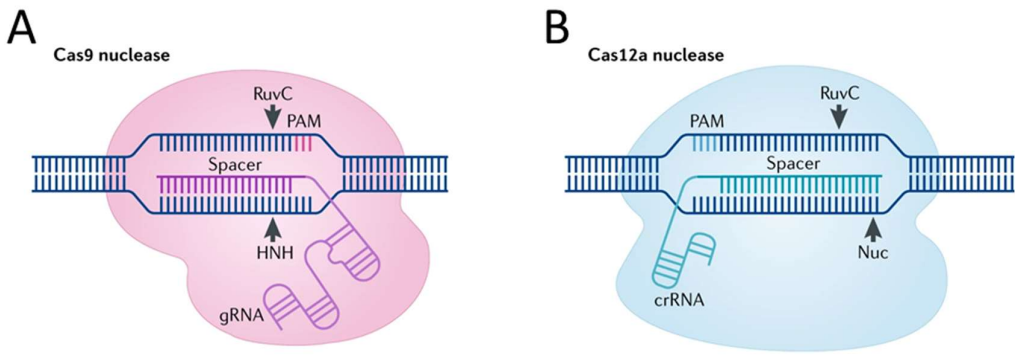

Figure 5 Schematic comparison of the CRISPR/Cas9 and the CRISPR/Cas12a system use for precise gene engineering of DNA (Pickar-Oliver and Gersbach, 2019). In contrast to Cas9 (A), the Cas12a nuclease (B) requires a 5'-located T-rich PAM sequence (TTN or TTTN) and cuts the DNA in a staggered pattern rather than giving a blunt cut. In addition, Cas12a is guided by a short crRNA and does not require a tracrRNA, which is essential for Cas9. It is assumed that the staggered pattern DNA cut by Cas12a is promoting homology-directed repair (HDR) of the target site. The Cas9 uses a RuvC- and a HNH-like protein domain to bind the target DNA site, while Cas12a contains a RuvC-like and a putative nuclease (Nuc) protein domain.

It was shown that Cas9 uses a RuvC- and a HNH-like protein domain to bind to the target DNA and mediate a double strand break (**Figure 5A**). In contrast, Cas12a binds to the DNA with a RuvC-like and a putative nuclease (Nuc)-like protein domain (**Figure 5B**). Cas12a also cuts the DNA with a DSB, but leaves behind a staggered overhang rather than a blunt end as it is the case for the Cas9 (Zetsche *et al.*, 2015). It is assumed that the DNA cut by Cas12a leads to higher rates of a homology-directed repair (HDR) of the host DNA, since the second DNA repair mechanism, non-homologous end-joining (NHEJ), would most-likely not result in a disruption of the target DNA in this scenario (Zetsche *et al.*, 2015; Pickar-Oliver and Gersbach, 2019). On the contrary, the blunt DNA cut that is mediated by Cas9 can predominantly lead to a high rate of NHEJ events, which is supposed to limit a subsequent HDR event, and thus result in an inefficient gene manipulation (Fagerlund *et al.*, 2015; Zetsche *et al.*, 2015). Besides single gene deletion events, multiple gene deletion is possible using a single CRISPR/Cas12a

and several crRNAs combined in a crRNA array as one system (Zetsche *et al.*, 2017; Ding *et al.*, 2018; Hong *et al.*, 2018; Zhang *et al.*, 2018b).

So far, CRISPR/Cas12a systems were successfully established for gene editing in *Saccharomyces cerevisiae* (Verwaal *et al.*, 2018), *Corynebacterium glutamicum* (Jiang *et al.*, 2017), and different cyanobacteria (Ungerer and Pakrasi, 2016). In addition, Cas12a was also applied to manipulate clostridia, such as *Clostridioides difficile* (Hong *et al.*, 2018), *Clostridium beijerinckii* (Zhang *et al.*, 2018a), and *Clostridium tyrobutyricum* (Zhang *et al.*, 2018b). Recently, CRISPR/Cas12a was implemented in *C. ljungdahlii* (Zhao *et al.*, 2019). The authors used a FnCas12a system to achieve gene deletion of the four genes *pyrE*, *pta*, *adhE1*, and *ctf* in *C. ljungdahlii*. Furthermore, it was possible to generate a deactivated form of the Cas12a nuclease, which was used as CRISPRi tool for the down regulation of genes in *C. ljungdahlii*, such as already reported for the Cas9 technique (Woolston *et al.*, 2018; Zhao *et al.*, 2019).

2.10. Nitrate reduction in clostridia

The ability of nitrate reduction is a wide-spread feature among many anaerobic and aerobic bacteria (Zumft, 1997). Dissimilatory nitrate reduction was thought to be an exclusive pathway that is only found in respiratory microbes, but completely absent in strict fermentative microbes (Hall, 1973; Zumft, 1997). However, it was observed that adding nitrate to a cultivation of strict fermentative bacteria, such as clostridia, contributed to an unexpected increase in growth yields (Hasan and Hall, 1975; Hasan and Hall, 1977; Caskey and Tiedje, 1980; Fröstl *et al.*, 1996). In consistence with the theory that the oxygen-dependent electron chain from respiratory bacteria must have evolved under anaerobic conditions with an alternative electron acceptor than free oxygen, it was assumed that nitrate reduction of fermentative bacteria is also coupled to the energy metabolism to some extent (Hall, 1971; 1973). There is a small number of studies from 60 years ago that already indicated such a potential connection between nitrate reduction and energy metabolism (Ishimoto and Egami, 1959; Takahashi *et al.*, 2012). In the following decades, scientists investigated the impact of nitrate on the growth of *Clostridium perfringens* (Hasan and Hall, 1975), *Clostridium tertium* (Hasan and Hall, 1977), an undefined *Clostridium* sp. (Caskey and Tiedje, 1980), and of the two acetogens *Clostridium thermoautotrophicus* and *Clostridium thermoaceticum* (Seifritz *et al.*, 1993; Fröstl *et al.*, 1996). When these bacteria were exposed to nitrate, heterotrophic growth was increased by up to 15-30%, while acetate concentration decreased slightly by 10 – 15%. This led to the hypothesis that the nature of the nitrate reduction in these microbes is from a dissimilatory rather than from an assimilatory character (Hasan and Hall, 1977). In the study of Hasan and Hall (1977), total ATP yields of *C. tertium* were slightly increased during nitrate reduction. However, the exact mechanism of ATP generation under nitrate

reducing conditions remained unclear. Later, the new type of energy conserving nitrate reduction was defined as fermentative nitrate reduction (Moreno-Vivián *et al.*, 1999). In conclusion, three nitrate reduction characters are known: 1) assimilatory nitrate reduction; 2) dissimilatory nitrate reduction; and 3) fermentative nitrate reduction. Only the latter two are described to be energy conserving, while assimilatory nitrate reduction is non-energy conserving and predominantly provides the metabolism with nitrogen (Hall, 1973; Zumft, 1997; Moreno-Vivián *et al.*, 1999). The first studies dealing with the impact of nitrate on autotrophic growth of acetogens were performed in the 1990s (Seifritz *et al.*, 1993; Fröstl *et al.*, 1996). Autotrophic growth was deficient when nitrate was added to the cultivation medium, while growth rates under heterotrophic conditions were slightly increased. The scientists argued that free electrons in the metabolism were predominantly used for the reduction of nitrate, which consequently impedes the WLP (Fröstl *et al.*, 1996). Interestingly, Fröstl *et al.* (1996) reported that cytochromes, which are usually found in the membrane, were absent in nitrate-reducing cells of *C. thermoaceticum* and *C. thermoautotrophicus*.

2.11. Nitrate reduction in *C. ljungdahlii*

For a long time, there was only a single study about nitrate reduction in *C. ljungdahlii* in which nitrate was tested as an alternative nitrogen source in an ammonium-free medium (Nagarajan *et al.*, 2013). However, the focus of this study was to investigate a genome-scale metabolic model for *C. ljungdahlii*. It was postulated that the nitrate reduction pathway of *C. ljungdahlii* is catalyzed by three enzymes: nitrate is first reduced by a soluble nitrate reductase (CLJU_c23710-30) to nitrite (NO_2^-), and, subsequently, converted *via* nitrite reductase (CLJU_c23750-70) and hydroxylamine reductase (CLJU_c07730) into ammonium (NH_4^+) (Köpke *et al.*, 2010; Nagarajan *et al.*, 2013). Another gene (CLJU_c23740) encoding for a putative nitrate/nitrite transporter was also predicted in the genome of *C. ljungdahlii.* Transcriptomic profiling of *C. ljungdahlii* cells that were grown under heterotrophic conditions with nitrate as sole nitrogen source, identified that all these genes are upregulated (>8-fold), with the highest upregulation found for genes encoding for the nitrate reductase, nitrite reductase, and the nitrate transporter (>400-fold) (Nagarajan *et al.*, 2013). Interestingly, the same authors mentioned that the nitrate reduction in *C. ljungdahlii* shares assimilatory and respiratory characteristics (based on their model), which was previously observed in the moderately thermophilic bacterium *Nautilia profundicola* (Campbell *et al.*, 2009). In that study, Campbell *et al.* (2009) proposed that *N. profundicola* uses a novel system to combine nitrate reduction to the energy metabolism in which a nitrate reductase, a putative hydroxylamine ubiquinone redox module, and an NADH-dependent hydroxylamine reductase must be involved, that are all located in the periplasm. Based on the genome-scale metabolic model of *C. ljungdahlii*, nitrate reduction under heterotrophic conditions was also associated with a reduced acetate production (Nagarajan *et al.*, 2013). This was explained by

the nitrate and nitrite molecules being additional electron sinks, however, an experimental test was not performed by Nagarajan *et al.* (2013). The only experimental data shown in this paper describe a stoichiometric reduction of nitrate and production of ammonium with *C. ljungdahlii* in a nitrate-containing but ammonium-free medium. The production of ethanol was not considered.

In 2019, a study was published in which the nitrate reduction in *C. ljungdahlii* and its impact on the autotrophic and heterotrohic metabolism was characterized in detail (Emerson *et al.*, 2019). For instance, it was shown that *C. ljungdahlii* is able to co-metabolize CO_2 and nitrate and uses both as final electron acceptor. Growth was enhanced during heterotrophic conditions with fructose and during autotrophic conditions with CO_2 and H_2. Interestingly, cultivation with CO as electron donor in nitrate-containing medium resulted in impaired growth rates and reduced product concentrations instead (Emerson *et al.*, 2019). The intracellular ATP/adenosine diphosphate (ADP) ratio and acetyl-CoA pools were increased by up to 5-fold and 3-fold during growth with nitrate under heterotrophic and autotrophic conditions with CO_2 and H_2. Transcriptomic analysis revealed that all genes involved in the nitrate reduction were significantly upregulated (log_2=2.9-6.2). This analysis showed also a simultaneous downregulation of 40% of the WLP involved genes of a culture grown with CO_2 and H_2 and nitrate supplementation. Emerson *et al.* (2019) explained this with a theoretical decoupling effect of ATP production from the WLP and proposed a schematic model (**Figure 6A**) for nitrate reduction in *C. ljungdahlii*, which has following stoichiometry: $4\ H_2 + 2\ H^+ + NO_3^- + 1.5\ ADP + 1.5\ P_i \rightleftharpoons 4\ H_2O + NH_4^+ + 1.5\ ATP$ with $\Delta r\ G'_0$=-150 kJ/mol H_2 (Thauer *et al.*, 1977; Emerson *et al.*, 2019).

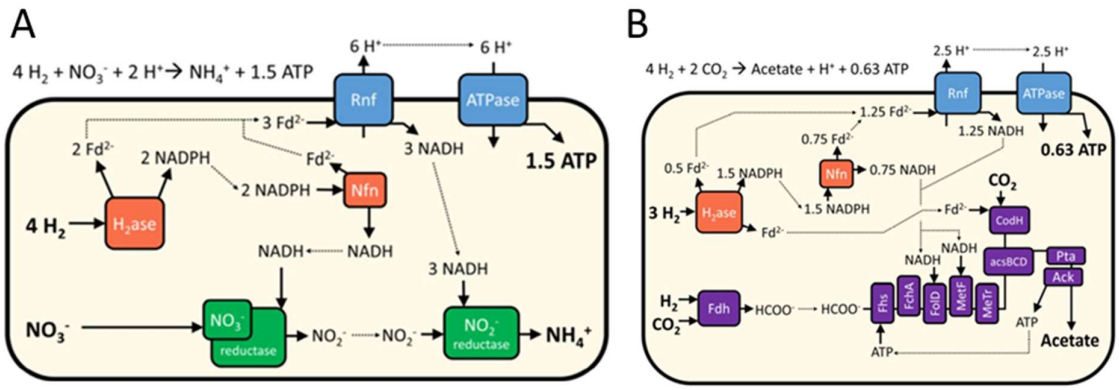

Figure 6 Postulated model for nitrate reduction in *C. ljungdahlii* under autotrophic conditions with H_2 and CO_2 (modified after Emerson et al., 2019). (A) The use of nitrate as final electron acceptor results in an increased ATP production up to 1.5 ATP *via* RNF complex and ATPase, and is independent from the carbon metabolism. Theoretically, one additional molecule of H_2 can be oxidized, while the nitrate reduction enzymes serve as NADH sink, and therefore accelerate the activity of the RNF. (B) The use of CO_2 as final electron acceptor leads to a theoretical maximum of 0.63 ATP, while acetate is produced as final fermentation product. Enzymes of the WLP are shown in purple. The nitrate reduction pathway is shown in green. Enzymes involved in electron bifurcation are shown in orange. The RNF complex and ATPase are shown in blue.

The ATP gained from this mechanism would be completely independent of the carbon metabolism but requires electron bifurcation mediated by hydrogenases (Buckel and Thauer, 2018). In contrast, the

theoretical maximum of ATP that *C. ljungdahlii* can gain during autotrophy with H_2 and CO_2 (without nitrate) is 0.63 ATP (**Figure 6B**) (Schuchmann and Müller, 2014). These theoretical predictions for the energy balance in *C. ljungdahlii* were broadly consistent with the measured ATP/ADP ratios from autotrophic nitrate reducing cells compared to cells growing without nitrate (Emerson *et al.*, 2019). However, the exact mechanism of electron flow and distribution within the cell during nitrate reduction remained unclear and requires further experimental data. In addition, it is not understood yet if other acetogens are also able to utilize nitrate and connect the nitrate reduction to their energy metabolism.

CHAPTER 3

NITRATE FEED IMPROVES GROWTH AND ETHANOL PRODUCTION IN *CLOSTRIDIUM LJUNGDAHLII* WITH H_2 AND CO_2 BUT RESULTS IN STOCHASTIC INHIBITION EVENTS.

Reproduced with permission from: Klask, C.M., Kliem-Kuster, N., Molitor, B., and Angenent L. T. (2020). Nitrate feed improves growth and ethanol production in *Clostridium ljungdahlii* with H_2 and CO_2 but results in stochastic inhibition events. Front. Microbiol., 11, 724. Copyright 2021 Frontiers in Microbiology.

3.1. Author's contribution

Christian-Marco Klask (C.M.K.) and Largus T. Angenent (L.T.A.) designed the Multi-Bioreactor-System. C.M.K., L.T.A., and Bastian Molitor (B.M.) planned the experiments. C.M.K. built, maintained, and sampled the bioreactors. Nikolai Kliem-Kuster (N.K.K.) supported in building, maintaining, and sampling the multi-bioreactor system as part of his bachelor thesis. L.T.A. and B.M. supervised the work. C.M.K. analyzed the experimental data and drafted the manuscript. L.T.A. and B.M. edited the manuscript. All authors revised the written text before submission.

3.2. Abstract

The pH-value in fermentation broth is a critical factor for the metabolic flux and growth behavior of acetogens. A decreasing pH level throughout time due to undissociated acetic acid accumulation is anticipated under uncontrolled pH conditions such as in bottle experiments. As a result, the impact of changes in the metabolism (*e.g.*, due to a genetic modification) might remain unclear or even unrevealed. In contrast, pH-controlled conditions can be achieved in bioreactors. Here, we present a self-built, comparatively cheap, and user-friendly multiple-bioreactor system (MBS) consisting of six pH-controlled bioreactors at a 1-L scale. We tested the functionality of the MBS by cultivating the acetogen *C. ljungdahlii* with CO_2 and H_2 at steady-state conditions (=chemostat). The experiments (total of 10 bioreactors) were addressing the two questions: (1) does the MBS provide replicable data for gas-fermentation experiments?; and (2) does feeding nitrate influence the product spectrum under controlled pH conditions with CO_2 and H_2? We applied four different periods in each experiment ranging from pH 6.0 to pH 4.5. On the one hand, our data showed high reproducibility for gas-fermentation experiments with *C. ljungdahlii* under standard cultivation conditions using the MBS. On

the other hand, feeding nitrate as sole N-source improved growth by up to 62% and ethanol production by 2-3-fold. However, we observed differences in growth, and acetate and ethanol production rates between all nitrate bioreactors. We explained the different performances with a pH-buffering effect that resulted from the interplay between undissociated acetic acid production and ammonium production and because of stochastic inhibition events, which led to complete crashes at different operating times.

3.3. Introduction

An increasing world population will likely lead to growing energy demands. To meet these demands in a sustainable way, we need to rethink the status quo of a fossil-based economy and transition into a renewable-based and circular economy. Furthermore, we have to mitigate the apparent climate effects of anthropogenic greenhouse gas emissions, such as carbon dioxide (CO_2), which are caused preliminary by industry, agriculture, and transportation. Biotechnology offers potential to contribute to climate-friendly and economically feasible solutions. One promising solution is synthesis gas (syngas) fermentation with microbes (Mohammadi *et al.*, 2011). For syngas fermentation, mixtures of the gases CO_2, hydrogen (H_2), and carbon monoxide (CO) are converted into products, such as acetate and ethanol, by acetogenic bacteria (Dürre, 2017). This process provides a promising way to produce chemicals and biofuels with a reduced CO2-footprint (Latif *et al.*, 2014; Molitor *et al.*, 2017; Phillips *et al.*, 2017).

In recent years, the company LanzaTech (Skokie, IL, USA) demonstrated that ethanol production from syngas with the acetogen *C. autoethanogenum* is possible at commercial scale, which further indicates the potential of this platform. While the LanzaTech technology is based on proprietary strains of *C. autoethanogenum*, in academic research the most frequently studied acetogen is the closely related microbe *C. ljungdahlii*. Both microbes produce acetic acid, ethanol, and some 2,3-butanediol from gaseous substrates (Tanner *et al.*, 1993; Abrini *et al.*, 1994; Köpke *et al.*, 2010; Brown *et al.*, 2014).

Different strategies are employed to optimize *C. autoethanogenum* and *C. ljungdahlii* for biotechnology. On the one hand, genetic engineering is used to generate modified strains that produce butyrate (Köpke *et al.*, 2010), butanol (Köpke and Liew, 2012; Ueki *et al.*, 2014), acetone, and isopropanol (Bengelsdorf *et al.*, 2016; Köpke *et al.*, 2016). In academic research, the physiological characterization of these genetically engineered strains is typically performed in batch experiments with serum bottles, which does not allow to control important process parameters such as the pH-value. On the other hand, bioprocess engineering is used to investigate and optimize the production of naturally occurring products, such as ethanol, in optimized bioreactor systems (Younesi *et al.*, 2005; Mohammadi *et al.*, 2012; Richter *et al.*, 2013; Abubackar *et al.*, 2015). While the impact of cultivation

parameters can be investigated within one study, these studies often are difficult to compare with each other, because very different bioreactor architectures and process parameters are used (Asimakopoulos *et al.*, 2018). Furthermore, because of the complexity, these setups are not suitable to perform preliminary experiments with genetically engineered strains. These issues can be partly overcome by utilizing commercially available bioreactor (chemostat) systems. However, these systems are costly, and therefore often not available to laboratories that do not focus on bioprocess engineering. Consequently, genetically engineered strains are typically not studied in fermentations beyond the serum bottle size, which leaves a gap between the construction of these strains and the investigation under controlled fermentation conditions.

To close this gap, we developed a cost-efficient, multiple-bioreactor system (MBS) that can be built from off-the-shelf components for a considerably smaller investment compared to the cost of commercial bioreactor systems. We give all information on purchasing the required parts, the assembly of the MBS, the process control elements (*e.g.*, stirring, pH, temperature), and further improvement ideas. We tested our MBS with *C. ljungdahlii* and CO_2 and H_2 as substrate under controlled pH conditions by addressing the two questions: (1) does the MBS provide replicable data for gas-fermentation experiments?; and (2) does feeding nitrate influence the product spectrum under controlled pH conditions with CO2 and H2? In a recent study, nitrate was used as an alternative electron acceptor for *C. ljungdahlii*, while it also served as sole nitrogen source (N-source) in batch cultivations (Emerson *et al.*, 2019). To our knowledge, this was the first study which investigated nitrate reduction by any known acetogen in detail. The co-utilization of CO_2 and nitrate enhanced the autotrophic biomass formation with CO_2 and H_2 compared to standard cultivation conditions with ammonium as the sole N-source. Contrarily, ethanol production was strongly reduced under nitrate conditions with CO_2 and H_2. The authors discussed that nitrate reduction consumes electrons, which would be no longer available for the reduction of acetate into ethanol. At the same time, nitrate reduction led to an accumulation of ammonium. This resulted in a continuous increase of the pH from 6.0 to 8.0 during the batch cultivations in serum bottles (Emerson *et al.*, 2019), which would intrinsically prevent ethanol production, because ethanol production is most likely triggered by a low pH (Mock *et al.*, 2015; Richter *et al.*, 2016a). It is well-known that growth of acetogens, such as *C. ljungdahlii*, is highly dependent on the pH (Drake *et al.*, 2008). Since their main fermentation product is acetate, which acts (in the form of the undissociated acetic acid) as a weak acid, a missing pH control, such as in serum bottles, intrinsically lowers the pH of the medium during growth. In contrast, the pH can be controlled in bioreactors such as in our MBS.

3.4. Materials and Methods

3.4.1. Microbial strains and medium composition

Wild type *C. ljungdahlii* PETC (DSM 13528) was obtained from the DSMZ (Braunschweig, Germany). Generally, pre-cultures were grown heterotrophically at 37°C (IN260 stand incubator, Memmert, Germany) in 100-mL serum bottles with 50 mL of standard PETC medium containing (per liter): 0.5 g yeast extract; 1.0 g NH_4Cl; 0.1 g KCl; 0.2 g $MgSO_4x7\ H_2O$; 0.8 g NaCl; 0.1 g KH_2PO_4; 0.02 g $CaCl_2x2\ H_2O$; 4 mL resazurin-solution (0.025 vol%); 10 mL trace element solution (TE, 100x); 10 mL Wolfe's vitamin solution (100x); 10 mL reducing agent (100x); and 20 mL of fructose/2-(N-morpholino)ethanesulfonic acid (MES) solution (50x). Vitamins, reducing agent, and fructose/MES solution were added after autoclaving under sterile conditions. TE was prepared as 100x stock solution containing (per liter): 2 g nitrilotriacetic acid (NTA); 1 g $MnSO_4xH_2O$; 0.8 g $Fe(SO_4)_2(NH_4Cl)2x6\ H_2O$; 0.2 g $CoCl_2{\cdot}6\ H_2O$; 0.0002 g $ZnSO_4x7\ H_2O$; 0.2 g $CuCl_2x2\ H_2O$; 0.02 g $NiCl_2x6\ H_2O$; 0.02 g $Na_2MoO_4x2\ H_2O$; 0.02 g Na_2SeO_4; and 0.02 g Na_2WO_4. The pH of the TE was adjusted to 6.0 after adding NTA. The solution was autoclaved and stored at 4°C. Wolfe's vitamin solution was prepared aerobically containing (per liter): 2 mg biotin; 2 mg folic acid; 10 mg pyridoxine-hydrochloride; 5 mg thiamin-HCl; 5 mg riboflavin; 5 mg nicotinic acid; 5 mg calcium pantothenate; 5 mg p-aminobenzoic acid; 5 mg lipoic acid; and 0.1 mg cobalamin. The vitamin solution was sterilized using a sterile filter (0.2 µm), sparged with N_2 through a sterile filter, and stored at 4°C. The 50x fructose/MES solution contained (per 100 mL): 25 g fructose; and 10 g MES. The pH was adjusted to 6.0 by adding KOH. The solution was sterilized, sparged with N_2 through a sterile filter, and stored at room temperature. The reducing agent was prepared under 100% N_2 in a glove box (UniLab Pro Eco, MBraun, Germany) and contained (per 100 mL): 0.9 g NaOH; 4 g cysteine-HCl; and 2.17 g/L Na_2S (60 weight%). Anaerobic water was used for the preparation of the reducing agent. The reducing agent was autoclaved and stored at 4°C.

For all bioreactor experiments, the standard PETC medium for the initial batch phase was supplemented with 0.5 g L^{-1} yeast extract and autoclaved inside the bioreactor vessel with an open off-gas line to enable pressure balance. The autoclaved bioreactors were slowly cooled down at room temperature overnight with an attached sterile filter at the off-gas line. After transferring each bioreactor to the MBS frame, the medium was continuously sparged with a sterile gas mixture of CO_2 and H_2 (20/80 vol-%). After 1 h, vitamins and reducing agent were added through the sampling port. N_2 gas was applied through a sterile filter to flush the sampling port after each addition of media components. Subsequently, each bioreactor was inoculated with 5 mL of an exponential heterotrophically grown PETC culture. All feed bottles for continuous mode containing 4 L of PETC medium with additions, as described below, were autoclaved, and stored overnight with an attached

sterile filter on the off-gas line. The bottles were sparged with N_2 for 2 h through a sterile filter. Vitamins and reducing agents were added under sterile conditions. A gas bag with N_2 gas was attached with a sterile filter to balance the pressure in the feed bottle during the bioreactor run. Standard PETC medium for continuous mode did not contain yeast extract and was adjusted to the respective pH of the period. One feed bottle was simultaneously used to provide medium for three bioreactors of the same triplicate. For all nitrate experiments we replaced NH_4Cl, with the equivalent amount of nitrogen as $NaNO_3$ (18.7 mM) in the feed medium.

3.4.2. Bioreactor setup and standard operating conditions

Six 1-L self-built bioreactors (**Figure 7, Supplementary Table S1, Supplementary Figure S1-S3**) with a working volume of 0.5 L were operated simultaneously for two experimental bioreactor runs, while four of these bioreactors were operated simultaneously for two additional experimental bioreactor runs, with a total of 10 bioreactors (**Figure 8-11, Supplementary Table S2-S9**). The cultivation temperature was 37°C and the agitation was set to 300 revolutions per minute (rpm). The gas flow rate was adjusted to 30 mL min^{-1} prior to inoculation. To establish microbial growth in the MBS after one inoculation event for each bioreactor, we operated the MBS in batch mode for 3-4 days before switching to continuous mode. The pH was set to 6.0 during the batch mode and the first 6 days (Period I) in continuous mode. Subsequently, the pH setting was lowered stepwise in 6 days to a pH of 5.5, 5.0, and 4.5 (Period II-IV). The pH of the feed medium was adjusted to the anticipated pH of each period. In our preliminary experiment (bioreactor 1/2/3) (**Figure 8, Supplementary Figure S4**) and the first nitrate experiment (bioreactor 4/5/6) (**Figure 9, Supplementary Table S3, S4, S5**), we did not use the acid feed to actively adjust the pH within the bioreactor. Instead, we let the pH decrease to the set value by the microbial production of undissociated acetic acid to avoid a pH shock. This took approximately one to two days of each 6-day period. For the preliminary experiment and the first nitrate experiment we chose a medium feed rate of 0.10 mL min^{-1}, which resulted in a 3.5-day hydraulic retention time (HRT), and which represents 1.7 HRT periods within each period of six days. In our second and third nitrate experiment, the medium feed rate was 0.19 mL min^{-1}. This was equal to a 2-day HRT and resulted in 3.2 HRT periods within each pH period, instead. We only used base feed to maintain the pH in the second nitrate experiment (bioreactor 7 and 8) (**Figure 10, Supplementary Table S6, S7**), while base and acid feed was actively applied for the third nitrate experiment (**Figure 11, Supplementary Table S8, S9**) to immediately adjust the pH of the bioreactor to the anticipated pH-value of each period. We used 2 M KOH and 2 M HCl in our experiments.

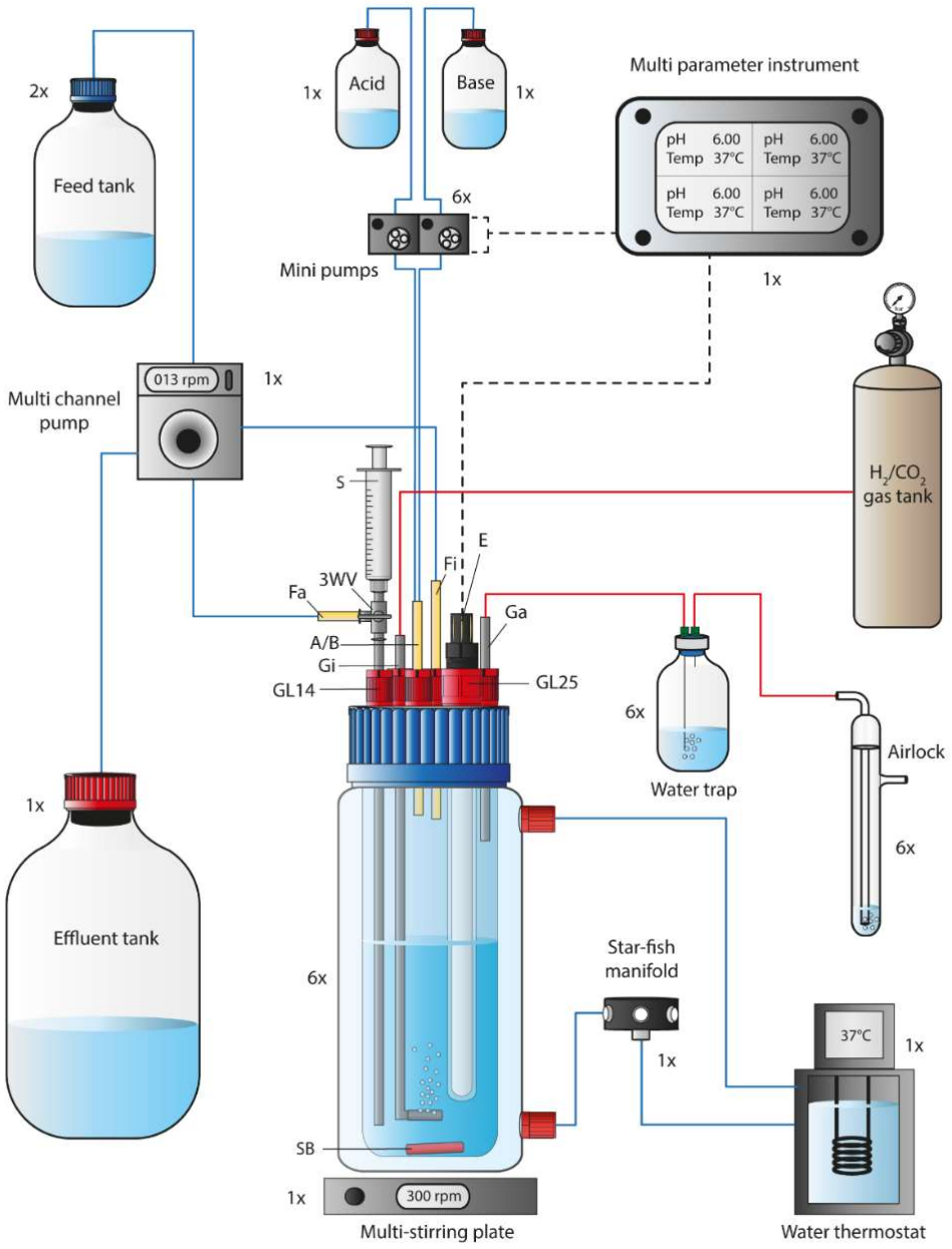

Figure 7 Flow chart of a single bioreactor operated in the MBS. The 1-L bioreactor vessel consisted of a double-walled glass vessel and a customized lid, while it was placed on a multi-stirring plate with up to six bioreactors. The bioreactor temperature was maintained through a water circulation unit at 37°C. The autoclavable lid offered connections for 5x GL14 and 1x GL25. A set of stainless-steel tubing was used for the gas-in/-out lines and for the medium feed-out line. The three-way valve at the medium feed-out line was required for sampling using a 5-mL syringe. The pH and bioreactor medium temperature were tracked *via* a pH/pt1000-electrode that was connected to a multi-parameter instrument. The multi-parameter instrument controlled and triggered two mini pumps (for base and acid) at programmable conditions. For continuous mode, the feed medium to each bioreactor was pumped *via* a single multi-channel pump from the feed tank into the bioreactor. The same pump was used to transfer the effluent from each bioreactor into the effluent tank. Sterile CO_2 and H_2 gas (20/80-vol-%) was sparged into the system through stainless-steel tubing with an attached sparger. The gas-out line was connected to a 100-mL serum bottle to serve as a water trap before the outgoing gas passed an airlock. The 1×, 2×, and 6× next to each unit in the figure describe the quantity, which is required to operate six bioreactors simultaneously. A/B, Acid and/or base feed line; E, pH/pt1000 electrode; Fa, medium feed-out line; Fi, medium feed-in line; Ga, gas-out line; Gi, gas-in line; GL14, screw joint connection size 14; GL25, screw joint connection size 25; rpm, revolutions per minute; SB, stirring bar; 3WV, three-way valve. Blue lines indicate liquid transfer, red lines contain gas, and dotted black lines provide electric power or signals.

3.4.3. Sampling and analyses

Bioreactors were sampled once or twice per day. A pre-sample of 3 mL of cell suspension was discarded, before taking a 2 mL sample (main sample) during batch mode. For sampling in continuous mode, the multi-channel pump was switched off during the sampling procedure. Cell growth was monitored by measuring the optical density at 600 nm (OD_{600}) (Nanophotometer NP80, Implen, Germany). For OD_{600}-values larger than 0.5, dilutions with 100 mM phosphate-buffered saline (PBS) at pH 7.4 were prepared. Nitrate and nitrite concentrations were qualitatively monitored using test stripes (Quantofix nitrate/nitrite, Macherey-Nagel, Germany). A correlation between cellular dry weight (CDW) and OD_{600} was calculated by harvesting 50 mL of culture sample from every bioreactor, centrifugation of the samples at 3428 relative centrifugal force (rcf) (Eppendorf centrifuge 5920R) for 12 min at room temperature (RT) and, subsequently, drying the pellet at 65°C for 3 days. The CDW for an OD_{600} of 1 was determined to be 0.24 g L^{-1} for cultures grown in PETC medium with ammonium and 0.29 g L^{-1} for cultures grown in PETC medium with nitrate as sole nitrogen source, respectively (**Supplementary Table S10**). Acetate and ethanol concentrations were analyzed *via* a high-pressure liquid chromatography (HPLC) (LC20, Shimadzu, Japan) system that was equipped with an Aminex HPX-87H column and operated with 5 mM sulfuric acid as eluent. The flow was 0.6 mL min^{-1} (LC-20AD). The oven temperature was 65°C (CTO-20AC). The sample rack of the HPLC was constantly cooled to 15°C in the autosampler unit (SIL-20ACHT). For HPLC sample preparation, all culture samples were centrifuged for 3 min at 15871 rcf (Centrifuge 5424, Eppendorf, Germany) in 1.5-mL reaction tubes. 750 µL of the supernatant was transferred into clean reaction tubes and stored at -20°C until use. Frozen samples were thawed at 30°C and 250 revolutions per minute (rpm) for 10 min (Thermomixer C, Eppendorf, Germany). The samples were centrifuged again and 500 µL of the supernatant was transferred into short thread HPLC/GC *via*ls (glass *via*l ND9, VWR, Germany) and sealed with short screw caps, which contained rubber septa (6 mm for ND9, VWR, Germany). New standards for acetate and ethanol were prepared for every analysis. All HPLC samples were randomized.

3.5. Results

3.5.1. Operating the MBS for replicable gas fermentation experiments

We based our experiments in this study on a versatile self-built multiple-bioreactor system (MBS). The MBS (**Figure 7, Supplementary Figure S1**) was designed to either perform heterotrophic or autotrophic cultivation experiments in batch or continuous mode. The MBS can be used to operate up to six bioreactors simultaneously, each individually at different pH conditions or, if necessary, with different feed medium. The MBS platform might be especially interesting for cost-effective research in academia. To show high comparability and reproducibility of our MBS, as a preliminary experiment

(control), we grew *C. ljungdahlii* simultaneously as triplicates in standard PETC medium with CO_2 and H_2 (ammonium, bioreactors 1/2/3) (**Figure 8, Supplementary Figure 4**).

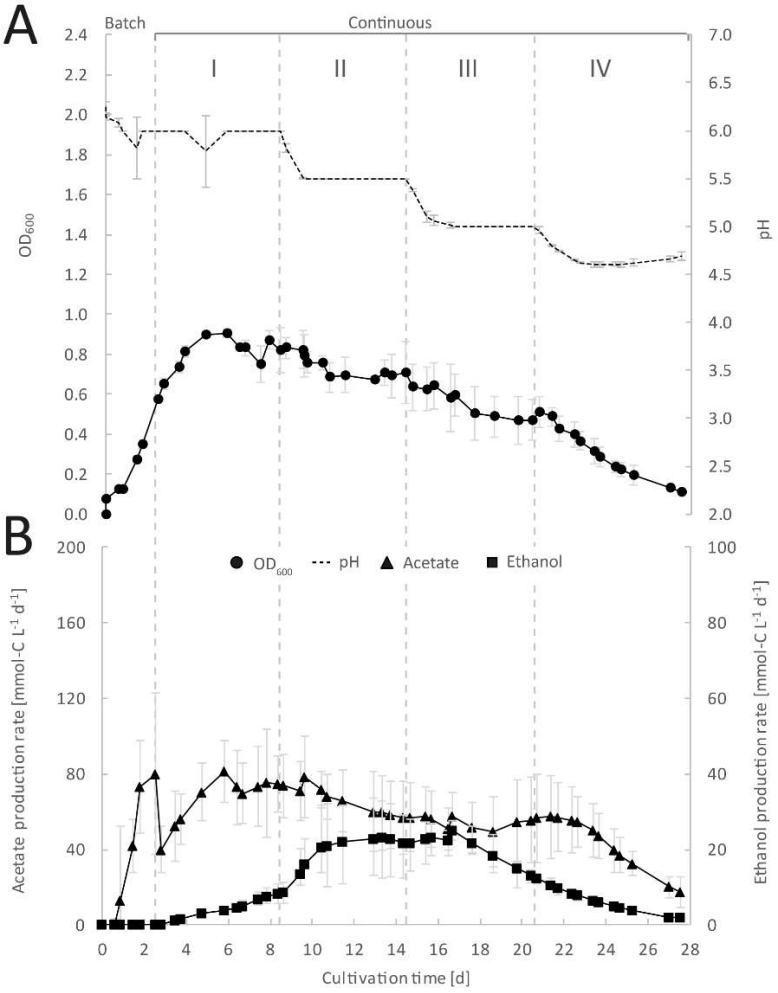

Figure 8 Continuous gas fermentation of *C. ljungdahlii* with CO_2 and H_2 in standard PETC medium at different periods in a preliminary experiment (bioreactor 1/2/3). (A) Mean values of triplicates with standard de*via*tion (n = 3) for pH and OD_{600}. (B) Acetate and ethanol production rates in mmol-C L^{-1} d^{-1}. The standard PETC medium contained 18.7 mM ammonium chloride as sole N-source. The horizontal dotted lines indicate the continuous process in which medium of different pH was fed to each bioreactor. Period: I, pH = 6.0; II, pH = 5.5, III, pH = 5.0; and IV, pH = 4.5.

We observed that growth was similar in the triplicate bioreactors during the cultivation of 27.5 days. During the initial batch mode, the average OD_{600} increased to 0.58 ± 0.01 (**Figure 8A**). After switching to continuous mode, the average OD_{600} increased further to values of 0.82 ± 0.04 during Period I. For Periods II, III, and IV, the average OD_{600} for the bioreactors constantly decreased to values of 0.69 ± 0.01, 0.51 ± 0.05, and 0.18 ± 0.06 (**Table 2, Figure 8A**). As expected, the pH of each bioreactor was decreasing during all periods by microbial acetate production (**Figure 8B**). The simultaneous and constant decrease of OD_{600} indicated reduced growth rates of *C. ljungdahlii* at a lower pH level in our system. In batch mode, the acetate production rates increased with increasing OD_{600}, but then

considerably dropped after switching to continuous mode (**Figure 8A and 8B**). The acetate production rates increased again to the highest measured average value of 73.1 ± 2.1 mmol-C L^{-1} d^{-1} for Period I (**Figure 8B**). The acetate production rates decreased to average values of 60.1 ± 3.4 mmol-C L^{-1} d^{-1}, and 53.7 ± 3.3 mmol-C L^{-1} d^{-1} for Periods II and III, respectively. For Period IV, the acetate production rate had only an average value of 29.2 ± 10.0 mmol-C L^{-1} d^{-1} (**Figure 8B**). Ethanol production rates were negligible during batch mode, but slowly increased after switching to continuous mode. The highest ethanol production rates were observed for Period II with average values of 22.5 ± 0.5 mmol-C L^{-1} d^{-1}. During the Periods III and IV, the ethanol production rates kept decreasing to average values of 18.7 ± 4.8 mmol-C L^{-1} d^{-1} and 3.4 ± 1.4 mmol-C L^{-1} d^{-1}, respectively (**Figure 8B**). The results of our preliminary experiment showed high reproducibility with small standard deviations for all tested parameters using the MBS (**Supplementary Table S2, Supplementary Figure S4**), which creates an environment to investigate the impact of different cultivation parameters simultaneously in a single system providing statistically relevant fermentation data.

Table 2 Average values for OD_{600} and acetate/ethanol production rates during the continuous fermentation of *C. ljungdahlii* with CO_2 and H_2 at four different pH conditions in standard PETC medium using the MBS.

Operating conditions	OD_{600}[1]	Acetate production rate [mmol-C L^{-1} d^{-1}] [1]	Ethanol production rate [mmol-C L^{-1} d^{-1}] [1]	$Ratio_{Et/Ac}$[2]
Period I (pH=6.0)	0.82 ± 0.04	73.1 ± 2.1	6.4 ± 1.6	0.1
Period II (pH=5.5)	0.69 ± 0.01	60.1 ± 3.4	22.5 ± 0.5	0.4
Period III (pH=5.0)	0.51 ± 0.05	53.7 ± 3.3	18.7 ± 4.8	0.3
Period IV (pH=4.5)	0.18 ± 0.06	29.2 ± 10.0	3.4 ± 1.4	0.1

[1] Values for the bioreactors with ammonium feed (n=3) are given as the average (± standard de*via*tion) from three bioreactors for the last 5 data points of every period.
[2] Et, Ethanol; Ac, Acetate.

3.5.2. Feeding nitrate to *C. ljungdahlii* in continuous operating bioreactors with H_2 and CO_2

In three main experiments with operating periods of 27.5 days (experiment 1) (**Figure 9**), and 28 days (experiment 2 and 3), we investigated the impact of nitrate as an alternative N-source on growth and the production of ethanol from CO_2 and H_2 (**Figure 10, 11**). For these experiments, the bioreactors (experiment 1, bioreactor 4/5/6; experiment 2, bioreactor 7/8; experiment 3, bioreactor 9/10) were fed with PETC medium containing nitrate instead of ammonium at an equivalent molar amount of nitrogen (=18.7 mM). We found an increasing pH due to ammonium production in preliminary bottle experiments in nitrate-containing PETC medium (**Supplementary Figure S5**). A pH increase was also observed in the nitrate bottle experiments of Emerson et al. (2019). Despite the pH-control in our experiments, all bioreactors with nitrate feed showed remarkable differences in growth, pH, acetate

production, and ethanol production rates. Therefore, we report individual data for each bioreactor and highlight lowest and highest values (**Table 3, 4**). We use the data of the preliminary experiment (ammonium, bioreactor 1/2/3) as the control in which ammonium served as the sole N-source (**Figure 8**). Unexpectedly, we observed a pH-buffering effect in experiment 1 (bioreactor 4/5/6) and experiment 2 (bioreactor 7/8) with nitrate feed during the fermentation (**Figure 9B, 10B**). This was most likely due to an interplay between the produced acetate and ammonium by the microbes. Overall, the pH was slowly decreasing in these bioreactors with nitrate feed (**Figure 9, 10, 11**), and we did not measure increasing pH values. To study this effect further, we actively reduced the pH in every pH period to the anticipated pH-value by feeding acid in experiment 3 (bioreactor 9/10).

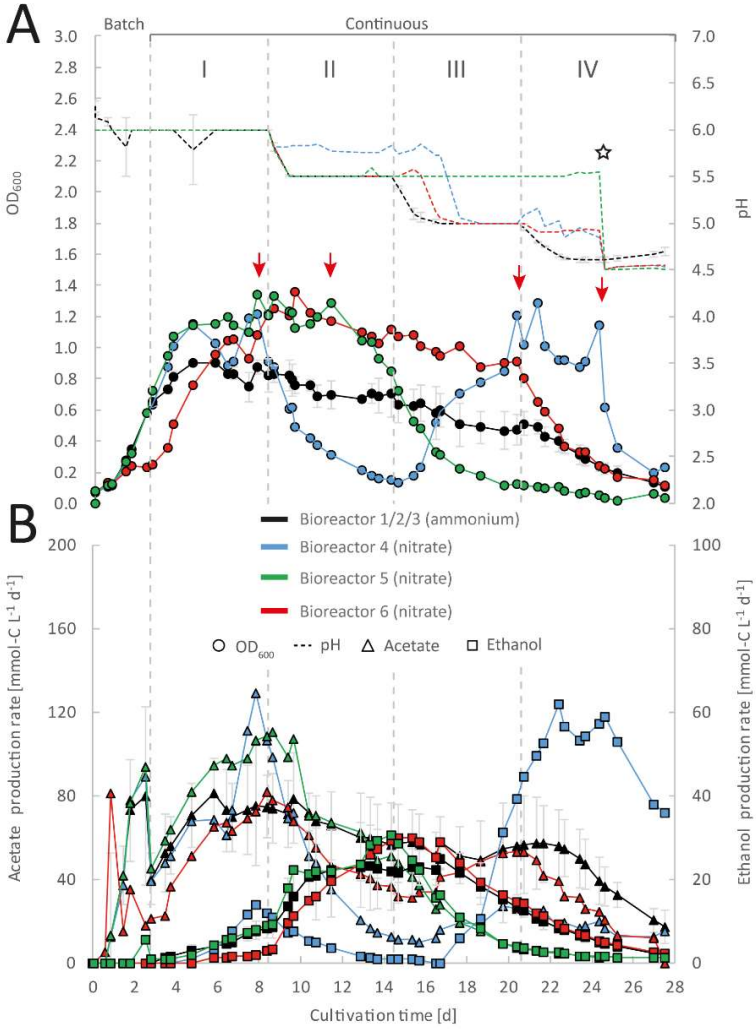

Figure 9 Impact of nitrate as an alternative N-source on continuous gas fermentation of *C. ljungdahlii* using CO_2 and H_2 at different periods with a medium feed rate of 0.10 mL min^{-1} (experiment 1). (A) Single values for pH and OD_{600}. (B) Acetate and ethanol production rates in mmol-C L^{-1} d^{-1}. The bioreactors with nitrate feed were grown in ammonium-free PETC medium supplemented with 18.7 mM Na-nitrate. The horizontal dotted lines indicate the continuous process in which medium of different pH was fed to each bioreactor. The red arrows indicate the crash in OD_{600} of each bioreactor with nitrate feed at different time points. The star symbol describes the time point where the pH was lowered manually by adding HCl to the system until a pH of 4.5 was reached. Period: I, pH = 6.0; II, pH = 5.5, III, pH = 5.0; and IV, pH = 4.5.

During the initial batch mode of all performed bioreactor experiments, growth was similar in each bioreactor and reached highest OD_{600}-values between 0.5-0.7 after 2-3 days (**Figure 8A, 9A, 10A, 11A**). In the first nitrate experiment, bioreactor 6 stagnated after two days of cultivation in batch with an OD_{600} of 0.23 (**Figure 9A**). However, after switching to continuous mode, all three nitrate bioreactors of experiment 1 (bioreactor 4/5/6) reached similar OD_{600}-values of ~1.2 during the end of Period I, which were 48% higher compared to the mean OD_{600}-value of the control bioreactors with ammonium feed and the same medium feed rate during Period I (**Table 2, 3**).

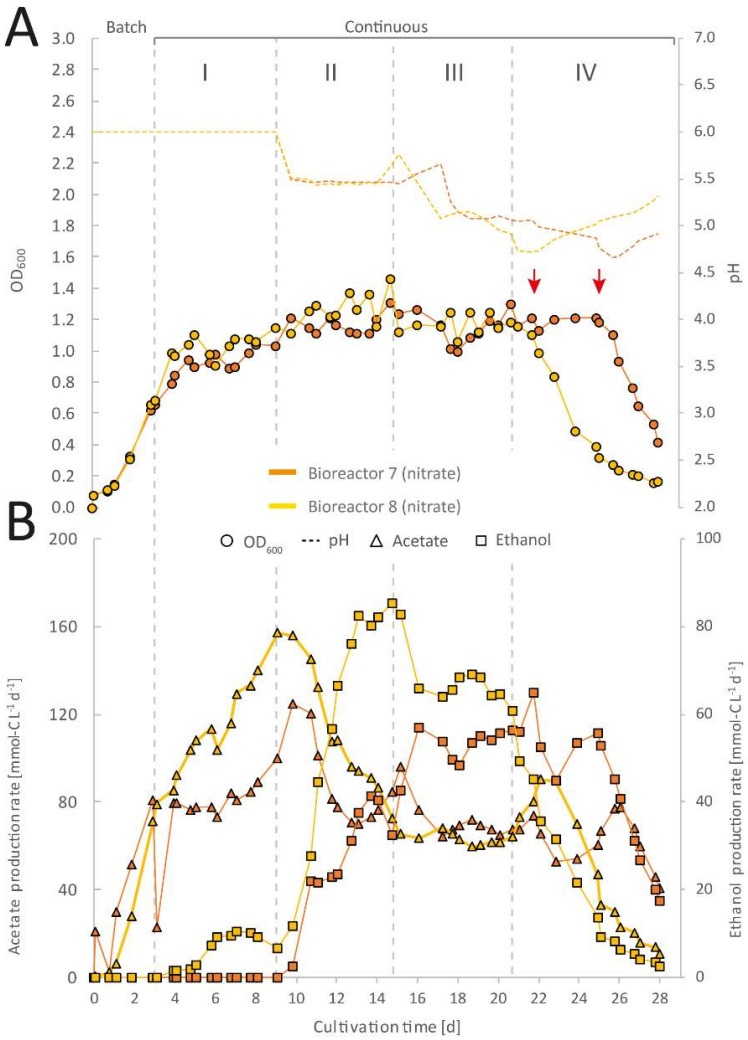

Figure 10 Impact of nitrate as an alternative N-source on continuous gas fermentation of *C. ljungdahlii* using CO_2 and H_2 at different periods with a medium feed rate of 0.19 mL min^{-1} (experiment 2). (A) Single values for pH and OD_{600}. (B) Acetate and ethanol production rates in mmol-C L^{-1} d^{-1}. The bioreactors were grown in ammonium-free PETC medium supplemented with 18.7 mM Na-nitrate. The horizontal dotted lines indicate the continuous process in which medium of different pH was fed to each bioreactor. The red arrows indicate the crash in OD_{600} of each bioreactor at different time points. Period: I, pH = 6.0; II, pH = 5.5, III, pH = 5.0; and IV, pH = 4.5.

The highest observed OD_{600} was 1.29 on day 21 during Period IV for bioreactor 4, 1.36 on day 10 during Period II for bioreactor 5, and 1.34 on day 8 during Period I for bioreactor 6 (**Figure 9A, Table 3**). In

comparison, the bioreactors with ammonium feed had the highest average OD_{600}-value of 0.90±0.02 on day 4 for Period I (**Table 2**). The increase of biomass was also observed in our second and third nitrate experiment (**Figure 10, 11**). When applying higher medium feed rates in these experiments, the highest OD_{600}-values were increased by 29-62% compared to the ammonium bioreactors (**Table 2, 4, Figure 8, 10, 11**). This indicated that the increased dilution rate did not exceed the growth rate of the microbes under our conditions. The highest OD_{600}-values for the bioreactors of experiment 2 and 3 were 1.31 for bioreactor 7 on day 15 during Period II, 1.46 for bioreactor 8 on day 15 during Period II, 1.16 for bioreactor 9 on day 15 during Period II, and 1.21 for bioreactor 10 on day 17 during Period III.

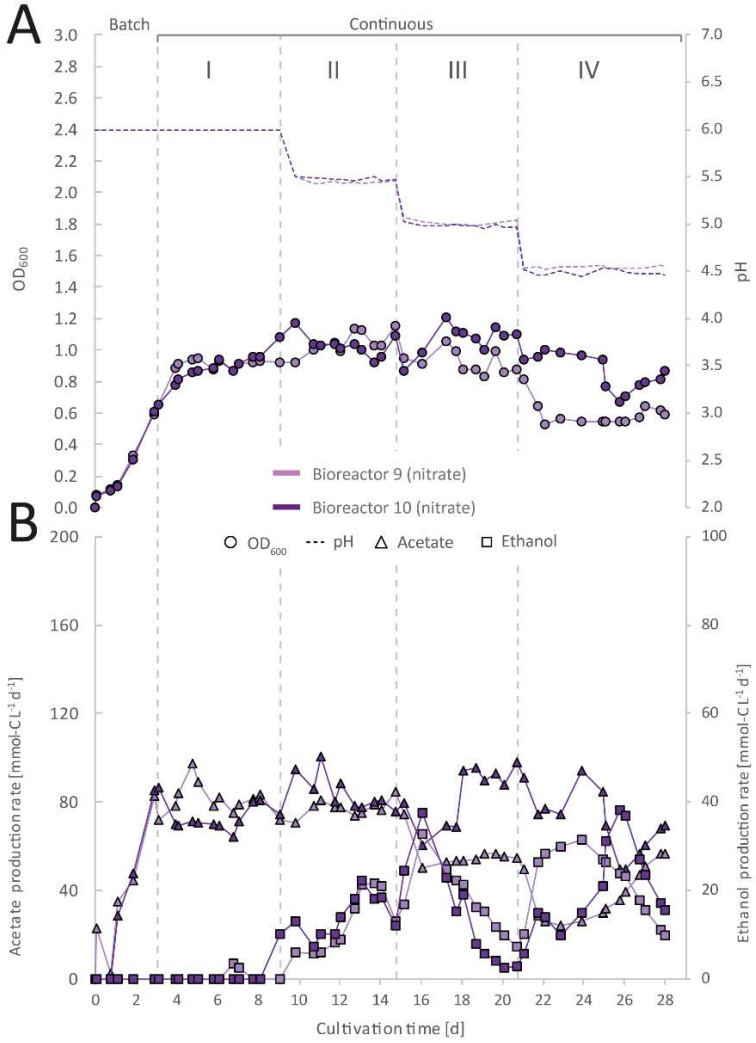

Figure 11 Impact of nitrate as an alternative N-source on continuous gas fermentation of *C. ljungdahlii* using CO_2 and H_2 at different periods with a medium feed rate of 0.19 mL min^{-1} (experiment 3). (A) Single values for pH and OD_{600} . (B) Acetate and ethanol production rates in mmol-C L^{-1} d^{-1}. The bioreactors were grown in ammonium-free PETC medium supplemented with 18.7 mM Na-nitrate. The horizontal dotted lines indicate the continuous process in which medium of different pH was fed to each bioreactor. Period: I, pH = 6.0; II, pH = 5.5, III, pH = 5.0; and IV, pH = 4.5.

A noticeable difference was that the OD_{600}-values were unstable for all bioreactors with nitrate feed (**Figure 9-11**). Instead, each nitrate bioreactor showed fluctuating OD_{600}-values of ±0.1 to ±0.3 during the experiment. This effect was not observed for the control bioreactors with ammonium feed, which showed continuously decreasing OD_{600}-values (**Figure 8A**). However, the fluctuating growth of the nitrate bioreactors was interrupted, when crash events occurred at different time points during the first and second nitrate experiment (**Figure 9, 10**). We observed these crash events in OD_{600} for bioreactor 4 on day 8 during Period I and again on day 24 during Period IV, for bioreactor 5 on day 20 during Period III, and for bioreactor 6 on day 11 at the end of Period III. The second crash event of bioreactor 4 was found after a previous phase of recovery during Period III in which the cells grew again to an OD_{600} of 1.2 on day 20 (**Figure 9A**). The recovery of growth was only observed for bioreactor 4. Crash events also occurred at the higher medium feed rates in our second nitrate experiment, but at later time points of the cultivation (**Figure 10**). Bioreactor 7 underwent a crash event on day 26 during Period IV, while bioreactor 8 crashed on day 21 during Period IV.

It is noteworthy, that we detected nitrate and nitrite in culture samples of all nitrate bioreactors undergoing a crash event, while neither nitrate nor nitrite were detectable in actively growing or recovering bioreactors with nitrate feed (**Supplementary Table S3, S4, S5, S6, S7, S8, S9**). This indicates a high uptake rate for nitrate by the microbes from the feed medium, and an immediate conversion of the nitrate to ammonium *via* nitrite as an intermediate. During our third nitrate experiment (bioreactor 9 and 10) (**Figure 11**), we neither observed crash events nor the accumulation of nitrate or nitrite in any culture sample. Nevertheless, both bioreactors showed a short duration of decreasing OD_{600}-values during Period IV, but their growth remained stable afterwards. Despite the occurrence of crash events, we found that all nitrate bioreactors showed high OD_{600}-values even at lower pH (Period II-IV) (**Table 3, 4, Figure 9, 10, 11**). In contrast, the bioreactors growing with ammonium feed, showed high OD_{600}-values only at pH 6.0, while the OD_{600} kept constantly decreasing at lower pH (**Figure 8A, Table 2**). The acetate production rates of all bioreactors with nitrate feed somewhat followed the OD_{600} profile and reached the highest values that we observed in all our experiments with a maximum value of 139 mmol-C L^{-1} d^{-1} for bioreactor 8 of experiment 2 during Period II (**Table 3, 4**). Overall, the acetate production rates were more stable during experiment 3, when the pH was actively decreased with an acid feed (**Figure 11B**). The acetate production rate considerably decreased at the time point of the OD_{600} crashes for the three bioreactors in experiment 1 and the two bioreactors in experiment 2 (**Figure 9B and 10B**).

Table 3 Highest observed values for OD_{600} and acetate/ethanol production rates at specific pH during continuous fermentation of *C. ljungdahlii* with CO_2 and H_2 in nitrate-containing medium with a feed rate of 0.10 mL min^{-1}.

Highest value for	Control[1,2]	Experiment 1[2]		
	Bioreactor 1-3 (ammonium)	Bioreactor 4 (nitrate)	Bioreactor 5 (nitrate)	Bioreactor 6 (nitrate)
OD_{600}	0.90 ± 0.02 (pH 6.0)	1.29 (pH 5.2)	1.36 (pH 5.5)	1.34 (pH 6.0)
Acetate production rate [mmol-C L^{-1} d^{-1}]	81.4 ± 3.0 (pH 6.0)	128.8 (pH 6.0)	81.5 (pH 6.0)	110.6 (pH 5.8)
Ethanol production rate [mmol-C L^{-1} d^{-1}]	25.0 ± 2.7 (pH 5.0)	62.0 (pH 5.0)	29.9 (pH 5.0)	30.6 (pH 5.5)
$Ratio_{Et/Ac}$[3]	0.4 (pH 5.5)	4.2 (pH 4.5)	1.0 (pH 5.6)	0.6 (pH 5.5)

[1] Values for the bioreactors with ammonium feed (n=3) are given as the average (± standard de*via*tion) from three bioreactors for the last 5 data points of every period.
[2] Only base was fed to maintain the pH, while a pH decrease was caused by microbial acetic acid production.
[3] Et, Ethanol; Ac, Acetate.

Ethanol production rates were negligible during batch mode for all bioreactors with nitrate feed and increased with decreasing pH during the different periods, after switching to continuous mode, and considerably dropped for each bioreactor that crashed (**Figure 9B, 10B, 11B**). In our first nitrate experiment with a medium feed rate of 0.10 mL min-1, we observed similar ethanol production rates for bioreactor 5 and 6 compared to the control experiment with ammonium feed (**Figure 9B**). The highest ethanol production rates were 30 mmol-C L^{-1} d^{-1} for bioreactor 5 on day 15 during Period III and 31 mmol-C L^{-1} d^{-1} for bioreactor 6 on day 14 during Period II. While for bioreactors 5 and 6 the ethanol production rates did not recover after the crashes, for bioreactor 4 the ethanol production rate increased with increasing OD_{600} after the crash and reached a maximum of 62 mmol-C L^{-1} d^{-1} on day 22 during Period IV. This value is ~2.5-fold higher compared to the highest ethanol production rate observed for *C. ljungdahlii* growing with ammonium (**Table 2, 3**) with the same medium feed rate of 0.10 mL min^{-1}. When we applied a higher medium feed rate of 0.19 mL min^{-1}, we found that ethanol production was strongly enhanced for bioreactor 7 and bioreactor 8 in experiment 2 (**Table 3, Figure 10**). Highest ethanol production rates were 65 mmol-C L^{-1} d^{-1} for bioreactor 7 on day 22 during Period IV and 85 mmol-C L^{-1} d^{-1} for bioreactor 8 on day 15 during Period II. On the contrary, the ethanol production rates of bioreactor 9 and bioreactor 10 in experiment 3 that operated with the same medium feed rate but with acid feed to control the pH, were lower with highest rates of 33 mmol-C L^{-1} d^{-1} for bioreactor 9 and 38 mmol-C L^{-1} d^{-1} for bioreactor 10, both on day 16 during Period III (**Table 4, Figure 11**). It should be noted that acetate production rates of bioreactor 4 remained low after the recovery, which led to the highest measured ethanol/acetate ratio of ~4.2 with CO_2 and H_2 in

this study (**Table 3**). To our knowledge it is also the highest ethanol/acetate ratio for published studies with acetogens and CO_2 and H_2, because Mock et al. (2019) achieved a ratio of ~1:1. In contrast, the acetate production rates of bioreactor 7, 8, 9, and 10 in experiment 2 and 3 were similar, even when we observed the high ethanol production rates in bioreactor 7 and 8 (**Table 4**).

Table 4 Highest observed values for OD_{600} and acetate/ethanol production rates at specific pH during continuous fermentation of *C. ljungdahlii* with CO_2 and H_2 in nitrate-containing medium with a feed rate of 0.19 mL min^{-1}.

Highest value for	Experiment 2[1]		Experiment 3[2]	
	Bioreactor 7 (nitrate)	Bioreactor 8 (nitrate)	Bioreactor 9 (nitrate)	Bioreactor 10 (nitrate)
OD_{600}	1.31 (pH 5.5)	1.46 (pH 5.6)	1.16 (pH 5.5)	1.21 (pH 5.0)
Acetate production rate [mmol-C L^{-1} d^{-1}]	124.8 (pH 5.5)	139.2 (pH 5.5)	97.4 (pH 6.0)	100.7 (pH 5.5)
Ethanol production rate [mmol-C L^{-1} d^{-1}]	65.1 (pH 5.1)	85.4 (pH 5.6)	32.6 (pH 5.0)	38.1 (pH 4.5)
$Ratio_{Et/Ac}$[3]	1.0 (pH 4.9)	1.4 (pH 5.8)	1.2 (pH 4.6)	0.8 (pH 4.5)

[1] Only base was fed to maintain the pH of the bioreactor, while a pH decrease was caused by microbial acetic acid production.
[2] Base and acid were fed to maintain the pH of the bioreactor. The pH was actively decreased to the feed medium pH when entering a new pH period.
[3] Et, Ethanol; Ac, Acetate.

We found in our first nitrate experiment with a medium feed rate of 0.10 mL min^{-1} that each bioreactor behaved differently and underwent stochastic crashes in the OD_{600} at different time points that were most likely connected to a simultaneous accumulation of nitrite (**Figure 9A**). One bioreactor recovered from this crash and showed increased ethanol production rates after the crash (**Table 3, Figure 9B**). When we increased the medium feed rate to 0.19 mL min^{-1} in experiment 2, we observed again crash events at different time points (**Figure 10A**). Interestingly, before these crashes, these bioreactors already showed increased ethanol production rates compared to experiment 1. Furthermore, we found that crash events did not occur in experiment 3 during which we actively and immediately decreased the pH to the anticipated pH-value (**Figure 11A**). However, overall ethanol production rates were lower then. It is likely that the simultaneous production of acetate from acetogenesis and ammonium from nitrate reduction creates a sensitive environment for *C. ljungdahlii*, which supports growth and production rates of ethanol through a self-buffering pH effect of the cell, but with a high instability of the system, as discussed in detail below.

3.6. Discussion

3.6.1. Our MBS resulted in reproducible gas-fermentation experiments with *C. ljungdahlii*

The MBS was successfully tested to cultivate *C. ljungdahlii* with CO_2 and H_2 under various pH conditions during four experiments (total of 10 bioreactors). The highly comparable growth behavior of the triplicate bioreactors under batch and continuous conditions in the preliminary experiment and in experiment 1, using standard medium with ammonium as the N-source (control), confirm a high stability of our MBS (**Table 1, Figure 8, Supplementary Table S2, Supplementary Figure S4**). We did observe minor differences in the ethanol and acetate production rates between replicates, which were connected to the same medium feed bottle under continuous conditions (**Figure 8, 9, 10, 11, Supplementary Table S2, S3, S4, S5, S6, S7, S8, S9**). These differences in single replicates may lead to different production rates, even in controlled bioreactors, and may result from slightly varying gassing or medium feed rates, variations in the pH control, or small but varying diffusion of oxygen into individual bioreactors. This finding clearly indicates the need for replicates during strain characterization and pre-selection in lab-scale bioreactor experiments before scaling up to larger fermentations. With our MBS, we can combine experiments at steady-state conditions for replicates, which saves time in generating statistically relevant data sets. Our future work to further optimize the MBS will target the additional integration of analytic equipment to calculate gas consumption and carbon uptake rates. We had sampled the inlet and outlet gases during all experiments, but our current setup was not adequate to obtain reliable results. Additional equipment, such as mass-flow controllers, will fill this gap and further increase the data quality during future experiments.

3.6.2. Feeding nitrate as sole N-source led to enhanced cell growth even at low pH

For our three main experiments (**Figure 9, 10, 11**), we tested the impact of nitrate as sole N-source on the growth and production rates of acetate and ethanol under pH-controlled conditions. It was recently demonstrated that *C. ljungdahlii* can use nitrate simultaneously for the generation of ammonium (assimilatory nitrate reduction) (Nagarajan *et al.*, 2013), and as an alternative electron acceptor (dissimilatory nitrate reduction) (Emerson *et al.*, 2019). This resulted in enhanced cell growth with sugars or CO_2 and H_2 in bottle experiments (Emerson *et al.*, 2019). From these findings and our own preliminary batch experiments (**Supplementary Figure S5**), we also expected enhanced cell growth in our bioreactor experiment. Our data confirmed that the use of nitrate as sole N-source is enhancing CO_2 and H_2-dependent growth of *C. ljungdahlii* by up to 62% (based on OD_{600}) in continuous mode (**Table 3, 4**, **Figure 9, 10, 11**). Emerson et al. (2019) observed 42% increased growth rates for bottle experiments with CO_2 and H_2, while the pH increased from 6.0 to 8.0. We observed a similar increase in the pH-value and a ~200% increased OD_{600} in our preliminary bottle experiments

(**Supplementary Figure S5**). All our bioreactors with nitrate feed had high OD_{600}-values even at low pH values, whereas the ammonium bioreactors showed a correlation between low pH and low OD_{600} (**Table 2, 3, 4**). We had not anticipated this uncoupling of pH and OD_{600}, because acetate production is becoming thermodynamically limited at lower pH (Richter *et al.*, 2016b). Consequently, less acetate is produced from acetyl-CoA and, in turn, less ATP is available for the Wood-Ljungdahl pathway (Schuchmann and Müller, 2014). One possible explanation for this observation is that the depleting pool of ATP at a low pH is refilled with ATP generated through the reduction of nitrate and concomitant redirection of reducing equivalents. This ATP can then be used for biomass formation.

Our data show that the highest OD_{600} in our bioreactors with nitrate feed ranged between an OD_{600} of 1.29 and 1.36 at a medium feed rate of 0.10 mL min^{-1} (**Table 3**), and an OD_{600} of 1.21 and 1.49 at a medium feed rate of 0.19 mL min^{-1} during different periods (**Table 4**). This indicates that ATP was not the limiting factor for growth for the bioreactors with nitrate feed. Thus, nitrate reduction, on the one hand, was sufficient to regenerate redox cofactors, and on the other hand, provided more ATP for biomass formation. Ethanol formation was neither observed in our bottle experiments nor in the experiments by Emerson et al. (2019). This led to the hypothesis by Emerson et al. (2019) that *C. ljungdahlii* predominantly shifts electrons into nitrate reduction rather than towards ethanol formation. Noteworthy, however, is that the generated ammonium was responsible for an increasing pH-value. Here, we demonstrated for all bioreactors with nitrate feed that ethanol production was still possible when the pH was controlled to lower values, which rejects the hypothesis by Emerson et al. (2019) (**Figure 9B, 10B, 11B**). We theorize here that ethanol formation was absent in the bottle experiments due to the increasing pH-value from ammonium production, which we were able to prevent with the bioreactors (**Supplementary Figure S5**). Again, this shows that observations with bottles should be followed up with pH-controlled bioreactors.

3.6.3. Nitrite accumulation indicated a metabolic crash of *C. ljungdahlii*

All bioreactors with nitrate feed showed different performance behavior during continuous mode (**Figure 9, 10, 11**). We observed crash events for nitrate bioreactors in which we did not force a decrease of the pH by feeding acid, but let the pH decrease by means of microbial acetate production (experiment 1 and 2) (**Figure 9, 10**). These crashes were stochastic, because they occurred at different time points of the cultivation. This was independent of the bioreactors, because we had already observed the reproducible nature of our MBS in our preliminary experiment with ammonium feed (**Figure 8, Supplementary Figure S4**). For each nitrate bioreactor that crashed, we measured an accumulation of nitrite and nitrate at the time point when the crash occurred and afterwards (**Supplementary Table S3, S4, S5, S6, S7**). Before the crashes, we were not able to detect nitrate in any

sample. Therefore, we assume that the applied nitrate feed rates of 0.11 mmol h^{-1} (18.7 mM x 0.10 mL min^{-1}) for the first nitrate experiment (bioreactor 4/5/6) and 0.21 mmol h^{-1} (18.7 mM x 0.19 mL min^{-1}) for the second and third nitrate experiment (bioreactor 7/8/9/10) was lower than the metabolic uptake rate for nitrate of *C. ljungdahlii*. However, our results indicate that an accumulation of nitrite and nitrate above a certain threshold is harmful to the microbes and leads to an abrupt halt of the metabolism for yet unknown reasons. A complete physiological characterization of the nitrate metabolism of *C. ljungdahlii*, or any other acetogen, is still missing in literature. Emerson et al. (2019) described that once the applied nitrate was depleted, the culture halted acetate production and crashed (as measured by the OD_{600}). The authors explained the crash with an abrupt end of the ATP supply, which is critical to maintain high cell densities for *C. autoethanogenum* (Valgepea *et al.*, 2017). However, the bottle cultures of Emerson et al. (2019) did not crash completely. The OD_{600} decreased by 50% but recovered after a short lag phase, indicating that the remaining CO_2 and H_2 was further consumed. An accumulation of nitrite was neither observed during the crash in these experiments nor in our own preliminary bottle experiments (**Supplementary Table S3, S4, S5, S6, S7, S8, S9, Supplementary Figure S5**). One explanation might be that the metabolic crash was triggered by an insufficient regeneration of NADH. *C. ljungdahlii* possesses two putative hydroxylamine reductases (CLJU_c22260, CLJU_c07730), which could catalyze the reduction of nitrite to ammonium with electrons from NADH (Köpke *et al.*, 2010; Nagarajan *et al.*, 2013). Since we observed simultaneous nitrite and nitrate accumulation in crashing cultures, a metabolic bottleneck at this catalytic step is possible. Another explanation might be that nitrite and/or nitrate inhibit one or several enzymes in *C. ljungdahlii*. Then, as soon as some nitrite and/or nitrate accumulated and inhibited the metabolism, a feedback loop was triggered that quickly led to a complete crash of the metabolism.

For recovering the culture, we assume that the inhibiting compounds must be washed out of the system to a certain critical threshold. In addition, some removal of the inhibiting compounds due to the recovering activity of the culture would also contribute. For bioreactor 4, we observed a constant decrease of the OD_{600} and acetate and ethanol production rates after the crash in Period I (**Figure 9, Supplementary Table 3**). However, on day 13-14 the decrease started to reach a valley, which indicates that the microbial growth was able to catch up with the dilution of our continuous process. For this bioreactor, the pH in Period II was still high enough to support sufficient growth, and after ~2 HRT periods the growth rate of the microbes exceeded the dilution rate again and the OD_{600} increased again (**Figure 9A**). The recovery of this bioreactor 4 in growth as well as in acetate and ethanol production rates indicates that: (1) the nitrate reduction pathway is not per se inhibited at low pH; and (2) the reduction of nitrate and the production of ethanol is possible simultaneously, and that most likely the low pH triggers a thermodynamic shift towards ethanol production (Richter *et al.*,

2016b). However, it remains elusive why the ethanol/acetate ratio in bioreactor 4 reached a nearly ten-fold higher value after recovering from the crash in the presence of nitrate compared to the bioreactors with ammonium feed (**Figure 8B, 9B**). Importantly, applying a higher feed rate and similar cultivation conditions with another set of bioreactors in experiment 2 reached only a maximum ethanol/acetate ratio of 1.4 (**Table 4**). In contrast, the crash occurred for bioreactor 5 in Period II. While the OD_{600} immediately decreased after the crash, the acetate and ethanol production rates remained somewhat constant until the switch to Period III. However, this bioreactor never recovered from the crash in terms of OD_{600}. We believe that the lower pH levels during Period III for bioreactor 5 prevented the growth recovery, which for bioreactor 4 took place at the higher pH level of Period II. We had found reduced growth conditions for bioreactors with ammonium at the lower pH levels, indicating that the growth rate is constantly decreasing while decreasing the medium pH (**Table 2, Figure 8, Supplementary Figure S4**). The same findings hold true for bioreactor 6 for which the crash occurred even later in the cultivation. When we applied the 90% higher medium feed rate but kept the same pH maintenance conditions for bioreactor 7 and bioreactor 8 in experiment 2, single crash events still occurred, but at later time points (**Figure 10**).

What could be the reason for the stochastic crashes? Valgepea et al. (2017) discussed occurring "crash and recover cycles" during syngas fermentation with *C. autoethanogenum*. They hypothesized that the WLP becomes the limiting factor during a period of ample supply of acetyl-CoA at higher biomass and acetate concentration. This can result in an insufficient supply of reducing equivalents due to a loss of H_2 uptake when the WLP cannot keep up anymore. Consequently, the cells are not able to deliver the ATP demand, resulting in a crash. The cells recovered once the extracellular acetate concentration went below a certain threshold but crashed again after exceeding the threshold. Unfortunately, these threshold acetate concentrations were not given.

We observed higher acetate production rates for bioreactor 4 and 6 before the crash, compared to those of the bioreactors with ammonium feed (**Figure 8B, 9B**). Bioreactor 5 did not reach a similarly high acetate concentration, but the crash occurred at the beginning of Period IV at the lower pH of 4.5. Intrinsically, the extracellular acetate concentration would be higher as a key to trigger the crash event. We assume a similar correlation for bioreactor 7 and bioreactor 8, which had a similar acetate production rate compared to bioreactor 5 at the time point of the crash event (**Figure 9B**).

3.6.4. A sensitive pH-environment based on an interplay between undissociated acetic acid and ammonium increased growth and ethanol production rates

To further tackle the question of why we observed the crash events, we applied active pH maintenance with base and acid feed in our third experiment (bioreactor 9 and 10) (**Figure 11**). This immediate

adjustment of the pH environment influenced growth, and acetate and ethanol production rates. At a pH of 5.5 (Period II), it caused stagnation of growth and acetate production rates, while simultaneously ethanol production started to increase. In contrast, the slow decrease of the pH in Period II due to microbial acetic acid production in bioreactor 7 and 8 accelerated ethanol production by 2-4-fold and biomass production by 11-28% compared to bioreactor 9 and 10, while acetate production first increased, but then quickly decreased (**Figure 10**). We believe that nitrate-reducing cells of *C. ljungdahlii* generate a sensitive pH-environment based on the buffering effect of the interplay between undissociated acetic acid production and ammonium production. This enables a more efficient pH balance and electron flow towards biomass production, and more reduced fermentation products, such as ethanol, but at the cost of a highly unstable environment. Small perturbations to the system seem to lead to a severe disbalance and immediate crash of the microbial growth. By feeding acid to actively lower the pH, this highly unstable environment can be controlled better, but at the cost of lower biomass and ethanol production rates. Without actively decreasing the pH with acid feed, the pH-environment remains sensitive to external influences. This could also explain the partly increasing pH-values during periods of higher (unbalanced) ammonium production with respect to acetate production. By a detailed look into literature and to the best of our knowledge there is no study that describes a similar pH effect for an acetogen. Our experiments showed highest ethanol production rates for nitrate-reducing cultures of *C. ljungdahlii* at pH 5.6 under fully controlled pH conditions. This indicates that optimum production conditions exist, and it will be of particular interest to maintain the bioreactors at this pH for longer cultivation times in future experiments (**Table 3, 4**).

In conclusion, nitrate reduction offers a great potential to further optimize gas fermentation of *C. ljungdahlii*. Because ATP limitation is one of the highest burdens to overcome for acetogens (Schuchmann and Müller, 2014; Molitor *et al.*, 2017), the surplus of ATP derived from nitrate reduction could be used to extent the product portfolio towards energy-intense products (Emerson *et al.*, 2019). However, our work clearly demonstrates that nitrate metabolism of *C. ljungdahlii* needs further investigation on both a physiological and a bioprocessing level. The stochastic metabolic crashes demonstrate the importance of replicated bioreactor experiments in the field of acetogen research.

3.7. Acknowledgment

This work was funded through the Alexander von Humboldt Foundation in the framework of the Alexander von Humboldt Professorship, which was awarded to LA. We are also thankful for additional funding to LA and BM from the Deutsche Forschungsgemeinschaft (DFG, German Research Foundation) under Germany's Excellence Strategy – EXC 2124 – 390838134. Finally, we acknowledge support by the DFG and Open Access Publishing Fund of University of Tübingen.

3.8. Supporting information

Supporting information is provided in the Appendix (**8.1.**) and contains ten supplementary tables and five supplementary figures. In addition, it provides further information about the concept and design of the MBS. The supplementary tables summarize all measured cultivation parameters and metabolites during each bioreactor experiment.

CHAPTER 4

REPROGRAMMING ACETOGENIC BACTERIA WITH CRISPR-TARGETED BASE EDITING *VIA* DEAMINATION

4.1. Author's contribution

Peng-Fei Xia (P.F.X.) designed the experiments, performed all genetic engineering, and evaluated the data. Isabella Casini (I.C.) performed the computational work. Christian-Marco Klask (C.M.K.) designed the heterotrophic and autotrophic cultivation experiments. C.M.K. conducted the heterotrophic cultivation experiments, while Sarah Schulz (S.S.) conducted the autotrophic cultivation experiments. C.K. and S.S. analyzed the culture samples and pre-evaluated the cultivation experiment data. Largus T. Angenent (L.T.A.) and Bastian Molitor (B.M.) supervised the work. P.F.X. and B.M. wrote the manuscript. All authors edited and revised the written text before submission.

4.2. Abstract

Acetogenic bacteria are rising in popularity as chassis microbes for biotechnology due to their capability of converting inorganic one-carbon (C1) gases to organic chemicals. To fully uncover the potential of acetogenic bacteria, synthetic biology tools are imperative to either engineer designed functions or to interrogate the physiology. Here, we report a genome-editing tool at a one-nucleotide resolution, namely base editing, for acetogenic bacteria based on CRISPR-targeted deamination. This tool combines nuclease deactivated Cas9 with activation-induced cytidine deaminase to enable cytosine-to-thymine substitution without DNA cleavage, homology-directed repair, and donor DNA, which are generally the bottlenecks for applying conventional CRISPR-Cas systems in bacteria. We designed and validated a modularized base-editing tool in the model acetogenic bacterium *C. ljungdahlii*. The editing principles were investigated, and an in-silico analysis revealed the capability of base editing across the genome and the potential for off-target events. Moreover, genes related to acetate and ethanol production were disrupted individually by installing premature STOP codons to reprogram carbon flux toward improved acetate production. This resulted in engineered *C. ljungdahlii* strains with the desired phenotypes and stable genotypes. Our base-editing tool promotes the

application and research in acetogenic bacteria and provides a blueprint to upgrade CRISPR-Cas-based genome editing in bacteria in general.

4.3. Introduction

Global climate change is challenging the future of human societies, resulting in the need for a sustainable food supply and greener synthesis of fuels and chemicals. One possible solution is by applying biotechnology to convert inorganic one-carbon (C1) gases, such as CO_2 and CO, into protein, biofuels, and commodity chemicals (Köpke *et al.*, 2010; Ueki *et al.*, 2014; Richter *et al.*, 2016b; Molitor *et al.*, 2019). Both gases are already available in large quantities, including in synthesis gas (syngas) and industrial waste gases (Molitor *et al.*, 2016b). Many studies have found that the model acetogenic bacterium *C. ljungdahlii* can convert these gases with hydrogen gas (H_2) into mainly acetate and ethanol *via* the WLP (Köpke *et al.*, 2010; Müller, 2019). LanzaTech, Inc. (Skokie, IL, USA) has already completed the industrial scale-up by utilizing a closely related acetogenic bacterium (*C. autoethanogenum*). However, synthetic biology and metabolic engineering are imperative to improve the productivity further and to expand the product spectrum (Köpke *et al.*, 2010; Leang *et al.*, 2013; Banerjee *et al.*, 2014; Ueki *et al.*, 2014). Currently, the lack of efficient genome-editing tools delays the progress at the molecular level to optimize acetogenic bacteria for biotechnology.

Clustered regularly interspaced short palindromic repeats (CRISPR)-Cas-based genome editing is a RNA programmable, precise, and robust approach for gene perturbation, and has been applied in a plethora of living organisms (Knott and Doudna, 2018), revolutionizing science. Recently, CRISPR-Cas systems were also adapted to be functional in acetogenic bacteria for gene deletion, insertion, and regulation. To date, different CRISPR-Cas systems (*e.g.*, Cas9 and Cas12a) have been established in *C. ljungdahlii* (Huang *et al.*, 2016; Huang *et al.*, 2019; Zhao *et al.*, 2019), *Eubacterium* limosum (Shin *et al.*, 2019), and *C. autoethanogenum* (Nagaraju *et al.*, 2016b). For these systems, first, the Cas protein (*e.g.*, Cas9 from *Streptococcus pyogenes*) is targeted to a highly specific site on the genome by a guide RNA (gRNA). Then, the Cas protein cleaves the genomic DNA at this site and introduces a double-strand break. To survive, the cell has to repair the double-strand break through DNA repairing mechanisms such as homology-directed repair or nonhomologous end joining (Selle and Barrangou, 2015). For homology-directed repair, a donor DNA has to be provided as a template, which has to contain homologies to the genome on both sides of the double-strand break. Depending on the design of the donor DNA, it is possible to generate a variety of desired mutations such as point mutations, gene deletions, and gene insertions. The homology directed repair of the double-strand break results in genome editing at the target site without leaving a selective marker (*i.e.*, antibiotic resistance gene) and scar.

However, CRISPR-Cas-based genome editing is generally challenging in bacteria, because the Cas nuclease is often toxic to bacteria, and bacteria typically lack efficient homology-directed repair or nonhomologous end joining machineries to repair the double-strand break (Vento *et al.*, 2019). Therefore, it is essential that a sufficient number of cells receive the CRISPR-Cas system to ensure that enough cells survive a DNA cleavage by undergoing the inefficient homology-directed repair process with donor DNAs (Selle and Barrangou, 2015). This renders the CRISPR-Cas system even more difficult for acetogenic bacteria, which are typically recalcitrant to receiving foreign DNA (Huang *et al.*, 2016; Molitor *et al.*, 2016a; Zhao *et al.*, 2019). Consequently, the process of cleavage-and-repairing, which is typically considered the important advantage of conventional CRISPR-Cas systems, becomes a bottleneck to perform CRISPR-Cas-based genome editing in acetogenic bacteria. Lately, a new CRISPR-Cas-based genome-editing tool, namely base editing, was developed by combining a CRISPR-Cas system with a deamination system to achieve genome editing at a one-nucleotide resolution without the necessity for DNA cleavage, homology-directed repair, and donor DNA (Komor *et al.*, 2016; Nishida *et al.*, 2016; Gaudelli *et al.*, 2017; Rees and Liu, 2018). By creating a fusion of a nuclease impaired Cas protein (*i.e.*, nuclease deactivated Cas9, dCas9) and a deaminase, this tool generates cytosine (C) to thymine (T) substitutions with cytidine deaminase (**Figure 12A**), or adenine (A) to guanine (G) substitutions with adenosine deaminase (Rees and Liu, 2018; Molla and Yang, 2019). Base editing provides distinctive advantages for genome editing in acetogenic bacteria by circumventing the bottlenecks of conventional CRISPR-Cas systems in bacteria. One such advantage is that the required DNA-uptake ability of acetogenic bacteria is minimized. Despite a few principal demonstrations in other bacteria (Banno *et al.*, 2018; Chen *et al.*, 2018; Gu *et al.*, 2018; Wang *et al.*, 2018; Li *et al.*, 2019; Tong *et al.*, 2019), the potential of base editing in acetogenic bacteria has not yet been unraveled.

Here, we developed a modularized base-editing tool for acetogenic bacteria by coupling dCas9 from *S. pyogenes* with activation-induced cytidine deaminase from the sea lamprey *Petromyzon marinus* (Banno *et al.*, 2018). Efficient base editing was validated, and the editing principles were investigated in the model acetogenic bacterium *C. ljungdahlii*. Genome-scale *in-silico* analysis revealed the capability of our base-editing tool and the potential for off-target events. As a first application, we employed base editing to reprogram the distribution of the carbon flux from acetyl-CoA to acetate and ethanol during heterotrophic and autotrophic fermentation, linking designed single-nucleotide variations with industrially relevant bacteria. Our base-editing tool will promote the research and application of C1 utilization with acetogenic bacteria, and more generally, provides an example for upgrading CRISPR-Cas-based genome-editing tools in bacteria.

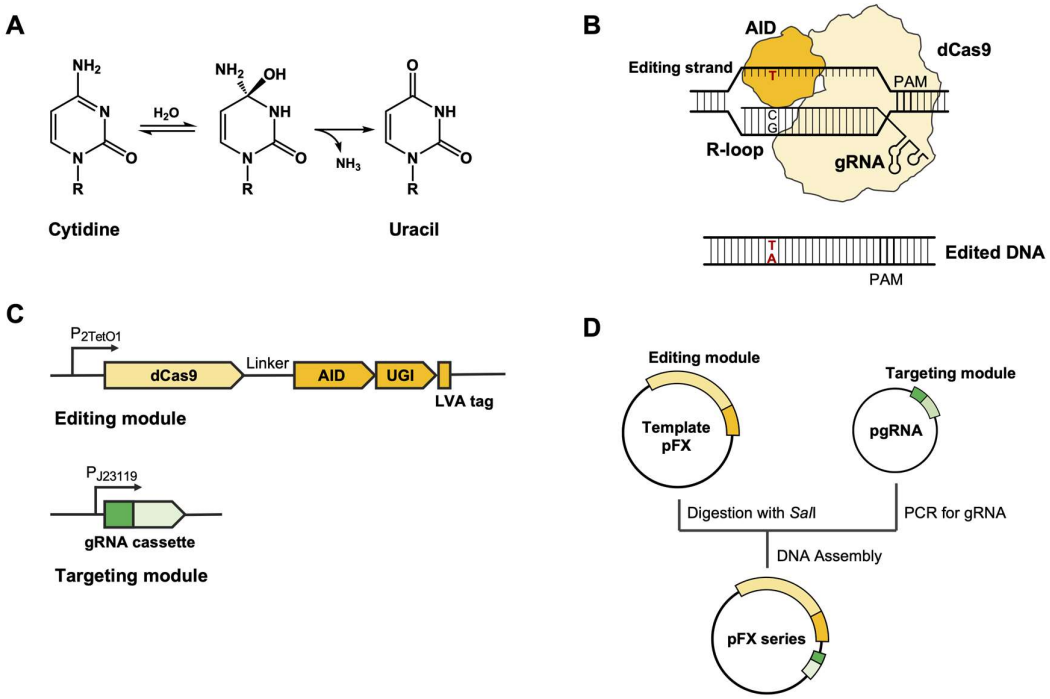

Figure 12 Design of base-editing tool in *C. ljungdahlii*. (A) Chemistry of deamination process converting cytidine to uracil. (B) Mechanism of base editing. Targeted by a gRNA, dCas9 binds to the target DNA and forms an R-loop. Activation-induced cytosine deaminase deaminates the Cs in the single strand DNA in the R-loop (Editing strand), resulting in C-to-T single-nucleotide variations in the genome. (C) The editing module consists of dCas9, activation-induced cytosine deaminase, uracil glycosylase inhibitor, and Leu-Val-Ala tag under the control of an inducible *tetR*-P_{tet} system, and the targeting module contains the gRNA cassette under the control of the constitutive P_{J23119} promoter. (D) Modularized strategy to generate editing plasmid series. To generate an editing plasmid, an inverse PCR is employed to generate the gRNA using pgRNA as a template. Template pFX plasmid is digested with SalI and then assembled with the amplified gRNA cassette, resulting in the editing plasmid (pFX series). (PAM: protospacer adjacent motif; AID: activation-induced cytosine deaminase; UGI: uracil glycosylase inhibitor; and LVA tag: Leu-Val-Ala tag.)

4.4. Material and Methods

4.4.1. Strains and Media

C. ljungdahlii DSM13528 was used as the wild-type strain, and all *C. ljungdahlii* strains that were used in this study are listed in **Supplementary Table S11**. Reinforced clostridial medium (RCM) was employed for general cultivation of *C. ljungdahlii* (Molitor *et al.*, 2016a). Modified PETC medium (ATCC 1754 medium) was used for fermentation experiments with 2 g/L (10 mM) of MES buffering the medium instead of $NaHCO_3$. For heterotrophic fermentation, 5 g/L (27.8 mM) of fructose were added in 250-mL serum bottles with 100 mL of medium as the carbon source. For autotrophic fermentation, an H_2/CO_2 mixture (80/20 vol-%, 1.5 bar) was added to the headspace of 1-L cultivation bottles (Pressure plus Duran bottle, VWR) with 100 mL of medium. The headspace was refilled to 1.5 bar every 24 h during fermentation. Clarithromycin (5 µg/L) was added when necessary. The manipulation of *C. ljungdahlii* was performed in an anaerobic chamber (UNILab Pro Eco, MBraun) with an O_2 level below 10 ppm. The cultivation was performed at 37°C. *E. coli* TOP10 (Invitrogen) was used for general

cloning and gene manipulation. *E. coli* was cultivated in Luria-Bertani (LB) medium. Ampicillin (100 µg/L), spectinomycin (60 µg/L), and erythromycin (400 µg/L on plates and 250 µg/L for liquid medium) were used to select and maintain plasmids in *E. coli*.

4.4.2. Plasmid construction

The plasmids used in this study are summarized in **Supplemental Table S12**. pMTLdCas9 was a generous gift from Gregory Stephanopoulos (Woolston *et al.*, 2018), pTargetF (Addgene plasmid # 62226) was a gift from Sheng Yang (Jiang *et al.*, 2015), and pScI_dCas-CDA-UL (Addgene plasmid # 108551) was a gift from Akihiko Kondo (Banno *et al.*, 2018). The pFX template was constructed by flanking the fragment consisting of activation-induced cytidine deaminase, uracil glycosylase inhibitor, and Leu-Val-Ala tag from pScI_dCas-CDA-UL with dCas9 on pMTLdCas9. The pgRNA01 plasmid was generated *via* inverse PCR using pTargetF as a template to recover the original P_{J23119} promoter and create the gRNA01 cassette, generating pgRNA01 (**Supplementary Figure S6**). Then, the pgRNA plasmid series containing the designed gRNA cassettes were constructed *via* inverse PCR using pgRNA01 as a template. Based on the pFX and pgRNA plasmid series, a modularized method was employed to construct the pFX plasmid series for base editing. First, the pFX template was digested with *Sal*I and the gRNA cassette was amplified by primers EBT-PFX-88 and -89. Second, the pFX plasmid series was generated by combining these two parts *via* Gibson assembly (New England labs, NEB) (**Figure 12B**). Plasmids were methylated *via* co-transformation with pANA1, which carries Φ3tI methyltransferase before transformation of *C. ljungdahlii* with the respective plasmid (Molitor *et al.*, 2016a). PCRs were performed using Q5 polymerase (New England Biolabs). The primers (Integrated DNA Technologies) for plasmid construction are summarized in **Supplemental Table S13**.

4.4.3. Transformation of *C. ljungdahlii*

Transformation of *C. ljungdahlii* was following a modified protocol previously established (Molitor *et al.*, 2016a). Briefly, RCM was inoculated and transferred twice with *C. ljungdahlii* at a 1:100 dilution. When the OD_{600} in the second culture reached 0.2 - 0.4, 12 - 16 mL of culture were harvested by stepwise centrifugation at 10,000 rpm for 1.5 min (mySPIN™ 12 Centrifuge, Thermo Fisher Scientific). The cells were then washed with ice-cold glycerol (10 vol-%) for three times and resuspended in 200 µL of 10 vol-% glycerol as electrocompetent cells. The methylated plasmids (2 µg) were mixed with the competent cells individually for electroporation (Micropulse system, 2.5 kV, 600 Ω and 25 µF, Bio-Rad) in 2-mm cuvettes. After electroporation, the cells were immediately transferred to pre-warmed RCM for a 12 - 18 h recovery. Subsequently, RCM medium with 5 µg/L of clarithromycin was inoculated with the cells, and the outgrowth cultures were used directly for base editing.

4.4.4. Base editing in *C. ljungdahlii*

The methylated pFX plasmid was transformed into *C. ljungdahlii* according to the protocol above. After electroporation, fresh RCM with 5 µg/L of clarithromycin and 100 ng/mL of anhydrotetracycline was inoculated (1:10 dilution) with the outgrowth culture (RCM with clarithromycin) in a Hungate-type culture tube and incubated for 18 - 24 h to induce base editing. After the induction, the culture was mixed with molten RCM agar (1.0 weight-%) with clarithromycin and poured into petri dishes. Single colonies were picked for further analysis. First, a colony PCR was conducted using Phire Plant Direct PCR Master Mix (Thermo Fisher Scientific) to amplify the fragment containing the target DNA sequence. Second, the fragment was sequenced to verify the single-nucleotide variations. Primers for amplifying the edited DNA fragments and sequencing are listed in **Supplemental Table S14**.

4.4.5. Plasmid curing

To cure the cells from the plasmid, a colony with the designed single-nucleotide variations was used to re-inoculate fresh RCM without clarithromycin and transferred for a second time. The second culture was poured with RCM agar (1.0 weight-%) at different dilutions. Subsequently, single colonies were picked to determine the loss of plasmids using colony PCR. If the colony PCR showed no PCR signal, the colony was further tested in RCM and RCM with clarithromycin to identify the curation from the plasmid. A colony that: 1) carries the designed single-nucleotide variations; 2) has no PCR signal for the editing plasmid; and 3) fails to grow in selective medium, was regarded as an edited strain for subsequent stability evaluation and fermentation experiments.

4.4.6. Serial transfer experiments

To test the stability of single-nucleotide variations in the edited strains, the obtained QX3, QX4, QX5, and QX6 strains were used to inoculate RCM from single colonies and transferred into fresh RCM at a 1:100 dilution after the OD_{600} reached late exponential or stationary phase (OD_{600} 1.3 to 2.0). The single-nucleotide variations were tested after each transfer and the sequencing results after the 10^{th} transfer are shown as a demonstration of the stability. The number of generations (n) was calculated by the following equation:

$$n = \frac{\log (OD_t) - \log(OD_0)}{\log 2}$$

where OD_t is the OD_{600} before each transfer and OD_0 is the initial OD_{600} after each transfer. The total number of generations is the sum of the generation numbers of each transfer.

4.4.7. Fermentation experiments

Fresh PETC medium was inoculated with *C. ljungdahlii* strains (from RCM cultures) and adapted to this medium in two transfers. Cells from the second preculture were harvested at late exponential phase and washed before inoculation. For heterotrophic fermentation, the wild-type, QX3, and QX4 strains were tested, and for autotrophic fermentation, the wild-type, QX5, and QX6 strains were tested. For all experiments, the initial OD_{600} was adjusted to 0.1 and samples were taken at different time intervals to analyze the growth and products. The fermentation products, including acetate, ethanol, and the substrate fructose, were measured using HPLC (LC20, Shimazu, Japan) with a RID detector and Aminex HPX-87H column (oven temperature 65°C) using 5 mM H_2SO_4 as elution solvent (0.6 mL/min).

The acetate and ethanol yields in the heterotrophic fermentations were calculated as following:

$$\text{Yield (mol/mol)} = \frac{C_{Acetate/Ethanol,t}}{C_{Fructose,0} - C_{Fructose,t}}$$

Where $C_{Acetate/Ethanol,t}$ is the concentration of acetate or ethanol at 107.50 h; $C_{Fructose,0}$ is the concentration of fructose at time 0; and $C_{Fructose,t}$ is the concentration of fructose at 107.50 h.

For autotrophic fermentation, the consumed CO_2 was first calculated by adding up the carbon in biomass ($C_5H_8O_2N$), acetate, and ethanol. 100 mL of a *C. ljungdahlii* culture with an OD_{600} of 1.0 equals 24.4 mg of biomass in dry cell weight (Klask *et al.*, 2020), which corresponds to 0.214 mmol of carbon. Then the yield was calculated by:

$$\text{Yield (mol/mol)} = \frac{C_{Acetate/Ethanol,t}}{\text{consumed } CO_2 \text{ per culture volume}}$$

Where $C_{Acetate/Ethanol,t}$ is the concentration of acetate or ethanol at 137.75 h.

4.4.8. Genome-scale algorithm design

We developed an algorithm to identify all editable sites at genome-scale to identify possible single-nucleotide variations and mutations at translation level. The algorithm was coded in Python (Pycharm 2018.1 with a virtual environment), and the commented scripts and necessary files have been uploaded to GitHub (https://github.com/isacasini/SNV_Xia_et_al_2020). In brief, the algorithm first reads the genomic DNA of *C. ljungdahlii* (NCBI GenBank, Access No. CP001666.1), as well as an additional file with the necessary genomic information (*i.e.*, NCBI identifier, NCBI annotations, *etc.*), and it identifies all protospacers by locating the protospacer adjacent motifs (nucleotides NGG) as potential editable sites. According to the editing principles of our base editing system, the algorithm finds Cs in the identified protospacers between position -11 and -19. If a C (or several Cs) is found, it considers the site as an editable site and changes C to T, returning the single-nucleotide variations. If

the editable site is located in a coding region, the algorithm also returns the resulting changes in amino acid. Additionally, the algorithm returns information about premature STOP codons in the first 70% of a gene. Another analysis based on the hot-spot editing window (position -16 to -19) was also conducted by adjusting the parameters of the algorithm. All editable sites and analysis are summarized in the Datasets and **Supplemental Table S15**.

4.4.9. Off-target event evaluation

Off-target events are a major concern of CRISPR-Cas-based genome editing tools, including base editing. We calculated the number of potential off-target sites by the following equations (Banno *et al.*, 2018):

$$\text{Correction factor} = 1 - 0.88^4$$

$$\text{Appearance rate} = \frac{D!}{4^m \times m! \times (D-m)!} \times \frac{1}{4^N} \times \frac{1}{4^2} \times \text{Correction factor}$$

$$\text{Potential off-target sites} = \text{Genome size} \times \text{Appearance rate} \times 2$$

Where D is the number of distal nucleotides, m is the number of matched nucleotides in distal sites, N is the number of nucleotides that should be identical to the target sequence. The correction factor indicates the probability of at least one C being located in the hot-spot editing window, which is determined under the assumption that most likely only Cs in the hot-spot editing window (position -16 to -19) can be edited by our base-editing tool, and by the A-T content (77%) of *C. ljungdahlii*. For the current design, we set D to 12, m to 5, and N to 8.28. The genome size of *C. ljungdahlii* is 4.63 Mb.

4.5. Results

4.5.1. Design of a modularized base-editing tool for *C. ljungdahlii*

For our base-editing tool, we constructed a fusion of a dCas9 with an activation-induced cytidine deaminase. We selected the dCas9 (D10A and H840A) from *S. pyogenes* and combined it with the activation-induced cytidine deaminase from *P. marinus* to minimize the toxicity of the Cas nuclease and to obtain promising deamination performance (Banno *et al.*, 2018). The dCas9, together with a gRNA, serves as a navigator to target a specific DNA sequence (a protospacer), which has to be located next to a protospacer adjacent motif (PAM), on the genome. When binding to the target an R-loop is formed (**Figure 12B**). Cytidine deaminase then converts cytidine to uracil *via* a deamination process (**Figure 12A**). In the following replication or repair of the DNA, the cell reads uridine as T, which results in a C-to-T single nucleotide variation (Banno *et al.*, 2018). The deamination occurs on the single-strand DNA (editing strand) in the R-loop and changes C to T in a defined editing window (**Figure 12B**) (Banno *et al.*, 2018; Rees and Liu, 2018). Based on previous reports, an uracil glycosylase inhibitor was fused

to an activation-induced cytidine deaminase to increase the editing efficiency and to prevent the excision of uracil on the editing strand. Furthermore, a fusion to a Leu-Val-Ala protein degradation tag was added, which has been reported to lead to an overall lower amount of the fusion protein in the cell, to minimize the potential toxicity of dCas9 and uracil glycosylase inhibitor (Banno *et al.*, 2018). We used a loose linker of 363 bp (121 amino acids) for our base-editing tool to expand the editing window and increase the editing efficiency (Banno *et al.*, 2018; Tan *et al.*, 2019). Finally, we employed a tetracycline repressor-promoter (*tetR*-P_{tet}) system, which is inducible with anhydrotetracycline in *C. ljungdahlii*, for the regulated expression of our base-editing tool (**Figure 12C**) (Woolston *et al.*, 2018).

To introduce our base-editing tool to *C. ljungdahlii*, we designed a modularized plasmid system, which contains: (1) a template plasmid (pFX) that carries the editing module, consisting of dCas9, activation-induced cytidine deaminase, uracil glycosylase inhibitor, and Leu-Val-Ala tag under the control of the inducible *tetR*-P_{tet} system; and (2) a helper plasmid (pgRNA01) for the streamlined generation of the targeting modules (gRNAs, **Figure 12C**). This modularization allows the use of inverse PCR on the helper plasmid to exchange the protospacer in the gRNA for a specific genome target site. The protospacer is driven by the P_{J23119} promoter and is flanked with the *S. pyogenes* Cas9 scaffold to form the new targeting module (**Supplementary Figure S6**). Afterward, the targeting module can be assembled with the pFX plasmid, creating the editing plasmid (**Figure 12D**). Finally, *C. ljungdahlii* can be transformed with the methylated editing plasmids to mediate base editing.

4.5.2. Validation of base-editing in *C. ljungdahlii*

To validate our system, *pta* (CLJU_c12770) from *C. ljungdahlii*, which codes for the phosphotransacetylase, was selected as a first target (**Figure 13, Supplementary Table S15**). We discovered efficient conversion from C to T on the editing strand, leading to a G-to-A single-nucleotide variation in the coding strand (**Figure 13A, B**). In total, 45 colonies from 5 individual rounds of base editing were picked to analyze the frequency and editing window (**Supplementary Table S16**). Three clean editing patterns were identified (**Figure 13B**). The highest editing frequency was found for position −16 of the protospacer in all three patterns (counting the site adjacent to the protospacer adjacent motif as position −1). Twelve out of 45 colonies showed a single mutation at this position −16, 12 colonies showed double mutations at positions −16 and −17, and 1 colony showed a double mutation at positions −12 and −16 (**Figure 13B**). We also identified 2 colonies with mutations at position −11 (**Figure 13B**) and −2 (**Supplementary Figure S7**), respectively, while the latter one (position −2) was a colony with mixed signals at position −17 (**Supplementary Figure S7**). Importantly, this finding did not considerably influence the chance to select colonies with the desired single-nucleotide variations in only one round of selection.

We further interrogated the editing principles of the base-editing tool. First, we targeted another site in *pta* (**Supplementary Table S15**). In this case, only 1 out of 8 colonies was found to be edited at position −7 (**Supplementary Figure S8A**), which suggests a lower editing efficiency at position −7. Accordingly, although editing is possible in a wide editing window, the editing efficiency of our base-editing tool might be lower between position −2 to −11. Second, our base-editing tool converts C to T on the editing strand, which indicates that it only deaminates C(s) in the protospacer (Nishida *et al.*, 2016; Banno *et al.*, 2018; Rees and Liu, 2018). Therefore, we designed two gRNAs with no Cs in the protospacers (**Supplementary Table S15**) to examine the base-editing mechanism further, because we hypothesized that in this case no base editing would occur. Importantly, this experiment can hardly be done in non-A-T-rich bacteria in which protospacers without a C are much less abundant. As anticipated, we did not observe single-nucleotide variations in any colony (**Supplementary Figure S8B**). Third, others have demonstrated that activation-induced cytidine deaminase-mediated base editing showed a hot-spot editing window of five nucleotides starting from the opposite end of the protospacer adjacent motif, and that the window shifts depending on the length of protospacers (Banno *et al.*, 2018; Rees and Liu, 2018).

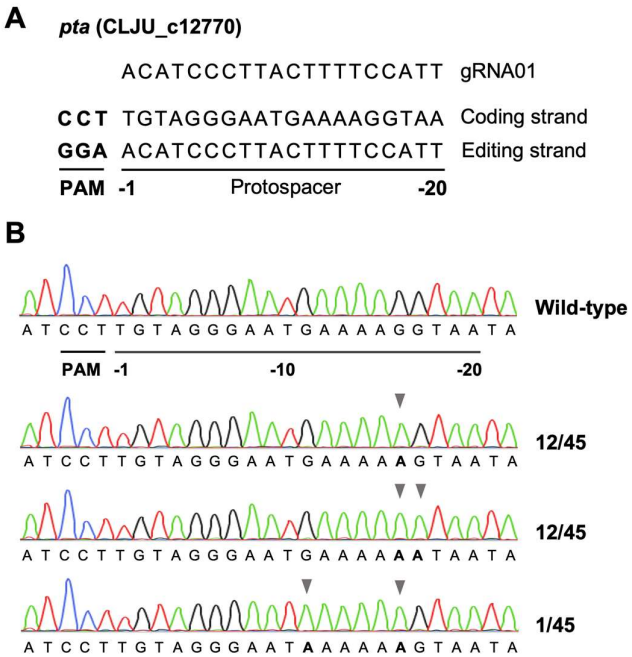

Figure 13 Design and validation of base editing on *pta* by gRNA01. (A) Genome sequence of editing location. The gRNA01 is complementary to the coding strand, while deamination occurs on the editing strand (protospacer). The position of nucleotides in the protospacer were counted from the first nucleotide adjacent to the protospacer adjacent motif (position −1). (B) Sequencing results to validate base editing using *pta* as a target. The protospacer adjacent motif is displayed on the complementary sequence. Arrows indicate identified single-nucleotide variations. (PAM: protospacer adjacent motif).

We discovered that our base-editing tool did not lead to mutations of the C at position −20 with neither a 20- or a 22-nucleotide protospacer (**Supplementary Table S15**). This suggests that the hot-spot

editing window with high editing efficiency in *C. ljungdahlii* starts from position −19 (**Supplementary Figure S8C**). However, more targets have to be investigated to determine whether editing is possible at position −20. To conclude, we observed that: (1) The C(s) within position −2 to −19 of the protospacer are editable; (2) a hot-spot editing window of our base-editing tool is located approximately between position −16 to −19; and (3) the editing efficiency is low in the range of position −2 to −11.

4.5.3. *In-silico* evaluation of base-editing capability on genome-scale

One doubt for applying base editing in acetogenic bacteria might be a questionable editing capability, because dCas9 from *S. pyogenes* recognizes the nucleotides NGG as the protospacer adjacent motif and *C. ljungdahlii* is an A-T-rich bacterium (77% A-T) (NCBI GenBank Access No. CP001666.1). To investigate the editing capability of our base-editing tool, we developed a genome-scale algorithm. The algorithm reads all possible protospacer adjacent motifs from the genome sequence, and then identifies Cs on the editing strand and converts those Cs to Ts within the editing window. This returns mutations at translational level and identifies the genome-wide capability to generate missense mutations, silent mutations, and nonsense mutations (by installing premature STOP codons). To avoid an overestimation of the capability, we defined position −19 to −11 as the editing window, which combined our results and previous reports (Rees and Liu, 2018). The editing outside this window might still have been possible but with low efficiency. We found that 314 800 sites could be potentially edited among which 257 133 sites are located in coding regions (**Figure 14A**). These editable sites involve 99.83% (4177 out of 4184) of all genes. Only 7 genes that encode short hypothetic proteins (25 to 50 amino acids) cannot be edited (**Supplementary Table S17**). We found that: (1) 99.69% (4171 out of 4184) genes can be edited to have missense mutations; (2) 99.04% (4144 out of 4184) genes can be edited to have silent mutations; and (3) 81.36% (3404 out of 4184) genes can be inactivated/ truncated by installing premature STOP codons (Kuscu *et al.*, 2017) (**Figure 14B**, **Supplementary Table S17**). Moreover, we found that 71.92% (3009 out of 4184) genes can be inactivated by installing premature STOP codons within the first 70% of the coding sequence (**Supplementary Table S17**). We also identified the editable sites, which can be edited with high efficiency by using the hot-spot editing window (position −16 to −19) to give a full evaluation of the capability of our base-editing tool (**Supplementary Table S16**). These *in-silico* results demonstrate a great capability of base editing even in an A-T-rich bacterium such as *C. ljungdahlii*.

On a genome scale, we discovered that, except for Trp and Met codons, all other amino acid codons can be edited to lead to silent mutations without changing the amino acid, while 15 out of 20 amino acids (excluding Phe, Ile, Lys, Asn, and Trp) can be changed to another amino acid (missense mutation)

by changing the codon *via* single-nucleotide variations (**Figure 14C**). Importantly, Gln, Arg, and Trp codons can be replaced to STOP codons. By changing CAA to TAA or CAG to TAG, 9329 Gln codons can be changed to STOP codons. Arg (427 sites) also shows potential to be mutated to a STOP codon by converting CGA to TGA. Trp (2989 sites) offers a different strategy to install premature STOP codons, because base editing changes CCA to TTA, TCA, or CTA on the editing strand and results in TAA, TGA, or TAG on the coding strand.

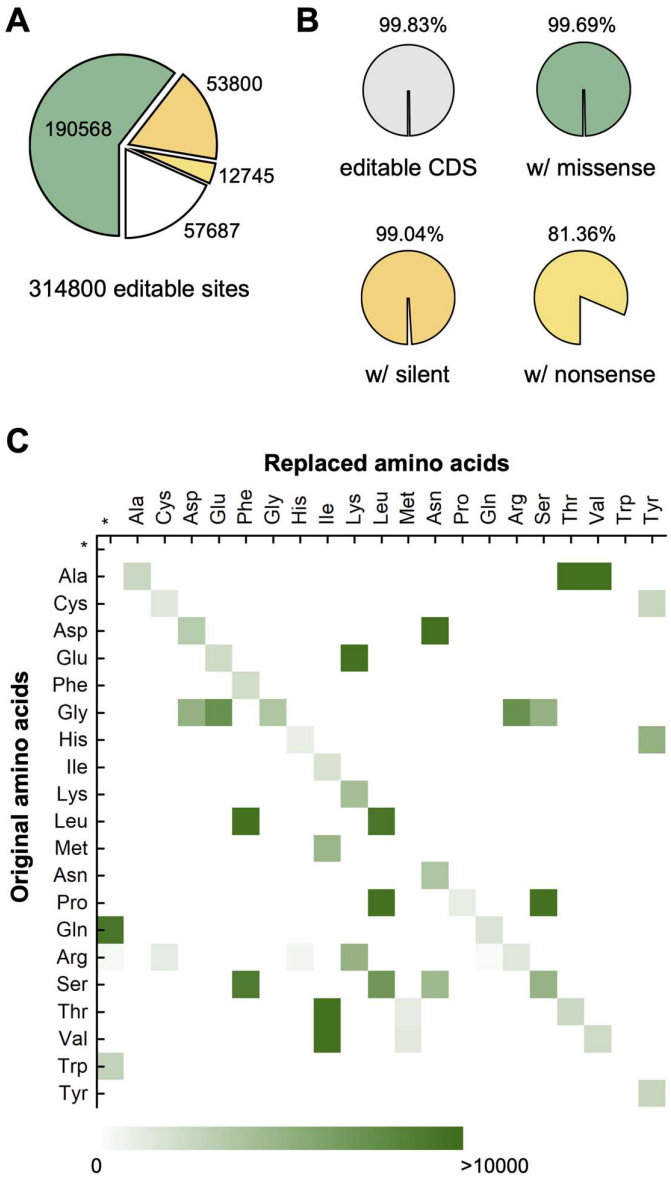

Figure 14 ***In-silico*** **evaluation of base-editing capability in *C. ljungdahlii*.** (A) Pie chart with the numbers of sites that can be edited on a genome scale. Green indicates missense mutations, orange indicates silent mutations, yellow indicates nonsense mutations, and white indicates single-nucleotide variations that are not located in coding regions. (B) Pie charts with the percentages of genes that can be edited in generating different kinds of mutations in coding regions. (C) Amino acid replacement matrix generated by base editing. The green squares indicate the possible mutations with a lighter green colour indicating fewer and a darker green colour indicating more possible mutations on genome-scale.

Compared with a predicted amino acid replacement matrix in G-C-rich Streptomyces species, only 3 out of 32 different amino acid replacement routines were not identified for *C. ljungdahlii* (Pro to Phe, Gly to Lys, and Gly to Asn) (**Figure 14C**), which probably results from the A-T-rich genome (Tong *et al.*, 2019). Moreover, we calculated the potential for off-target events. We investigated off-target sites, which partially match the target sequence, with a modified equation from a previous report in which a similar design of the base-editing tool was used for *E. coli* (Banno *et al.*, 2018). On the basis of this previous report, eight nucleotides in an off-target DNA sequence have to be identical with the gRNA sequence from position −1 to −8, and additional five nucleotides have to match between position −9 to −20 to lead to an off-target event. Besides these parameters, we assumed that editing in a potential off-target site would most likely occur when: (1) the editing site is located in the hot-spot editing window (position −16 to −19); and (2) only when C(s) are present in the hot-spot editing window. Moreover, we added a correction factor for *C. ljungdahlii* due to the A-T-rich genome, which results in low abundance of C(s) in the hot-spot editing window. We found that off-target sites occur approximately 2.7 times per random gRNA in *C. ljungdahlii*, which is much lower than in *E. coli* (8 times) (Banno *et al.*, 2018). According to the genome-scale evaluation, approximately 1.8 potential off-target sites would be located in a coding region, and might lead to missense/nonsense mutations if these sites were edited. Based on these numbers, the probability of actual off-target events can be considered to be very low. However, we want to acknowledge that there is a risk to have off-target events when using base-editing tools.

4.5.4. Reprogramming carbon flux by installing premature STOP codons

To further demonstrate the application potential of our base-editing tool, we disrupted genes involved in ethanol production in *C. ljungdahlii* to reprogram the carbon flux for improved acetate production as a first application. To achieve this, we targeted four genes in two different metabolic pathways individually. First, we targeted *adhE1* (CLJU_c16510) and *adhE2* (CLJU_c16520), which encode isoenzymes of the bifunctional aldehyde-alcohol dehydrogenase. This enzyme converts acetyl-CoA to ethanol *via* acetaldehyde as an intermediate under heterotrophic conditions (**Figure 15A**) (Leang *et al.*, 2013; Richter *et al.*, 2016b). The premature STOP codons were successfully installed in *adhE1* (STOP after 19.4% of the coding region with gRNA10, **Supplementary Table S15**) and *adhE2* (STOP after 3.8% of the coding region with gRNA11, **Supplementary Table S15**), respectively, generating strains QX3 (*adhE1* Trp169*) and QX4 (*adhE2* Gln33*) (**Figure 15B**). Second, we targeted *aor1* (CLJU_c20110) and *aor2* (CLJU_c20210), which encode isoenzymes of the aldehyde:ferredoxin oxidoreductase. This enzyme converts acetate (in the form of undissociated acetic acid) to acetaldehyde under autotrophic conditions (**Figure 15A**) (Richter *et al.*, 2016b). Accordingly, we inactivated *aor1* (STOP after 44.0% of the coding region) and *aor2* (STOP after 44.0% of the coding region) by installing STOP codons with

gRNA19 and gRNA14 (**Supplementary Table S15**), generating strains QX5 (*aor1* Gln267*) and QX6 (*aor2* Gln267*), respectively (**Figure 15B**).

We first tested the stability of all four strains by serial transfer experiments. We confirmed the correct genotype (single-nucleotide variations) at the edited location after 10 transfers with more than 65 generations, indicating that our base-editing tool resulted in stable genotypes (**Figure 15**).

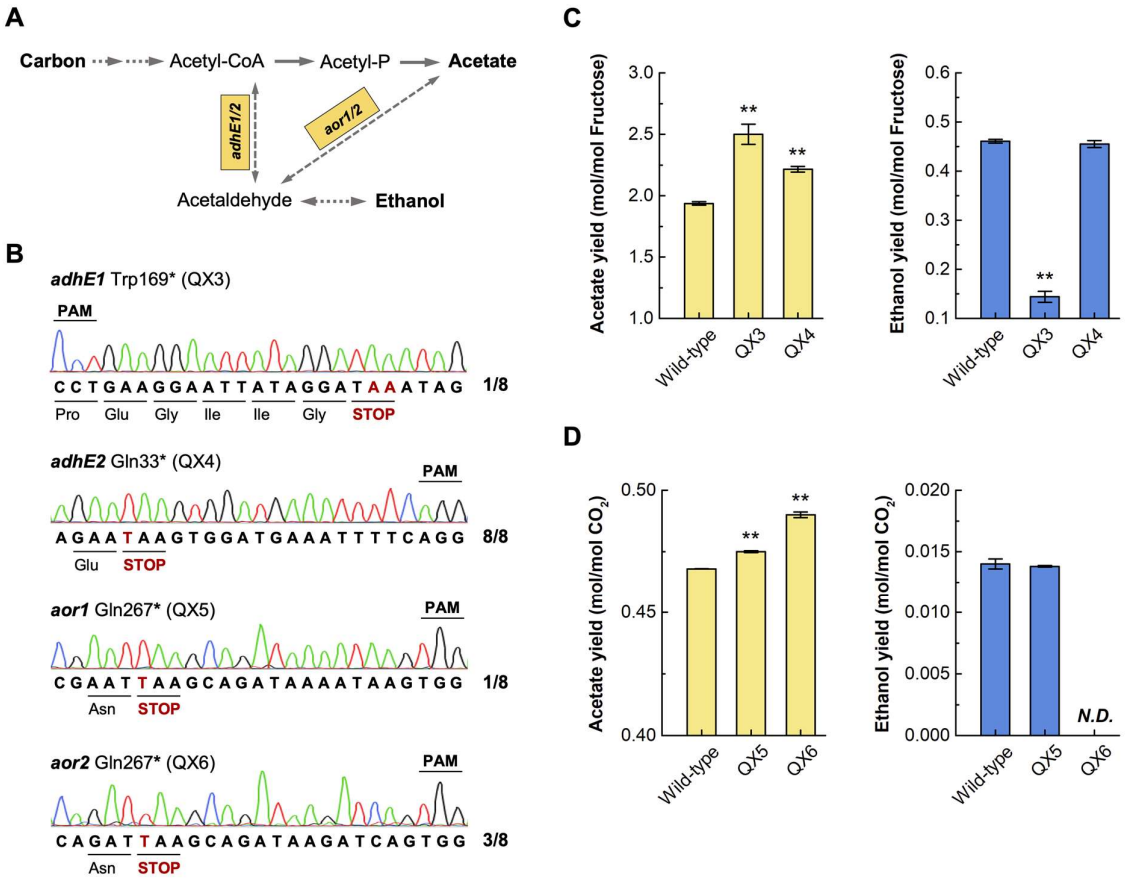

Figure 15 Reprogramming carbon flux toward improved acetate production. (A) Metabolic pathway from acetyl-CoA to acetate and ethanol. Under heterotrophic conditions, ADHE1/2 (encoded by *adhE1/2*) convert acetyl-CoA to ethanol *via* acetaldehyde as an intermediate, while under autotrophic conditions, AOR1/2 (encoded by *aor1/2*) convert acetate to acetaldehyde. (B) Validation of premature STOP codons in the four edited strains (QX3, QX4, QX5, and QX6). The edited sequences and amino acids are shown in the protospacer region. (C) Acetate and ethanol yields of wild-type, QX3, and QX4 under heterotrophic conditions with 5 g/L (27.8 mM) of fructose as the carbon source. (D) Acetate and ethanol yields of wild-type, QX5, and QX6 under autotrophic conditions with a gas mixture of H_2/CO_2 (80/20 vol %, 1.5 bar) as the substrate. The fermentation experiments were conducted in triplicate (N = 3), and the error bars indicate the standard de*via*tions. The differences in acetate yield and ethanol yield were verified by t-test with a $P < 0.05$ as a significant difference and a $P < 0.001$ as a highly significant difference (**).

Next, we investigated the physiology with bottle experiments. For heterotrophic conditions, QX3 and QX4 showed growth defects compared to the wild-type strain, and did not consume all of the provided fructose (**Supplementary Figure S10A, S10B**). However, both QX3 and QX4 achieved higher final acetate yields, because at similar final biomass and acetate concentrations, these strains achieved

lower final ethanol concentrations (**Figure 15C, Supplementary Figure S10C, S10D**). Especially for QX3, we observed a 28.9% higher acetate yield and a 68.6% reduced ethanol yield compared to the wild-type strain (**Figure 15C**), which is in agreement with a previous report on an adhE1 deletion in *C. ljungdahlii*. For autotrophic conditions, we also found growth defects for QX5 and QX6 compared to the wild-type strain, and less overall substrate (H_2/CO_2) consumption (**Supplementary Figure S11A, S11B**). QX5 showed wild-type-like patterns in the yield of acetate and ethanol, however, at an overall lower absolute level of final concentrations (**Figure 15D, Supplementary Figure S11C, S11D**).

QX6 showed a slight, but significant, increase of 4.6% in the final acetate yield (0.490 mol acetate/mol consumed CO_2) compared to the wild-type strain (0.468 mol acetate/mol consumed CO_2), while ethanol was below our detection limit (**Figure 12D, Supplementary Figure S11C**). The higher acetate yield likely resulted from a redistribution of carbon from biomass and/or ethanol to acetate production. The final biomass and acetate concentrations were considerably lower compared to the wild-type strain (**Supplementary Figure S11A, S11D**), while we further acknowledge that this increase (4.6%) in acetate yield by QX6, although significant, is only marginal. However, this increase brings the acetate yield (0.490 mol acetate/mol consumed CO_2) closer to the theoretical limit (0.500 mol acetate/mol consumed CO_2). In addition, we calculated the acetate and ethanol yields based on the dry cell weight under either heterotrophic (**Supplementary Figure S11A, S11B**) or autotrophic conditions (**Supplementary Figure S11C, D**). We found that the yields per dry cell weight of the edited strains shared similar variation patterns with those calculated based on consumed carbon (**Figure 15, Supplementary Figure S11**). Except for QX5, which showed an increased ethanol yield per dry cell weight, but had a similar ethanol yield per consumed carbon compared to the wild-type strain.

These results are in agreement with the results from previous studies with *C. ljungdahlii* and the closely related acetogenic bacterium *C. autoethanogenum* in which full knockout strains of the respective genes were investigated (Leang *et al.*, 2013; Liew *et al.*, 2017). Therefore, although we cannot eliminate the possibility for off-target events, the probability that our fermentation results are caused by off-target events is very low. We found that a single-gene inactivation by introducing a premature STOP codon (*adhE1* and *aor2*) could be enough to generate strains with higher acetate yield and lower ethanol yield under either heterotrophic or autotrophic conditions. To further optimize the metabolism, it is also possible to obtain multigene inactivation in one strain with multiplex base editing by employing established assembly approaches to generate gRNA arrays with protospacers targeting different genes as described by others (Banno *et al.*, 2018; Woolston *et al.*, 2018).

4.6. Discussion

4.6.1. An expanded synthetic biology toolkit for acetogenic bacteria

We developed a base-editing tool for the model acetogenic bacterium *C. ljungdahlii* and enabled genome editing at a one-nucleotide resolution without DNA cleavage, homology-directed repair, and donor DNA. Base editing bypasses the general bottlenecks of applying CRISPR-Cas systems in bacteria, which include the toxicity of Cas nucleases and inefficient DNA repairing mechanisms. It also lowers the requirement of transformation efficiency in *C. ljungdahlii* compared to conventional CRISPR-Cas-based genome editing (Huang *et al.*, 2016; Vento *et al.*, 2019; Zhao *et al.*, 2019). We discovered a great capability of our base-editing tool. With base editing, we can: (1) install STOP codons to 3404 genes in *C. ljungdahlii* to reprogram the metabolism directly; (2) generate silent mutations in 4144 genes to interrogate codon preference; and (3) replace amino acids *via* missense mutations in 4171 genes to perform protein research and engineering *in vivo*. Moreover, we observed that desired single-nucleotide variations could be obtained in a single round of selection. Only in two cases, we observed both wild-type and edited signals in one colony. In a previous study, mixed populations have been reported as an issue for base editing in *C. beijerinkii*, making a second round of selection necessary (Li *et al.*, 2019). Notably, we observed high precision single-nucleotide variations in *C. ljungdahlii* with limited bystander nucleotide substitutions (undesired single-nucleotide variations within the editing window on the editing strand) (**Figure 15B**). This is an advantage returned by the A-T-rich genome of *C. ljungdahlii*, which naturally overcomes bystander base editing with limited Cs in a target sequence and leads to precise base editing. We designed a modularized system to enable fast generation of the base-editing plasmid series. The employed plasmid backbone, replicon for clostridia, antibiotic resistances markers, and the dCas9 protein have been separately demonstrated to be functional in various species in the order Clostridiales, including *A. woodii* (dCas9 has not yet been validated) (Hoffmeister *et al.*, 2016; Beck *et al.*, 2020), *E. limosum* (Shin *et al.*, 2019), and *C. autoethanogenum* (Nagaraju *et al.*, 2016b). Accordingly, the system could be generalized in acetogenic bacteria, which mainly belong to the order Clostridiales.

4.6.2. Linking base editing with microbial C1 utilization

Base editing was first invented to revert single-nucleotide mutations related to human diseases (Komor *et al.*, 2016). Despite an increasing utilization in medicine and agriculture (Rees and Liu, 2018; Molla and Yang, 2019), only a few reports validated bacterial base-editing principles, especially for bacterial pathogens (Chen *et al.*, 2018; Gu *et al.*, 2018; Wang *et al.*, 2018). Furthermore, only few reports exist for biotechnologically relevant bacteria, and these do not demonstrate a specific biotechnological application (Banno *et al.*, 2018; Li *et al.*, 2019; Tong *et al.*, 2019). Presumably, base

editing in bacteria might be hindered by a low editing capability in relevant genes or low stability of resulting single-nucleotide variations, which would not be favorable for industrial biotechnology. To overcome this presumption, we inactivated four genes related to ethanol production in *C. ljungdahlii* as a first application, with the goal to increase the acetate yield. This would improve the production of certain platform chemicals that require acetate as an intermediate (Nevin *et al.*, 2011; Nangle *et al.*, 2017). For instance, our acetate-producing strain can be considered to further improve the two-stage bioprocess for single-cell protein production from C1 gases, with acetate as the carbon-fixing intermediate product before being fed to aerobic yeasts, especially for industrial gases that contain CO (Molitor *et al.*, 2019). Importantly, single-nucleotide variations generated by base editing are clean mutations in the genome, which may also occur in natural evolution. Thus, our base-editing tool, in principle, provides a unique venue to engineer industrially relevant bacteria without creating genetically modified organisms (GMOs). However, this advantage is not recognized in the legislation of all countries, and especially in Europe, CRISPR-Cas-based genome editing is often per se considered to generate GMOs, irrespective of the outcome of the editing.

4.6.3. Limitations and perspectives for base editing in A-T-rich bacteria

Not surprisingly, base editing has its limitations in A-T-rich bacteria. First, the editing sites are still limited in A-T-rich genomes, because of the protospacer adjacent motif (nucleotides NGG) that is recognized by dCas9 from *S. pyogenes*. Despite a large number of editable sites, not the entire genome can be covered. To overcome this, possible strategies include using a dCas protein with a different protospacer adjacent motif, such as Cas12a with nucleotides TTTV as a protospacer adjacent motif (Li *et al.*, 2018) or xCas9 with nucleotides NG as a protospacer adjacent motif (Hu *et al.*, 2018). Second, base editing is site-specific, and not all sites following the editing principles can be edited (Molla and Yang, 2019). Evidently, when we tried to introduce a STOP codon at Gln235 in *aor1* with gRNA13, no colonies with the expected single-nucleotide variations were identified (data not shown), while we obtained 2 out of 8 colonies with Gln237* replacement by using gRNA19. A different deaminase may be necessary to circumvent this limitation. Third, base editing, although in low probability, arouses off-target events in bacteria, which should not be underestimated. Possible ways to minimize editing at off-target sites would include: (1) optimizing the gRNAs based on a pre-off-target evaluation; and (2) employing a CRISPR-Cas system with higher specificity (Zuo *et al.*, 2020). Finally, base editing intrinsically cannot insert DNA fragments into the genome. Yet, it offers a new angle to edit the genome with CRISPR-Cas systems without DNA cleavage. Starting from this perspective, a recent report demonstrated DNA insertion into the genome without cutting the DNA by coupling a CRISPR-Cas system to a reverse transcriptase (Anzalone *et al.*, 2019).

In summary, we established an efficient base-editing tool for gene manipulation in acetogenic bacteria. Further, we demonstrated the use of this genome-editing tool in C1 utilization with the industrially relevant acetogenic bacterium *C. ljungdahlii*. Our strategy provides an example for upgrading bacterial genome-editing tools with CRISPR systems in general, especially for bacteria that are sensitive to heterologously expressed Cas nucleases (*e.g.*, cyanobacteria (Xia *et al.*, 2019)) and those with limited capability of receiving foreign DNA.

4.7. Acknowledgment

This work was supported by the Alexander von Humboldt Foundation in the framework of the Alexander von Humboldt Professorship (L.T.A.) and the Humboldt Research Fellowship for Postdoctoral Researchers (P.-F.X.). S.S. thanks the support from the German Federal Environmental Foundation (Deutsche Bundesstiftung Umwelt, DBU). B.M. and L.T.A are grateful to funding from the Deutsche Forschungsgemeinschaft (DFG, German Research Foundation) under Germany´s Excellence Strategy – EXC 2124 – 390838134. Finally, L.T.A. is supported as a Max Planck Fellow by the Max Planck Institute for Developmental Biology.

4.8. Supporting information

Supporting information is provided in the Appendix (**8.2.**). It contains four supplementary tables and seven supplementary figures, which detail the evaluation and interpretation of the base-editing work. Furthermore, it compiles the growth data of the autotrophic and heterotrophic cultivation experiment of the base-edited strains.

CHAPTER 5

GENETIC EVIDENCE REVEALS THE INDISPENSABLE ROLE OF THE *RSEC GENE FOR AUTOTROPHY* AND THE IMPORTANCE OF A FUNCTIONAL ELECTRON BALANCE FOR NITRATE REDUCTION IN *CLOSTRIDIUM LJUNGDAHLII*

Reproduced with permission from: Klask, C.M., Jäger, B., Angenent L. T. , and Molitor, B. Genetic evidence reveals the indispensable role of the *rsec gene for autotrophy* and the importance of a functional electron balance for nitrate reduction in *Clostridium ljungdahlii*. Submitted to mBio, 02.08.2021.

5.1. Author's contribution

Christian-Marco Klask (C.M.K.) and Bastian Molitor (B.M.) designed the experiments. C.M.K. performed the genetic work, conducted the growth experiments, analyzed the metabolites, and performed the *in-silico* research. C.M.K. and Benedikt Jäger (B.J.) performed the qRT-PCR experiments. C.M.K. analyzed all experimental data. Largus T. Angenent (L.T.A.) and B.M. supervised the work. C.M.K. and B.M. wrote the manuscript, and all authors edited the paper and approved the final version.

5.2. Abstract

For *Clostridium ljungdahlii*, the RNF complex plays a key role for energy conversion from gaseous substrates such as hydrogen and carbon dioxide. In a previous study, a disruption of RNF-complex genes led to the loss of autotrophy, while heterotrophy was still possible *via* glycolysis. Furthermore, it was shown that the energy limitation during autotrophy could be lifted by nitrate supplementation, which resulted in an elevated cellular growth and ATP yield. Here, we used CRISPR-Cas12a to delete: 1) the RNF complex-encoding gene cluster *rnfCDGEAB*; 2) the putative RNF regulator gene *rseC*; and 3) a gene cluster that encodes for a putative nitrate reductase. The deletion of either *rnfCDGEAB* or *rseC* resulted in a complete loss of autotrophy, which could be restored by plasmid-based complementation of the deleted genes. We observed a transcriptional repression of the RNF-gene cluster in the *rseC*-deletion strain during autotrophy and investigated the distribution of the *rseC* gene among acetogenic bacteria. To examine nitrate reduction and its connection to the RNF complex, we compared autotrophic and heterotrophic growth of our three deletion strains with either ammonium or nitrate. The *rnfCDGEAB*- and *rseC*-deletion strains failed to reduce nitrate as a metabolic activity in

non-growing cultures during autotrophy but not during heterotrophy. In contrast, the nitrate reductase deletion strain was able to grow in all tested conditions but lost the ability to reduce nitrate. Our findings highlight the important role of the *rseC* gene for autotrophy and contribute to understand the connection of nitrate reduction to energy metabolism.

5.3. Introduction

Acetogenic bacteria (*i.e.*, acetogens), such as *Clostridium ljungdahlii*, maintain autotrophic growth with mixtures of the gaseous substrates carbon dioxide, carbon monoxide, and hydrogen as carbon and energy sources (Drake *et al.*, 2008; Katsyv and Müller, 2020). The pathway that allows carbon fixation for autotrophic growth in acetogens is the Wood-Ljungdahl pathway (Wood *et al.*, 1986; Ljungdahl, 2009). Overall, the Wood-Ljungdahl pathway is considered the most energy-efficient pathway for carbon fixation that exists in nature (Fast and Papoutsakis, 2012; Song *et al.*, 2020). In the Wood-Ljungdahl pathway, two molecules of carbon dioxide are reduced to one carbonyl group and one methyl group, which are then combined with coenzyme A to the central metabolite acetyl-coenzyme A (Ljungdhal, 1986). The electrons for these reductions can be derived from the oxidation of hydrogen or carbon monoxide, while carbon monoxide can also enter the pathway directly to provide the carbonyl group (Wood, 1991). For carbon fixation, acetyl-coenzyme A is channeled into the anabolism for cellular growth (Ragsdale and Pierce, 2008). For energy conservation, acetyl-coenzyme A is converted to acetate, which generates cellular energy by substrate level phosphorylation (Schuchmann and Müller, 2014). One mole of ATP is generated per mole of acetate that is produced. However, in the first step of the pathway, after carbon dioxide was reduced to formate, one mole of ATP is invested to activate the formate to formyl-tetrahydrofolate (Wood *et al.*, 1986; Ljungdahl, 2009). Thus, the energy balance of the Wood-Ljungdahl pathway alone is net zero (Schuchmann and Müller, 2014). All required cellular energy for the anabolism of the microbes during autotrophy is generated *via* membrane-coupled phosphorylation (Katsyv and Müller, 2020). In *C. ljungdahlii*, the membrane-bound transhydrogenase *Rhodobacter* nitrogen fixation (RNF) complex (Schmehl *et al.*, 1993; Biegel *et al.*, 2011) utilizes two electrons from the oxidation of reduced ferredoxin to reduce NAD^+ to NADH, while simultaneously one proton is translocated across the membrane (Tremblay *et al.*, 2012; Schuchmann and Müller, 2014). A proton-dependent F_1F_O ATPase then consumes the chemiosmotic proton gradient to generate ATP (Köpke *et al.*, 2010; Al-Bassam *et al.*, 2018). In the presence of carbon dioxide and hydrogen, theoretically, *C. ljungdahlii* can generate a maximum of 0.63 moles ATP per mole acetate for the anabolism *via* membrane-coupled phosphorylation. Thus, the conservation of cellular energy during autotrophy occurs at the thermodynamic limit of life (Schuchmann and Müller, 2014).

For *C. ljungdahlii*, the RNF complex is encoded by the RNF-gene cluster *rnfCDGEAB*. Although the RNF complex plays an essential role for energy conservation during autotrophy in *C. ljungdahlii* (Tremblay *et al.*, 2012), fundamental knowledge about the regulation and gene expression control of the encoding RNF-gene cluster is missing. Transcriptome studies with *C. ljungdahlii* revealed that the RNF complex is under strict gene expression control and strongly induced during autotrophy (Tan *et al.*, 2013; Al-Bassam *et al.*, 2018). The regulatory mechanisms behind this remain unknown. However, the small gene *rseC*, which is located directly upstream of *rnfC* in *C. ljungdahlii,* is also highly expressed during autotrophy and follows the expression profile of *rnfC* (Al-Bassam *et al.*, 2018). The gene *rseC* is annotated to contain the conserved protein domain family RseC_MucC (pfam04246) (Köpke *et al.*, 2010). The domain family RseC_MucC is found in positive transcriptional regulators in other microbes. The one representative, RseC, was found to be involved in the oxidative stress response in *Escherichia coli* (De Las Peñas *et al.*, 1997; Missiakas *et al.*, 1997; Koo *et al.*, 2003), and in thiamine synthesis in *Salmonella typhimurium* (Beck *et al.*, 1997). The other representative, MucC, was found to be involved in the regulation of the alginate formation of *Azotobacter vinelandii* (Martinez-Salazar *et al.*, 1996) and *Pseudomonas aeruginosa* (Boucher *et al.*, 1997). Others identified a transcription start site for *C. ljungdahlii*, which is located upstream of the *rseC* gene, and a putative terminator sequence, which is located between *rseC* and *rnfC* were identified. This indicates that *rseC* is expressed as an individual transcript apart from the RNF-gene cluster transcripts (Al-Bassam *et al.*, 2018). Altogether, this leads to the assumption that the *rseC* gene product is closely linked to the RNF complex, and could be important for the regulation of autotrophy in *C. ljungdahlii*.

While autotrophy in acetogens results in low cellular energy yields, Emerson *et al.* (2019) reported that *C. ljungdahlii* is able to couple the reduction of nitrate to the generation of ATP during growth with carbon dioxide and hydrogen. This relieved the energy limitation during autotrophy and resulted in a significantly higher biomass yield (Emerson *et al.*, 2019). We confirmed this in a bioreactor study, and biomass yields were considerably higher with nitrate, but resulted in stochastic crashes of the continuous bioreactor cultures (Klask *et al.*, 2020). Emerson *et al.* (2019) proposed that electrons, which are required for nitrate reduction, are provided by NADH. One route to regenerate NADH is by the RNF complex where reduced ferredoxin is consumed (Biegel *et al.*, 2011), which would link nitrate reduction to the energy metabolism. It was assumed that nitrate reduction is accelerating the RNF-complex activity and more protons are translocated across the membrane, which can be used by the F_1F_O ATPase for the generation of ATP (Emerson *et al.*, 2019). This way, the co-utilization of carbon dioxide and nitrate with hydrogen was suggested to yield up to 1.5 ATP through the concerted action of the RNF complex and the ATPase (Emerson *et al.*, 2019). This would be a 2.4-fold increase in ATP

yield compared to the ATP yield with carbon dioxide and hydrogen alone (Schuchmann and Müller, 2014).

To investigate the autotrophy in *C. ljungdahlii* with respect to regulatory aspects and the interplay with nitrate reduction, we addressed three main questions: **1)** Is the *rseC* gene involved in the regulation of the RNF-gene cluster?; **2)** Is nitrate reduction dependent on a functional RNF complex?; and **3)** Is nitrate reduction abolished by the deletion of the nitrate reductase that is annotated in the genome of *C. ljungdahlii*?

5.4. Material and Methods

5.4.1. Bacterial strains and growth

Escherichia coli TOP10 (Invitrogen), *E. coli* EPI300 (Lucigen), and *E. coli* HB101 PKR2013 (DSM 5599) were grown at 37°C in Luria Broth (LB) medium containing (per liter): 5 g NaCl; 10 g peptone; and 5 g yeast extract. *C. ljungdahlii* ATCC13528 was generally cultivated in anaerobic Rich Clostridial Medium (RCM) containing per liter: 5 g fructose; 3 g yeast extract; 10 g meat extract; 10 g peptone; 5 g NaCl; 1 g soluble starch; 3 g sodium acetate; 0.5 g L-cysteine HCl; and 4 mL resazurin-solution (0.025 vol-%). For growth experiments with *C. ljungdahlii*, standard PETC medium (Klask *et al.*, 2020) was used containing (per liter): 1 g yeast extract; 1.0 g NH_4Cl; 0.1 g KCl; 0.2 g $MgSO_4x7\ H_2O$; 0.8 g NaCl; 0.1 g KH_2PO_4; 0.02 g $CaCl_2x2\ H_2O$; 4 mL resazurin-solution (0.025 vol-%); 10 mL trace element solution (TE, 100x); 10 mL Wolfe's vitamin solution (100x); 10 mL reducing agent (100x); and 20 mL of fructose/2-(N-morpholino)ethanesulfonic acid (MES) solution (50x). TE was prepared as 100x stock solution containing (per liter): 2 g nitrilotriacetic acid (NTA); 1 g $MnSO_4xH_2O$; 0.8 g $Fe(SO_4)2(NH_4Cl)2x6\ H_2O$; 0.2 g $CoCl_2x6$ H2O; 0.0002 g $ZnSO_4x7\ H_2O$; 0.2 g $CuCl_2x2\ H_2O$; 0.02 g $NiCl_2x6\ H_2O$; 0.02 g $Na_2MoO_4x2\ H_2O$; 0.02 g Na_2SeO_4; and 0.02 g Na_2WO_4. The pH of the TE was adjusted to 6.0 after adding NTA. The solution was autoclaved and stored at 4°C. Wolfe's vitamin solution was prepared aerobically containing (per liter): 2 mg biotin; 2 mg folic acid; 10 mg pyridoxine-hydrochloride; 5 mg thiamin-HCl; 5 mg riboflavin; 5 mg nicotinic acid; 5 mg calcium pantothenate; 5 mg p-aminobenzoic acid; 5 mg lipoic acid; and 0.1 mg cobalamin. The vitamin solution was sterilized using a sterile filter (0.2 µm), sparged with N_2 through a sterile filter, and stored at 4°C. The 50x fructose/MES solution contained (per 100 mL): 25 g fructose; and 10 g MES. The pH was adjusted to 6.0 by adding KOH. For autotrophic experiments, fructose was omitted. In nitrate experiments, ammonium chloride was replaced with sodium nitrate ($NaNO_3$) in the equal molar amount (=18.7 mM). The reducing agent solution contained (per 100 mL): 0.9 g NaCl and 4 g L-cysteine HCl and was prepared with anaerobic water under anaerobic conditions. The reducing agent was stored at room temperature. For solid LB medium, 1.5 weight-% agar was added. For solid RCM or PETC medium 1.0-2.0 weight-% agar was added. For

conjugation of *C. ljungdahlii* cells (see below) a modified PETC medium (PETC+5gS) was used containing additionally (per liter): 5 g peptone and 5 g meat extract.

Liquid *E. coli* cultures and autotrophic *C. ljungdahlii* cultures were agitated at 150 revolutions per minute (rpm) (Lab Companion Incubater Shaker ISS-7100R, Jeio Tech). Heterotrophic cultures of *C. ljungdahlii* and LB plates with *E. coli* cells were incubated without shaking (Incubator IN260, Memmert). Anaerobic work was performed in an anaerobic chamber (Glovebox-System UNIlab Pro, MBraun) with an N_2 (100 vol-%) atmosphere. However, *C. ljungdahlii* cultures in bottles were transferred at the bench with sterile syringes and needles. Before each transfer between serum bottles, we flamed the top of the rubber stopper with ethanol (70 vol-%) at a Bunsen burner. All plating work with *C. ljungdahlii* was performed in the anaerobic chamber with a maximum of 5 parts per million (ppm) oxygen in the atmosphere. All plating work with *E. coli* was carried out in a lamina flow bench (Hera Safe KS18, Thermo Fischer Scientific). Antibiotics (see below) were added to maintain plasmid stability in recombinant cultures of *E. coli* and *C. ljungdahlii*.

5.4.2. Antibiotics

Chloramphenicol (30 mg/mL), ampicillin (100 mg/mL), and kanamycin (50 mg/mL) were applied to maintain plasmids in *E. coli* strains, while thiamphenicol (5 mg/mL) was used for recombinant strains of *C. ljungdahlii*. Thiamphenicol was prepared as aerobic stock solution (25 mg/mL) in DMSO (100 vol-%) and diluted with sterile water (1:10) before use. The diluted thiamphenicol solution (2.5 mg/mL) was transferred into a sterile 1 mL syringe. 100 µL of this solution was used to add to a 50 mL RCM or PETC medium (final concentration of 5 mg/mL). The use of DMSO over ethanol as solvent for thiamphenicol prevented the addition of external ethanol to cultures of *C. ljungdahlii*, which is a metabolite. The thiamphenicol stock solution was stored at -20°C.

5.4.3. Design and generation of CRISPR-FnCas12a plasmids for gene deletion

The broad-host plasmid pMTL83152 (Heap et al. 2009) was used as backbone (**Table 5**). All PCR steps were performed with Q5® High-Fidelity DNA Polymerase (New England Biolabs) and primers provided by IDT (Integrated DNA Technologies) (**Table 6**). PCR products were purified with QIAquick PCR Purification Kit (Qiagen). The gene *Fncas12a* of *Francisella novicida* (Zetche et al. 2015) was obtained from plasmid pY001 (Addgene #69973) and amplified with primers cas12a_fwd_BamHI and cas12a_rv_NcoI generating *Bam*HI and *Nco*I restriction sites for a subsequent restriction cloning to generate pMTL83152_*Fn*Cas12a. Two homology-directed repair arms (HDR1/HDR2) each with a size of 1000-1200 bp, which flank the targeted gene, were individually amplified with HDR_upst_fwd/rv and HDR_dwst_fwd/rv primers generating an overlap of 25-40 bp to each other.

Table 5 Plasmids used in this study.

plasmid	function	source
pMTL83151	shuttle-vector	(Heap *et al.*, 2009)
pMTL83152	shuttle-vector with constitutive thiolase promoter P_{thl}	(Heap *et al.*, 2009)
pMTL2tetO1gusA	pMTL82254 with pminiThl:tetR and p2tetO1:gusA	(Woolston *et al.*, 2018)
pMTL8315tet	shuttle-vector with inducible promoter system *tetR-O1*	this study
pMTL83151_P_{nat}_*rnfCDGEAB*	overexpression of *rnfCDGEAB* through native promoter P_{nat}	this study
pMTL83152_*rseC*	overexpression of *rseC* through constitutive promoter P_{thl}	this study
pMTL83152_*nar*	overexpression of *nar* through constitutive promoter P_{thl}	this study
pY001_FnCpf1(Cas12a)	expression of FnCas12a	(Zetsche *et al.*, 2015), Addgene 69973
pMTL83152_FnCas12a	constitutive expression of FnCas12a through P_{thl}	this study
pMTL83152_FnCas12a_ΔrseC	constitutive expression of FnCas12a through P_{thl}, constitutive expression of a single sgRNA targeting *rseC* on the genome, fused repair HDR1/2 fragment for homologous recombination and marker-less gene deletion	this study
pMTL83152_FnCas12a_Δ*nar*	constitutive expression of FnCas12a through P_{thl}, constitutive expression of two sgRNA targeting *nar* on the genome, fused repair HDR1/2 fragment for homologous recombination and marker-less gene deletion	this study
pMTL83152_FnCas12a_Δ*rnfCDGEAB*	constitutive expression of FnCas12a through P_{thl}, constitutive expression of two sgRNA targeting *rnfCDGEAB* on the genome, fused repair HDR1/2 fragment for homologous recombination and marker-less gene deletion	this study
pMTL8315tet_FnCas12a	inducible expression of FnCas12a through tetR-O1 promoter system	this study
pMTL8315tet_FnCas12a_Δ*rseC*	inducible expression of FnCas12a through tetR-O1 promoter system, constitutive expression of a single sgRNA targeting *rseC* on the genome, fused repair HDR1/2 fragment for homologous recombination and marker-less gene deletion	this study
pMTL8315tet_FnCas12a_Δ*nar*	inducible expression of FnCas12a through tetR-O1 promoter system, constitutive expression of two sgRNA targeting *nar* on the genome, fused repair HDR1/2 fragment for homologous recombination and marker-less gene deletion	this study
pMTL8315te_FnCas12a_Δ*rnfCDGEAB*	inducible expression of FnCas12a through tetR-O1 promoter system, constitutive expression of two sgRNA targeting *rnfCDGEAB* on the genome, fused repair HDR1/2 fragment for homologous recombination and marker-less gene deletion	this study

The fragments were purified, and 50-100 ng of both fragments were used as template for a subsequent fusion PCR using HDR_upst_fwdOv and HDR_dwst_rvOv primers, which generated new overlaps at 5' and 3' (fusion fragment HDR1/2).

Table 6 Primers used in this study.

primer	sequence (5'-> 3')	function
rnfCDGEAB+213bp_fw_BamHI	GGATCCGTAATTTGTGTACAAACTTTAATTAATGGAGAGAC	amplification of the RNF complex gene cluster (CLJU_c11360-410) + and promoter sequence (P_{nat})
rnfCDGEAB_rv_NcoI	CCATGGTTATGAATTTGCAGCAGCTTCATTCTTG	amplification of the RNF complex gene cluster (CLJU_c11360-410) + and promoter sequence (P_{nat})
rseC_fwd_BamHI	GGATCCAGGAGGTTAAGAATGAAAAGAGAATCGGAGGGTATTG	amplification of the putative RNF regulator gene *rseC* (CLJU_c11350)
rseC_rv_NcoI	CCATGGTCAATACAATATCTTTGTGATTACTGGC	amplification of the putative RNF regulator gene *rseC* (CLJU_c11350)
nar-full_fwd_BamHI	GGCAGCTTACCGGGATCCAGGAGGTTAAGAATGAATTACGTGGAAGTAAAACAATCAAC	amplification of a gene cluster (CLJU_c23710-30) encoding for a nitrate reductase
nar-full_rv_NcoI	GCACGGTCGTCGCCATGGTTAAAAAGTATACTCTAAATTTTCCTTTATATTAAAAAAGTC	amplification of a gene cluster (CLJU_c23710-30) encoding for a nitrate reductase
Seq1_RNF_744bp_fwd	GGAAAATTCAGACAAGGTAGTTGC	sanger sequencing of the *rnfCDGEAB* fragment
Seq2_RNF _1502bp_fwd	CAGAAAATAGAGCTGCAGGTGAAAG	sanger sequencing of the *rnfCDGEAB* fragment
Seq3_RNF _2268bp_fwd	CTGGCAGATTCCAGTAGTAATGATTG	sanger sequencing of the *rnfCDGEAB* fragment
Seq4_RNF _3000bp_fwd	GGGACAGTTTAAGGATAAAAAGGCAG	sanger sequencing of the *rnfCDGEAB* fragment
Seq5_RNF_3787bp_fwd	GCAAATGGAGGTGAAGCATAATG	sanger sequencing of the *rnfCDGEAB* fragment
Seq6_RNF _4502bp_fwd	GTGAATCCACTTGTAGACTTAGTAGAAG	sanger sequencing of the *rnfCDGEAB* fragment
Seq7_RNF_5047bp_rv	TTATGAATTTGCAGCAGCTTCATTCTTG	sanger sequencing of the *rnfCDGEAB* fragment
Seq1 _nar_456bp_rv	GCACCTCCTTATACTCTAAAAGATTTTG	sanger sequencing of the *nar* fragment
Seq2 _nar_610bp_fwd	CTGTTTCAGATTTTCTCGGGTCAATTG	sanger sequencing of the *nar* fragment
Seq3 _nar_1059bp_rv	CCAAAGCATAGAGAAGAAATTGC	sanger sequencing of the *nar* fragment
Seq4 _nar_1186bp_fwd	CCCACAATGCCTTAATTTCTCCG	sanger sequencing of the *nar* fragment
Seq5 _nar_1677bp_rv	GTAAAGCTCATTTATGAAGATGCAGCC	sanger sequencing of the *nar* fragment
Seq6 _nar_1798bp_fwd	CCCTAGTTCTAGTCTGGGTATGC	sanger sequencing of the *nar* fragment
Seq7 _nar_2303bp_rv	CCAGATACCGGTATTGTAGAGTACG	sanger sequencing of the *nar* fragment
Seq8 _nar_2476bp_fwd	CATCTAGCTACACACTGCGG	sanger sequencing of the *nar* fragment
Seq9 _nar_2902bp_rv	GATGCACAAAAAATAAAGGATGCAGC	sanger sequencing of the *nar* fragment
Seq10 _nar_3086bp_fwd	CTTCATATCTGCCTGCTGCA	sanger sequencing of the *nar* fragment
Seq11 _nar_3385bp_rv	GGAATTGTAGCAGCTAGTAATATGGC	sanger sequencing of the *nar* fragment
tetR-O1_fwd_SbfI	CCTGCAGGATAAAAAAATTGTAGATAAATTTTATAAAATAG	amplification of the inducible promoter system tetR-O1

tetR-O1_rv_BamHI	GGATCCTATTTCAAATTCAAGTTTATCGCTCTAATGAAC	amplification of the inducible promoter system tetR-O1
repH _401bp_rv	CTCTAACGGCTTGATGTGTTGG	primer binding in the backbone of pMTL83151 and pMTL83152 upstream of *repH*
fdhA_fwd	AGTGCAGCGTATTCGTAAGG	amplification of a 501 bp fragment of the *fdhA* gene in *C. ljungdahlii*
fdhA_rv	TAATGAGCCACGTCGTGTTG	amplification of a 501 bp fragment of the *fdhA* gene in *C. ljungdahlii*
repH_643bp_rv	GCACTGTTATGCCTTTTGACTATCAC	primer binding in the backbone of pMTL83151 and pMTL83152 upstream of *repH*
traJ_60bp_fw	CATGCGCTCCATCAAGAAGAG	primer binding in the backbone of pMTL83151 and pMTL83152 downstream of *traJ*
rnfC_250bp_rv	CTCCTATATCTACAACCTTTCCAGAAGTAG	primer binding 250 bp upstream of *rnfC*, which was used for sanger sequencing and PCR screening
cas12a_fwd_BamHI	GGTACCGGATCCATGTCAATTTATCAAGAATTTGTTAATA	amplification of *Fncas12a*
cas12a_rv_NcoI	GGTACCCCATGGTTAGTTATTCCTATTCTGCAC	amplification of *Fncas12a*
Seq1_cas12a	CACAGATATAGATGAGGCG	sanger sequencing of *Fncas12a*
Seq2_cas12a	GCTTCTGGAGCTTTGTCT	sanger sequencing of *Fncas12a*
Seq3_cas12a	GTAGTTACAACGATGCAAAG	sanger sequencing of *Fncas12a*
Seq4_cas12a	CCGCTGTACCAATAACAC	sanger sequencing of *Fncas12a*
Seq5_cas12a	GGCTAATGGTTGGGATAA	sanger sequencing of *Fncas12a*
Seq6_cas12a	CTTATTCATCACACCCAG	sanger sequencing of *Fncas12a*
Seq7_cas12a	CAAGATGTGGTTTATAAGC	sanger sequencing of *Fncas12a*
Seq8_cas12a	CCTCTTTAGCTGGGTGAGTG	sanger sequencing of *Fncas12a*
Seq9_cas12a	CAAGGTAGAGAAGCAGGTC	sanger sequencing of *Fncas12a*
Seq10_cas12a	GCTCTAAGCACTCCCCCAG	sanger sequencing of *Fncas12a*
Seq11_cas12a	GCTAAGCTAACTAGTGTC	sanger sequencing of *Fncas12a*
Seq12_cas12a	CCATTTACATCTGCTACTGG	sanger sequencing of *Fncas12a*
HDR_rnfB_fwdOv	TGTAAAAATTATTGAAAGAGGTGTTTAAGATGGCAGTGGAGCAAAGCTT	amplification of homology-directed repair arm downstream of *rnfB* with overhang to the homology-directed repair arm upstream of *rnfC*
HDR_rnfB_rv	ATGTAAAGGGTTCACATAAAATAGCTGT	amplification of homology-directed repair arm downstream of *rnfB*
HDR_rnfC_fwdOv	CAAGTTGAAAAATTTAATAAAAAAATAAGTGGCTTGAAATCAATAGTTAACGCAATAG	amplification of homology-directed repair arm upstream of *rnfC* with overhang to the *Fncas12a* sequence
HDR_rnfC_fwd	GGCTTGAAATCAATAGTTAACGCAATAG	amplification of homology-directed repair arm upstream of *rnfC* without overhang
HDR_rnfC_rvOV	TCAGCAAATTTAAGCTTTGCTCCACTGCCATCTTAAACACCTCTTTCAATAATTTTTACAGC	amplification of homology-directed repair arm upstream of *rnfC* with overhang to the homology-directed repair arm downstream of *rnfB*
Seq_HDR_rnfB_881bp_fwd	GACCTGGTTCGGATATCCATCC	sanger sequencing of the HDR_rnfB fragment
minigene_crRNA_RNF_fwd	TTTATGTGAACCCTTTACATTTGACAAATT	amplification of crRNA array consisting of 22-bp overhang to HDR_rnfB , p4-promoter,

		direct repeats, sgRNA (TTA), and rrnB-T1 terminator for genome target *rnfCDGEAB*
minigene_crRNA_all_rv	GTTGGTAGCTTAATATATAAGAATAAAACGAAAGG	amplification of crRNA array consisting of 22-bp overhang to pMTL83152-Cas12a, p4-promoter, direct repeats, sgRNA (TTA), and rrnB-T1 terminator for genome target *rnfCDGEAB, rseC,* and *nar*
outside_RNF_HDR_dwst_rv	GCATGGGAGTGTTAATATGAAAAAAGGG	verification of *rnfCDGEAB* deletion
outside_RNF_HDR_upst_fwd	GGAGGCTATTAAGGGACCGT	verification of *rnfCDGEAB* deletion
HDR_rseC_dwst_fwdOv	CGCTAACAAATAATAGGAGGTGTATTATGTAATTTGTGTACAAACTTTAATTAATGGAGAGAC	amplification of a homology-directed repair arm downstream of *rseC* with 28-bp overlap to HDR_rseC_upst
HDR_rseC_dwst_rv	TAGTTGTAACCCTCTGTATAAGTGGAATTC	amplification of a homology-directed repair arm downstream of *rseC*
HDR_rseC_upst_fwd	CTCATTGAAGTATATGTTAATGGCAGAAAAAAGTTC	amplification of a homology-directed repair arm upstream of *rseC*
HDR_rseC_upst_fwdOv	CAAGTTGAAAAATTTAATAAAAAAATAAGTCTCATTGAAGTATATGTTAATGGCAGAAAAAAAGTTC	amplification of a homology-directed repair arm upstream of *rseC* with 30-bp overlap to pMTL83152-Cas12a
HDR_rseC_upst_rvOv	TCCATTAATTAAAGTTTGTACACAAATTACATAATACACCTCCTATTATTTGTTAGCGTTTTC	amplification of a homology-directed repair arm upstream of *rseC* with 30-bp overlap to fragment HDR_rseC_dwst
minigene_crRNA_rseC_fwd	CTTATACAGAGGGTTACAACTATTGACAAATT	amplification of crRNA array consisting of 22-bp overhang to HDR_rseC_dwst, p4-promoter, direct repeats, sgRNA (TTA), and rrnB-T1 terminator for genome target *rseC*
outside_rseC_HDRdwst_rv	CCCATCATAGGTCCACCTGAAA	verification of *rseC* deletion
outside_rseC_HDRupst_fwd	CGAGCTGAAGGTTGTAAAAATATCCG	verification of *rseC* deletion
seq_rseC_145bpupst_fwd	GAAGGTAATACTGTTCAATATCGATACAGA	verification of *rseC* deletion
HDR_nar_dwst_fwdOv	TCTTTTTCATAAATTTAGAGTATACTTTCTCCACTTCTCAATATTTTTTACTGAAAATAC	amplification of a homology-directed repair arm downstream of nar with overhang to HDR_nar_upst
HDR_nar_dwst_rv	TTGGAATGACAGGACTCTATATAGTTATGG	amplification of a homology-directed repair arm downstream
HDR_nar_upst_fwd	TACAACCTCTGTTAGTACTGCTGATATTACATC	amplification of a homology-directed repair arm upstream of nar
HDR_nar_upst_fwdOv	CAAGTTGAAAAATTTAATAAAAAAATAAGTTACAACCTCTGTTAGTACTGCTGATATTACATC	amplification of a homology-directed repair arm upstream of nar with overhang to *Fncas12a*
HDR_nar_upst_rvOv	GTATTTTCAGTAAAAAATATTGAGAAGTGGAGAAAGTATACTCTAAATTTATGAAAAAGAATTTTA	amplification of a homology-directed repair arm upstream of *nar* with overhang to HDR_nar_dwst
minigene_nar_fwd	ATATAGAGTCCTGTCATTCCAATTGACAAATT	amplification of crRNA array consisting of 22-bp overhang to HDR_nar_dwst, p4-promoter, direct repeats, sgRNA (TTA), and rrnB-T1 terminator for genome target *nar*
seq_nar_95bp_dwst_fwd	CCGGATAACCTTTAGTGGGAAGT	verification of *nar* deletion
seq_nar_132bp_upst_rv	GCGCCATAATTCAAGGGGAT	verification of *nar* deletion
outside_nar_HDRdwst_rv	GGGTTGACGTAGATGGAGGAAG	verification of *nar* deletion
outside_nar_HDRupst_fwd	CCTTTAAGCTTCCACCATTTGCC	verification of *nar* deletion
qPCR_rseC_fwd	GCTAGTAGACACGGAGATTG	amplification of a 142 bp fragment from *rseC*
qPCR_rseC_rv	CTGCCCATAACATATTTGC	amplification of a 142 bp fragment from *rseC*

qPCR_rnfC_fwd	GCACCTATACCAGATAAGGT	amplification of a 160 bp fragment from *rnfC*
qPCR_rnfC_rv	CCTTTCCAGAAGTAGATGCAT	amplification of a 160 bp fragment from *rnfC*
qPCR_rnfD_fwd	CCTCATGTTCGTTGTGATG	amplification of a 157 bp fragment from *rnfD*
qPCR_rnfD_rv	CAAAGTACTCCGTAACTACAGC	amplification of a 157 bp fragment from *rnfD*
qPCR_rnfG_fwd	CATCACCAGTAGCAGCG	amplification of a 156 bp fragment from *rnfG*
qPCR_rnfG_rv	CTGCAGGTACAACATATGC	amplification of a 156 bp fragment from *rnfG*
qPCR_rnfE_fwd	TGTGTCCAGCACTGGC	amplification of a 138 bp fragment from *rnfE*
qPCR_rnfE_rv	CAGGGACACGTACCTTAG	amplification of a 138 bp fragment from *rnfE*
qPCR_rnfA_fwd	GCATCTGTAGGTATGGGTATG	amplification of a 136 bp fragment from *rnfA*
qPCR_rnfA_rv	CAATAAGAAGTACAAAAACTACCG	amplification of a 136 bp fragment from *rnfA*
qPCR_rnfB_fwd	GCAATGGAAGTGAATCCAC	amplification of a 155 bp fragment from *rnfB*
qPCR_rnfB_rv	GCTGCTTTTCCAGGTAC	amplification of a 155 bp fragment from *rnfB*
qPCR_rho_fwd	GGACTCTTTCAGGAGGACTA	amplification of a 243 bp fragment from *rho*
qPCR_rho_rv	ATACATCTATGGCAGGGAAT	amplification of a 243 bp fragment from *rho*

An crRNA array was synthesized and cloned as minigene into plasmid pUC19 by IDT (Integrated DNA Technologies) (**Table 7**). The crRNA array sequence contained the mini-promoter P4 (5'-TTGACAAATTTATTTTTTAAAGTTAAAATTAAGTTG-3') (Xu *et al.*, 2015), the FnCas12a-specific directed repeats (DR) sequence (5'-TAATTTCTACTGTTGTAGAT-3') (Zetsche *et al.*, 2015), 1-2 sgRNA for the targeted gene(s) (Pam sequence TTV for target RNF and TTTV for target *rseC* and *nar*), and the rrbn-T1-terminator (Orosz *et al.*, 1991).

Table 7 Synthesized mini genes that contain crRNA arrays for this study. Gene synthesis was performed by IDT (Integrated DNA Technologies). Each mini gene contains 20-22-bp overhang to the pMTL-backbone and to the fused homology-directed repair arms. Directed-repeats sequence of 20 bp (underlined). sgRNA with TTV PAM for the RNF complex gene cluster deletion and with TTTV PAM for the *nar* and *rseC* deletion (bold). Two sgRNAs were used to target RNF and *nar*.

name	sequence (3'-> 5')
minigene_crRNA-RNF	TTTATGTGAACCCTTTACATTTGACAAATTTATTTTTTAAAGTTAAAATTAAGTTGTAATTTCTACT GTTGTAGATAAAAGTTTTCGAGGTGGAGTACATAATTTCTACTGTTGTAGATCAACAGCAGAGC AAGAATGAAGCATAAAACGAAAGGCTCAGTCGAAAGACTGGGCCTTTCGTTTTATTCTTATATA TTAAGCTACCAAC
minigene_crRNA-*rseC*	CTTATACAGAGGGTTACAACTATTGACAAATTTATTTTTTAAAGTTAAAATTAAGTTGTAATTTCT ACTGTTGTAGATATAGATCTACAAGCAAAAATGAGATAAAACGAAAGGCTCAGTCGAAAGACT GGGCCTTTCGTTTTATTCTTATATATTAAGCTACCAAC
minigene_crRNA-*nar*	ATATAGAGTCCTGTCATTCCAATTGACAAATTTATTTTTTAAAGTTAAAATTAAGTTGTAATTTCT ACTGTTGTAGATTATTTCTTGTTTATAGCTTTCATTAATTTCTACTGTTGTAGATTACAGCAAAATC CATCATTTACCATAAAACGAAAGGCTCAGTCGAAAGACTGGGCCTTTCGTTTTATTCTTATATAT TAAGCTACCAAC

The crRNA array fragment was amplified with primers minigene_crRNA_fwd/rv creating overhangs to the fused HDR1/2 fragment and the plasmid backbone. For gene targets with a size >2 kb, such as *rnfCDGEAB* and *nar*, two sgRNA (and two DRs) were used in the same crRNA array (**Table 7**). For the assembly reaction (Gibson Assembly Ultra Kit, Synthetic Genomics), the plasmid

pMTL83152_*Fncas12a* was first digested using *Bbv*CI and CIP (New England Biolabs) for 3h at 37°C, purified by PCR-clean, and then mixed with the purified fused HDR1/2 fragment and the crRNA array fragment. Using electrocompetent E. coli EPI300 cells (TransforMax™, Lucigen) and electroporation for transformation highly increased cloning efficiency for the CRISPR-Cas12a constructs in *E. coli*. For inducible Cas12a expression, the P_{thl} module was replaced with the *tetR-O1* promoter module ($P_{tetR-O1}$) (Woolston *et al.*, 2018) using restriction sites *Sbf*I and *Bam*HI, for all generated CRISPR-Cas12a plasmids.

5.4.4. Generation of overexpression and complementation plasmids

The broad-host shuttle-vector system pMTL80000 (Heap *et al.*, 2009) was used for all cloning steps. All generated plasmids of this study (**Table 5**) were cloned with restriction endonucleases and T4 ligase from NEB (New England Biolabs) or Gibson assembly (NEBuilder® HiFi DNA Assembly, New England Biolabs). PCR work was carried out with primers provided by IDT (Integrated DNA Technologies) (**Table 6**) and with a proof-reading Q5® High-Fidelity DNA Polymerase (New England Biolabs) according to the manufacture's guidelines. Genomic DNA (gDNA) was purified from 2 mL of exponential cultures of *C. ljungdahlii* with the NucleoSpin Tissue Mini kit (Macherey-Nagel) and used as PCR-template. Notably, instead of performing harsh cell disruption according to the manufacture's recommendation, we applied a 6x10 sec vortex interval during the procedure. The *rnfCDGEAB* gene cluster (CLJU_c11360-410) and a 213-bp sequence located upstream of *rnfC*, which contains the putative native promoter sequence (P_{nat}), were amplified as one fragment using primers rnfCDGEAB+213bp_fwd and rnfCDGEAB_rv. The *rseC* gene (CLJU_c11350) was amplified using primers *rseC*_fwd and *rseC*_rv. The gene cluster CLJU_c23710-30, here referred to as *nar*, was amplified as one fragment using primers nar-full_fwd and nar-full_rv. All PCR products were purified with the QIAquick PCR Purification kit (Qiagen). Subsequently, the purified fragments were ligated into pMinit2.0 (New England Biolabs) and used for transformation of $CaCl_2$-competent *E. coli* TOP10 cells (Sambrook and Russell, 2006a). Next, the plasmid DNA was digested using the restriction sites determined by the used PCR primers and the fragment was cloned into the pMTL83151 plasmid generating pMTL83151_P_{nat}_*rnfCDGEAB* or into the pMTL83152 plasmid generating pMTL83152_*rseC* and pMTL83152_*nar*. Subsequently, all cloned fragments were verified again with test-digestion of the plasmid DNA and Sanger sequencing to exclude mutations in the gene sequences.

5.4.5. Screening for correct plasmid DNA and genome editing

For screening and continuous purity control of our *C. ljungdahlii* strains (**Table 8**), we performed PCRs from culture samples or from purified DNA with the Phire Plant Direct PCR Master Mix (Thermo Fischer Scientific).

Table 8 Used and generated *C. ljungdahlii* strains in this study.

clostridial strain	plasmid	phenotype	
		heterotrophic	autotrophic
C. ljungdahlii DSM13528	-	yes	yes
C. ljungdahlii DSM13528	pMTL83151	yes	yes
C. ljungdahlii DSM13528	pMTL83151_$P_{tetR-O1}$	yes	yes
C. ljungdahlii DSM13528	pMTL83152	yes	yes
C. ljungdahlii DSM13528	pMTL83151_P_{nat}_*rnfCDGEAB*	yes	yes
C. ljungdahlii DSM13528	pMTL83152_*rseC*	yes	yes
C. ljungdahlii DSM13528	pMTL83151_*nar*	yes	yes
C. ljungdahlii ΔRNF[a]	-	yes (reduced)	no
C. ljungdahlii ΔRNF[a]	pMTL83151	yes (reduced)	no
C. ljungdahlii ΔRNF[a]	pMTL83151_P_{nat}_*rnfCDGEAB*	yes	yes
C. ljungdahlii ΔrseC	-	yes	no
C. ljungdahlii ΔrseC	pMTL83152	yes	no
C. ljungdahlii ΔrseC	pMTL83152 _*rseC*	yes	yes
C. ljungdahlii Δnar	-	yes	yes
C. ljungdahlii Δnar	pMTL83152	yes	yes
C. ljungdahlii Δnar	pMTL83152_*nar*	yes	yes

[a] ΔRNF = Δ*rnfCDGEAB*

E. coli colonies grown on selective LB plates after receiving plasmid constructs were analyzed for the correctly assembled plasmids using the Phire Plant Direct PCR Master Mix (Thermo Fischer Scientific). A small amount of recombinant *E. coli* cell material was directly transferred to the reaction mix. For *C. ljungdahlii* cells, 0.5-1 mL culture sample was harvested by centrifugation for 3 min at 13806 rpm (Centrifuge 5424, FA-45-24-11, Eppendorf) and resuspended in 100-500 µL 10 mM NaOH depending on the size of the cell pellet. Subsequently, cell suspensions were boiled for 10 min at 98°C. The hot reaction tubes were incubated on ice for 1 min and quickly vortexed before they served as a DNA template. In general, we used 20 µL PCR master mix, which consisted of 10 µL Phire Plant Mix 2x, 0.8 µL of each primer, 1 µL cell lysate sample, and 7.4 µl nuclease-free water. The PCR reaction was carried out according to the manufacture's guidelines. We generally used the primers tra60bp_fwd and repH_401bp_rv or repH_643bp_rv for these control PCRs (**Table 6**), because they bind to the plasmid backbone of every pMTL plasmid used in this study. Verification of gene deletion in the genome of *C. ljungdahlii* was performed with "outside" primers, which bound upstream and downstream of the used homology-directed repair arms (HDR1/2) on the genomic DNA (**Table 6**). In addition, we performed test-digestion of the generated plasmids with restriction enzymes (New England Biolabs),

and analyzed the fragment pattern *via* gel electrophoresis. The final plasmid sequence was verified by Sanger sequencing. Plasmid DNA was purified from *E. coli* with hand-made purification buffers (described below). Correct plasmid DNA was then purified with the QIAprep Spin Miniprep kit (Qiagen) *prior* to further use.

5.4.6. A fast method for plasmid purification from *E. coli* without use of a commercial kit

For screening of successfully transformed *E. coli* cells we used a time- and money-saving protocol to purify plasmid DNA from multiple samples without using a commercial kit, which is a modified alkaline lysis protocol adapted from (Sambrook *et al.*, 1989). All centrifugation steps were performed at 13806 rpm for 5 min (Centrifuge 5424, FA-45-24-11, Eppendorf). Recombinant *E. coli* cells were grown overnight in 5 mL selective liquid LB at 37°C and 150 rpm. 1.5-3 mL cell suspension were harvested in 1.5 mL reaction tubes. The supernatant was discarded, and the pellet was resuspended by vortexing in 150 µl P1-buffer (50 mM Tris, 10 mM EDTA, 100 µg/mL RNAseA, pH 8.0 with HCl). Cells were lysed in 150 µl P2-buffer (200 mM NaOH, 1 vol-% SDS) and inverted five times. Proteins were precipitated by adding 250 µl P3-buffer (2.55 M Na-acetate, pH 4.8 with acetic acid). The samples were inverted five times and centrifuged. Subsequently, 500 µL of the supernatant were transferred into new 1.5 mL tubes and mixed with 500 µl isopropanol. The samples were quickly vortexed and centrifuged again. Afterwards, the supernatant was discarded. At this step, the precipitated and non-visible plasmid-DNA pellet remained on the bottom of the tube. The pellet was washed twice with ice-cold EtOH (70 vol-%) omitting resuspending the DNA. After the second washing, the supernatant was discarded completely and the remaining EtOH was first removed by snapping the tube on a piece of clean paper towel and then through drying at 50-65°C for 10 min. The dried pellet was resuspended in 30 µL elution buffer (Tris/EDTA, pH 7.2) or deionized water. Purified plasmid-DNA with a concentration of 250-500 ng/µL was clean enough for subsequent cloning steps and test-digestion, however, an additional clean-up with the QIAquick PCR Purification Kit (Qiagen) was carried out when a Sanger sequencing reaction was necessary. P1-buffer needed to be stored at 4°C to maintain RNAse activity for up to 3 months. P2- and P3-buffer were stored at room temperature.

5.4.7. A modified conjugation protocol for *C. ljungdahlii*

This protocol was adapted and modified according to Mock *et al.* (2015). Cells of *C. ljungdahlii* were grown in RCM overnight to mid exponential growth until an OD_{600} of 0.4-0.8 was reached (NanoPhotometer® NP80, Implen). *E. coli* HB101 pKR2013 (DSM 5599) harboring the desired CRISPR-Cas12a-plasmid was grown as pre-culture in selective 5 mL LB medium overnight. The plasmid pKR2013 contains essential genes to mediate conjugation and a kanamycin resistance cassette. 1-2 mL of the *E. coli* cells were used to inoculate 10 mL selective LB medium in 50 mL baffled flask and

cultivated until mid-exponential growth (OD_{600} 0.5-1.0). Subsequently, the *E. coli* culture was cooled to 4°C and 2 mL were transferred into sterile 2 mL reaction tubes. The *C. ljungdahlii* culture was kept at room temperature until use. Inside the anaerobic chamber, *E. coli* cells were centrifuged softly at 2900 rpm (mySpin^{TM} 12 mini centrifuge, Thermo Fischer Scientific) to protect pili, and washed once with sterile and anaerobic 0.1 M phosphate buffer saline (PBS) at pH 6.0. Afterwards, the washed pellet was resuspended gently in 100-150 µL cell suspension of *C. ljungdahlii* and directly transferred to well-dried RCM-agar plates (2 vol-% agar). Spot-mating was carried out at 37°C inside the anaerobic chamber overnight. After 8-24 h the spot was resuspended with anaerobic PBS (pH 6.0) and centrifuged at 10000 rpm (mySpin^{TM} 12 mini centrifuge, Thermo Fischer Scientific) for 3 min. The supernatant was discarded, and the pellet was resuspended in the remaining volume of the tube. Subsequently, 100 µL of the cell suspension was plated onto selective PETC+5gS-agar plates, which contained 5 g/L of peptone and 5 g/L meat extract to support growth. Selective agar plates should not be older than 2-3 days. Thiamphenicol was added for plasmid selectivity. Trimethoprim (10 mg/mL) was added to counter-select against *E. coli*. Growth was obtained after 4-5 days at 37°C inside the anaerobic chamber. *C. ljungdahlii* colonies were transferred into Hungate tubes containing 5 mL RCM with the respective antibiotics. A successful transformation of *C. ljungdahlii* with the correct plasmid was confirmed as follow: **1)** Growth in selective RCM with a characteristic pH decrease due to acetogenesis; **2)** control PCRs with primers for plasmid specific fragments; and **3)** plasmid purification from the culture and re-transformation into *E. coli* TOP10 cells.

5.4.8. Electroporation of *C. ljungdahlii* cells

Electroporation of *C. ljungdahlii* cells was performed as previously reported (Xia *et al.*, 2020) and applied for all non-CRISPR-based plasmids. Single colonies growing on selective plates were verified by PCR analyses and by re-transformation of plasmid DNA, which was extracted from *C. ljungdahlii* into *E. coli*.

5.4.9. Growth experiments with *C. ljungdahlii*

In general, all recombinant *C. ljungdahlii* strains were pre-grown in 50 mL RCM in 100 mL serum bottles for 24-48 h. Subsequently, 2 mL cell suspension were used to inoculate 50 mL PETC medium in 100 mL serum bottles. This PETC pre-culture was cultivated for 40-48h at 37°C until mid-exponential growth phase at OD_{600} of 0.5-1.0. Afterwards, cells were transferred anaerobically into 50 mL reaction tubes, which were equilibrated for 3-5 days inside the anaerobic chamber. Cell harvest was performed outside the anaerobic chamber at 3700 rpm for 12 min (Centrifuge 5920R, S-4x1000, Eppendorf) at room temperature. After the centrifugation, the tubes were transferred back immediately into the anaerobic chamber, to keep the time at aerobic conditions at a minimum. Inside the anaerobic

chamber, the supernatant was discarded, and the pellet was resuspended in fresh PETC medium to adjust to an OD_{600} of 5-10. The concentrated cell suspension was then transferred into sterile and anaerobic 10 mL Hungate tubes, sealed carefully, and used to inoculate main cultures outside of the anaerobic chamber. 1 mL of the cell suspension was used to inoculate 100 mL PETC main cultures. For heterotrophic growth experiment, 240 mL serum bottles were used. Autotrophic growth experiments were performed in 1000 mL Duran pressure plus bottles (Schott), to provide a high medium-to-headspace ratio. The Duran pressure plus bottles were sealed with butyl stoppers and a GL45 ring cap. Before inoculation of autotrophic cultures, the N_2 headspace was replaced with a sterile gas mixture consisting of H_2/CO_2 (80/20 vol-%). Each bottle contained 0.5 bar overpressure. All cultures were cultivated in biological triplicates as batch cultures. The gas headspace was not refilled during the experiments. However, for the strain *C. ljungdahlii* pMTL83151_P_{nat}_*rnfCDGEAB* and the control strain *C. ljungdahlii* pMTL83151 we refilled the headspace during this experiment with the same gas mixture to 0.5 bar overpressure at time points 44.5 h, 73.5 h, and 148.5 h (**Supplementary Figure S15**). Culture samples of 3 mL were taken at the bench and used for: **1)** OD_{600} measurement; **2)** pH measurement; **3)** HPLC analyses (acetate and ethanol); and **4)** FIA analyses (nitrate, nitrite, and ammonium). All culture samples were stored at -20°C until use. OD_{600} samples were diluted with medium or PBS buffer when the absorbance was > 0.5. We applied a two-tailed student's t-test for all cultivation data. All p-values (*P*) below 0.001 indicate high significance and are given as ≤ 0.001.

5.4.10. HPLC analyses

HPLC analyzes were performed as described before (Klask *et al.*, 2020). In addition, all frozen supernatant samples were thawed at 30°C for 10 min and 300 rpm, vortexed briefly, and centrifuged for 3 min at 13806 rpm (Centrifuge 5424, FA-45-24-11, Eppendorf) before use. All HPLC samples were randomized.

5.4.11. Measurement of nitrate, nitrite, and ammonium

Nitrate and nitrite concentrations were measured in a FIA continuous-flow analyzer system (AA3 HR AutoAnalyzer System, Seal Analytical GmbH, Germany) as described before (Klueglein *et al.*, 2014). Briefly, nitrate is reduced to nitrite with hydrazine and then reacts with sulfanilamide and NEDD (N-1-Naphthylethylenediamine di-HCl) to form a pink complex, which can be quantified photo-metrically at 550 nm. The protocol follows the DIN 38405/ISO 13395 standard methods. Ammonium concentrations were measured in the same system but with salicylate and dichloroisocyanuric acid forming a blue complex that is measured at 660 nm instead. The protocol was following DIN 38406/ISO 11732 standard methods. Culture samples of *C. ljungdahlii* were treated as explained above for HPLC preparation. However, we prepared 1:50 dilution in 1 mL with deionized water *prior*

to the FIA analyses. Standards for nitrate, nitrite, and ammonium were measured before and during the analyses for a standard curve and to minimize drift effects. Nitrate concentrations of each sample were calculated by the difference of the amount of nitrite measured with and without the *prior* reduction by hydrazine.

5.4.12. Growth experiment for RNA extraction from *C. ljungdahlii*

For the expression analyses, we grew the strains *C. ljungdahlii* WT, *C. ljungdahlii* ΔRNF, and *C. ljungdahlii* Δ*rseC* under autotrophic and heterotrophic conditions as described above. The cultivation medium was PETC with ammonium as nitrogen source. Pre-cultures were grown in heterotrophic medium for 48 h. Next, the cells were transferred into the anaerobic chamber and harvested for 12 min at 25°C and 3700 rpm (Centrifuge 5920 R, S-4x1000, Eppendorf) outside of the anaerobic chamber. The supernatant was discarded under anaerobic conditions and the pellet was resuspended in fresh medium of the main cultures. The start OD_{600} for autotrophic main cultures was 0.2, while it was 0.15 for heterotrophic conditions. The cultures were cultivated at 37°C. 10 mL culture samples were taken after 3 h and 20 h. The samples were immediately cooled on ice and centrifuged for 12 min at 4°C and 3700 rpm (Centrifuge 5920 R, S-4x1000, Eppendorf). The cell pellets were stored at -20°C until RNA extraction.

RNA was purified from *C. ljungdahlii* with the RNeasy Mini Kit (Qiagen) as described before (Liu *et al.*, 2013). For the RNA extraction, we used $2 \cdot 10^8$ cells, which was approximately 10 mL of a *C. ljungdahlii* culture at OD_{600} 0.2. The cell lysis was performed in the lysis buffer of the kit with 50 mg glass beads (0.1 mm silica spheres, MP Biomedicals) in a bead beater (5G-FastPrep, MP Biomedicals) for 2x 60s at 9 m/s. RNA samples were eluted in 30 µL nuclease-free water. After the extraction procedure, an additional DNase I digest (RNase free Kit, Thermo-Scientific) was performed to remove potential DNA contamination. Elimination of genomic DNA was confirmed with PCR analyses and gel electrophoresis. cDNA synthesis was performed with the QuantiTect Reverse Transcriptase Kit (Qiagen) according to the manufacturer´s instructions. We used 500 ng RNA as template for each reaction. cDNA was stored at -20°C until further use.

5.4.13. qRT-PCR analyses

All qRT-PCR analyses were performed in a Quantstudio 3 Thermocycler (Applied Biosystems, Thermo Scientific). The PCR reaction mix contained 10 µL SYBR Green Master mix (Thermo Scientific), 1 µL of a fwd and rv qRT-PCR primer (final concentration 500 nM) (**Table 6**), and 1 µL (~5 ng) cDNA template. We used the *rho* gene as reference gene, which was described before as suitable candidate for qRT-PCR experiments with *C. ljungdahlii* (Liu *et al.*, 2013). We added RNA controls to further exclude gDNA contamination in our samples. All qRT-PCR reactions were performed in technical triplicate according

to the manufacturer's instructions. We set the Ct threshold to 0.1. The fold change in gene expression between the samples was determined with the $2^{-\Delta\Delta Ct}$ method as described before (Livak and Schmittgen, 2001). We examined the PCR efficiency of our qPCR master mix by using plasmid DNA containing the sequence of each tested gene in a series of dilutions (10^{-1}, 10^{-2}, $5{\cdot}10^{-3}$, 10^{-3}, $5{\cdot}10^{-4}$, 10^{-4}). The slopes were ranging from 0.04-0.09 for the RNF-gene cluster genes and 0.17 for *rseC*, and were thus, close to zero, which proofs that the efficiencies are similar and the $2^{-\Delta\Delta Ct}$ can be used for interpretation of the qRT-PCR data (Livak and Schmittgen, 2001). We applied a two-tailed student's t-test based on our ΔCt values for each gene to analyze the significance of our samples in comparison to the wild type.

5.4.14. Strain preservation

Cultures of *C. ljungdahlii* were stored at -80°C. For this, cultures were grown in RCM until late exponential growth phase (OD_{600} 0.8-1.2) at 37°C for 36-48 h. The cells were transferred into anaerobic 50 mL reaction tubes inside the anaerobic chamber and harvested outside of the anaerobic chamber for 12 min at 4°C and 3700 rpm (Centrifuge 5920 R, S-4x1000, Eppendorf). The supernatant was discarded inside the anaerobic chamber and the pellet was resuspended in fresh RCM medium to an OD_{600} of 5-10. 2 mL of the cell suspension was transferred into 10 mL serum bottles, which were previously filled with 2 mL of 25-50 vol-% anaerobic and autoclaved glycerol. The serum bottles were briefly vortexed outside the anaerobic chamber, incubated on ice for 10-15 min and subsequently frozen at -80°C. For inoculation of a new RCM culture, a single serum bottle was quickly thawed up under rinsing water and 1-2 mL of the cell suspension was immediately transferred with a syringe into the medium bottle. Cultures of *E. coli* were stored at- 80°C in sterile screw-cap tubes filled with 25-50 vol-% glycerol.

5.5. Results

5.5.1. A full deletion of the RNF complex confirmed its indispensable role for autotrophy in *C. ljungdahlii*

We first attempted to generate a full deletion of the RNF-gene cluster to further investigate autotrophy in *C. ljungdahlii*. Others had demonstrated that a mutant strain of *C. ljungdahlii*, for which the *rnfAB* genes were disrupted with an antibiotic resistance cassette, had lost the ability to grow during autotrophy (Tremblay *et al.*, 2012). However, this genome modification was not stable, and the wild-type genotype was restored during the cultivation time of the experiments (Tremblay *et al.*, 2012). In addition, it was demonstrated recently that a full RNF-gene cluster deletion led to the loss of autotrophic growth in the acetogen *Acetobacterium woodii* (Westphal *et al.*, 2018). Here, we achieved

a full deletion of the RNF-gene cluster in *C. ljungdahlii* with a clustered regularly interspaced short palindromic repeats (CRISPR)-associated protein 12a (CRISPR-Cas12a) system, which we implemented and used to generate all deletion strains in this study (**Figure 16A, Supplementary Text S1A**).

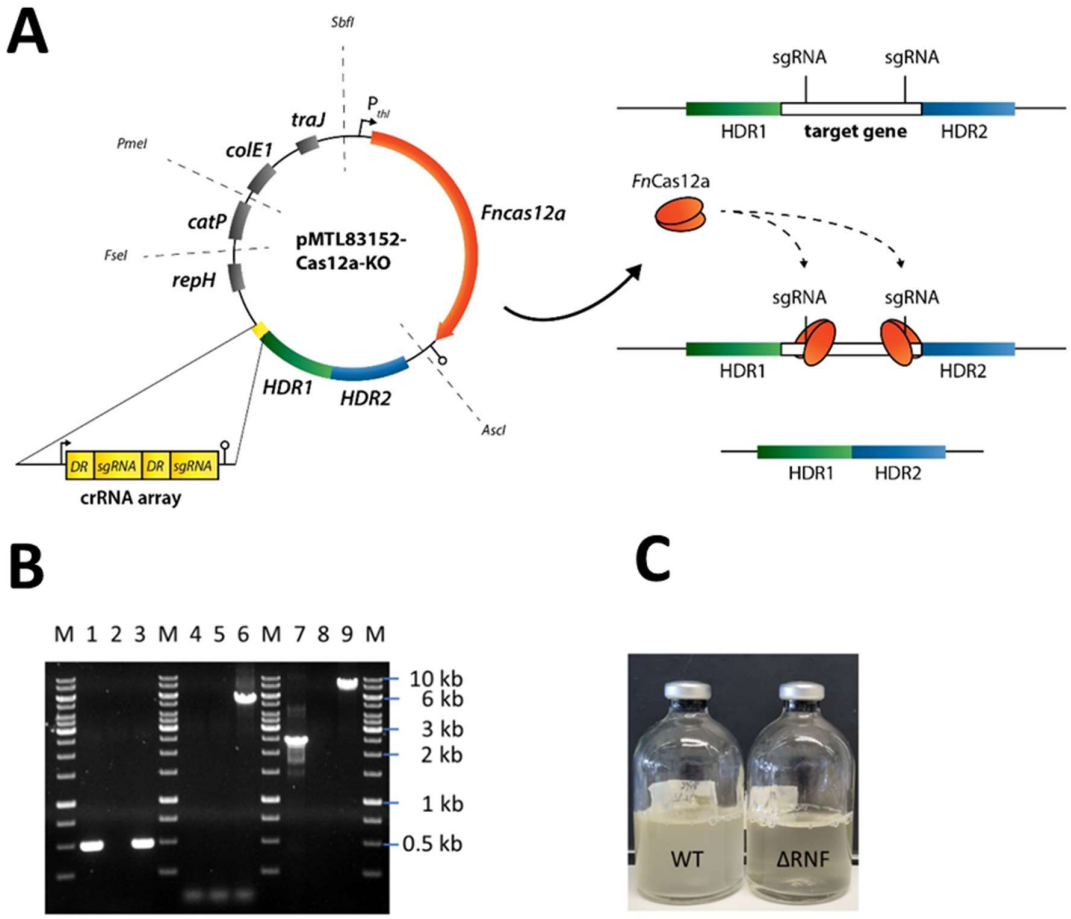

Figure 16 CRISPR-Cas12a-mediated *rnfCDGEAB* gene cluster deletion in *C. ljungdahlii*. A, modular CRISPR-Cas12a system established in the pMTL80000 shuttle-vector system (Heap *et al.*, 2009). The final CRISPR-Cas12a plasmid for deletion of *rnfCDGEAB* contained the *Fncas12a* gene, homology-directed repair arms (HDRs), and a specific crRNA array comprising two directed repeats (DRs) and two sgRNA, which targeted the *rnfC* and *rnfB* genes. **B**, agarose gel with PCR-samples for the *fdhA* fragment (WT: 501 bp, deletion strain: 501 bp), *rnfCDGEAB* fragment (WT: 5047 bp, deletion strain: no fragment), and for a fragment that was amplified with primers that bind ~1250 bp upstream and downstream of the rnfCDGEAB gene cluster locus (WT: 7550 bp, deletion strain: 2503 bp). DNA-template: gDNA of *C. ljungdahlii* ΔRNF (lane 1, 4, and 7); gDNA of *C. ljungdahlii* WT (lane 3, 6, and 9); and water (lane 2, 5, 8). M: Generuler™ 1 kb DNA ladder. **C**, growth of the wild type (WT) and reduced growth of the deletion strain (ΔRNF) with fructose in PETC medium. HDR1/2, homology-directed repair arm flanking the targeted gene; crRNA array, sequence containing FnCas12a-specific DRs and sgRNAs; sgRNA, guide RNA; *repH*, Gram-positive origin of replication; *catP*, antibiotic resistant cassette against chloramphenicol/thiamphenicol; *colE1*, Gram-negative origin of replication; *traJ*, conjugation gene; P_{thl}, promoter sequence of the thiolase gene in *Clostridium acetobutylicum*; *Asc*I, *Fse*I, *Pme*I, and *Sbf*I are unique-cutting restriction sites, which were preserved during the cloning to maintain the modular functionality of the plasmid backbone.

After successfully generating the RNF-gene cluster deletion strain (*C. ljungdahlii* ΔRNF) and confirming the identity of this strain (**Figure 16B, Supplementary Text S1B**), we compared the growth of *C. ljungdahlii* wild-type (WT) to the growth of *C. ljungdahlii* ΔRNF. We performed growth experiments

with carbon dioxide and hydrogen (autotrophy) and with fructose (heterotrophy), while we added equimolar amounts of either ammonium or nitrate as nitrogen source to the medium for both autotrophy and heterotrophy (***Materials and Methods*, Figure 17, Supplementary Figure S13**).

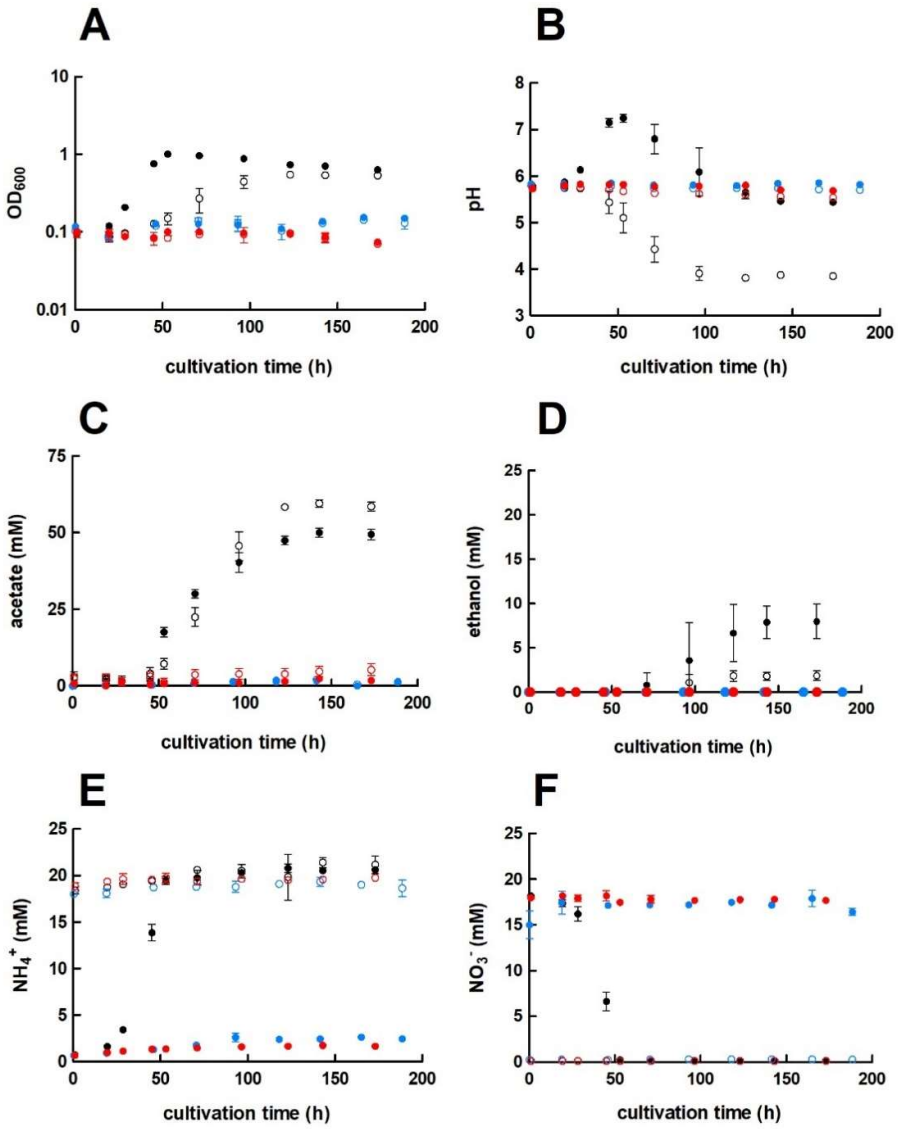

Figure 17 Cultivation of *C. ljungdahlii* WT, *C. ljungdahlii* ΔRNF, and *C. ljungdahlii* Δ*rseC* in nitrate- or ammonium-containing medium with H_2 and CO_2. Cultures of *C. ljungdahlii* strain WT (●, ○), ΔRNF (●, ○), and Δ*rseC* (●, ○) were grown in 100 mL PETC medium in 1 L bottles at 37°C and 150 rpm. The headspace consisted of H_2 and CO_2 (80/20 vol-%) and was set to 0.5 bar overpressure. The medium contained either 18.7 mM nitrate (NO_3^-) (filled circles) or 18.7 mM ammonium (NH_4^+) (open circles) as nitrogen source. The cultivation times were 173 h for cultures of *C. ljungdahlii* WT and *C. ljungdahlii* ΔRNF and 186 h for cultures of *C. ljungdahlii* Δ*rseC*. All cultures were grown in biological triplicates, data is given as mean values, with error bars indicating the standard deviation. **A**, growth; **B**, pH-behavior; **C**, acetate concentrations; **D**, ethanol concentration; **E**, ammonium concentration; and **F**, nitrate concentrations. WT, wild type; ΔRNF, RNF-gene cluster deletion; Δ*rseC*, *rseC* gene deletion.

We had added a small amount of yeast extract (0.1 weight-%) in all cultivation conditions (***Material and Methods***). As expected, we observed growth for *C. ljungdahlii* WT in all growth experiments (**Figure 17A, Supplementary Figure S13A**). However, the nitrogen source had a distinct influence on the growth rate, final OD_{600}, fermentation product spectrum, and pH (**Table 9, Figure 17B, Supplementary Text S1C, Supplementary Figure S13B**).

Table 9 Performance of all tested *C. ljungdahlii* strains in autotrophic batch cultivation experiments. Cultures were grown with carbon dioxide and hydrogen (autotrophy) in PETC medium, which contained either ammonium or nitrate as nitrogen source. A gas atmosphere of H_2/CO_2 (80/20 vol-%) with 0.5 bar overpressure was applied. Growth was not detected for any culture of *C. ljungdahlii* ΔRNF or *C. ljungdahlii* Δ*rseC*. Data is represented as mean values from biological triplicates ± standard deviation. WT, *C. ljungdahlii* wild type; ΔRNF, *C. ljungdahlii* with deleted *rnfCDGEAB* gene cluster; Δ*rseC*, *C. ljungdahlii* with deleted *rseC* gene; and Δ*nar, C. ljungdahlii* with deleted nitrate reductase gene cluster. CO_2, carbon dioxide; and H_2, hydrogen.

strain	nitrogen source	growth rate (μ in h)[a]	maximum OD_{600} value	maximum acetate concentration (mM)	maximum ethanol concentration (mM)
WT	ammonium	0.024±0.002	0.56±0.01	59.5±1.8	1.9±0.4
WT	nitrate	0.072±0.004	1.00±0.06	50.1±2.1	8.0±1.6
ΔRNF	ammonium	-	-	5.7±3.0	n.d.[b]
ΔRNF	nitrate	-	-	2.3±1.1	n.d.[b]
Δ*rseC*	ammonium	-	-	2.0±0.5	n.d.[b]
Δ*rseC*	nitrate	-	-	1.9±0.1	n.d.[b]
Δ*nar*	ammonium	0.018±0.001	0.44±0.01	44.8±0.2	3.3±0.2
Δ*nar*	nitrate	0.017±0.003	0.44±0.01	41.9±1.9	2.9±0.4

[a] μ values were calculated based on the individual OD_{600} values of each triplicate in the exponential growth phase.

[b] n.d., not detectable.

We found that nitrate reduction occurred rapidly in our growth experiments (**Figure 17F, Supplementary Figure S13F**). *C. ljungdahlii* WT utilized all provided nitrate within 53 h of cultivation with carbon dioxide and hydrogen (**Figure 17F**) and within 47 h of cultivation with fructose (**Supplementary Figure S17F**). The ammonium concentrations increased concomitant with decreasing nitrate concentrations when nitrate was provided in the medium (**Figure 17E, Supplementary Figure S13E**). Noteworthy, we also observed an increase in the ammonium concentration when ammonium was provided as the nitrogen source during autotrophy (**Figure 17F**). We did not measure any nitrite as an intermediate of the nitrate reduction pathway (discussed below).

In contrast, the *C. ljungdahlii* ΔRNF strain was unable to grow with carbon dioxide and hydrogen regardless of the nitrogen source (**Figure 17A**). We did not observe a pH decrease, and also not an accumulation of ethanol as a metabolic activity of non-growing cultures of *C. ljungdahlii* ΔRNF, however, some minor amounts of acetate were detected (**Figure 17B, 17C, 17D, Table 9**).

Furthermore, nitrate reduction as a metabolic activity of non-growing cultures was not detectable in *C. ljungdahlii* ΔRNF with carbon dioxide and hydrogen (**Figure 2F**). Thus, we confirmed the essential role of the RNF complex for autotrophy in *C. ljungdahlii*.

5.5.2. The deletion of the RNF complex influenced nitrate reduction during heterotrophy

For the *C. ljungdahlii* ΔRNF strain, heterotrophic growth with fructose was still possible but notably reduced (**Figure 16C, Supplementary Figure S13A**). The growth rates of *C. ljungdahlii* ΔRNF were significantly reduced by 34% (0.052 h^{-1}, $P \leq 0.001$) and by 42% (0.042 h^{-1}, $P \leq 0.001$) with ammonium and nitrate, respectively, when compared to *C. ljungdahlii* WT (**Supplementary Table S18**). The observed maximum OD_{600} values were also significantly reduced by 53% ($P \leq 0.001$) and 56% ($P \leq 0.001$) for *C. ljungdahlii* ΔRNF, respectively (**Supplementary Figure S13A**). In addition, the maximum acetate concentrations in the deletion strain were significantly reduced by 32% ($P \leq 0.001$) with ammonium and by 42% ($P \leq 0.001$) with nitrate compared to the maximum acetate concentration in the wild type. The maximum ethanol concentration was significantly reduced by 41% ($P \leq 0.001$) with fructose and ammonium, while ethanol was not produced at all by *C. ljungdahlii* ΔRNF during growth with fructose and nitrate (**Supplementary Table S18, Supplementary Figure S13C, S13D**). During heterotrophy, *C. ljungdahlii* ΔRNF was able to utilize nitrate but considerably slower when compared to *C. ljungdahlii* WT (**Supplementary Figure S13F**). At the end of the cultivation, cultures of *C. ljungdahlii* ΔRNF had only consumed 49% of the provided nitrate (**Supplementary Figure S13F**). Overall, we observed a halt in growth and metabolic activity for cultures of *C. ljungdahlii* ΔRNF with fructose after 47 h of cultivation in nitrate-containing medium and after 56 h of cultivation in ammonium-containing medium (**Supplementary Figure S13**). Fructose concentrations at the end of the cultivation remained at a concentration of 8.0-9.7 mM, which is still 30-35% of the initially provided concentration (**Supplementary Figure S13G**). The pH did not increase during heterotrophy with nitrate in *C. ljungdahlii* ΔRNF, but instead slowly decreased until the end of the cultivation (**Supplementary Figure S13B**). Notably, the final pH for heterotrophic cultures of *C. ljungdahlii* ΔRNF with nitrate was still higher compared to cultures with ammonium (**Supplementary Figure S13B**). For none of the culture samples with *C. ljungdahlii* ΔRNF during heterotrophy, decreasing ammonium concentrations were observed, even when ammonium was provided as the nitrogen source (**Supplementary Figure S13E**). Overall, we confirmed that the RNF complex plays a pivotal role for the distribution of electrons in the metabolism of *C. ljungdahlii* during heterotrophy, but that it was not essential in these conditions.

5.5.3. The *rseC* gene is essential for autotrophy in *C. ljungdahlii*

After we confirmed the indispensable role of the RNF complex for autotrophy and the influence on nitrate reduction during heterotrophy, we investigated the role of the small putative regulator gene *rseC* (CLJU_c11350), which is located directly upstream of the *rnfCDGEAB* gene cluster. A transcriptomic study with *C. ljungdahlii* had revealed that *rseC* is expressed in a similar pattern compared to *rnfC* and is highly expressed during autotrophy (Al-Bassam *et al.*, 2018). We applied our CRISPR-Cas12a system to delete the *rseC* gene from the genome (**Supplementary Figure S14A**). Next, we performed growth experiments with the generated *C. ljungdahlii* Δ*rseC* strain under the same conditions as for the *C. ljungdahlii* WT and ΔRNF strains. Cultures of *C. ljungdahlii* Δ*rseC* did not grow with carbon dioxide and hydrogen, neither with ammonium nor with nitrate, during a total cultivation time of 189 h (**Figure 17A**). Non-growing cultures for this strain did not accumulate notable concentrations of acetate or ethanol during the cultivation time (**Figure 17C, 17D**). Furthermore, we did not observe nitrate reduction or a remarkable change in pH as a metabolic activity of non-growing cultures for this strain during autotrophy (**Figure 17B, 17E, 17F**).

Heterotrophic growth of *C. ljungdahlii* Δ*rseC* was possible, and in contrast to *C. ljungdahlii* ΔRNF, the impact was less pronounced for growth with ammonium but limited to some extent with nitrate (**Supplementary Figure S13A**). Heterotrophic growth rates were increased by 6% (0.084 h^{-1}, $P = 0.08$) with ammonium and significantly reduced by 34% (0.048 h^{-1}, $P \leq 0.001$) with nitrate as nitrogen source, respectively, when compared to *C. ljungdahlii* WT under the same conditions (**Supplementary Table 18**). The maximum observed OD_{600} values for *C. ljungdahlii* Δ*rseC* were 1.90±0.15 for ammonium and 1.58±0.03 for nitrate cultures, which is a reduction of 24% ($P = 0.05$) and a significant reduction of 30% ($P \leq 0.001$) compared to the wild type. The maximum acetate concentrations of *C. ljungdahlii* Δ*rseC* were similar to those observed for *C. ljungdahlii* WT, while the maximum ethanol concentrations were significantly reduced by 29% ($P \leq 0.001$) for ammonium cultures and by 42% ($P \leq 0.001$) for nitrate cultures instead (**Supplementary Table 18, Supplementary Figure S13C, S13D**). Nitrate reduction was not restricted during heterotrophy in *C. ljungdahlii* Δ*rseC* (**Supplementary Figure S13E, S13F**). Indeed, we observed a rapid utilization of all supplied nitrate within 60 h of cultivation, which is similar to the observations that we had made for *C. ljungdahlii* WT (**Supplementary Figure S13F**). Thus, *rseC* seems to be involved in positively regulating the expression of the RNF-gene cluster during autotrophy, but not during heterotrophy. However, the exact impact on gene expression of the RNF-gene cluster cannot be deduced from these findings.

5.5.4. Plasmid-based complementation relieved the phenotypes of the *C. ljungdahlii* ΔRNF and Δ*rseC* strains

After we had characterized the *C. ljungdahlii* ΔRNF and *C. ljungdahlii* Δ*rseC* strains, we questioned whether the wild-type phenotype, particularly with respect to autotrophy, can be restored by plasmid-based gene complementation. Therefore, we generated the plasmid-carrying strains *C. ljungdahlii* ΔRNF pMTL83151_P_{nat}_*rnfCDGEAB* and *C. ljungdahlii* Δ*rseC* pMTL83152_*rseC*. The plasmids encode the RNF-gene cluster under the control of the native promoter region upstream of the *rnfC* gene from the genome (P_{nat}) in pMTL83151_P_{nat}_*rnfCDGEAB* and the *rseC* gene under the control of the constitutive thiolase promoter (P_{thl}) in pMTL83152_*rseC*, respectively. We investigated the complementation strains in ammonium-containing medium with carbon dioxide and hydrogen for growth (**Figure 18**). Indeed, the plasmid-based expression of the deleted genes relieved the phenotype and enabled autotrophy with carbon dioxide and hydrogen for both strains (**Table 10**, **Figure 18**).

Table 10 Performance of the plasmid-based complemented deletion strains of *C. ljungdahlii* in autotrophic batch cultivation experiments. Cultures were grown with carbon dioxide and hydrogen (autotrophy) in PETC medium, which contained either ammonium or nitrate as nitrogen source. A gas atmosphere of H_2/CO_2 (80/20 vol-%) with 0.5 bar overpressure was applied. Data is represented as mean values from biological triplicates ± standard deviation. The WT data from Table 1 are shown again for comparison. WT, wild type; ΔRNF, deletion of the *rnfCDGEAB* gene cluster; Δ*rseC*, deletion of the *rseC* gene; Δ*nar*, deletion of the nitrate reductase gene cluster; ΔRNF compl., complementation strain *C. ljungdahlii* pMTL83151_P_{nat}_*rnfCDGEAB*; Δ*rseC* compl., complementation strain *C. ljungdahlii* pMTL83152_*rseC*; and Δ*nar* compl., complementation strain *C. ljungdahlii* pMTL83152_*nar*.

strain	nitrogen source	growth rate (μ in h)[a]	maximum OD_{600} value	maximum acetate concentration (mM)	maximum ethanol concentration (mM)
WT	ammonium	0.024±0.002	0.56±0.01	59.5±1.8	1.9±0.4
ΔRNF compl.	ammonium	0.024±0.001	0.40±0.03	46.7±3.7	2.2±0.2
Δ*rseC* compl.	ammonium	0.022±0.002	0.66±0.03	63.2±0.2	n.d.[b]
WT	nitrate	0.072±0.004	1.00±0.06	50.1±2.1	8.0±1.6
Δ*nar* compl.	nitrate	0.054±0.001	1.54±0.03	41.7±2.5	3.4±0.5

[a] μ values were calculated based on the individual OD_{600} values of each triplicate in the exponential growth phase.

[b] n.d., not detectable.

The control strains that carried an empty plasmid failed to grow autotrophically, as we had already observed for the non-complemented deletion strains. However, *C. ljungdahlii* ΔRNF pMTL83151_P_{nat}_*rnfCDGEAB* reached only 71% (P = 0.02) of the maximum OD_{600} with ammonium when compared to the wild type, which is significantly less (**Table 10**). Furthermore, the complemented strain had a prolonged *lag* phase of 71 h (**Figure 18A**). The pH decrease occurred slower compared to the wild type (**Figure 18B**). The *C. ljungdahlii* ΔRNF pMTL83151_P_{nat}_*rnfCDGEAB* strain reached a maximum acetate concentration of 46.7±3.4 mM, which is a significant reduction of 22% (*P*

= 0.009) when compared to the wild type (**Table 10, Figure 18C**). The maximum ethanol concentration was similar in comparison to the wild type (**Figure 18D**). In contrast, the *C. ljungdahlii* Δ*rseC* pMTL83152_*rseC* strain reached a maximum OD_{600} of 0.66±0.03, which is a significant increase of 17% (*P* = 0.02) compared to the wild type (**Table 10, Figure 18A**). Instead of a prolonged *lag* phase, we observed a shortened *lag* phase for this strain when compared to the wild type (**Figure 17A, 18A**).

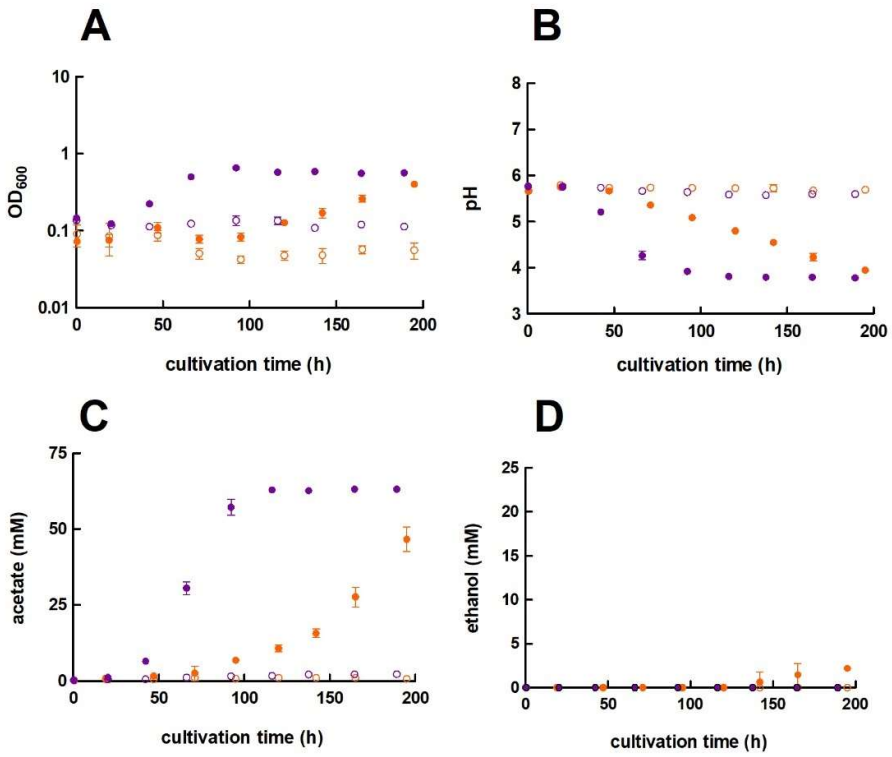

Figure 18 Growth and pH behavior of plasmid-based complementation of *C. ljungdahlii* ΔRNF and *C. ljungdahlii* Δ*rseC* with H_2 and CO_2. Cultures were grown in 100 mL PETC medium in 1 L bottles at 37°C and 150 rpm for 195 h and 189 h, respectively. The headspace consisted of H_2 and CO_2 (80/20 vol-%) and was set to 0.5 bar overpressure. Only 18.7 mM ammonium (NH_4^+) but no nitrate was added to the medium. All cultures were grown in biological triplicates, data is given as mean values, with error bars indicating the standard deviation. **A**, growth and **B**, pH-behavior of *C. ljungdahlii* ΔRNF strains. **C**, growth and **D**, pH-behavior of *C. ljungdahlii* Δ*rseC* strains. ● *C. ljungdahlii* ΔRNF pMTL83151_P_{nat}_*rnfCDGEAB*; ○ *C. ljungdahlii* ΔRNF pMTL83151; ● *C. ljungdahlii* Δ*rseC* pMTL83152_*rseC*; and ○ *C. ljungdahlii* Δ*rseC* pMTL83152. ΔRNF, rnfCDGEAB gene cluster deletion; Δ*rseC*, deletion of *rseC*; P_{nat}, native promoter sequence upstream of *rnfC*; P_{thl}, promoter of the thiolase gene in *C. acetobutylicum*; rpm, revolutions per minute; CO_2, carbon dioxide; and H_2, hydrogen.

Notably, the medium for the complementation experiments always contained antibiotics, which generally caused a slightly negative impact on growth of plasmid-carrying *C. ljungdahlii* strains such as in the *C. ljungdahlii* ΔRNF pMTL83151_P_{nat}_*rnfCDGEAB* strain. In contrast, this was not the case for the *C. ljungdahlii* Δ*rseC* pMTL83152_*rseC* strain. The complemented strain reached a maximum acetate concentration of 63.2±0.2 mM (**Figure 18C**), which is a significant increase of 6% (*P* = 0.04) when

compared to the wild type (**Table 10, Figure 17**). However, this strain did not produce any detectable ethanol during the cultivation (**Table 10, Figure 18D**). Furthermore, the pH value did not show any notable change, when compared to the wild type (**Figure 18B**).

5.5.5. Plasmid-based overexpression of the *rseC* gene enhanced autotrophic growth

We observed a growth stimulating effect in the *C. ljungdahlii* Δ*rseC* pMTL83152_*rseC* strain. To investigate whether overexpression of *rseC* in the wild-type strain increases autotrophic growth further, we generated the *C. ljungdahlii* pMTL83152_*rseC* strain. This strain carries the complementation plasmid with the constitutive P_{thl} promoter in the wild-type background. During autotrophy with carbon dioxide and hydrogen in ammonium-containing medium, the *C. ljungdahlii* pMTL83152_*rseC* strain had a shortened *lag* phase and a 13.2% faster but not significantly increased growth rate (0.21 h^{-1}, $P = 0.2$) compared to the wild type (**Figure 18A**, **Supplementary Figure S15A**). In addition, this overexpression strain reached similar maximum OD_{600} values (**Supplementary Figure S15A**). The maximum acetate concentration was significantly reduced by 22% ($P \leq 0.001$), and ethanol was not produced (**Supplementary Figure S15C, S15D**).

We also attempted to generate a plasmid that carries the *rnfCDGEAB* gene cluster under the control of a constitutive promoter. However, any attempts to generate a fusion of the constitutive promoter P_{thl} with the *rnfCDGEAB* gene cluster failed already during the cloning steps in *E. coli*. Thus, for the expression of *rnfCDGEAB* in the wild type, we also used the native P_{nat} promoter sequence, which most likely is under the same expression control as the genomic copy of the RNF-gene cluster. Not surprisingly, the cultivation of *C. ljungdahlii* pMTL83151_P_{nat}_*rnfCDGEAB* did not show any notable impact on growth and product formation when compared to the control strain that carried an empty plasmid (**Supplementary Figure S15**).

5.5.6. The gene expression profiles of *rnf* genes and the *rseC* gene in the deletion strains revealed regulatory effects

We had found that autotrophy was abolished in the *rseC* deletion strain, while heterotrophy was not impacted. Thus, we further investigated the activating or repressing function on the gene expression of the RNF-gene cluster by RseC. For this, we performed qRT-PCR analyses to investigate the individual expression profiles of the genes *rnfC, rnfD, rnfG, rnfE, rnfA, rnfB*, and *rseC* in the *C. ljungdahlii* Δ*rseC* strain. We included the *C. ljungdahlii* ΔRNF and *C. ljungdahlii* WT strains as controls (***Materials and Methods***). We analyzed samples after 3 h and 20 h of cultivation time to investigate the transcriptomic response after inoculating the autotrophic and heterotrophic main cultures from heterotrophic pre-cultures. During the cultivation of the six main cultures (three strains, two conditions), *C. ljungdahlii*

WT grew during autotrophy and heterotrophy, while *C. ljungdahlii* ΔRNF and *C. ljungdahlii* Δ*rseC* only grew during heterotrophy.

The qRT-PCR results in this paragraph are given as $\log_2$ (fold change in gene expression), where a value of ≤ -1 (0.5-fold) refers to a significant downregulation, and a value of ≥ +1 (2-fold) refers to a significant upregulation (**Figure 19**). We did not measure any expression signals for any of the deleted RNF genes in the *C. ljungdahlii* ΔRNF strain and for the deleted *rseC* gene in the *C. ljungdahlii* Δ*rseC* strain. We found that all RNF-gene cluster genes were significantly downregulated (ranging from -1.8 to -4.7) in the *C. ljungdahlii* Δ*rseC* strain, when cultivating non-growing cells of this strain autotrophically with hydrogen and carbon dioxide (**Figure 19**).

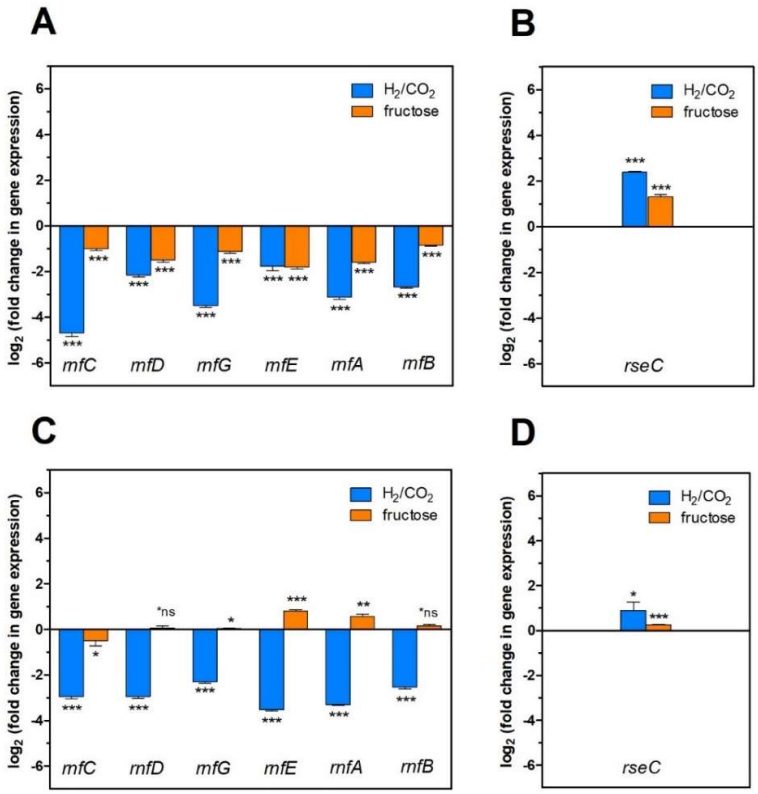

Figure 19 Gene expression change of the *rnfCDGEAB* cluster genes and the *rseC* gene in the ΔRNF and Δ*rseC* deletion strains. A, gene expression change for the genes *rnfC*, *rnfD*, *rnfG*, *rnfE*, *rnfA*, and *rnfB* in strain *C. ljungdahlii* Δ*rseC* after 3h cultivation time; **B**, gene expression change for the gene *rseC* in strain *C. ljungdahlii* ΔRNF after 3 h cultivation time; **C**, gene expression change for the genes *rnfC*, *rnfD*, *rnfG*, *rnfE*, *rnfA*, and *rnfB* in strain *C. ljungdahlii* Δ*rseC* after 20 h cultivation time; and **D**, gene expression change for the gene *rseC* in strain *C. ljungdahlii* ΔRNF after 20 h cultivation time. RNA samples were purified from cultures that were cultivated either autotrophically with hydrogen and carbon dioxide (blue bars) or heterotrophically with fructose (orange bars). cDNA was synthesized from the purified RNA samples and used as template for qRT-PCR analyses. The individual gene expression profiles of each gene was calculated using the wild-type strain as reference, which was grown under the same conditions. The *rho* gene was used as "housekeeping" gene. The fold change in gene expression was determined with the $2^{-\Delta\Delta CT}$ method (Livak and Schmittgen, 2001). ***, $P \leq 0.001$; **, $P \leq 0.01$; *, $P \leq 0.05$; *ns, not significant ($P > 0.05$). We defined $\log_2$ (fc) ≤ -1 as downregulated genes and ≥ +1 as upregulated genes.

We observed a similar pattern of downregulation for the 3-h and 20-h samples of the *C. ljungdahlii* Δ*rseC* strain (**Figure 19A, 19C**). In the heterotrophic samples, all RNF-gene cluster genes, except of *rnfB*, were significantly downregulated in the 3-h samples (ranging from -1.0 to -1.8). However, after 20 h of cultivation time during heterotrophy, we observed a less pronounced but still significant downregulation of the *rnfC* gene, while all other genes were either not significantly different from the wild type (*rnfD*) or significantly upregulated (**Figure 19**). In the *C. ljungdahlii* ΔRNF strain as a control, we found that *rseC* expression was significantly upregulated in the 3-h samples during autotrophy (+2.4) and during heterotrophy (+1.3) (**Figure 19B**). The upregulation was less pronounced but still significant after 20 h of cultivation (**Figure 19D**). For the wild type, all genes (except for *rnfE* in the 3-h sample) were significantly upregulated during autotrophy when compared to heterotrophy for the 3-h samples (ranging from +1.0 to +5.4), and for the 20 h samples (ranging from +2.8 to +3.8), respectively (**Supplementary Figure S16**). Thus, RseC positively regulated the RNF-gene cluster during autotrophy, but not during heterotrophy.

5.5.7. The *rseC* gene is abundantly found among acetogens

While *rseC* was annotated as a putative transcriptional regulator, the regulatory function was not known. We had found in our cultivation experiments and qRT-PCR analyses that the *rseC* gene plays a critical role for the function of the RNF complex, and thus for autotrophy. We investigated whether *rseC* genes are also present in genomes of other microbes that possess RNF complex genes. Indeed, we found putative *rseC* genes in the genomes of *C. ljungdahlii*, *Clostridium autoethanogenum, A. woodii*, *Eubacterium limosum, Clostridium carboxidovorans, Clostridium kluyveri, R. capsulatus,* and *E. coli*. On the contrary, we did not find a putative *rseC* gene in the genome of *Moorella thermoacetica* or *Thermoanaerobacter kivui,* which possess an energy-converting hydrogenase (Ech) complex instead of an RNF complex (Hess *et al.*, 2014). Next, we took a detailed look at the genomic location and distance to the RNF-gene cluster (**Figure 20**). We noticed that the *rseC* gene was located directly upstream of the RNF complex gene cluster in *C. ljungdahlii* (CLJU_c11350), *C. autoethanogenum* (CAETHG_3225), *C. carboxidovorans* (Ccar_25725), and *C. kluyveri* (CKL_1263). The *rseC* gene in *A. woodii* (Awo_C21740) and *E. limosum* (B2M23_08890), however, was not in direct genetic vicinity of the RNF-gene cluster. Furthermore, we identified a second gene with homologies to *rseC* in *C. carboxidovorans* (Cca_07835) and *C. kluyveri* (CKL_2767), but neither RNF complex genes nor other genes that are involved in the autotrophic metabolism, such as the genes for the Wood-Ljungdahl pathway, are located in the direct vicinity of this second *rseC* homolog (**Table 11**). Notably, we also identified a *rseC* gene in the non-acetogenic bacterium *R. capsulatus*, which is the microbe in which the RNF complex was first described (Schmehl *et al.*, 1993). The *rseC* gene in *R. capsulatus* is located upstream of *rnfF* instead of *rnfC*, which is separated by five genes (**Figure 20**).

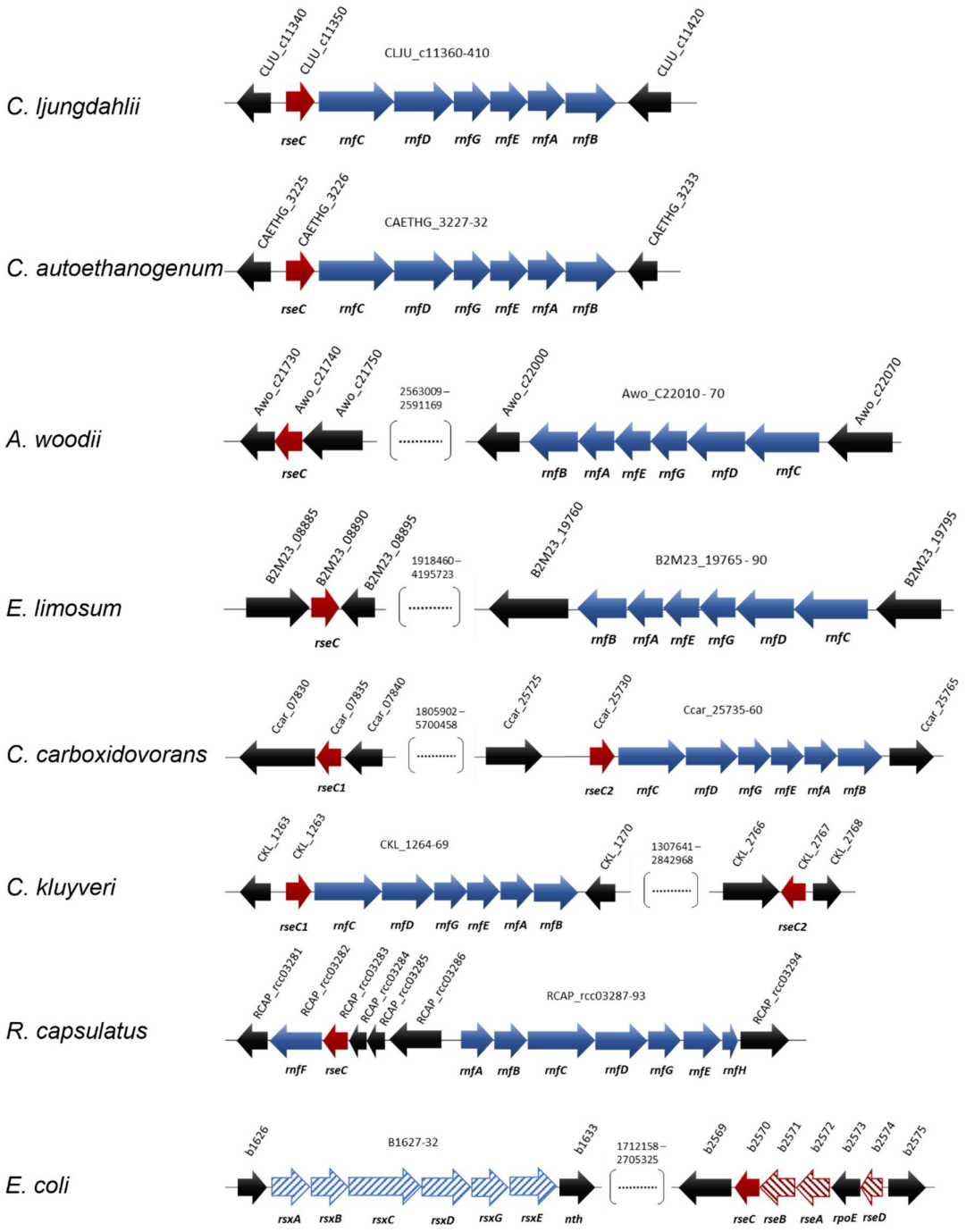

Figure 20 Location and orientation of *rseC* genes in microbes that possess RNF complex gene clusters. The conserved protein domain RseC_MucC (pfam04246) was identified in the *rseC* protein sequence of *C. ljungdahlii* and used to search for putative *rseC* genes in the genome of *C. autoethanogenum, A. woodii*, *E. limosum, C. carboxidovorans, C. kluyveri, R. capsulatus,* and *E. coli*. All sequence analyses and gene arrangements were adapted from the JGI platform and the NCBI database (03/2021). The type strains are listed in Table 3. In red, putative *rseC* genes; in red pattern fill, *rseC*-associated genes in *E. coli*; in blue, RNF-complex gene cluster; in blue pattern fill, *rsx* genes, which are homologous to the *rnf* genes in *R. capsulatus*.

Also *E. coli* possesses one *rseC* gene that is organized in the *rseABC* gene cluster (**Figure 20, Supplementary Text S1D**) (Koo *et al.*, 2003). The conservation of the RseC amino-acid sequence was between 59% and 100% for *C. ljungdahlii*, *C. autoethanogenum*, *C. carboxidovorans,* and *C. kluyveri*, which is a high similarity (**Supplementary Table S19, Supplementary Figure S16**). In addition, the amino-acid sequence length is nearly identical with 138 amino acids (*C. ljungdahlii*, *C. autoethanogenum*, and *C. carboxidovorans*) and 137 amino acids (*C. kluyveri*), respectively.

Table 11 Distribution of *rseC* genes.

microbe[a]	amount of *rseC* genes[b]	RNF or Ech	*rseC* associated with RNF genes	gene locus
Clostridium ljungdahlii	1	RNF[c]	yes	CJLU_c11350
Clostridium autoethanogenum	1	RNF[c]	yes	CAETHG_3226
Clostridium carboxidovorans	2	RNF[c]	yes, one of them	Ccar_07835, Ccar_025730
Clostridium kluyveri	2	RNF[c]	yes, one of them	CKL_1263, CKL_2767
Eubacterium limosum	1	RNF[d]	no	B2M23_08890
Acetobacterium woodii	1	RNF[d]	no	Awo_c21740
Thermotoga maritima	1	RNF[d]	no	THEMA_1487
Moorella thermoacetica	0	Ech	no	-
Thermoanaerobacter kivui	0	Ech	no	-
Rhodobacter capsulatus	1	RNF[e]	yes	RCAP_rcc03283
Escherichia coli	1	Rsx[f]	no, but with Rsx	b2570

[a] The type strains were: *C. ljungdahlii* DSM13528; *C. autoethanogenum* DSM10061; *C. carboxidovorans* P7; *C. kluyveri* DSM555; *E. limosum* ATCC8486; *A. woodii* DSM1030; *T. maritima* DSM3109; *M. thermoacetica* ATCC39073; *T. kivui* DSM2030; *R. capsulatus* SB1003; and *E. coli* K-12.

[b] The pfam domain pfam04426 was used to search for putative *rseC* genes in each genome.

[c] The RNF complex uses (or is supposed to use) protons.

[d] The RNF complex uses (or is supposed to use) sodium ions.

[e] The RNF complex either uses protons or sodium ions. Experimental data are missing.

[f] Rsx is encoded by *rsxABCDGE* and is homologous to the RNF-gene cluster in *R. capsulatus.*

The second RseC homolog from *C. carboxidovorans* and *C. kluyveri* shared an identity of 65% with each other, but only between 25% and 49% to all other RseC proteins (**Supplementary Table S19, Supplementary Figure S17**). The RseC from *A. woodii* and *E. limosum* shared a similarity of 57% with each other, and only of 34% to 35% with the RseC proteins that are encoded directly upstream of the RNF-gene clusters (**Figure 20, Supplementary Table S19, Supplementary Figure S17**). The RseC proteins from *R. capsulatus* and *E. coli* have the same amino-acid sequence length (159 amino acids), but shared low similarities to each other (31%) as well as to the RseC proteins from the other microbes (18-34%) (**Supplementary Table S19, Supplementary Figure S17**). The similarity of the RseC protein

from *C. ljungdahlii* and *R. capsulatus* was only 23%, while it was 36% for the RseC protein from *C. ljungdahlii* in comparison to the RseC protein from *E. coli*. Overall, the RseC protein sequence seems to be highly conserved in acetogens that contain an RNF-gene cluster.

5.5.8. The *nar* gene cluster encodes a functional nitrate reductase in *C. ljungdahlii*

We had found that nitrate reduction during heterotrophy is impacted for the *C. ljungdahlii* ΔRNF strain but not the *C. ljungdahlii* Δ*rseC* strain. Thus, we aimed to explore nitrate metabolism and the interplay with the RNF complex further. For *C. ljungdahlii*, it was postulated that nitrate is reduced by nitrate reductase to nitrite and, subsequently, converted *via* nitrite reductase and hydroxylamine reductase into ammonium, and the involved genes were predicted in the genome (Köpke *et al.*, 2010; Nagarajan *et al.*, 2013). Emerson *et al.* (2019) had found that in the presence of nitrate the expression level of the genes that encode the putative nitrate reductase (CLJU_c23710-30) were significantly increased. The three genes are annotated as nitrate reductase NADH oxidase subunit (CLJU_c23710), nitrate reductase electron transfer subunit (CLJU_c23720), and nitrate reductase catalytic subunit (CLJU_c23730) (Köpke *et al.*, 2010). We refer to these three genes (CLJU_c23710-30) as the *nar* gene cluster. We verified the absence of the *nar* gene cluster from the genome of the *C. ljungdahlii* Δ*nar* strain, after mediating the deletion with our CRISPR-Cas12a system (**Supplementary Figure S14B**). This strain was able to grow during autotrophy and heterotrophy, but had completely lost the ability to reduce nitrate under both conditions (**Figure 21F**, **Supplementary Figure S18F**). We observed similar growth and pH behavior for cultures of *C. ljungdahlii* Δ*nar* during autotrophy with either ammonium or nitrate (**Figure 21A, 21B**). Enhanced autotrophic growth in nitrate-containing medium when compared to ammonium-containing medium, such as with the wild-type strain, was not detected (**Figure 21A**). However, we still observed differences in the growth when compared to *C. ljungdahlii* WT. Growth rates during autotrophy of *C. ljungdahlii* Δ*nar* were 0.018 h^{-1} for ammonium- and 0.017 h^{-1} for nitrate-containing medium, which is a significant reduction of 24% ($P = 0.04$) and 76% ($P \leq 0.001$) in comparison to the wild type (**Table 9**). The maximum observed OD_{600} values were both 0.44±0.01, which is a significant decrease of 21% ($P \leq 0.001$) for ammonium cultures and 55% ($P = 0.002$) for nitrate cultures when compared to the wild type (**Figure 21A**). A pH increase as a consequence of ammonium production, such as observed for the wild type, was not observed in cultures of *C. ljungdahlii* Δ*nar* (**Figure 21B**). The maximum acetate concentrations were significantly reduced by 25% (44.8±0.2 mM, $P \leq 0.001$) for ammonium cultures and by 16% (41.9±1.9 mM, $P = 0.01$) for nitrate cultures of *C. ljungdahlii* Δ*nar* (**Figure 21C, Table 9**). The maximum ethanol concentrations were significantly increased by 79% (3.3±0.2 mM, $P = 0.02$) and significantly decreased by 64% (2.9±0.4 mM, $P = 0.02$) for ammonium and for nitrate conditions with carbon dioxide and hydrogen, respectively

(**Figure 21D, Table 9**). Even though *C. ljungdahlii* Δ*nar* was not able to use nitrate, cultures still accumulated 3-4 mM ammonium until the end of the cultivation in nitrate-containing medium (**Figure 21E**).

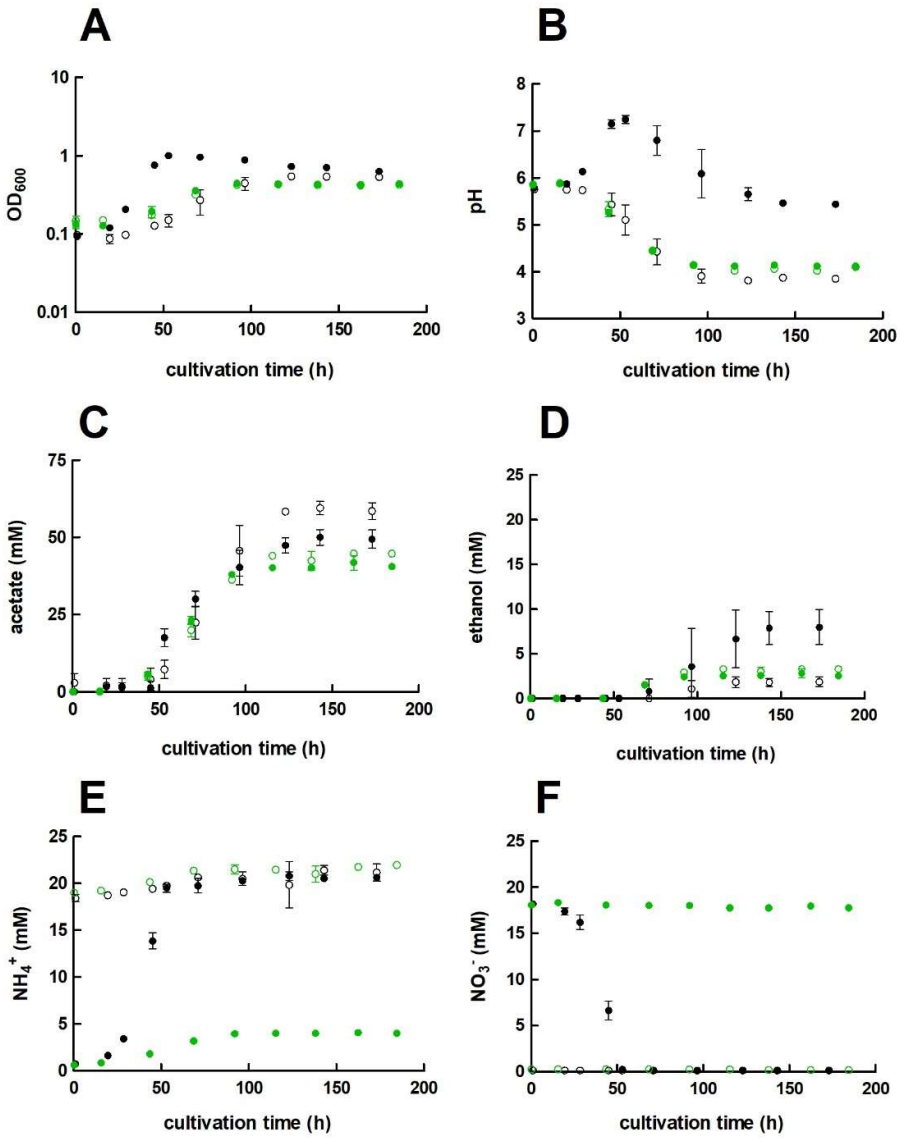

Figure 21 Growth, pH behavior, nitrate reduction of *C. ljungdahlii* Δ*nar* with H_2 and CO_2. Cultures were grown in 100 mL PETC medium in 1 L bottles at 37°C and 150 rpm for 185 h. The headspace consisted of H_2 and CO_2 (80/20 vol-%) and was set to 0.5 bar overpressure. The medium contained either 18.7 mM nitrate (NO_3^-) (●) or 18.7 mM ammonium (NH_4^+) (○) as nitrogen source. The *C. ljungdahlii* WT data (●, ○) from Supplementary Figure S1 is given for comparison. All cultures were grown in biological triplicates, data is given as mean values, with error bars indicating the standard deviation. **A**, growth; **B**, pH-behavior; **C**, acetate concentrations; **D**, ethanol concentration; **E**, ammonium concentration; and **F**, nitrate concentrations. Δ*nar,* deletion of nitrate reductase gene cluster; rpm, revolutions per minute; CO_2, carbon dioxide; and H_2, hydrogen.

The growth rates for heterotrophic cultures were 0.071 h^{-1} for ammonium- and 0.067 h^{-1} for nitrate containing medium (**Supplementary Table S18**). The maximum observed OD_{600} value was 2.35±0.04 for ammonium cultures of *C. ljungdahlii* Δ*nar*, which is similar to the performance of *C. ljungdahlii* WT (**Supplementary Figure S18A**). For nitrate cultures the maximum observed OD_{600} value was 1.51±0.03 and corresponds to a significant reduction of 32% ($P \leq 0.001$) when compared to *C. ljungdahlii* WT under the same conditions (**Supplementary Figure S18A**). The maximum acetate concentrations were 51.9±0.9 mM for ammonium- and 28.7±1.1 for nitrate-containing medium, which is a reduction of 1% ($P = 0.6$) and a significant reduction of 34% ($P \leq 0.001$), respectively (**Supplementary Figure S18C**). Interestingly, the maximum ethanol concentrations for *C. ljungdahlii* Δ*nar* significantly increased by 45% (15.3±0.1 mM, $P \leq 0.001$) when ammonium and fructose were provided, and by 234% (16.6±0.2, $P \leq 0.001$) when nitrate and fructose were provided (**Supplementary Table S18, Supplementary Figure S18D**). The provided fructose was only consumed completely by *C. ljungdahlii* Δ*nar* in ammonium-containing but not in nitrate-containing medium (**Supplementary Figure S18G**).

Finally, we confirmed that the complementation of *C. ljungdahlii* Δ*nar* with the plasmid pMTL83152_*nar*, which encodes the *nar* gene cluster under the expression control of the constitutive P_{thl} promoter, enabled the *C. ljungdahlii* Δ*nar* pMTL83152_*nar* strain to utilize nitrate under autotrophic conditions again, while this was not possible in an empty plasmid control strain (**Supplementary Figure S19**). The nitrate cultures of *C. ljungdahlii* Δ*nar* pMTL83152_*nar* reached a growth rate of 0.054 h^{-1} and maximum observed OD_{600} values of 1.54±0.03, which is a significant reduction of 26% ($P = 0.004$) and a significant increase of 54% ($P \leq 0.001$) in comparison to the wild type when growing with nitrate (**Table 10**). Maximum acetate concentrations were 41.7±2.5 mM, while maximum ethanol concentrations were 3.4±0.5 mM (**Supplementary Figure S19C, S19D**). This is a significant reduction of 17% ($P = 0.02$) and of 57% ($P \leq 0.001$) in contrast to the nitrate-grown cultures of *C. ljungdahlii* WT (**Table 10**). Therefore, we revealed that the expression of the *nar* gene cluster led to the only functional nitrate reductase in *C. ljungdahlii* under the tested conditions.

5.6. Discussion

A functional RNF complex is essential for autotrophy but not for heterotrophy in *C. ljungdahlii*

Here, we provided further insight into the autotrophy of *C. ljungdahlii* and the connection to nitrate metabolism. With the strain *C. ljungdahlii* ΔRNF, we confirmed that the absence of the RNF complex leads to a complete loss of autotrophy in *C. ljungdahlii*. Unlike in a previous study by Tremblay *et al.* (2012), this strain provides a stable genotype that cannot revert back to the wild-type genotype, which can be used to further study the energy conservation principles in this acetogen (**Figure 16B, 17**). Heterotrophic growth in this strain was still possible, but considerably reduced when compared to the

wild type (**Figure 16C, Supplementary Figure S13**). While we did not measure the difference in the headspace gas composition during heterotrophy for *C. ljungdahlii* ΔRNF and wild type, we argue that *C. ljungdahlii* ΔRNF lost the ability to fixate the carbon dioxide that is released during glycolysis, which is the defining feature of acetogens (Drake *et al.*, 2008; Schuchmann and Müller, 2014). Thus, even though the Wood-Ljungdahl pathway was still present, this strain was not able to balance the electrons in the metabolism to drive the Wood-Ljungdahl pathway. Further research is required to confirm this hypothesis. The RNF deletion in *A. woodii* did also lead to reduced acetate production during heterotrophy, but the strain reached similar OD_{600} values compared to the *A. woodii* wild type (Westphal *et al.*, 2018). In comparison to *C. ljungdahlii*, the RNF complex of *A. woodii* uses sodium ions instead of protons to generate the chemiosmotic gradient, which is then consumed by a sodium-dependent F_1F_O ATPase to generate ATP (Biegel and Müller, 2010; Hess *et al.*, 2013). Overall, this further confirms the meticulous differences in the energy conservation and redox balancing in different acetogens (Katsyv and Müller, 2020), which have to be considered to apply acetogens for biotechnological purposes.

RseC is a positive regulator of the RNF complex genes and plays a critical role during autotrophy

We further investigated the regulation of the RNF-gene cluster by the putative regulator RseC. The *rseC* gene is known to encode a transcriptional regulator in other microbes such as *E. coli* and *S. typhimurium* (**Supplementary Text S1D**) (Beck *et al.*, 1997; De Las Peñas *et al.*, 1997; Yura and Nakahigashi, 1999; Koo *et al.*, 2003). Our results demonstrated that RseC played a critical role for the formation of a functional RNF complex in *C. ljungdahlii* (**Table 10, Figure 17**). A deletion of the *rseC* gene led to the complete loss of autotrophy (**Figure 17**). With our qPCR analyses, we confirmed that RseC, indeed, had a positive regulatory effect on the expression of the RNF-gene cluster during autotrophy. Our results indicate that RseC is essential for the activation of RNF-gene cluster expression during autotrophy, but not during heterotrophy, while we cannot rule out other modulating activities (**Figure 19A, 19C, 22, Supplementary Figure S16, Supplementary Text S1E**). Further biochemical and molecular biological investigations, such as the purification of the RseC protein and DNA-binding assays, or the study of the subcellular localization, will be required to unravel the regulatory functions of RseC in *C. ljungdahlii* and other acetogens with an RNF complex in more detail.

Nitrate reduction does not require a functional RNF complex but benefits from a correct electron balance

Furthermore, we investigated the nitrate metabolism in *C. ljungdahlii*. We confirmed that the genes CLJU_c23710-30 encode the functional subunits of the only nitrate reductase under the tested conditions for *C. ljungdahlii* (**Figure 21, Supplementary Figure S14, S18**). In the presence of nitrate,

C. ljungdahlii WT quickly utilized all nitrate even though a sufficient amount of nitrogen-source was covered by the added yeast extract (**Figure 17F, Supplementary Figure S13F**). Thus, nitrate reduction in *C. ljungdahlii* is mainly used for energy conversion, and therefore must be of a dissimilatory function (Emerson *et al.*, 2019) (**Supplementary Text S13F**). The stoichiometry for nitrate reduction in *C. ljungdahlii* is proposed as follows: 4 H_2 + 2 H^+ + NO_3^- + 1.5 ADP + 1.5 P_i ⇌ 4 H_2O + NH_4^+ + 1.5 ATP with $\Delta_rG'_0$ = -150 kJ/mol H_2 (Thauer *et al.*, 1977; Emerson *et al.*, 2019). This mechanism would require electron bifurcation from the hydrogenases and the activity of the RNF complex, but would then provide ATP completely independent of the Wood-Ljungdahl pathway (or more general, independent of the carbon metabolism) (Buckel and Thauer, 2018; Emerson *et al.*, 2019). Thus, we hypothesized that nitrate reduction in *C. ljungdahlii* requires a functional RNF complex for a correct electron balance. Indeed, non-growing cells of both *C. ljungdahlii* ΔRNF and *C. ljungdahlii* Δ*rseC* were not able to reduce nitrate during autotrophy (**Figure 17F**). However, nitrate reduction still proceeded in both deletion strains during heterotrophy (**Supplementary Figure S13F**). In *C. ljungdahlii* ΔRNF a functional RNF complex was not present during heterotrophy because the RNF-complex encoding genes were deleted, but the required reducing equivalents for nitrate reduction were likely provided by glycolysis (**Figure 22**). In contrast, in *C. ljungdahlii* Δ*rseC*, nitrate reduction was not impacted during heterotrophy, because the RNF complex genes were not repressed under these conditions and a functional RNF complex was formed (**Figure 19, 22**). It remains to be answered whether there is a direct interplay between the nitrate reductase and the RNF complex, and whether this interplay is different during heterotrophy and autotrophy.

The electron balance in the deletion strains is impacted beyond nitrate reduction

In general, the reduced growth indicated that *C. ljungdahlii* ΔRNF was not able to balance the electrons from glycolysis efficiently during heterotrophy. This led to the reduction in biomass and acetate production, while ethanol production was completely absent in heterotrophic cultures of *C. ljungdahlii* ΔRNF, which indicates that reducing power for a further reduction of acetate was not available (**Supplementary Table S18, Supplementary Figure S13D**). In the batch experiments of Emerson *et al.* (2019), *C. ljungdahlii* WT did not produce considerable amounts of ethanol when growing with nitrate (and carbon dioxide and hydrogen). When *C. ljungdahlii* WT was cultivated in pH-controlled bioreactors under continuous conditions, enhanced biomass and increased ethanol production rates were observed (Klask *et al.*, 2020). This observation could not be fully explained yet, but it was assumed that electrons are predominantly used for the reduction of nitrate rather than for the reduction of acetate. This distribution of electrons changed in the absence of the nitrate reductase in the *C. ljungdahlii* Δ*nar* strain and higher maximum ethanol concentrations were observed (**Supplementary Text S1G**).

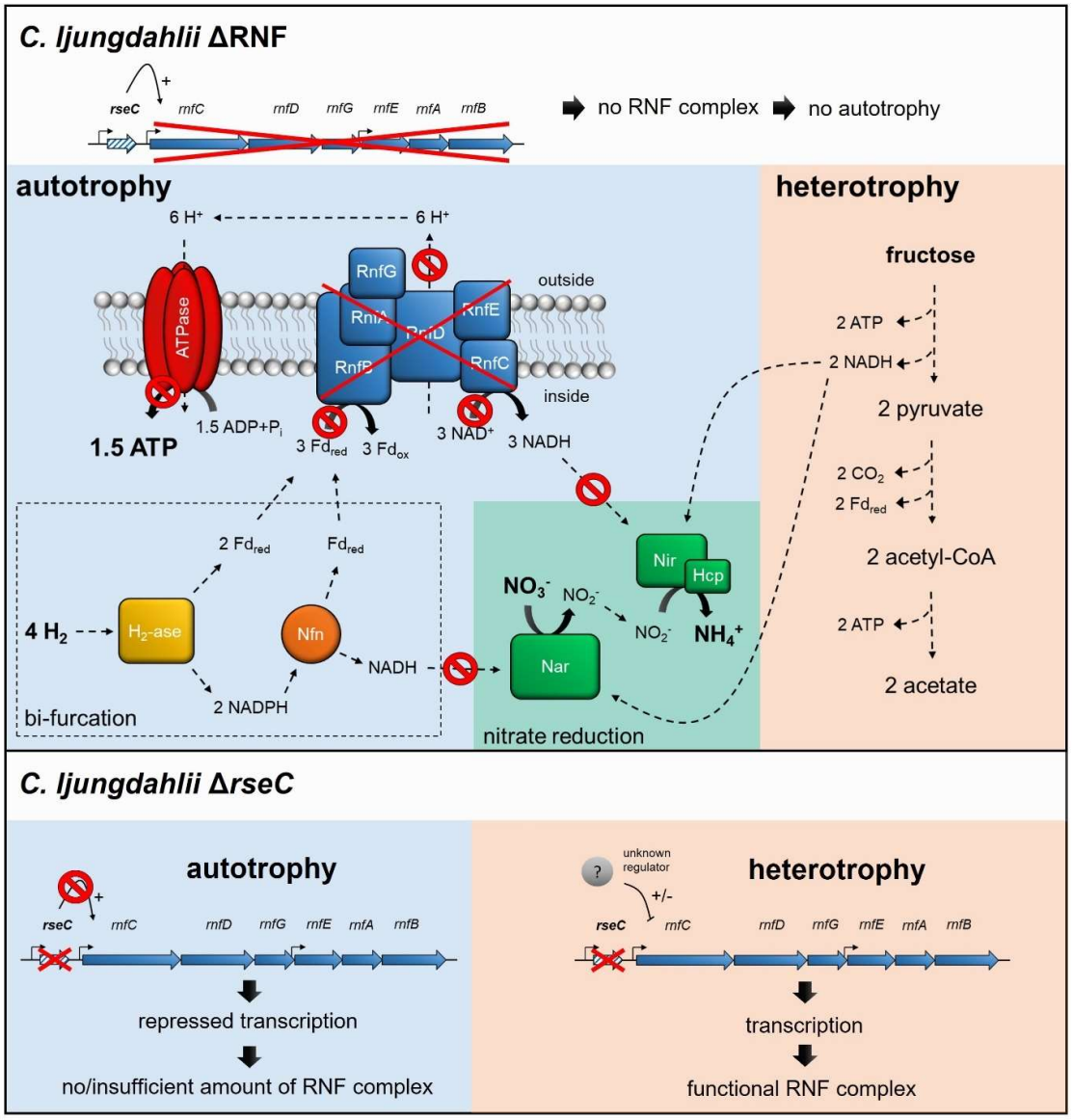

Figure 22 Schematic model of RNF-gene regulation and nitrate reduction in the deletion strains *C. ljungdahlii* ΔRNF and *C. ljungdahlii* Δ*rseC* during autotrophy and heterotrophy. In both deletion strains, nitrate reduction is not possible in non-growing cells during autotrophy with carbon dioxide and hydrogen due to the lack of a functional RNF complex, and thus the missing regeneration of reducing equivalents such as NADH. On the contrary, nitrate reduction can proceed in *C. ljungdahlii* ΔRNF during heterotrophy with NADH, which is provided by glycolysis of fructose. In *C. ljungdahlii* Δ*rseC*, the RNF complex genes are repressed during autotrophy but not during heterotrophy, which indicates a further unknown regulation mechanism during heterotrophy. Thus, a functional RNF complex is formed, and nitrate reduction can proceed such as proposed for the wild type. Abbreviations: H_2, hydrogen; H^+, proton, CO_2, carbon dioxide; NO_3^-, nitrate; NO_2^-, nitrite; NH_4^+, ammonium; ATP, adenosine triphosphate; ADP + P_i, adenosine diphosphate + phosphate; $Fd_{red/ox}$, reduced/oxidized ferredoxin; NADH/NAD^+, reduced/oxidize nicotinamide adenine dinucleotide; NADPH/$NADP^+$, reduced/oxidized nicotinamide adenine dinucleotide phosphate; RnfCDGEAB, RNF-complex subunits; Nar, nitrate reductase; Nir, nitrite reductase; Hcp, hydroxylamine reductase; H_2-ase, bifurcating hydrogenase/lyase; Nfn, bifurcating transhydrogenase; e^-, electron; ΔRNF, *C. ljungdahlii* ΔRNF; and Δ*rseC*, *C. ljungdahlii* Δ*rseC*. The model was adapted from Emerson *et al.* (2019).

It remains elusive, how the change in the distribution of electrons affects other NADH-dependent metabolic pathways in more detail. While further research is required to understand the regulatory mechanisms during autotrophy and the mechanism of energy conservation during nitrate reduction, with this work, we provide a deeper insight into the autotrophic metabolism and nitrate reduction in *C. ljungdahlii*.

5.7. Acknowledgement

This work was funded through the Alexander von Humboldt Foundation in the framework of the Alexander von Humboldt Professorship, which was awarded to L.T.A. We are also thankful for additional funding to L.T.A. and B.M. from the Deutsche Forschungsgemeinschaft (DFG, German Research Foundation) under Germany's Excellence Strategy – EXC 2124 – 390838134. The plasmid pMTL2tet01gusA was kindly provided by Dr. Gregory Stephanopoulos (Department of Chemical Engineering, Massachusetts Institute of Technology). We acknowledge support by the DFG and Open Access Publishing Fund of the University of Tübingen. We thank Dr. Peng-Fei Xia (Environmental Biotechnology Group, University of Tübingen) for his advice for the CRISPR design and Franziska Schädler (Geomicrobiology and Microbial Ecology, University of Tübingen) for her support with the nitrate and ammonium measurements. We thank Nicole Smith (Environmental Biotechnology Group, University of Tübingen) for her support in medium preparations.

5.8. Supporting information

Supporting information is provided in the Appendix (**8.3.**) and contains additional results and further explanations. The six supplementary table provide information for all used plasmids and sequences. The seven supplementary figures show graphs for further cultivation experiment and more detailed information about the *in-silico* research and qPCR results.

CHAPTER 6

SYNTHESIS OF CYANOPHYCIN IN RECOMBINANT STRAINS OF *CLOSTRIDIUM LJUNGDAHLII*

Klask, C.M., Ernst, M., Lemke, S., Angenent L.T. and Molitor, B. Synthesis of cyanophycin in recombinant strains of *Clostridium ljungdahlii*. Preliminary manuscript.

6.1. Author's contribution

Christian-Marco Klask (C.M.K.) and Bastian Molitor (B.M.) designed the experiments. C.M.K. performed the genetic work. Sylvia Lemke (S.L.) supported the genetic work as part of her Bachelor thesis. C.M.K. conducted the bioreactor and growth experiments. Marco Ernst (M.E.) performed the biochemical work, and the purification and analyses of the cyanophycin, while C.M.K. supervised this work. C.M.K. and M.E. evaluated the experimental data. C.M.K. wrote the preliminary manuscript. Largus T. Angenent (L.T.A.) and B.M. supervised the project and revised the written text.

6.2. Abstract

Acetogenic bacteria are well-known for their capability to convert gaseous one-carbon molecules into biofuels such as bioethanol. The implementation of alternative metabolic pathways (*e.g.,* through genetic engineering) is used to expand the product range. This is often restricted by the fundamental energy limitations in the acetogenic metabolism. For instance, the acetogenic bacterium *C. ljungdahlii* conserves only a maximum of 0.63 ATP/mol H_2 when growing with hydrogen and carbon dioxide. Therefore, ATP-demanding heterologous pathways, which are implemented in recombinant strains of this microbe must compete with basal metabolism of the cell for the limited amount of available ATP. A recent study has shown that *C. ljungdahlii* can gain up to 1.5 ATP/mol H_2 when co-utilizing nitrate and carbon dioxide with hydrogen. In this process, nitrate is reduced *via* nitrite as an intermediate into ammonium, while carbon dioxide is used for the carbon metabolism. The exact mechanism on how this nitrate reduction is linked to the energy metabolism is not understood yet. However, wild type *C. ljungdahlii* uses the extra ATP gain from nitrate reduction for an enhanced biomass production. Since biomass is a low-value product of a gas fermentation with acetogens, a re-direction of the ATP from the reduction of nitrate into a more valuable product would be of great interest.

In this study, we report the implementation of a cyanophycin (CGP) synthesis pathway in *C. ljungdahlii* by constitutively overexpressing *cphA* genes. We provided nitrate as alternative electron acceptor to overcome the energy limitations of the acetogenic metabolism. CGP is synthesized by a single enzyme

called cyanophycin synthetase, which links arginine to a poly-aspartic backbone under the consumption of 2 ATP per cycle. The constitutive overexpression of the *cphA* gene from the cyanobacterium *Anabaena* sp. resulted in a high cyanophycin accumulation in a recombinant *E. coli* strain, which was used for cloning. However, neither this gene nor the constitutive overexpression of the native *cphA* gene, which is found in the genome of *C. ljungdahlii* enabled detectable CGP synthesis in *C. ljungdahlii*. We discuss the possible reasons for the CGP synthesis limitation and provide recommendations for future experiments.

6.3. Introduction

During the past years, gas fermentation with acetogenic bacteria (acetogens) has been developed into a promising technology to convert C1 gases, such as carbon monoxide (CO) and CO_2, into valuable bio-chemicals (Latif *et al.*, 2014; Phillips *et al.*, 2017). Gas fermentation with acetogens reduces the CO_2 footprint of the chemical bioproduction, and thus provides a suitable and sustainable way to combine industrial interest with the global fight against rising CO_2 emissions (Dürre, 2017; Takors *et al.*, 2018). First commercial plants, such as developed by the company LanzaTech, showed that this technology can produce bioethanol at industrial scale with minimal CO_2 emissions using off-gas streams from steel mills. Besides drop-in fuels, such as bioethanol, research is conducted to further optimize acetogenic bacteria (*e.g.,* with genetic engineering) to expand the fermentation product range (Humphreys and Minton, 2018). However, only a few alternative fermentation products have exceeded the laboratory level and further optimization is required (Molitor *et al.*, 2017). In addition to genetic engineering, acetogens are combined with other wild-type microbes in defined co-cultures or two-stage bioprocessing systems to expand the product range (Diender *et al.*, 2016; Richter *et al.*, 2016a; Benito-Vaquerizo *et al.*, 2020; Cui *et al.*, 2020). Such a concept was developed in which gas fermentation of acetogens is combined in a two-stage system with the growth of yeast for the production of single-cell protein as a source of human food (Molitor *et al.*, 2019; Mishra *et al.*, 2020). In this concept, the acetogenic bacteria produce the natural fermentation product acetate form hydrogen (H_2) and CO_2 in an anaerobic first stage, which is then utilized in an aerobic second stage by a yeast to form biomass. The yeast biomass has high potential to be sold as single-cell protein (Mishra *et al.*, 2020). Furthermore, it was shown that clostridial cells can be cultivated in a two-stage system to produce acetate from gaseous substrate, which serves then as a substrate for production of lipids by an engineered oleaginous yeast in a second bioreactor (Hu *et al.*, 2016). The lipids could provide a suitable precursor for liquid biofuel production. In another concept, a two-stage system was recently used to produce acetate from H_2 and CO_2 with the acetogen *Acetobacterium woodii*, which is then utilized by *Cupriavidus necator* for the synthesis of the bioplastic Polyhydroxyalkanoate (PHA) (Al Rowaihi *et al.*, 2018). A potential use of the acetogenic biomass as a source of protein was patent by Lanzatech

(Simpson *et al.*, 2016), but is less discussed in academia and would further optimize the sustainability of both concepts.

While Lanzatech is working with the acetogen *Clostridium autoethanogenum*, the academic community often investigates *Clostridium ljungdahlii* as model microbe. Both microbes share high genetic similarities (~98%), but can show different performances in growth, pH behavior, and metabolic response (Martin *et al.*, 2016). The natural fermentation products of *C. ljungdahlii* are acetate, ethanol, and minor amounts of 2,3-butanediol (Tanner and Laopaiboon, 1997; Köpke *et al.*, 2010). Other heterologous fermentation products were obtained with genetic engineered strains of *C. ljungdahlii* (Molitor *et al.*, 2016a; Humphreys and Minton, 2018). However, all known acetogens, such as *C. ljungdahlii*, suffer from energy limitations in their metabolism (Schuchmann and Müller, 2014). The central acetogenic pathway is the Wood-Ljungdahl-Pathway (WLP), which has no net ATP gain (Hess *et al.*, 2013). One ATP is required for the fixation of carbon, while one ATP is regenerated by the dephosphorylation of acetyl phosphate into acetate (Wood, 1991; Drake *et al.*, 2008). The only ATP available for the metabolism and cell growth in *C. ljungdahlii* is based on the *Rhodobacter nitrogen fixation-like* complex (RNF complex) activity (Schmehl *et al.*, 1993; Köpke *et al.*, 2010; Tremblay *et al.*, 2012). In *C. ljungdahlii*, this membrane-bound enzyme complex uses electrons from reduced ferredoxin (Fd_{red}) to translocate H^+-ions across the membrane and regenerate NADH from NAD^+ (Tremblay *et al.*, 2012; Schuchmann and Müller, 2014). The H^+-gradient is then used by a proton-dependent F_1F_O ATPase to generate ATP (Köpke *et al.*, 2010; Tremblay *et al.*, 2012). For growth with H_2 and CO_2, *C. ljungdahlii* can generate up to 0.63 ATP/mol H_2 through this mechanism, which provides enough energy for the anabolism and growth, but at the thermodynamic limit of feasibility (Schuchmann and Müller, 2014). Therefore, the energy limitation is most-likely the highest burden to overcome to produce high-value chemicals, which often require ATP for their biosynthesis (Molitor *et al.*, 2017; Katsyv and Müller, 2020).

In two recent studies, co-feeding of nitrate was described to provide more ATP by nitrate reduction during autotrophic growth with H_2 and CO_2 in *C. ljungdahlii* (Emerson *et al.*, 2019; Klask *et al.*, 2020). Nitrate was used as alternative electron acceptor while it provides a carbon independent route for energy conservation. With this pathway *C. ljungdahlii* can gain up to 1.5 ATP/mol H_2, which is used by the wild type (WT) for enhanced biomass production (Emerson *et al.*, 2019; Klask *et al.*, 2020). This extra gain of ATP could theoretically increase the yields for fermentation products that are based on ATP-demanding heterologous pathways (Emerson *et al.*, 2019). However, experimental data to support this idea is missing. To evaluate whether the extra ATP that is gained through nitrate reduction in *C. ljungdahlii* can be re-directed from biomass production into a bioproduct, a relatively simple heterologous pathway should be tested. Such a pathway could be the synthesis of the intracellular

biopolymer cyanophycin (CGP). CGP consists of a poly-L-aspartic acid backbone with arginine side chains attached to the β-carboxyl group of every aspartyl moiety (Simon and Weathers, 1976). It naturally occurs in various bacteria, such as cyanobacteria, as intracellular nitrogen and carbon storage polymer (Füser and Steinbüchel, 2007; Watzer and Forchhammer, 2018). CGP itself attracts biotechnological interest as a precursor for the synthesis of poly-aspartic acid (PASP), which can be used as a bioplastic precursor. In addition, CGP dipeptides could find application in the food and feed industry (Frey et al., 2002; Aboulmagd et al., 2001). CGP-containing cells are rich in protein, and thus could provide a suitable single-cell protein source due to their high arginine and aspartate content. The CGP synthesis is a non-ribosomal process and is catalyzed by a single enzyme called cyanophycin synthethase (CphA) (Ziegler *et al.*, 1998; Stubbe *et al.*, 2005; Füser and Steinbüchel, 2007). This enzyme consumes two moles of ATP for every chain elongation step of the CGP molecule (Berg *et al.*, 2000). Furthermore, it requires aspartate, arginine, and the two cations Mg^{2+} and K^{+}. However, the most important factor for a successful synthesis is the presence of an amino acid primer, which is essential for the start of the polymerization (Ziegler *et al.*, 1998). An *in vitro* synthesis of cyanophycin without this primer was not possible (Ziegler *et al.*, 1998; Aboulmagd *et al.*, 2000). The exact structure and composition of the primer still remains elusive (Watzer and Forchhammer, 2018). It was shown that the primer required at least three Asp-Arg building blocks $(\beta\text{-Asp-Arg})_3$ for a detectable CphA activity *in-vitro* (Berg *et al.*, 2000). Furthermore, other peptides, such as intermediates of the cell wall biosynthesis, seem to serve as an alternative primer and enable cyanophycin synthesis (Hai *et al.*, 2002). It is postulated that these alternative primers enable heterologous cyanophycin synthesis also in non-cyanophycin-accumulating microbes (Watzer and Forchhammer, 2018).

Besides the higher ATP levels in nitrate-reducing *C. ljungdahlii*, elevated amounts of arginine and aspartate where also observed in the metabolism (Emerson *et al.*, 2019). However, the heterologous cyanophycin synthesis in *C. ljungdahlii* would still suffer from energy limitation based on the stoichiometry. Therefore, a high accumulation of cyanophycin might be unlikely. On the contrary, a functional synthesis of cyanophycin in *C. ljungdahlii* would, consequently, deprive ATP from biomass formation. Interestingly, the genome of *C. ljungdahlii* contains already a native *cphA* gene that might encode for a CphA enzyme (Köpke et al., 2010). The *cphA* gene was not characterized yet, neither is cyanophycin known to be accumulated naturally by acetogens. Only a single study is available in literature in which a potential function of CGP in the sporulation and germination of *Clostridium perfringens* was speculated (Liu *et al.*, 2016). However, if cyanophycin genes are present in the genome of *C. ljungdahlii* a suitable amino acid primer might be also available.

Here, we investigate the potential of recombinant *C. ljungdahlii* strains that overexpress *cphA* genes to synthesize cyanophycin in nitrate-containing medium. We question whether the expression of *cphA*

genes provides functional CphA enzymes in *C. ljungdahlii*, and leads to the synthesis of cyanophycin, and thus to a re-direction of energy from biomass production into a valuable bioproduct. This will serve as proof–of-concept to further unravel the potential of using nitrate reduction in the gas fermentation of *C. ljungdahlii*.

6.4. Material and Methods

6.4.1. Bacterial strains and growth

General cloning was performed with *Escherichia coli* TOP10 (Thermo Fisher Scientific, Massachusetts, USA). *C. ljungdahlii* ATCC13528 was obtained from the DSMZ and transformed with plasmids by electroporation according to Molitor *et al.* (2016a). *E. coli* cultures were grown in Luria Broth (LB) medium at 37°C. Liquid LB cultures were agitated at 150 revolutions per minute (rpm). Clostridial cells were cultivated in serum bottles containing anaerobic Rich Clostridial Medium (RCM) at 37°C but not shaken. All anaerobic work was carried out in an anaerobic chamber (MBraun) with a N_2 (100 vol-%) atmosphere. *C. ljungdahlii* cultures in serum bottles were sampled and transferred under aerobic conditions using sterile syringes, needles, and a Bunsen burner. The rubber stopper of each serum bottle was cleaned with ethanol (70 vol-%) and flamed *prior* to use. All plating work with *C. ljungdahlii* was performed under anaerobic conditions with a maximum of 5 parts per million (ppm) oxygen inside the anaerobic chamber. Transfer of *E. coli* cells was performed under sterile conditions (HeraSafe KS 18, Thermo Fisher Scientific). The cyanobacterium *Anabaena* sp. PCC7120 was a gift of Professor Forchhammer (University of Tübingen, Germany) and was provided as grown culture on an agar plate. The agar plate was stored at 4°C. Chloramphenicol (30 mg/mL) or/and ampicillin (100 mg/mL) was used to maintain plasmids in *E. coli* strains. Thiamphenicol (5 mg/mL) was used for recombinant strains of *C. ljungdahlii* and dissolved in ethanol (100 vol-%). All antibiotics were stored at -20°C for up to three months.

6.4.2. Cloning

PCR fragments for a subsequent cloning event were amplified with the Q5® High-Fidelity DNA Polymerase (New England Biolabs), according to the manufacturer's instructions. All primers we used are listed in **Supplementary Table S20**. The PCR fragments were purified (QIAquick PCR Purification kit, Qiagen) and sub-cloned into pMinit2.0 (NEB® PCR Cloning Kit, New England Biolabs). Restriction endonucleases (New England Biolabs) were used for digestion of correct subcloning plasmids and cloning of correct fragments into the pMTL80000 shuttle vector system (Heap *et al.*, 2009). Ligation was performed with a T4-ligase (New England Biolabs). All generated plasmids we used are listed in **Supplementary Table S21**. A successful cloning event was verified using Sanger sequencing and test-digestion with subsequent gel electrophoresis analyses. Cell lysate of *C. ljungdahlii* or *Anabaena* sp.

served as DNA template. For this, a small cell pellet from a 1-2 mL culture suspension or a small amount of cell material from a plate was boiled in 100 µL deionized water for 10 min at 98°C and directly used for PCR after short period of cooling on ice. Plasmid DNA was purified with the QIAprep Spin Miniprep kit (Qiagen). Transformation of *E. coli* TOP10 and *C. ljungdahlii* was carried out as described before (Sambrook and Russell, 2006a; Molitor *et al.*, 2016a). All generated strains (**Supplementary Table S22**) were verified by test PCRs with the Phire Plant Direct PCR Master Mix (Thermo Fisher Scientific) according to the manufacturer's instructions.

6.4.3. Bioreactor experiment

The multi-bioreactor system (MBS) was used for the bioreactor experiment as described before (Klask *et al.*, 2020). However, we performed batch experiments in a modified minimal medium (modified PETC medium), which contained 10 g/L fructose, and 3.2 g/L sodium nitrate instead of ammonium chloride. In addition, we reduced the phosphate concentration by 50 weight-%. Thiamphenicol (5 µg/mL) was added to each reactor. The reactor wet volume was 750 mL and maintained at pH 6.0 (hysteresis ± 0.02) with 2 M KOH and 2 M HCl. The headspace of each bioreactor contained N_2 (100 vol-%) and was sealed from the atmosphere with an airlock. The bioreactors were not sparged with gas during the cultivation. Pre-cultures were grown for 48 h at 37°C without shaking in standard PETC medium (without nitrate) as described before (Klask *et al.*, 2020). Cells were harvested aerobically at 5000 relative centrifugal force (rcf) for 20 min and 4°C (Avanti JXN-26 centrifuge, Beckman Coulter). The rotor was cooled down to 4°C for 5 h *prior* to use. The pellet was resuspended in 40 mL of the supernatant and transferred to 50 mL reaction tubes. Subsequently, the concentrated cell suspension was centrifuged at 3492 rcf for 20 min at 4°C (Centrifuge 5920 R, Eppendorf). After removing the supernatant, each pellet was weighted, resuspended in 37.5-40 mL PBS, and distributed in 10x 1 mL aliquots, which corresponded to approximately 20 mL of initial bioreactor volume. The samples were stored at -20°C for later use.

6.4.4. HPLC

All HPLC analysis were performed as previously described (Klask *et al.*, 2020). Fructose standards were prepared as concentrations of 2.5 mM, 5 mM, 10 mM, 25 mM, and 50 mM. All samples were randomized for the analysis.

6.4.5. Transmission Electron Microscopy

For transmission electron microscopy (TEM), 2.5% (w/v) glutaraldehyde/4% (w/v) formaldehyde (in PBS, pH 7.2) was added to a heterotrophic 5 mL *C. ljungdahlii* culture, which was grown in RCM for 48 h. The fixed cells were then frozen in capillaries under high pressure (HPF Compact 03, Engineering

Office M. Wohlwend GmbH), and subsequently freeze-substituted (AFS2, Leica Microsystems) with 2% (w/v) OsO_4 and 0.4% (w/v) uranyl acetate in acetone as substitution medium and embedded in EPON™ Resin 828 (Hexicon). Ultrathin sections were then stained with uranyl acetate and lead citrate. The microscopic images were analysed with a Tecnai Spirit (Thermo Fisher Scientific) operated at 120 kV.

6.4.6. Sakaguchi staining

Staining of arginine was carried out with a modified protocol for the Sakaguchi reaction as described before (Messineo, 1966; Watzer *et al.*, 2015). Briefly, a cell pellet sample was centrifuged for 10 min at 3000 *g* and washed once with 500 µL phosphate-buffered saline (PBS) (2.7 mM KCl, 1.5 mM KH_2PO_4, 137 mM NaCl, 8.1 mM Na_2HPO_4) at 4°C. The washed pellet was resuspended in 500 µL PBS with 2.5% (w/v) glutaraldehyde and incubated for 30 min on ice. Next, the cell suspension was centrifuged again at 4°C and washed with 500 µL PBS. The washed pellet was gently resuspended in 80 µL of 5 M KOH. Subsequently, 10 µL of 1 weight-% 2,4-Dichloro-1-naphthol dissolved in ethanol (100 vol-%) were added. The cell suspension was then mixed gently with 10 µL 5 vol-% sodium hypochlorite (NaClO) and centrifuged again for 6 min. The supernatant was discarded, and the pellet was resuspended in 100 µL PBS. 15 µL of this sample was mixed with 2 weight-% molten agar and transferred immediately onto a microscopic slide. Microscopy (Olympus BX41) was carried out either in bright field or phase contrast at a resolution of 400x or 1000x. A successful Sakaguchi reaction will stain all arginine containing protein and cell compartments in red.

6.4.7. Cell lysis

Cell lysis of *C. ljungdahlii* cells was performed in a tissue and cell homogenizer (FastPrep®-24, MP Biomedicals) followed by ultra-sonification (Ultrasound cleaning bath USC, VWR) for 5 min. For cell lysis with the FastPrep instrument, the collected cell pellet was mixed with 2-3 g of glass beads and 10 mL of lysis buffer (150 mM NaCl, 100 mM Tris/HCl, 5 mM 1,4- dithiothreitol, 10 mM $MgCl_2$). Furthermore, 10 µL proteinase inhibitor (proteinase inhibitor cocktail, VWR), 0.5-1 mg DNAse I and 10 µL lysozyme was added to the lysis mix before use. The frequency setting for the FastPrep was two times 6.5/s for 30 sec with a 5 min break. The FastPrep method was applied multiple consecutive times if necessary. All samples were cooled to 4°C prior to disruption. Ice was added into the ultra-sonication tray for additional cooling. *E. coli* cells were only lysed by ultra-sonification. The lysed cell suspension was centrifuged for 15 min at 17900 rcf at 4°C. Supernatant and cell pellet were separated and stored individually at -20°C.

6.4.8. Extraction of CGP

Extraction of water insoluble CGP was performed as described elsewhere (Elbahloul *et al.*, 2005). However, following modifications were applied: The cell pellet was resuspended in 1 mL acetone. After a 30 min incubation period at 600 rpm (ThermoMixer C, Eppendorf), the cells were centrifuged at 25000 rcf for 10 min. The supernatant was discarded, and the pellet resuspended in 1 mL of 0.1 M HCl and incubated at 60°C with 600 rpm (ThermoMixer C, Eppendorf) for 1-18 h. On the next day, the sample was centrifuged again for 30 min at 4°C. The supernatant was transferred into a new 1.5 mL reaction tube and mixed with 500 µL of 3 M Tris/HCl (pH 7.5). The mix was incubated for 50 min on ice to allow precipitation of the CGP. Afterwards, the sample was centrifuged again for 40 min at 4°C. The supernatant was discarded, and the pellet (hardly visible) was resuspended in 100 µL of deionized water. The samples were stored at 4°C for up to 5 days. Extraction of water soluble CGP was carried out as described in Watzer *et al.* (2015). In addition, following changes were made: The cell pellet was resuspended in 10 mL B-PER™ Bacterial Protein Extraction Buffer (Thermo Fisher Scientific) supplemented with 3 mg/mL lysozyme (Muramidase, Merck), 0.1-0.5 mg/mL DNAse I (DNase I, Merck), and 1 µg/mL RNAse A (Thermo Fischer Scientific). Next, the suspension was centrifuged for 1 h at 3492 rcf. The resulting pellet was washed twice with 1.5 mL acetone and centrifuged afterwards for 15 min at 25000 rcf. 1.2 mL HCl was added to the pellet. The suspension was mixed and afterwards incubated for 2 h at 60°C while shaking with 2000 rpm (ThermoMixer C, Eppendorf). Subsequently, 0.5 mL of 1 M Tris/HCl (pH 7.5) and 150 µg Proteinase K (Proteinase K, Carl Roth) was added. The mix was again incubated for 30 min at 60°C and 1400 rpm. The sample was placed on ice for cooling and then centrifuged for 15 min at 25000 rcf. The resulting pellet was washed again with 2 mL acetone and then dissolved in 1 mL 0.1 M HCl. The supernatant was transferred into new 1.5 mL reaction tubes, mixed with 300 µL of 1 M Tris/HCl (pH 7.5), and centrifuged again. The supernatant was discarded, and the final pellet was resuspended in 400 µL of 0.1 M HCl for further analyses.

6.4.9. SDS-PAGE

Electrophoresis of protein were performed with standard SDS-PAGE (Sambrook and Russell, 2006b). We used SDS gels with 12 weight-% acrylamide for a separation range of ~12-60 kDa. The SDS-PAGE parameters were 80 V for 5 min and 160 V for 50-60 min. The gels were stained with Instant Blue™ (Instant Blue™ protein stain, VWR) for 30-40 min and de-stained with deionized water.

6.4.10. NMR analysis

NMR analyses were performed with a Bruker AV-III 600 MHz spectrometer (operating at 14 Tesla) equipped with a TXI-z gradient probe head. The analysis method was as described before (Erickson *et al.*, 2001). However, following modifications were applied: All NMR spectra was measured at 40°C. The

NMR tubes (Norell® Standard Series™ 5 mm NMR tubes frequency 400 MHz, Merck) had a volume of 500 µL. Samples were diluted with TSP in D_2O (final concentration of 10 mM). For quantification, a calibration curve was measured with purified CGP. NMR spectra were evaluated using the TopSpin software version 3 (https://bruker-labscape.store/collections/other-mr-items/products/topspin-for-processing-academic-government).

6.5. Results

6.5.1. Generation of recombinant *E. coli* strains overexpressing *cphA* genes

We used the broad-host shuttle vector system pMTL80000 to generate recombinant strains of *C. ljungdahlii*, which overexpress either the native *cph*A gene of *C. ljungdahlii* (*Clj*) or the *cph*A gene of the cyanobacterium *Anabaena* sp. PCC7120. We selected the promoter P_{thl} of the pMTL83152 plasmid for constitutive expression of the *cphA* genes. The generated plasmids were pMTL83152_$cphA_{An.}$ (*cphA* of *Anabaena* sp.) and pMTL83152_$cphA_{Clj}$ (*cphA* of *C. ljungdahlii*). We transformed *E. coli* cells and subsequently grew the recombinant strains on selective LB plates. Interestingly, the colonies of *E. coli* pMTL83152_$cphA_{An.}$ revealed a considerable opaque phenotype, which was neither observed for *E. coli* pMTL83152_$cphA_{Clj}$ nor for the empty-vector-carrying control strain *E. coli* pMTL83152 (**Figure 23A**). Next, we grew all recombinant *E. coli* strains in liquid medium for 24 h and visualized the cells under the light microscope (**Figure 23B, 23C, 23D**).

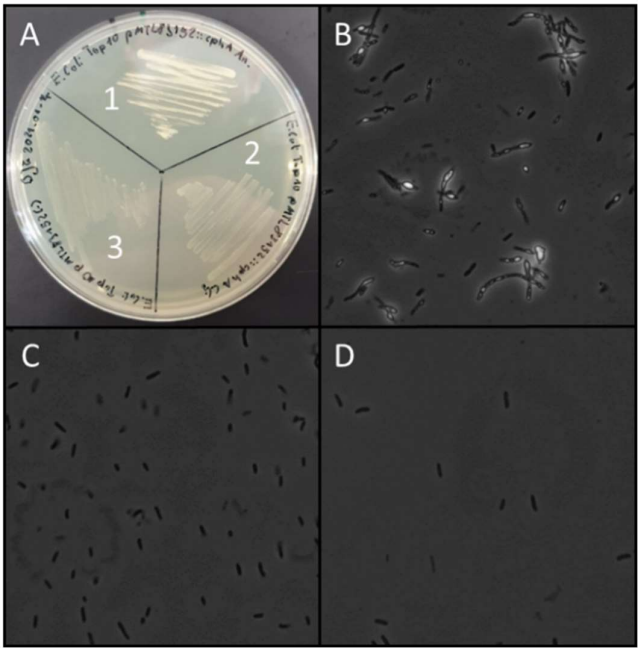

Figure 23 Phenotype of recombinant *E. coli* strains expressing *cphA* genes. Cells were grown in selective LB medium and incubated for 24 h at 37°C. Cells of *E. coli* pMTL83152_$cphA_{An.}$ showed an opaque phenotype and most cells were elongated and contained intracellular inclusions. (A) Growth on selective LB-agar plates of *E. coli* pMTL83152_$cphA_{An.}$: (1), *E. coli* pMTL83152_$cphA_{Clj}$ (2), and the control strain *E. coli* pMTL83152 (3). Light microscopic pictures in phase contrast of *E. coli* pMTL83152_$cphA_{An.}$ (B), *E. coli* pMTL83152_$cphA_{Clj}$ (C), and *E. coli* pMTL83152 (D).

Notably, liquid cultures of *E. coli* pMTL83152_*cphA*$_{An.}$ grew remarkably slower in contrast to the two other strains. Under the microscope, we observed that the majority of *E. coli* pMTL83152_*cphA*$_{An.}$ cells were elongated and contained cell inclusions (**Figure 23B**). Such intracellular inclusions are well known to appear in microbes that natuarally accumulated intracellular biopolymers such as polyhydroxyalkanoates (PHA) or CGP. We did not observe a similar phenotype neither for *E. coli* pMTL83152_*cphA*$_{Clj}$ nor for cells of the control strain *E. coli* pMTL83152. This indicated that the clostridial promoter P$_{thl}$ seems to be also functional in *E. coli*.

6.5.2. Microscopic analyses of CGP in recombinant *C. ljungdahlii* cells

After we had observed that one of our recombinant *E. coli* strains was already able to produce CGP, we next transformed *C. ljungdahlii* with our CGP plasmids. The generated *C. ljungdahlii* strains did not show a change in growth behaviour or in production of acetate or ethanol compared to the control strains harboring empty plasmids. We analyzed again culture suspension of the recombinant strains after growth for 48 h in RCM under the light microscope, but we could not detect any visible cell inclusions for any strain. Noteworthy, the *C. ljungdahlii* cells are Gram-positive, which could prohibit a simple visualization with light microscopy because of the cell-wall thickness. Therefore, we decided to treat the cells with the Sakagushi staining, which is a suitabel method to visualize CGP inside of natural CGP producers, such as cyanobacteria (Messineo, 1966; Watzer and Forchhammer, 2018). In this method, 1-naphthol and sodium hypobromid react with the guanidine group of arginines, which forms a red-coloured complex. CGP usually contains a high amount of arginine (Simon and Weathers, 1976). However, the Sakagushi staining did also not work for the *C. ljungdahlii* cell samples. We could not detect any red staining neither outside nor inside of the cell. To the best of our knowledge, literature does not report about a sucessful staining of Gram-positive cells with the Sakagushi method. This could indicate, that again the Gram-positive cell wall might hinder the chemicals from entering the cell. We also applied TEM for culture samples of our recombinant *C. ljungdahlii* strains. In literature, TEM was succesfully used to show accumulated CGP granules in cells of cyanobacteria. We could not detect any cell inclusions, which would indicate a biopolymer accumulation inside of our recombinant *C. ljungdahlii* cells (**Supplementary Figure S20**).

6.5.3. Bioreactor experiment to gain large amounts of biomass from recombinant strains

To gain enough biomass for a subsequent chemical purification of CGP from *C. ljungdahlii* cells, we performed a heterotrophic bioreactor experiment in which we grew *C. ljungdahlii* pMTL83152_*cphA*$_{An}$, *C. ljungdahlii* pMTL83152_*cphA*$_{Clj}$, and *C. ljungdahlii* pMTL83152 in minimal medium with nitrate as sole nitrogen source (**Figure 24**). In addition, we doubled the concentration of fructose from 5 g/L to 10 g/L to ensure that carbon is not a limitting factor. We did the same for the nitrogen source. Our

Multibioreactor system (Klask *et al.*, 2020) allows simultaneous cultivation of *C. ljungdahlii* under pH-controlled conditions in up to six bioreactor. *C. ljungdahlii* has its pH optimum at pH 6.0, thus, we set the pH controller to maintain the medium pH at 6.0 during the entire cultivation experiment. In our previous study (Klask *et al.*, 2020), we observed that nitrate reduction of autotrophic grown cells of *C. ljungdahlii* can increase the pH, while acetic acid production through the microbial acetogenesis is lowering the medium pH at the same time. For our present experiment, we argued that keeping the cells under optimal physiological conditions might be benefically for the ATP-demanding synthesis of CGP. Furthermore, we cultivated our bioreactors in batch to obtain a large amount of biomass, which was required for the subsequent chemical treatment. During the bioreactor experiment, we took cell samples and analyzed the purity of our cultures through PCR analysis (**Supplementary Figure S21**).

Figure 24 Bioreactor cultivation of recombinant *C. ljungdahlii* cells overexpressing *cphA* genes. Cultures (n=2) of *C. ljungdahlii* pMTL83152_$cphA_{An.}$, *C. ljungdahlii* pMTL83152_$cphA_{Clj}$, and *C. ljungdahlii* pMTL83152 were grown as duplicates in 750 mL minimal medium with nitrate as N-source under batch conditions. The pH was maintained at pH 6.0, which is the physiological optimum for *C. ljungdahlii*. The temperature was 37°C and stirring was 300 rpm. The fructose concentration was doubled to 10 g/L to exclude carbon limiting conditions. The headspace of each bioreactor contained N_2 (100 vol-%). The cultures were harvested after 52 h, when the remaining fructose concentration fell below 5 mM. At this timepoint all cultures entered the stationary growth phase. A detailed description of the bioreactor system can be found in Klask *et al.* (2020).

In addition, we tracked the consumption of fructose through HPLC analyses. We set a treshold value at 5 mM fructose and stopped the cultivation immediately, when the culture fell below this value. This point was reached after 52 h, and cells simultabeously stopped to grow, indicating the start of the stationary growth phase. We selected this treshold to ensure that our *C. ljungdahlii* cells are not suffering from a carbon or nitrogen limitation, which could fascilitate a potential re-uitilization of the cyanophycin. Furthermore, we believed that in the early stationary growth phase (not limitted by carbon or nitrogen), less ATP is required for cellular processes, such as cell division, and thus can be

used by the CphA to form CGP. After the cell harvest, we obtained two cell pellets for each strain with a total cell wet weight (CWW) of 3.9-4.2 g/750 mL culture. We used our extraction and analysis methods (**Material and Methods**) but could not detect any CGP from our recombinant strains grown with fructose in our bioreactors (see below).

6.5.4. Biochemical analysis of CGP *via* SDS-PAGE

For the chemical purification and verification of CGP, we took advantage of the special solubility characters of the CGP polymer. While CGP is usually soluble in HCl, it precipitates at a neutral pH. Therefore, we argued that an acid treatment of our cell samples would be suitable to extract any accumulated CGP. As CGP is a polymer that consists of amino acids, it can be detected *via* SDS-PAGE analyses. We decided to perform an initial cell-lysis step to overcome potential problems due to the Gram-positive cell wall, which might lower the efficiency of the extraction. Thus, we applied bead beating in combination with a subsequent ultra-sonification of our cell samples.

We separated the cell fragments from the supernatant and treated the latter with an acid and neutralization treatment. Subsequently, we performed SDS-PAGE to verify the presence of CGP in our samples (**Figure 25**). Albeit we could detect protein bands in our gel, the acid and neutralization steps had led to the removal of nearly all protein, in comparison to the samples that were loaded to the gel without undergoing the purification steps. In addition, we observed similar protein patterns for all samples including the control sample. We believed that this indicates that either our purification had not been successful or that our strains did not accumulate CGP under the tested conditions. Next, we tried to apply the Sakagushi staining directly on our gel. We hypothesized that we this would reveal potential ariginine-enriched protein bands. Unfortunately, this step stained the entire gel reddish but not selective protein bands. The staining was removed by a subsequent washing step with dionized water, however, this showed that the staining was not sufficient to identify CGP in our samples. Since we did not know, whether our cell lysis procedure was sufficient, and thus, we might have discarded all CGP containing cell material at our first lysis step, we next performed multiple lysis steps of our samples. During this procedure we frequently checked the degree of lysis by light microscopy. Notably, we could detect only slight changes of the cell shape and cell condition after our three subsequent lysis steps (bead beating and ultra-sonification). We analyzed again the cell samples in an SDS-PAGE. In comparison to our first attempt, this time we detected higher overall protein concentrations (**Supplementary Figure S22, S23**). However, we found again that neither the acid and neutralization treatment nor the multiple lysis steps revealed protein bands that could indicate the presence of CGP. In addition, all tested culture samples showed similar protein patterns such as observed in our first attempt.

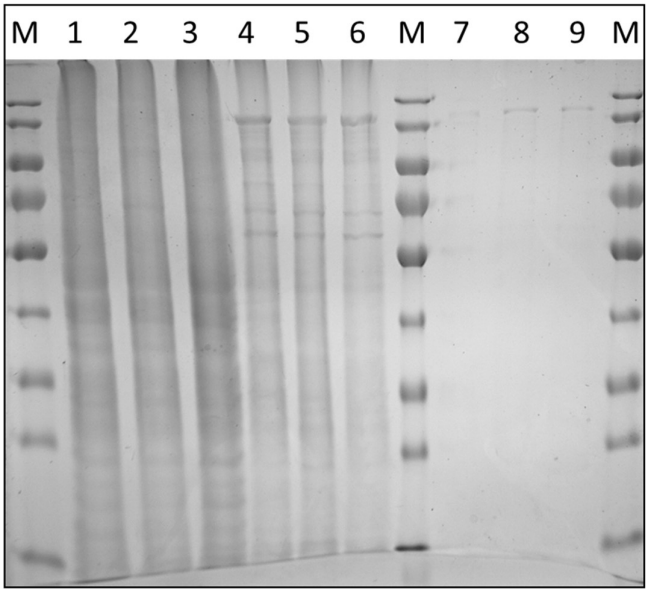

Figure 25 SDS-PAGE of *C. ljungdahlii* cell samples after lysis and treatment for the purification of CGP. Samples were loaded in the order *C. ljungdahlii* pMTL83152, *C. ljungdahlii* pMTL83152_*cphA*$_{Clj}$, and *C. ljungdahlii* pMTL83152_*cphA*$_{An.}$ (from left to right). 1-3, supernatant after lysis; 4-6, pellet after lysis; and 7-9, CGP sample after acid and neutralization treatment. M, PageRuler™ Prestained Protein Ladder. The gel was stained with InstantBlue™ for 30-40 min and washed with deionized water before imaging.

From literature it is known that CGP can sometimes possess an unusual solubility character being soluble under physiological conditions but insoluble at high or low pH. Therefore, we questioned if the CGP produced by our *C. ljungdahlii* cells might have this characteristic. As a consequent, our previous mentioned purification would have been counter-productive, because we would have discarded the purified CGP in the washing procedure. We repeated the CGP purification steps but this time we also loaded cell samples, which were treated with HCl but not neutralized onto the SDS-PAGE gel. As a second control, we also used cell samples from the *E. coli* strains that overexpress the *cphA* genes. The *E. coli* cells were only lysed by ultra-sonification. After staining the SDS-PAGE gel, we found a prominent smear for the cell sample of *E. coli* pMTL83152_*cphA*$_{An.}$, which we had treated with the acid and neutralization steps for CGP purification (**Figure 26, lane 8**). This indicated the presence of CGP in our cell sample of *E. coli* pMTL83152_*cphA*$_{An}$.

We had expected to find CGP here, because of our observation that cells of *E. coli* pMTL83152_*cphA*$_{An.}$ formed opaque colonies and microscopic analyses showed intracellular inclusions. In addition, such a smear also appears when purified CGP isolated from cyanobacteria is applied in an SDS-PAGE (**Supplementary Figure S24**). All other cell sample, which we had treated with the CGP purification steps did not show this smear. Furthermore, none of the supernatant samples from the *E. coli* and *C. ljungdahlii* cells showed a difference or indication for the presence of CGP that is soluble at physiological pH in the supernatant.

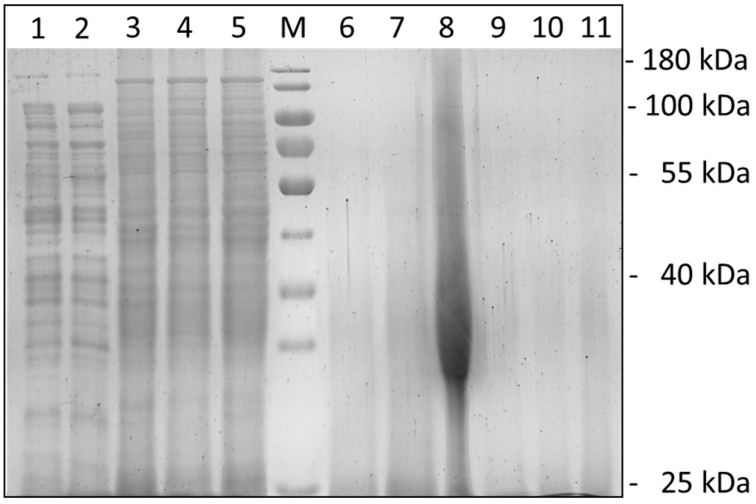

Figure 26 SDS-PAGE of *C. ljungdahlii* and *E. coli* cell samples after lysis and treatment for the purification of CGP. 1, Supernatant of *E. coli* pMTL83152_$cphA_{Clj}$; 2, Supernatant of *E. coli* pMTL83152_$cphA_{An.}$; 3-5, supernatant of *C. ljungdahlii* pMTL83152, *C. ljungdahlii* pMTL83152_$cphA_{Clj}$, and *C. ljungdahlii* pMTL83152_$cphA_{An.}$ (from left to right); 6-8, CGP sample after extraction from *E. coli* pMTL83152, *E. coli* pMTL83152_$cphA_{Clj}$, and *E. coli* pMTL83152_$cphA_{An.}$; 9-11, CGP sample after extraction from *C. ljungdahlii* pMTL83152, *C. ljungdahlii* pMTL83152_$cphA_{Clj}$, and *C. ljungdahlii* pMTL83152_$cphA_{An.}$. M, PageRuler™ Prestained Protein Ladder. The gel was stained with InstantBlue™ for 30-40 min and washed with deionized water before imaging. *E. coli* cells were lysed by ultra-sonification, while *C. ljungdahlii* cells were lysed with bead beating and a subsequent ultra-sonification.

6.5.5. CGP detection by NMR analyses

Since we only detected CGP in samples of *E. coli* pMTL83152_$cphA_{An.}$, we questioned whether the CGP content in our recombinant *C. ljungdahlii* strains might be too low for a detection with SDS-PAGE. Furthermore, we knew from our results above that the expression at for $cphA_{An.}$ provides a functional enzyme at least in *E. coli* and that the promoter P_{thl} is well characterized to function in *C. ljungdahlii.* We found a method in which nuclear magnetic resonance (NMR) spectroscopy was used to identify small amounts of CGP with a high sensitivity (Erickson *et al.*, 2001). Briefly, the NMR technique measures H^+-ions, such as attached to the N-carbon of arginine. Typical CGP is rich in arginine, which gives a distinct peak for arginine in the NMR spectrum. Against 3-(trimethylsilyl)-tetradeutero sodium propionate) (TSP) as standard, CGP concentrations can then be calculated with a standard curve. This allows a sensitive detection of CGP even below 0.1 mg/mL, and thus might be suitable to test our collected bioreactor cell samples. We first performed a calibration curve with the purified CGP sample isolated from cyanobacteria against TSP (**Supplementary Table S23**). As reported by Erickson *et al.* (2001), NMR analyses also showed a high sensitivity for CGP in our tests. The calibration curve had a high accuracy (R^2= 0.9995), and we were even able to measure CGP at a concentration of 0.05 mg/mL (**Figure 27, Supplementary Figure S25**). Next, we tested our purified CGP sample of *E. coli* pMTL83152_$cphA_{An.}$ and checked if the purity of this sample was sufficient for the NMR analyses and did not cause high background noise. In the subsequent analysis, we did not observe a high background

noise and were able to measure a concentration of 9.95 mg/mL from our *E. coli* cell sample. We could not detect any NMR peaks for CGP in any of the *C. ljungdahlii* samples we had analyzed for a potential insoluble soluble CGP character (in water soluble or not in water soluble) (**Supplementary Figure S26, S27**).

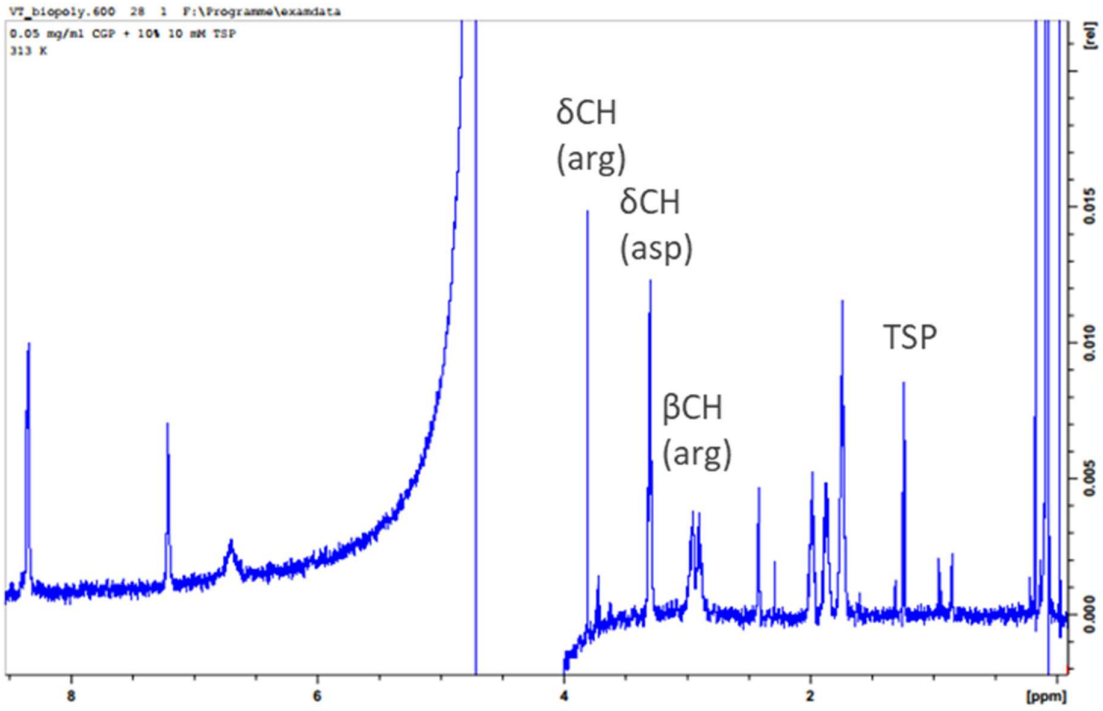

Figure 27 NMR spectrum for 0.05 mg/ml CGP. The purified CGP was obtained from cyanobacteria. TSP was applied as standard. The NMR analyses was performed as described before (Erickson *et al.*, 2001).

6.6. Discussion

The synthesis of CGP is highly ATP-dependent (Watzer and Forchhammer, 2018), and thus, unlikely to be efficient in microbes that already suffer from energy limitations such as *C. ljungdahlii* (Schuchmann and Müller, 2014). On the contrary, nitrate reduction is connected to energy metabolism in *C. ljungdahlii* and provides increased levels of ATP for the cell (Emerson *et al.*, 2019). Therefore, ATP-demanding synthesis of metabolic products could be possible with *C. ljungdahlii* when growing in the presence of nitrate. We addressed this hypothesis with the generation and cultivation of recombinant strains of *C. ljungdahlii* overexpressing *cphA* genes. Although, we could not detect any CGP in the *C. ljungdahlii* strains, we showed that the *cphA* gene of *Anabaena* sp. is active in *E. coli*. This is surprising, because the P_{thl} promoter was originally derived from *Clostridium acetobutylicum* and was, to our knowledge, not described before to function in *E. coli*. In our experiments, a successful CGP synthesis in *E. coli* pMTL83152_$cphA_{An.}$ was indicated by the change into the opaque color of the colonies on plates. This could be an interesting screening feature for further experiments, such as screening for

functional *cphA* genes in *E. coli*. However, we showed with our experiments that this does not provide evidence for a functional CGP synthesis also in *C. ljungdahlii*. What is the reason that we could not detect any CGP in our recombinant strains of *C. ljungdahlii*? One hypothesis could be that the CphA enzyme is not synthesized correctly, which could be reasoned by missing transcript or a different codon usage in *C. ljungdahlii*. This could be addressed with further optimization on the gene sequence such as implementing a different promoter or cloning a condon-optimized gene sequence. The amount of transcript could be analyzed with qRT-PCR with purified RNA samples of the recombinant strains. Another hypothesis for the absence of CGP accumulation in *C. ljungdahlii* could be that the CphA enzyme is, indeed, successfully synthesized by the cell, but its catalytic function is surpressed or blocked. It was reported that CphA requires an amino acid primer to start the polymerization reaction (Ziegler *et al.*, 1998). However, only little is known about the structure and composition of this amino acid primer (Ziegler *et al.*, 1998; Watzer and Forchhammer, 2018). In recombinant strains of *E. coli* that express *cphA* genes, it is speculated that this amino acid primer is coincidentally available as an intermediate of the cellular protein biosynthesis pathways. This scenario could be different in *C. ljungdahlii*, and therefore a missing amino acid primer would restrict the CGP synthesis. Another hypothesis for absence of CGP synthesis in *C. ljungdahlii* could be based on a potential degradation of the CGP in *C. ljungdahlii*. Beside the native *cphA* gene (CLJU_c02100), the genome of *C. ljungdahlii* also contains a *cphB* gene (CLJU_c02090), which might encode for a cyanophycin kinase. Cyanophycin kinases are known to play a key role in the depolymerization of the CGP polymer. Therefore, it could be that CGP was indeed synthesize in our recombinant *C. ljungdahlii* strains but was immediately degraded by CphB. Accumulated CGP provides a suitable energy, carbon, and nitrogen source, which could provoke a CGP degradation for the already energy limited metabolism. Since any experimental data for the physiological meaning of the cyanophycin genes in *C. ljungdahlii* is missing, it remains unclear if *cphB* of *C. ljungdahlii* encodes for a functional enzyme. However, it would be recommended to verify if *cphB* is expressed under the tested conditions. RNA-analysis, such as qPCR-analysis, could be helpful to get further insights in a potential CGP degradation. Eventually, the *cphB* gene should be removed from the genome or silenced with recently developed CRISPR tools (Huang *et al.*, 2016; Zhao *et al.*, 2019; Xia *et al.*, 2020). It was previously shown that *C. ljungdahlii* can use an arginine deiminase pathway to generate ATP from the oxidation of arginine (Valgepea *et al.*, 2017). Since arginine is one major component of the CGP molecule, it might be reasonable that this pathway could also be involved in a potential degradation of the CGP. A third hypothesis for the failure of CGP synthesis in the recombinant strains could rely on not ideal growth conditions and wrong media composition. For our bioreactor experiment, we have tried to provide optimal conditions (*e.g.*, pH control, excess of carbon, excess of nitrogen) for a non-limited growth of *C. ljungdahlii*. However, the minimal medium

composition could still be disadvantageous for an excessive amino acid synthesis in the anabolism. Thus, the available arginine and aspartate pools could be too small and not sufficient for the CGP synthesis. For future experiments, it should be tested if an additional supplementation of the medium with amino acids, such as arginine or aspartate, could prevent such a possible limitation. Furthermore, also an additional supply with K^+ or Mg^{2+}-ions could be beneficial for the CGP synthesis as described elsewhere (Simon and Weathers, 1976; Ziegler *et al.*, 1998).

Another approach to enable CGP synthesis in *C. ljungdahlii* could be made by overexpressing alternative *cphA* genes in *C. ljungdahlii*. Interestingly, an amino acid primer independent CphA was identified in *Thermosynechococcus elongatus* (Arai and Kino, 2008). If this CphA is also active in *C. ljungdahlii* this could exclude that the CGP synthesis in *C. ljungdahlii* is limited by missing amino acid primers. It was postulated that heterologous CphAs in non-native cyanophycin accumulating microbes, such as *E. coli*, are only functional because an intermediate of the cell wall biosynthesis functions as artificially amino acid primer (Hai *et al.*, 2002; Watzer and Forchhammer, 2018). In contrast to the Gram-negative bacterium *E. coli*, *C. ljungdahlii* is Gram-positive. Therefore, the cell wall biosynthesis differs a lot from the mechanisms in Gram-negative cells (Scheffers and Pinho, 2005; Madigan *et al.*, 2009). A suitable amino acid primer might not be available in *C. ljungdahlii*. This would explain why we could observe a functional cyanophycin synthesis in the recombinant *E. coli* strain overexpressing $cphA_{An.}$, but not in the respective *C. ljungdahlii* strain. On the contrary, it was already reported that cyanophycin could be successfully produced heterologously in recombinant strains of *Corynebacterium glutamicum*, which is a Gram-positive bacterium (Aboulmagd *et al.*, 2001). In conclusion, the various aspects of our discussion indicate that further experiments are required to unravel if cyanophycin synthesis is possible in *C. ljungdahlii*. In this context, it will be mandatory to further investigate the native cyanophycin synthesis pathway in *C. ljungdahlii.* In addition, future experiments should address if cyanophycin plays a relevant role in the sporulation of clostridial cells, which would be a further benefit to understand the clostridial metabolism.

6.7. Acknowledgement

This work was funded through the Alexander von Humboldt Foundation in the framework of the Alexander von Humboldt Professorship, which was awarded to LA. We are also thankful for additional funding to LA and BM from the Deutsche Forschungsgemeinschaft (DFG, German Research Foundation) under Germany's Excellence Strategy – EXC 2124 – 390838134. We acknowledge support by the DFG and Open Access Publishing Fund of University of Tübingen. Finally, we are thanking Professor Karl Forchhammer and Dr. Björn Watzer for the purified cyanophycin samples, the cyanobacteria cell samples, and protocols for the purification of cyanophycin. We also thank

Dr. Vincent Truffault for the conduction of the NMR analyses and Dr. Katharina Hipp for the TEM analyses at the Max Planck Institute for Developmental Biology, Tübingen.

6.8. Supporting information

Supporting information is provided in the Appendix (**8.4.**) and contains further information about generated strains, used primers, and plasmids. The additional eight supplementary figures give more details about the cyanophycin purification and analysis steps.

CHAPTER 7

CLOSING SUMMARY AND FURTHER RECOMMONDATION FOR FUTURE EXPERIMENTS

7.1. Closing summary

The results presented in this dissertation give new fundamental insights into the autotrophy and energy metabolism of *C. ljungdahlii*. Gas fermentation with acetogens, such as *C. ljungdahlii*, provides a promising technology to produce next-generation fuels and biochemicals in a sustainable and eco-friendly way. However, further research is still required to unravel the full potential of these microbes as future industrial biocatalyst. One critical factor is the acetogenic energy metabolism. Only a functional energy metabolism (*e.g.,* through a correct electron balancing) will enable the production of valuable heterologous products. Therefore, its understanding is an indispensable prerequisite for future work with acetogens. In Chapter 3, we demonstrated the efficient gas fermentation of *C. ljungdahlii* in a self-built multi-bioreactor system and showed that ethanol production is possible in a continuous cultivation with nitrate and carbon dioxide as co-electron acceptors. The system provides a suitable platform for a physiological characterization of anaerobic microbes in replicates. In addition, it demonstrated the importance of cultivating acetogens under pH-controlled conditions. For instance, batch cultures of *C. ljungdahlii* indicated that ethanol production is absent when nitrate was provided (Emerson *et al.*, 2019). Consequently, this would limit the motivation of using nitrate in a bioreactor to produce any biofuel. However, with our bioreactor experiments, we showed that ethanol production was even enhanced for *C. ljungdahlii* in nitrate containing medium under continuous conditions with pH-control. Thus, the energy metabolism must have been limited in the batch cultivation where the pH increased due to ammonium production, but not in the bioreactors. Furthermore, the nitrate feed in the bioreactors resulted in metabolic crash events, which means that further research is highly required. In addition, we could demonstrate that continuous operating bioreactors for gas fermentation of obligate anaerobic bacteria does not require a technically demanding setup and expensive investments as it is often the case for commercially available bioreactor systems. The self-built system presented in Chapter 3 is flexible, expandable, and easy to re-build, which makes it particularly interesting for academic research. In Chapter 4, we developed an ideal cultivation concept for the physiological characterization of *C. ljungdahlii* in batch cultures. We showed that characterization of the genetic manipulated recombinant strains of *C. ljungdahlii* in bottles provided high-quality cultivation data with low variance. Furthermore, we learnt during the work in this chapter fundamental knowledge for the generation of a CRISPR-Cas system, which was

later the basis for my genetic work in Chapter 5. In Chapter 5, we studied in detail the essential role of the RNF complex for the autotrophy in *C. ljungdahlii*. We developed a CRISPR-Cas12a gene deletion system and applied this successfully in *C. ljungdahlii* to delete three important genetic loci from the genome. Genetic manipulation of acetogens is still limited, and often takes a lot of time or complex experimental approaches. Therefore, the work we presented gives insights in the genetic relevance of the RNF complex gene cluster and associated genes in *C. ljungdahlii* for the first time. Moreover, our qPCR work unraveled the critical role of the *rseC* gene for the RNF-complex gene expression and most-likely for a functional RNF-complex formation. Thus, its indispensable role for autotrophy is another milestone to understand the energy metabolism of *C. ljungdahlii* and other acetogens. Furthermore, we used my cultivation setup developed in Chapter 4 for a detailed physiological characterization of all deletion strains in nitrate- and ammonium-containing medium. The mechanisms of nitrate reduction, especially its connection to the energy metabolism, was just recently found and still lacks fundamental understanding (Emerson *et al.*, 2019; Katsyv and Müller, 2020). The results of Chapter 5, contributed to address this knowledge gap. In addition, we revealed that nitrate reduction required a functional RNF complex and correct electron balance under autotrophic conditions. We demonstrated by gene deletion and complementation that the annotated nitrate reductase encodes for the only functional nitrate reductase in *C. ljungdahlii*. By plasmid-based complementation of the ΔRNF and Δ*rseC* deletion strain, we confirmed that the wild-type phenotype could be restored, and that the gene deletion was exclusively responsible for the phenotype of the deletion mutant. Furthermore, the generated deletion strain ΔRNF will have a great value for future investigation of the autotrophy and energy metabolism in an RNF-complex free background. In Chapter 6, we demonstrated the use of the nitrate reduction of *C. ljungdahlii* to channel the extra gain in ATP into the valuable bioproduct cyanophycin rather than being invested in the formation of extra biomass. We successfully generated recombinant strains of *E. coli* and *C. ljungdahlii,* which most-likely express the key gene of the cyanophycin synthesis (*cphA*). We successfully applied the multi-bioreactor system for the generation of large amounts of biomass samples from the *C. ljungdahlii* cells. These were required for the subsequent analysis and purification of the cyanophycin. We showed that one recombinant *E. coli* strain produced high amounts of cyanophycin, while the *C. ljungdahlii* strain did not. We established several analysis methods for the detection and purification of cyanophycin (*e.g.*, microscopy, staining, NMR-analyses). The results of Chapter 6 showed that native cyanophycin from a cyanobacterium, and the cyanophycin from the accumulating recombinant *E. coli* strain could be detected already in small concentrations. The reason why cyanophycin was not produced by the *C. ljungdahlii* strains was discussed in detail and future experiments recommended to overcome this problem were stated. Once cyanophycin synthesis is also functional in *C. ljungdahlii*, this provides a first indication for the

possibility to re-direct energy from nitrate reduction and expand the current product range of acetogens.

7.2. Further recommendation for future experiments

This dissertation provides several novel results and findings, which increase the understanding of the acetogen *C. ljungdahlii*, its energy metabolism, and therefore its potential use as an industrial biocatalyst. By concluding and connecting the main results of each chapter it becomes obvious that future work is highly recommended. For instance, the potential of using nitrate in continuously operated bioreactor with hydrogen and carbon dioxide misses further experimental data. Although high-quality data was obtained in Chapter 3 using the multi-bioreactor system, the different performance of each bioreactor questions the reasons for the physiological response to nitrate as alternative electron acceptor in *C. ljungdahlii*. More cultivation parameters should be considered in future experiments with the bioreactors. One useful optimization would be to evaluate a full carbon balance for each bioreactor. On the one hand, this requires steady-state conditions, such as already provided through the multi-bioreactor system, and on the other hand, individual tracking of the gas feed rates and gas composition for each bioreactor. A carbon balance will give a detailed view on the flow of carbon in the metabolism and reveal potential limitations in metabolic pathways. In addition, it will allow to calculate the electron balance. After the experiments of Chapter 3 were done, several modifications were already applied to the multi-bioreactor system to further optimize this system (**Figure 28**). I installed mass flow controllers in front of each of the six bioreactors. These will enable to use accurate gas feed rates for each bioreactor, and will balance eventual pressure drops throughout different gas uptake rates of the microbes during the cultivation. Furthermore, I optimized the system with a drum-type gas meter. This analytic instrument measures flow rates based on volumetric displacement independent from the used gas or gas mixture. Because the microbes in our multi-bioreactor system are gas-liquid mass transfer limited, and thus can only use a small amount of the gas volume provided, the composition of the off-gas stream of each bioreactor can be different. Furthermore, gas-composition analyses can be performed with gas samples taken from each bioreactor in gas chromatographic analyses. Required gas sampling ports were already installed at the multi-bioreactor system. Future experiments should also address the use of carbon monoxide as carbon and energy source for nitrate-grown cells. While it was reported that nitrate reduction was restricted in batch cultures containing carbon monoxide in the headspace (Emerson *et al.*, 2019), it remains open if this is also true for continuous and pH-controlled bioreactors. In addition, it will be from particular interest to investigate the response of *C. ljungdahlii* growing under continuous conditions but with varying gas-compositions that are changed during the cultivation. For instance, future bioreactor experiments could address if an increasing carbon monoxide concentration in the

used gas mixture is leading to a physiological response of nitrate reducing cells of *C. ljungdahlii*. And if so, how this would change the energy metabolism and fermentation product spectrum. A similar scenario could be tested with changing hydrogen concentrations. However, a change of the gas composition during a bioreactor experiment without the need to interrupt the operation is technically challenging. To overcome this, I have already upgraded the multi-bioreactor system with a self-designed gas mixing system (**Figure 28**).

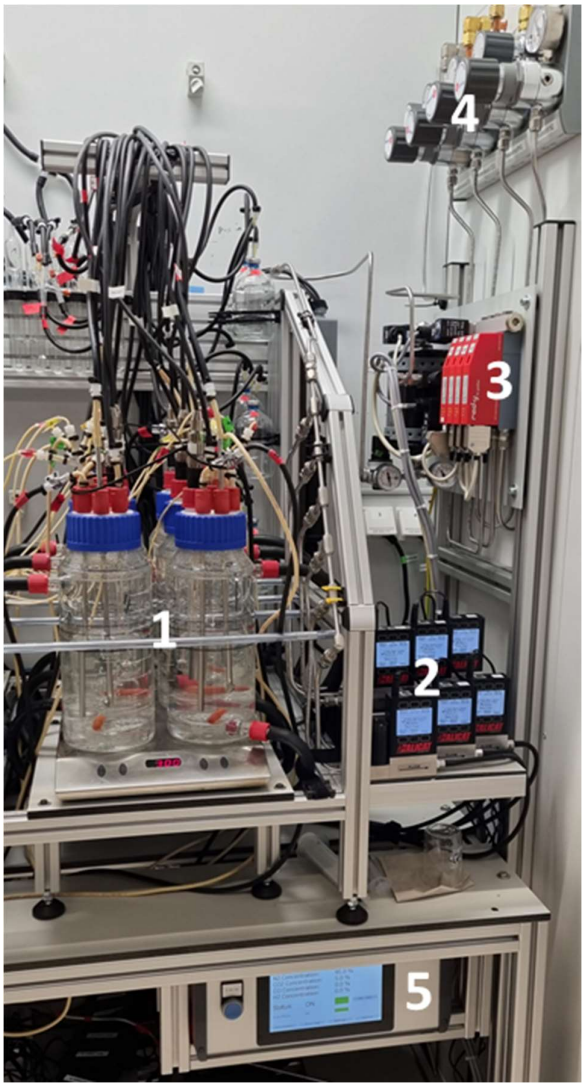

Figure 28 The self-built multi-bioreactor system (MBS) in April 2021. The MBS (1) was further expanded with six mass flow controllers (2) for a precise gas flow control for each bioreactor. A self-designed gas mixing system (3) was installed and can mix the pure gases CO, CO_2, H_2, and N_2 (4) into any required gas mixture. The gas mixing system is controlled by the gas mixing controller (5), which enables the change of the provided gas mixture without the need for a stop of the cultivation experiment. All MBS upgrades were installed to gain more accurate and high-quality data from gas fermentation experiments with acetogens such as *C. ljungdahlii.* The MBS system was operated for maintenance reasons with water in this picture.

This gas mixing system can mix the pure gases carbon monoxide, carbon dioxide, hydrogen, and nitrogen into any required gas mixture and provide the mixture to each bioreactor individually by

separate mass flow controllers. In addition, also pure gases can be used. A further great benefit of this system is that the gas composition can be changed during an ongoing bioreactor experiment without the need to interrupt the cultivation. This will be helpful to investigate further the robustness and resilience of the biocatalyst using different gas feed streams as substrates.

Besides the bioreactor approach, also the genetic work performed in this dissertation (Chapter 4-6) revealed some open questions for future experiments. The base-editing tool (Chapter 4), which we developed for precise genetic repression in *C. ljungdahlii*, showed a high editing efficiency. However, the full potential of this tool for a multiple gene-editing was only discussed but not tested yet. Therefore, future experiments could address the simultaneous gene-editing of several targets by using multiple sgRNAs in the pFX plasmid (multiplexing). In addition, the dCas9 nuclease could be replaced with alternative nucleases such as a deactivated form of the Cas12a (dCas12a) (Zhao *et al.*, 2019). This could increase the potential editing sites since the Cas12a requires a T-rich PAM sequence in contrast to the G-rich PAM of the Cas9. This might be beneficial for the typical A-T-rich genomes of acetogens. However, it is not clear yet if the dCas12a can be fused to the deaminase and still be functional (Master thesis Caroline Schlaiß). The different binding and DNA breaking mechanism could be decreasing the activity of the fused dCas12a/deaminase enzyme complex. In addition, the poor transformation efficiency of *C. ljungdahlii* was still a limiting factor in the CRISPR work. Future experiments should include a further optimization of this DNA-transfer method. Especially for multiple gene editing a sufficient and fast transformation will be mandatory. The poor transformation efficiency was also a bottle neck in the deletion strain generation with the CRISPR-Cas12a system (Chapter 5). The size of each generated CRISPR-Cas12a deletion plasmids was >10 kb. Transformation by electroporation was not feasible, indicating that the plasmid size is a critical factor for the transformation efficiency. Transformation *via* conjugation overcame this problem. But still varying conjugation efficiencies between the different experiments limited the generation of the recombinant strains. Furthermore, the DNA-repair mechanism after the double-strand break through the Cas12a seemed to further limit the success of transformation. A poor transformation efficiency was also reported for Cas9-mediated gene deletion in *C. ljungdahlii* (Huang *et al.*, 2016). Thus, future experiments should consider possibilities to enhance the DNA-repair event. It could be tested if the co-transformation with PCR-amplified linear repair template DNA (homologous flanking regions) supports the regeneration process in the targeted cell. In the work presented in Chapter 5 it was demonstrated that at least the constitutive production of FnCas12a based on the control plasmid (no sgRNAs, no repair template) always lead to a great number of successfully transformed *C. ljungdahlii* cells. This makes it unlikely that the Cas12a activity inside the cell is causing tremendous damage, and thus limiting the

transformation efficiency. Testing different promoter strengths, however, could also be part of a further investigation of the used CRISPR systems from this dissertation.

Understanding the physiological response of *C. ljungdahlii* during autotrophy was one major objective of this dissertation. The deletion strains generated in Chapter 5 provide an ideal platform to get further insights into the energy metabolism. For instance, one future experiment could investigate the proteome, transcriptome, and metabolome of the generated strain *C. ljungdahlii* ΔRNF strain. In particular, the reduced growth of *C. ljungdahlii* ΔRNF under heterotrophic conditions must be a result of an inefficient energy balance. Thus, other genes and proteins associated with the energy metabolism are likely to be affected. Unravelling such potential dependencies and connections will help to understand the physiological behavior of *C. ljungdahlii* in more detail. The results of this dissertation showed that the nitrate reduction is highly dependent on a functional RNF complex (Chapter 5). The fact that *C. ljungdahlii* utilizes the provided nitrate quickly to conserve energy was described before (fermentative nitrate reduction) (Emerson *et al.*, 2019). But how are the electrons transferred to the nitrate reduction enzymes? It is assumed that NADH is the main electron carrier for nitrate reduction, because NADH binding sites are present in the nitrate reductase enzymes (Nagarajan *et al.*, 2013; Emerson *et al.*, 2019) (**Figure 27A and 27B**). In such a scenario, the nitrate reduction pathway would always compete with other NADH-dependent pathways for the NADH pool. For instance, the ADHE1/2 enzymes, which are the main contributor for ethanol production under heterotrophic conditions, would suffer from this drain of NADH. Consequently, less ethanol would be produced. Indeed, we could confirm with our deletion strain *C. ljungdahlii* Δ*nar* that ethanol concentrations were increased for heterotrophy in bottle experiments. On the one hand, this would agree to the hypothesis that more NADH is available if nitrate reduction is absent. On the other hand, this would not explain why nitrate reduction was completely abolished in mutants of *C. ljungdahlii*, which lacked a functional RNF complex under autotrophic conditions. A possible explanation could be that the nitrate reductase is directly linked to the RNF by protein-protein interactions under autotrophic conditions. Thus, electrons could be directly transferred from the RNF complex onto the nitrate reductase (Nar) (**Figure 27C**). Such a mechanism would be independent from the NADH pool, and maybe more efficient than using electron carries. Since nitrate reduction in *C. ljungdahlii* ΔRNF was still possible but considerably reduced under heterotrophic conditions it could be assumed that the nitrate reductase might interact with another electron donor under these conditions but in a relatively inefficient manner. Instead, under autotrophic conditions, a direct protein-protein interaction between the RNF and nitrate reductase would explain why the nitrate reduction is: 1) accruing rapidly, 2) is connected to the generation of ATP; and 3) requires a functional RNF complex. However, for electron balancing reasons 2 mol of NADH must be still provided by the RNF complex,

which is then used by the nitrite reductase and hydroxylamine reductase (**Figure 27C**). A further alternative to this could be the formation of a super-complex consisting of the RNF complex proteins and all three nitrate reduction enzymes (**Figure 27D**). This would mean that the electrons are distributed directly from the RNF complex onto the nitrate reduction proteins without the further need of NADH regeneration. In this scenario, the electron balance would still fit the proposed model for energy conservation through nitrate reduction by Emerson *et al.* (2019). Furthermore, it would explain why nitrite accumulation was not observed for nitrate reducing cells of *C. ljungdahlii*. Neither Emerson *et al.* (2019), nor the result of our bottle experiments showed relevant concentrations of nitrite in culture samples. In contrast, we detected nitrite accumulation in continuous cultures of *C. ljungdahlii* during the crash events reported in Chapter 3. However, the reason for its accumulation requires further investigations. In the super-complex scenario, the residence time of the nitrite molecule would be extremely short, because it would be directly reduced in the next step and not being released to the cytosol. Overall, this would mean that the RNF complex and nitrate reduction enzymes are highly organized for a sufficient multiple protein-protein interaction (**Figure 27D**). Super-complex formation of respiratory enzymes is well-known from literature (Enríquez, 2016). However, it is still under debate if they follow a rigid and highly organized manner or a fluid-state mechanism in which the interaction partners randomly collide while floating in the membrane (Porras and Bai, 2015; Enríquez, 2016). A recent study showed that the nitrate reduction enzymes in *Pseudomonas aeruginosa* most-likely formed a super-complex with multiple proteins such as an NADH dehydrogenase and an F_1F_O ATPase (Borrero-de Acuña *et al.*, 2017). This could argue for a similar super-complex structure in *C. ljungdahlii*. However, *P. aeruginosa* possesses a membrane-bound nitrate reductase and electron transport proteins, such as cytochromes and ubiquinones, but *C. ljungdahlii* does not. Thus, it remains open if a direct protein-protein interaction or even a super-complex structure of the RNF complex and the nitrate reduction enzymes is present in *C. ljungdahlii* (**Figure 27D**). Future experiments should, therefore, investigate potential protein-protein interactions with the RNF complex. For instance, interacting protein partners could be identified in pull-down assays or cross-linking experiments. Furthermore, a biochemical purification of the RNF complex and the nitrate reductase and their characterization could show if the nitrate reductase can reduce nitrate with NADH or requires an RNF complex for this reaction. A post-doc in the Environmental Biotechnology Group of Prof. Angenent is following already up on this. The purification of the RNF complex from *C. ljungdahlii* and reconstitution in liposomes, described before (Kuhns *et al.*, 2020), could further be used for *in-vitro* assays to screen for potential interaction partners.

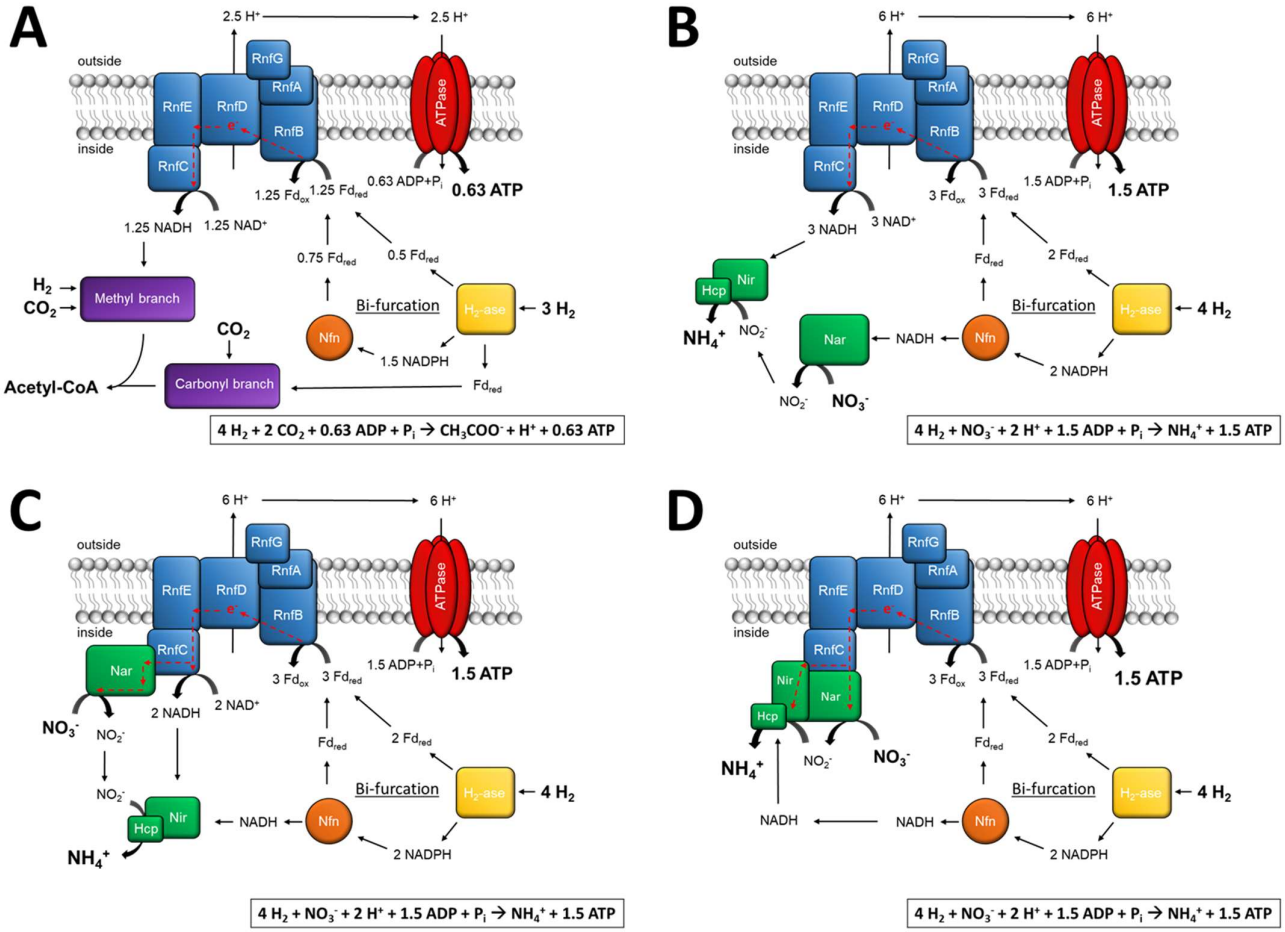

Figure 17. Models for energy conservation during nitrate reduction in *C. ljungdahlii* with potential protein-protein interaction (PPi) between the RNF complex and the nitrate reduction enzymes. A, Energy conservation with H_2 and CO_2 in the absence of nitrate; B, Energy conservation during nitrate reduction without PPi by (Emerson *et al.*, 2019); C, Energy conservation during nitrate reduction with direct electron transfer through PPi between RnfC and Nar; and D, Energy conservation during nitrate reduction with direct electron transfer through PPi between RnfC, Nar, and Nir. All models require electron bifurcation. The red arrows indicate flow of electrons. Abbreviations: H_2, hydrogen; H^+, proton, CO_2, carbon dioxide; NO_3^-, nitrate; NO_2^-, nitrite; NH_4^+, ammonium; ATP, adenosine triphosphate; ADP + P_i, adenosine diphosphate + phosphate; $Fd_{red/ox}$, reduced/oxidized ferredoxin; NADH/NAD^+, reduced/oxidize nicotinamide adenine dinucleotide; NADPH/$NADP^+$, reduced/oxidized nicotinamide adenine dinucleotide phosphate; RnfCDGEAB, RNF-complex subunits; Nar, nitrate reductase; Nir, nitrite reductase; Hcp, hydroxylamine reductase; H_2-ase, bifurcating hydrogenase/lyase; Nfn, bifurcating transhydrogenase; and e^-, electron.

Because the RNF complex is the only respiratory enzyme in *C. ljungdahlii* and crucial for autotrophy, it is likely that multiple protein-protein interactions are possible such as between RnfC and Nar and RnfC and the nitrite reductase (Nir). The direct interaction would be a benefit for the cell to maintain sufficient electron transfer mechanisms with a minimized loss of energy in the metabolism. Since acetogens, such as *C. ljungdahlii*, are known to live at the thermodynamic limit of life, it becomes obvious that energy conservation, especially during autotrophy, must have been evolved into a very efficient process. Thus, proteins associated with the energy metabolism, such as the RNF complex or the nitrate reductase enzymes, must underlie a high selective pressure. Consequently, a super-complex structure becomes reasonable (**Figure 27D**).

The *rseC* gene and its encoded protein RseC also provides an interesting subject for future experiments. Neither functional nor exact regulatory mechanisms are understood for this protein. Furthermore, it seems obvious that the *rseC* in an acetogen, such as *C. ljungdahlii*, might not have the same function in oxidative stress response as reported for *E. coli* (De Las Peñas *et al.*, 1997; Koo *et al.*, 2003). Therefore, future investigations should aim for a complete physiological and biochemical characterization of the encoded protein RseC in *C. ljungdahlii*. The results of this dissertation (Chapter 5) showed that *rseC* plays a critical role for the expression of the RNF-complex encoding genes in *C. ljungdahlii* during autotrophy. Therefore, future experiments should aim for *rseC* gene deletions in other acetogens. If similar results can be found as stated in Chapter 5, it could be a hint for a conserved protein feature among acetogens, and thus relevant for various other studies. Furthermore, this could further reveal if the *rseC* genes, which are clearly separated from the RNF complex genes, such as in *A. woodii* or *E. limosum*, are also essential for a functional RNF complex. Beside future experiments dealing with genetic manipulation of *rseC* genes, the RseC protein also provides a promising target for further investigations. So far, literature describes RseC as putative positive transcriptional regulator. For instance, RseC could potentially bind to the promoter sequence in front of *rnfC* to regulate gene expression of the RNF complex genes. Such a mechanism could be similar to the positive transcriptional control of the Calvin-Benson-Bassham (Cbb) pathway genes by the regulator protein CbbR (Kusian and Bowien, 1997). The Cbb genes are organized in a *cbb* operon and are a widely distributed pathway to fix CO_2 for many litho-, chemo-, and photoautotrophic microbes such *Cupriavidus necator* (Kusian and Bowien, 1997). In *C. necator*, the regulator protein CbbR binds as a tetramer upstream of the *cbb* operon and initializes the gene expression to enable autotrophy with H_2 and CO_2 and oxygen (O_2) as final electron acceptor. Interestingly, a *cbbR* gene deletion mutant of *C. necator* lost its ability for autotrophic growth but heterotrophic growth was still possible (Bowien and Kusian, 2002). This is similar to the observations made for the deletion of the *rseC* gene in *C. ljungdahlii* (Chapter 5). Therefore, future experiments should investigate if and at which

position RseC can bind to DNA. This could be achieved in an electromobility shift assay (shift assay) in which the RseC protein would bind to DNA fragments (*e.g.*, a fragment containing the RNF-complex gene cluster), and thus will migrate less in a native gel electrophoresis gel than DNA fragments that do not interact with RseC. Such a method was recently successfully applied to identify the regulator of the lactate metabolism and its binding site in the acetogen *A. woodii* (Schoelmerich *et al.*, 2018). However, it could also be that RseC is also interacting with other proteins rather than only controlling gene expression and interacting with DNA sequences. A hint for this is given by two predicted transmembrane helices in the amino acid sequence of RseC. For instance, RseC could have a potential chaperone-like function, which would mediate a correct protein folding of the RNF-complex subunits and their final complex formation. Alternatively, RseC could also be involved in the stabilization of the RNF complex inside the membrane, and thus maintain the protein-protein interactions between each subunit of the RNF complex. The two potential transmembrane domains would argue for such a helper protein character. Both hypotheses would require experiments, which address the characterization of protein-protein interactions between the RNF complex proteins and the RseC as discussed above for the nitrate reduction enzymes. A future experiment could aim for an *in-vitro* reassemble assay of the RNF complex in liposomes mediated by RseC. In case, RseC has a chaperone-like function the reassembling should be only possible in presence of RseC. In contrast, if RseC is located together with the RNF complex in the membrane a protein tag could be fused to RseC and then used to detect the presence of RseC in purified membranes of *C. ljungdahlii*.

In conclusion, more research is required with *C. ljungdahlii* to unravel the essential role of the RNF complex and associated proteins for autotrophy. Many of these future experiments will surely contribute to a better understanding of the acetogenic energy metabolism. The fundamental knowledge gained through this research will be from high value also for other acetogens, and thus, a major step to increase the potential of using acetogens as biocatalysts in biotechnological application.

APPENDIX

8.1. Supplementary information for Chapter 3

Supplementary Results

Supplementary Table S1-S10

Supplementary Figure S1-S5

8.1.1. Supplementary Results

Concept and assembly of the MBS

All required materials for the MBS (**Supplementary Figure S1**) were purchased from different manufacturers in Germany or France. We provide a list with all information for each unit of the MBS including manufacturer's names, required amounts, and expected costs (**Supplementary Table S1**). The basis for our MBS concept was a commercially available 1-L double-walled glass bottle with GLS 80 neck as the bioreactor vessel. The neck of the bottle was additionally flattened by a glass blower to increase the surface contact area between glass and lid. Furthermore, the custom-made lid was sealed with an additional O-ring. We designed a custom-made lid (**Supplementary Figure S2**), because it had to offer as many ports as possible to attach pH-regulation and all lines required for a continuous gas and medium feed-in and -out, and we could not find commercially available options that fulfilled our requirements. In addition, the lid had to be autoclavable and gas tight. Our customized lid is made of PTFE and provides vertically attached connection ports for five GL14 fittings and one GL25 fitting. Before attaching the lid, vacuum grease was applied to the glass thread of the bioreactor. One water bath thermostat maintained the temperature of all bioreactors. The equal distribution of the water through black rubber tubing was achieved by installing a starfish manifold. The water outlets of the individual bioreactors were merged into a single line before entering the thermostat again. Stirring bars were used for continuous and unitary agitation of the medium with a multi stirring plate for six bioreactor vessels. Autoclavable pH-electrodes with integrated temperature sensors were installed at the GLS25 port, which was sealed with a PTFE ring that contained a GL25 screw cap. A multi parameter controller, which includes four internal pH/temperature modules, two external pH/temperature modules, and two external relay controllers, was used to track the temperature and to control the pH. All wiring and connections were installed according to the manufacturer's instructions. Twelve peristaltic mini pumps were added to the MBS system and connected to the multi parameter controller to control the pH with base and acid feed for all six bioreactors (**Supplementary Figure S3**). A three-part stainless-steel tubing set: a sampling tube, an off-gas tube, and an inlet-gas tube with attached

micro sparger was designed, custom-built, and attached to each bioreactor. In addition, the sampling tube was extended by a stainless-steel three-way valve. All GLS14 ports of the bioreactor lid were sealed with 3-part GL14 caps containing PTFE/ETFE replacement inner parts. To maintain continuous feed-in and feed-out conditions, a multichannel pump head equipped with twelve channels was attached to a peristaltic pump. For the mini pumps, a chemical-resistant rubber tubing was used. Furthermore, the multichannel pump head was equipped with 2-stop rubber tubing. All rubber parts were connected *via* Luer-Lock adapters and autoclaved *prior* to use. However, the 2-stop rubber tubing was sterilized with bleach (10 vol-%) and rinsed with sterile water. To keep the feed bottles anaerobic, holes for tubing were drilled through GL45 butyl stoppers. Each feed bottle contained three feed lines, which were connected to the 2-stop rubber tubing of the multichannel pump, one tubing line to add sterile vitamins and reducing agents, and one line (made of rubber tubing and a 10-cm piece of a 1-mL glass pipette). For the gas-out line, rubber tubing coming from the bioreactor went first through a 100-mL serum bottle, which was used as water trap before ending in a fermentation airlock for each bioreactor. The effluent of all bioreactors was collected in a single 10-L bottle or six 1-L bottles to track individual effluent levels.

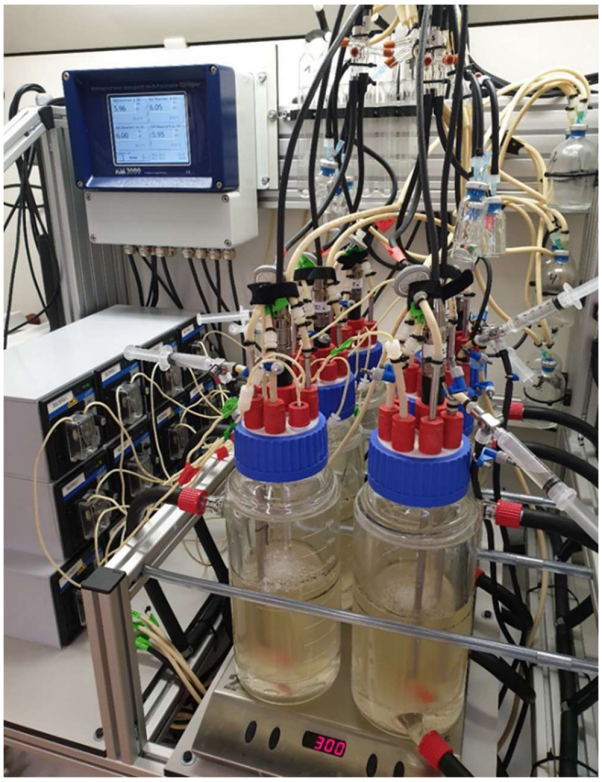

Supplementary Figure S1 The MBS under operating conditions. *C. ljungdahlii* was cultivated under continuous conditions with CO_2 and H_2 in up to six bioreactors with pH- and temperature control. The reactor volume was 0.5 L. The bioreactors were stirred at 300 rpm and maintained at 37°C with a water jacket. The pH was controlled with a multi-meter instrument and automatically adjusted if necessary. The MBS provides an ideal platform for the characterization of acetogenic bacteria under continuous conditions in replicates and is a cheap and off the shelf alternative to commercially available bioreactor system.

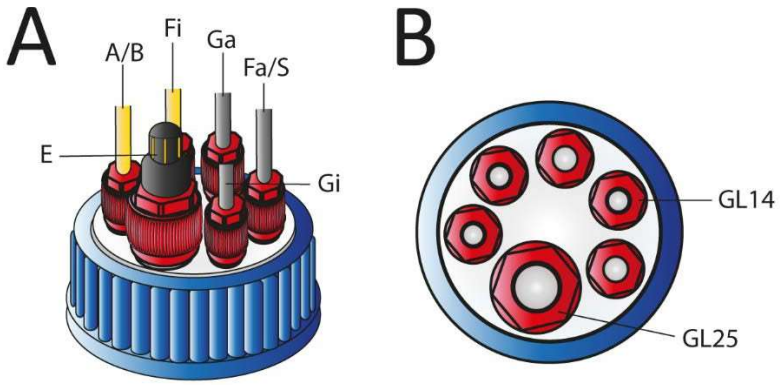

Supplementary Figure S2 Side and top view of the customized lid designed for the MBS. Side view on the lid with connected tubing, ports, and pH-electrode (A). Top view on the lid surface (B). The lid meets all requirements to perform either heterotrophic or autotrophic cultivation experiments with attached pH-control and continuous medium feed-in and -out. Abbreviations: E, pH-electrode; A/B, acid or/and base feed; Fi, medium feed-in line; Ga, gas-out line; Fa/S, medium feed-out line/sampling port *via* three-way valve; Gi, gas inlet, GL14, thread size GL14; GL25, thread size GL25.

Supplementary Figure S3 Wiring of the multi parameter controller KM3000 to operate six pH- electrodes and twelve pumps *via* relay and CAN bus interface. Four internal relay signals are used to control four pumps directly through 3-wire cables (1). The other eight pumps are controlled as in- line signal *via* CAN bus (2). Four internal interfaces are used to connect four pH/Pt-1000 electrodes (3). It is important to have small bridge connectors for the white and the green wire (not provided with the cable combinations). The other two pH/Pt-1000 electrodes are connected in-line *via* CAN bus. The yellow and brown wire are not required and insulated for safety reasons (4). Unless otherwise stated, all connections were made according to the manufacturer's instructions.

Supplementary Table S1 Required materials for the MBS to operate six bioreactors. The list comprises details about every item and summarizes the total cost of the system (as of Spring, 2019).

Item	Manufacturer	Item no.	Quantity	Approx. cost in €*
1-L double-walled bottle	Duran/VWR	215-4157	6	2000
Customized bioreactor lid	Bohlender/Zinnstag	XZ019-182117	6	2000
O-ring (70x3 mm, FPM30)	Reif	4141280	6	25
Multi stirring plate	2mag	2MAG_10020	1	1250
Set of customized stainless-steel tubing, Ø 6mm, tube (320 mm) with sparger, sample tubing (280 mm), off-gas tubing (100 mm)	bbi-biotech	quote (BZV-2018100900491)	6	2250
Gas manifold for 6 lines (self-built)	Swagelock	-	1	1500
KM3000 Multi-Parameter controller, including 4 internal relays + Can-Bus-Interface (standard version)	Xylem/Si-analytics	90278011	1	2050
Internal pH/temp module	Xylem/Si-analytics	90278011	4	1500
External pH/temp module for KM3000	Xylem/Si-analytics	90278011	2	850
REL 2000 CAN (external module) 4 relays, CAN-Bus-Interface	Xylem/Si-analytics	90278017	2	850
pH-electrode (SL 81-225 pHT VP, pt1000)	Xylem/Si-analytics	90279050	6	2600
Cable combination for SL 81-225 pHT VP	Xylem/Si-analytics	85442000	6	1100
Set of shrink tubing green/yellow (3 mm)	Conrad	541743-62	1	5
Set of wire end ferrule 0.25 mm x 6 mm	Conrad	739539-62	1	5
Masterflex C/L Mini pumps (13 to 80 rpm)	ColeParmer	77122-14	12	9400
Heating thermostat (CC-104A)	Huber	461-1056	1	1600
Octagon-Manifold	Interchim	343938	1	440
Customized bioreactor frame	Item24		1	1200
Plastic 10mm, ESD, grey (300x600mm)	Item24	0.0.614.87	2	15
Plastic 10mm, ESD, grey (300x200mm)	Item24	0.0.614.87	1	5
GL14 cap, 3-parts, including PTFE/ETFE fittings (6 mm)	Bola	D590-06	30	550
GL25 cap with PTFE ring	Bola	H984-03 + H975-18	6	60
Magnetic stirring bar (38 mm)	Carl Roth	A954.1	6	40
Airlock	Chemglass/VWR	AF-0513	6	350
Water trap (240-mL serum bottle)	Glasgerätebau Ochs	102.041	10	20
Masterflex Multichannel pump head + 12 cartridges	ColeParmer	HV-07519-25/SI-07519-85	1	2900
Masterflex L/S pump (100 RPM)	ColeParmer	HV-07528-30	1	1600
2-Stop pump tubing for multichannel pump	ColeParmer	HV-06431-26	1	150
Masterflex mini pump tubing	ColeParmer	GZ-95809-30	6	30
Norprene tubing in size 14	ColeParmer	GZ-06402-14	1	75
Norprene tubing in size 16	ColeParmer	GZ-06402-16	1	75
Masterflex I/P Norprene Tubing A 60 G	ColeParmer	GZ-06404-73	1	50
Luer/Lock fittings in different sizes	Carl Roth	CT59.1-64.1	100	150
3-way valves	Carl Roth	P340.1	6	200
5-L duran bottle	Duran/VWR	215-0057	4	360
10-L duran bottle	Duran/VWR	215-0058	1	150
Butyl stoppers for GL45	Glasgerätebau Ochs	444704	4	15
Tube clamps	Carl Roth	YE70-1	50	100
Zip ties and holder for 6 mm	Hornbach (hardware store)	-	100	30
Screws and nuts	Hornbach (hardware store)	-	20	10
* includes 19% tax		Total cost		**37560**

8.1.2. Cultivation data of *C. ljungdahlii* growing with ammonium or nitrate as N-source

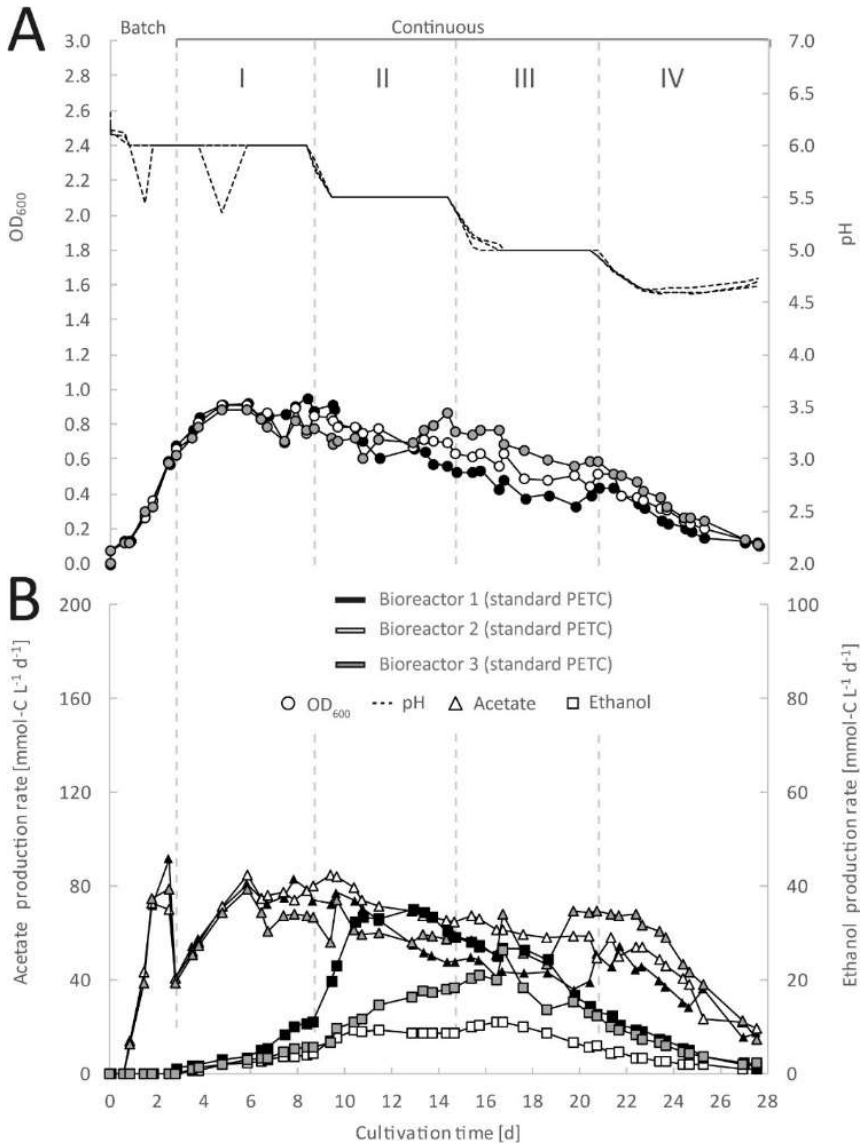

Supplementary Figure S4 Single bioreactor data for continuous gas fermentation of *C. ljungdahlii* with CO_2 and H_2 in standard PETC medium with ammonium at different pH periods. Single values for pH and OD_{600} (A), and for acetate and ethanol production rates in mmol-C L^{-1} d^{-1} (B). The horizontal dotted lines indicate the continuous mode in which medium with different pH was fed to each bioreactor. The pH was not regulated with feeding acid in continuous mode, but by adjusting the feed medium pH to the desired value and by biological acetic acid production. The cultivation volume was initially 500 mL but was tracked daily during the experiment ranging from 500-650 mL. The gas feed rate was 30 mL min^{-1}. The medium feed was 0.10 mL min-1 (HRT= ~0.25 d^{-1}). The bioreactors were operated at 37°C and 300 rpm for 27.5 days. pH Period: I, pH=6.0; II, pH=5.5, III, pH=5.0; and IV, pH=4.5.

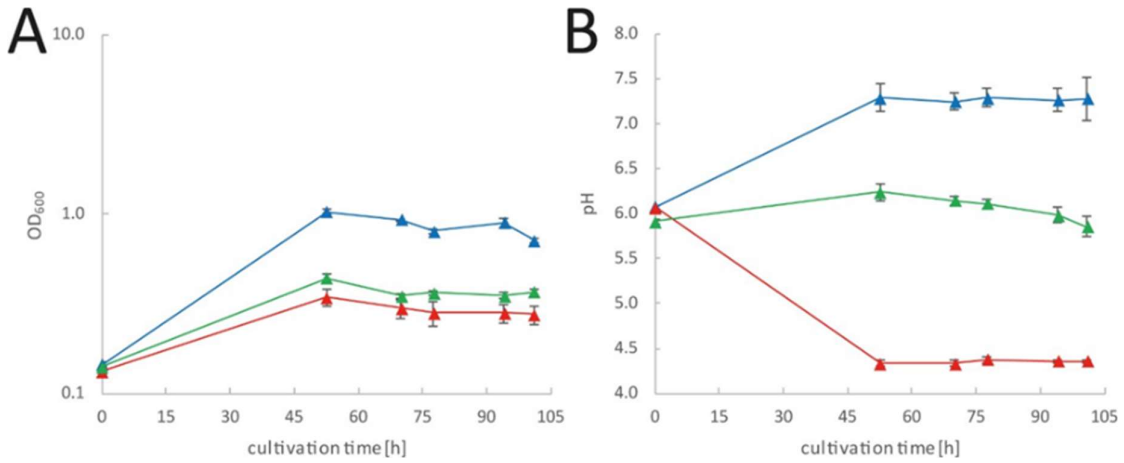

Supplementary Figure S5 Bottle cultivation of *C. ljungdahlii* with CO_2 and H_2 using ammonium, nitrate, or a mixture of both as N-source. Growth as OD_{600} in triplicate (n=3) under each tested condition (A). Changes in pH (B). 50 mL PETC medium supplemented with 0.5 g/L yeast extract but without fructose and ammonium chloride was provided in 240-mL serum bottles. Na-nitrate, ammonium chloride, or a mixture of both N-sources were added as sterile and anaerobic solution. The bottles were filled with sterile CO_2 and H_2 gas (20/80 vol%) to 1 bar overpressure before inoculation. Pre-cultures were grown heterotrophically in PETC with fructose for 48 h at 37°C in a stand incubator, washed once with sterile PBS, concentrated, and directly used for inoculation. Cultivation of main cultures were carried out at 150 rpm in a shaking incubator (Lab companion, ISS-7100R, Jeio Tech, Korea) at 37°C for 101 hours. *C. ljungdahlii* growing with 20 mM Na-nitrate (▲); *C. ljungdahlii* growing with 20 mM ammonium chloride (▲); and *C. ljungdahlii* growing with a mixture of 10 mM Na-nitrate and 10 mM ammonium chloride (▲).

Supplementary Table S2 Averaged data obtained from the cultivation of *C. ljungdahlii* WT in ammonium-containing medium with H_2 and CO_2 using the self-built MBS (Reactor 1-3). Growth parameter: medium feed rate = 0.0986 mL min^{-1}; gas low rate = 30 mL min^{-1}, ammonium feed rate = 0.002 mM min^{-1}; CDW/L/OD_{600} [g] = 0.242 and total cultivation time = 661 h. The pH (6.0 – 4.5) was maintained with base but not with acid. Any negative production rate was set = 0. n.m. = not measured.

						Bioreactor 1/2/3 (ammonium, control)																	
	sample	date	time	cultivation time [h]	cultivation time [d]	OD600	SD (OD600)	pH	SD pH	CDW_{total} [g]	SD (CDW)	acetate [mM]	SD	ethanol [mM]	SD	acetate production rate [mmol-C L^{-1} d^{-1}]	SD	ethanol production rate [mmol-C L^{-1} d^{-1}]	SD	acetate production rate [g L^{-1} d^{-1}]	SD	ethanol production rate [g L^{-1} d^{-1}]	SD
Batch	0	29.07.19	7.45 PM	0.0	0.0	0.000	0.000	6.24	0.06	0.000	0.000	0	0	0	0	0	0	0	0	0	0	0	0
	1	29.07.19	8.00 PM	0.3	0.0	0.075	0.000	6.13	0.02	0.018	0.000	1.8	0.1	0	0	0	0	0	0	0	0	0	0
	2	30.07.19	10.45 AM	14.5	0.6	0.128	0.007	6.08	0.05	0.031	0.002	1.6	0.1	0	0	0	0	0	0	0	0	0	0
	3	30.07.19	4.00 AM	20.0	0.8	0.126	0.006	6.00	0.00	0.030	0.001	3.0	0.1	0	0	13.0	1.0	0	0	0.4	0.0	0	0
	4	31.07.19	8.30 AM	35.5	1.5	0.276	0.019	5.82	0.32	0.067	0.005	16.5	1.0	0	0	41.8	2.8	0	0	1.3	0.1	0	0
	5	31.07.19	4.00 PM	43.0	1.8	0.349	0.023	6.00	0.00	0.084	0.006	27.9	0.8	0	0	73.0	1.5	0	0	2.2	0.0	0	0
	6	01.08.19	9.00 AM	60.0	2.5	0.577	0.008	6.00	0.00	0.140	0.002	56.2	3.8	1.8	1.0	79.9	11.0	0.0	0.0	2.4	0.3	0	0
continuous, pH 6.0	7	01.08.19	4.30 PM	67.5	2.8	0.652	0.028	6.00	0.00	0.158	0.007	71.8	1.8	2.2	1.3	40.0	1.0	0.0	0.0	1.2	0.0	0	0
	8	02.08.19	9.00 AM	84.0	3.5	0.735	0.027	6.00	0.00	0.178	0.006	93.9	3.7	2.4	0.7	52.3	2.0	1.4	0.4	1.6	0.1	0.0	0.0
	9	02.08.19	3.30 PM	90.5	3.8	0.813	0.031	6.00	0.00	0.197	0.008	100.6	2.6	2.7	0.6	56.1	1.4	1.5	0.3	1.7	0.0	0.0	0.0
	10	03.08.19	3.30 PM	114.5	4.8	0.898	0.016	5.78	0.38	0.217	0.004	126.3	2.5	5.4	1.9	70.4	1.4	3.0	1.1	2.1	0.0	0.1	0.0
	11	04.08.19	7.00 PM	140.0	5.8	0.903	0.021	6.00	0.00	0.219	0.005	146.1	5.4	6.8	1.6	81.4	3.0	3.8	0.9	2.4	0.1	0.1	0.0
	12	05.08.19	9.30 AM	154.5	6.4	0.832	0.006	6.00	0.00	0.201	0.001	152.3	7.1	9.6	2.2	72.8	3.3	4.6	1.1	2.2	0.1	0.1	0.0
	13	05.08.19	4.00 PM	161.0	6.7	0.832	0.041	6.00	0.00	0.201	0.010	154.0	20.9	10.9	3.1	69.7	8.3	5.0	1.4	2.1	0.2	0.1	0.0
	14	06.08.19	9.00 AM	178.0	7.4	0.748	0.093	6.00	0.00	0.181	0.022	168.3	12.4	15.3	3.0	73.3	5.0	6.7	1.9	2.2	0.1	0.2	0.0
	15	06.08.19	7.30 PM	188.5	7.9	0.872	0.045	6.00	0.00	0.211	0.011	171.5	1.6	16.9	3.7	75.0	7.6	7.5	2.4	2.3	0.2	0.2	0.1
	16	07.08.19	8.00 AM	201.0	8.4	0.822	0.111	6.00	0.00	0.199	0.027	173.4	7.5	18.9	4.9	74.6	6.3	8.3	2.7	2.2	0.2	0.2	0.1
continuous, pH 5.5	17	07.08.19	2.30 PM	207.5	8.6	0.833	0.053	5.82	0.04	0.202	0.013	175.9	10.0	20.2	6.0	73.7	6.6	8.5	2.8	2.2	0.2	0.2	0.1
	18	08.08.19	9.00 AM	226.0	9.4	0.822	0.096	5.50	0.01	0.199	0.023	166.5	13.8	30.7	11.7	71.1	14.3	13.5	6.6	2.1	0.4	0.3	0.2
	19	08.08.19	11.00 AM	228.0	9.5	0.793	0.104	5.50	0.00	0.192	0.025	n.m.	n.m.	n.m.	n.m.	n.m.	n.m.	n.m.	n.m.	n.m.	n.m.	n.m.	n.m.
	20	08.08.19	2.30 PM	231.5	9.6	0.760	0.053	5.50	0.00	0.184	0.013	164.4	15.0	33.1	12.3	78.5	5.2	16.0	6.7	2.4	0.2	0.4	0.2
	21	09.08.19	9.00 AM	250.0	10.4	0.760	0.035	5.50	0.00	0.184	0.008	152.7	19.3	42.0	15.4	71.6	9.0	20.7	10.9	2.2	0.3	0.5	0.3
	22	09.08.19	4.30 PM	257.5	10.7	0.687	0.074	5.50	0.00	0.166	0.018	151.4	23.4	44.1	14.9	68.0	7.5	21.1	11.2	2.0	0.2	0.5	0.3
	23	10.08.19	9.30 AM	274.5	11.4	0.697	0.086	5.50	0.00	0.169	0.021	145.2	25.7	46.5	11.5	65.7	5.7	22.1	9.7	2.0	0.2	0.5	0.2
	24	11.08.19	8.30 PM	309.5	12.9	0.672	0.016	5.50	0.00	0.163	0.004	138.4	34.2	49.4	11.9	60.0	7.9	22.9	10.6	1.8	0.2	0.5	0.2
	25	12.08.19	7.30 AM	320.5	13.4	0.707	0.063	5.50	0.00	0.171	0.015	134.9	36.4	49.3	11.4	59.5	7.7	23.1	9.9	1.8	0.2	0.5	0.2
	26	12.08.19	4.00 PM	329.0	13.7	0.692	0.111	5.50	0.00	0.167	0.027	134.1	38.3	48.9	10.3	58.3	8.2	22.7	9.4	1.8	0.2	0.5	0.2
	27	13.08.19	7.00 AM	344.0	14.3	0.707	0.153	5.50	0.00	0.171	0.037	130.8	39.6	47.7	7.1	56.8	9.0	21.9	7.4	1.7	0.3	0.5	0.2
continuous, pH 5.0	28	13.08.19	3.30 PM	352.5	14.7	0.637	0.115	5.38	0.01	0.154	0.028	131.6	39.9	47.3	6.2	57.1	8.5	21.6	6.6	1.7	0.3	0.5	0.2
	29	14.08.19	8.30 AM	369.5	15.4	0.625	0.109	5.10	0.06	0.151	0.026	127.0	37.0	48.5	6.3	57.7	8.9	22.8	4.6	1.7	0.3	0.5	0.1
	30	14.08.19	4.00 PM	377.0	15.7	0.643	0.115	5.06	0.05	0.156	0.028	123.6	35.5	49.3	6.1	56.3	8.8	23.1	3.9	1.7	0.3	0.5	0.1
	31	15.08.19	11.00 AM	396.0	16.5	0.582	0.169	5.02	0.03	0.141	0.041	115.7	40.0	49.2	7.3	51.0	10.1	22.4	2.6	1.5	0.3	0.5	0.1
	32	15.08.19	4.00 PM	401.0	16.7	0.598	0.107	5.00	0.00	0.145	0.026	117.3	37.8	49.8	6.0	57.5	12.5	25.0	2.6	1.7	0.4	0.6	0.1
	33	16.08.19	2.00 PM	423.0	17.6	0.505	0.135	5.00	0.00	0.122	0.033	111.9	37.3	45.2	3.3	51.2	8.2	21.7	4.4	1.5	0.2	0.5	0.1
	34	17.08.19	2.00 PM	447.0	18.6	0.488	0.102	5.00	0.00	0.118	0.025	114.1	39.8	39.7	2.9	49.4	7.6	18.4	5.5	1.5	0.2	0.4	0.1
	35	18.08.19	5.00 PM	474.0	19.8	0.467	0.120	5.00	0.00	0.113	0.029	116.7	38.5	32.2	2.9	54.7	17.0	15.2	1.7	1.6	0.5	0.3	0.0
	36	19.08.19	9.00 AM	490.0	20.4	0.472	0.099	5.00	0.00	0.114	0.024	118.5	34.2	27.7	2.8	55.6	15.0	13.1	1.6	1.7	0.5	0.3	0.0
continuous, pH 4.5	37	19.08.19	4.30 PM	497.5	20.7	0.513	0.075	4.96	0.04	0.124	0.018	120.1	25.3	26.3	0.4	56.5	11.2	12.4	0.5	1.7	0.3	0.3	0.0
	38	20.08.19	9.00 AM	513.0	21.4	0.488	0.045	4.80	0.01	0.118	0.011	120.5	28.5	21.9	2.7	57.3	11.2	10.5	1.8	1.7	0.3	0.2	0.0
	39	20.08.19	4.00 PM	521.0	21.7	0.428	0.064	4.74	0.01	0.104	0.016	119.6	21.6	20.4	0.2	57.1	9.0	9.7	0.5	1.7	0.3	0.2	0.0
	40	21.08.19	9.30 AM	537.5	22.4	0.397	0.065	4.65	0.01	0.096	0.016	113.0	23.2	16.6	2.0	55.6	11.7	8.2	1.3	1.7	0.4	0.2	0.0
	41	21.08.19	4.00 PM	544.0	22.7	0.365	0.045	4.62	0.01	0.088	0.011	106.6	21.9	15.0	1.5	54.6	8.7	7.8	1.4	1.6	0.3	0.2	0.0
	42	22.08.19	9.30 AM	561.5	23.4	0.313	0.063	4.60	0.03	0.076	0.015	93.8	19.5	12.2	1.3	49.8	10.3	6.5	1.1	1.5	0.3	0.2	0.0
	43	22.08.19	4.00 PM	568.0	23.7	0.286	0.048	4.61	0.03	0.069	0.012	88.5	19.2	11.3	1.2	47.0	10.3	6.1	1.0	1.4	0.3	0.1	0.0
	44	23.08.19	9.30 AM	585.5	24.4	0.237	0.028	4.61	0.03	0.057	0.007	73.2	16.0	9.1	0.8	39.4	8.3	4.9	0.6	1.2	0.2	0.1	0.0
	45	23.08.19	4.00 PM	592.0	24.7	0.222	0.037	4.60	0.03	0.054	0.009	68.2	14.9	8.4	0.8	36.7	7.6	4.5	0.6	1.1	0.2	0.1	0.0
	46	24.08.19	6.00 AM	606.0	25.3	0.196	0.047	4.62	0.03	0.047	0.011	57.9	12.5	6.8	0.7	32.5	8.2	3.8	0.2	1.0	0.2	0.1	0.0
	47	25.08.19	11.30 PM	647.5	27.0	0.133	0.007	4.66	0.03	0.032	0.002	35.0	8.0	3.7	0.5	20.1	4.1	2.2	0.3	0.6	0.1	0.0	0.0
	48	26.08.19	1.00 PM	661.0	27.5	0.111	0.005	4.69	0.04	0.027	0.001	29.4	7.1	3.0	0.5	17.1	2.4	1.8	0.4	0.5	0.1	0.0	0.0

Supplementary Table S3 Single data obtained from the cultivation of *C. ljungdahlii* WT in nitrate-containing medium with H_2 and CO_2 using the self-built MBS (Reactor 4). Growth parameter: medium feed rate = 0.0986 mL min^{-1}; gas low rate = 30 mL min^{-1}, nitrate feed rate = 0.002 mM min^{-1}; CDW/L/OD_{600} [g] = 0.288 and total cultivation time = 661 h. The pH (6.0 – 4.5) was maintained with base but not with acid. Any negative production rate was set = 0. n.m. = not measured.

						Reactor 4 (nitrate)														
	sample	date	time	cultivation time [h]	cultivation time [d]	measured OD	DF	OD600nm	wet volume [L]	CDW_{total} [g]	pH	acetate measured [mM]	ethanol measured [mM]	acetate production rate [mmol-C L^{-1} d^{-1}]	ethanol production rate [mmol-C L^{-1} d^{-1}]	acetate production rate [g L^{-1} d^{-1}]	ethanol production rate [g L^{-1} d^{-1}]	ratio (ethanol/acetate)	nitrate	nitrite
Batch	0	29.07.19	7.45 PM	0.0	0.0	0	1	0	0.500	0	6.00	0	0	0	0	0	0	0	no	no
	1	29.07.19	8.00 PM	0.3	0.0	0.075	1	0.075	0.500	0.022	6.00	1.9	0	0	0	0	0	0	no	no
	2	30.07.19	10.45 AM	14.5	0.6	0.102	1	0.102	0.500	0.029	6.00	1.6	0	0.0	0	0.0	0	0	no	no
	3	30.07.19	4.00 AM	20.0	0.8	0.115	1	0.115	0.500	0.033	6.00	3.0	0	12.2	0	0.4	0	0	no	no
	4	31.07.19	8.30 AM	35.5	1.5	0.244	1	0.244	0.500	0.070	6.00	15.0	0	37.3	0	1.1	0	0	no	no
	5	31.07.19	4.00 PM	43.0	1.8	0.322	1	0.322	0.500	0.093	6.00	27.2	0	77.7	0	2.3	0	0	no	no
	6	01.08.19	9.00 AM	60.0	2.5	0.288	2	0.576	0.500	0.166	6.00	58.8	0	89.2	0	2.7	0	0	no	no
continuous, pH 6.0	7	01.08.19	4.30 PM	67.5	2.8	0.318	2	0.636	0.500	0.183	6.00	70.0	0	39.0	0	1.2	0	0	no	no
	8	02.08.19	9.00 AM	84.0	3.5	0.438	2	0.876	0.500	0.253	6.00	86.0	0	48.0	0	1.4	0	0	no	no
	9	02.08.19	3.30 PM	90.5	3.8	0.202	5	1.010	0.500	0.291	6.00	92.2	0	51.4	0	1.5	0	0	no	no
	10	03.08.19	3.30 PM	114.5	4.8	0.231	5	1.155	0.500	0.333	6.00	121.5	1.7	67.7	0.9	2.0	0.0	0.0	no	no
	11	04.08.19	7.00 PM	140.0	5.8	0.206	5	1.030	0.600	0.297	6.00	148.1	6.9	68.8	3.2	2.1	0.1	0.0	no	no
	12	05.08.19	9.30 AM	154.5	6.4	0.177	5	0.885	0.650	0.255	6.00	143.3	13.3	61.4	5.7	1.8	0.1	0.1	no	no
	13	05.08.19	4.00 PM	161.0	6.7	0.182	5	0.910	0.600	0.262	6.00	157.7	16.3	73.2	7.6	2.2	0.2	0.1	no	no
	14	06.08.19	9.00 AM	178.0	7.4	0.237	5	1.185	0.500	0.342	6.00	199.2	20.7	111.0	11.6	3.3	0.3	0.1	no	no
	15	06.08.19	7.30 PM	188.5	7.9	0.243	5	1.215	0.500	0.350	6.00	231.1	25.1	128.8	14.0	3.9	0.3	0.1	no	no
	16	07.08.19	8.00 AM	201.0	8.4	0.183	5	0.915	0.500	0.264	6.00	190.9	21.4	106.4	11.9	3.2	0.3	0.1	yes	yes
continuous, pH 5.5	17	07.08.19	2.30 PM	207.5	8.6	0.176	5	0.880	0.500	0.254	5.81	177.2	19.4	98.8	10.8	3.0	0.2	0.1	yes	yes
	18	08.08.19	9.00 AM	226.0	9.4	0.122	5	0.610	0.550	0.176	5.82	136.1	14.4	69.0	7.3	2.1	0.2	0.1	yes	yes
	19	08.08.19	11.00 AM	228.0	9.5	0.123	5	0.615	0.500	0.177	5.83	n.m.	n.m.	n.m.	n.m.	n.m.	n.m.	n.m.	yes	yes
	20	08.08.19	2.30 PM	231.5	9.6	0.099	5	0.495	0.500	0.143	5.83	128.9	13.4	71.8	7.5	2.2	0.2	0.1	yes	yes
	21	09.08.19	9.00 AM	250.0	10.4	0.084	5	0.420	0.525	0.121	5.83	96.5	10.1	51.2	5.4	1.5	0.1	0.1	yes	no
	22	09.08.19	4.30 PM	257.5	10.7	0.075	5	0.375	0.525	0.108	5.84	89.5	9.1	47.5	4.8	1.4	0.1	0.1	yes	no
	23	10.08.19	9.30 AM	274.5	11.4	0.158	2	0.316	0.550	0.091	5.77	69.0	6.9	35.0	3.5	1.0	0.1	0.1	yes	no
	24	11.08.19	8.30 PM	309.5	12.9	0.105	2	0.210	0.625	0.061	5.76	45.3	3.8	20.2	1.7	0.6	0.0	0.1	yes	no
	25	12.08.19	7.30 AM	320.5	13.4	0.089	2	0.178	0.675	0.051	5.76	40.5	3.1	16.7	1.3	0.5	0.0	0.1	yes	no
	26	12.08.19	4.00 PM	329.0	13.7	0.078	2	0.156	0.725	0.045	5.76	38.2	2.7	14.7	1.0	0.4	0.0	0.1	yes	no
	27	13.08.19	7.00 AM	344.0	14.3	0.075	2	0.150	0.725	0.043	5.83	32.7	2.2	12.6	0.8	0.4	0.0	0.1	yes	no
continuous, pH 5.0	28	13.08.19	3.30 PM	352.5	14.7	0.067	2	0.134	0.775	0.039	5.74	31.2	2.1	11.2	0.7	0.3	0.0	0.1	no	no
	29	14.08.19	8.30 AM	369.5	15.4	0.091	2	0.182	0.700	0.052	5.79	28.2	1.9	11.2	0.7	0.3	0.0	0.1	no	no
	30	14.08.19	4.00 PM	377.0	15.7	0.115	2	0.230	0.800	0.066	5.84	28.0	1.8	9.8	0.6	0.3	0.0	0.1	no	no
	31	15.08.19	11.00 AM	396.0	16.5	0.259	2	0.518	0.800	0.149	5.73	34.1	0	11.9	0.0	0.4	0.0	0.0	no	no
	32	15.08.19	4.00 PM	401.0	16.7	0.294	2	0.588	0.600	0.170	5.73	34.6	0	16.1	0.0	0.5	0.0	0.0	no	no
	33	16.08.19	2.00 PM	423.0	17.6	0.142	5	0.710	0.700	0.205	5.06	48.0	15.1	19.1	6.0	0.6	0.1	0.3	no	no
	34	17.08.19	2.00 PM	447.0	18.6	0.156	5	0.780	0.900	0.225	5.00	58.6	34.6	18.2	10.7	0.5	0.2	0.6	no	no
	35	18.08.19	5.00 PM	474.0	19.8	0.169	5	0.845	0.600	0.244	5.00	58.3	66.9	27.1	31.1	0.8	0.7	1.1	no	no
	36	19.08.19	9.00 AM	490.0	20.4	0.242	5	1.210	0.600	0.349	5.00	55.7	84.1	25.9	39.1	0.8	0.9	1.5	no	no
continuous, pH 4.5	37	19.08.19	4.30 PM	497.5	20.7	0.203	5	1.015	0.600	0.293	5.08	54.0	96.0	25.1	44.6	0.8	1.0	1.8	no	no
	38	20.08.19	9.00 AM	513.0	21.4	0.258	5	1.290	0.600	0.372	5.16	51.6	106.3	24.0	49.4	0.7	1.1	2.1	no	no
	39	20.08.19	4.00 PM	521.0	21.7	0.202	5	1.010	0.575	0.291	4.97	51.6	108.3	25.0	52.5	0.8	1.2	2.1	no	no
	40	21.08.19	9.30 AM	537.5	22.4	0.184	5	0.920	0.575	0.265	5.03	33.4	128.0	16.2	62.0	0.5	1.4	3.8	no	no
	41	21.08.19	4.00 PM	544.0	22.7	0.184	5	0.920	0.575	0.265	4.84	40.1	116.7	19.4	56.6	0.6	1.3	2.9	no	no
	42	22.08.19	9.30 AM	561.5	23.4	0.176	5	0.880	0.650	0.254	4.95	38.9	124.3	16.7	53.3	0.5	1.2	3.2	no	no
	43	22.08.19	4.00 PM	568.0	23.7	0.183	5	0.915	0.650	0.264	4.91	41.4	126.3	17.7	54.2	0.5	1.2	3.1	no	no
	44	23.08.19	9.30 AM	585.5	24.4	0.228	5	1.140	0.650	0.329	4.84	45.7	133.2	19.6	57.1	0.6	1.3	2.9	yes	yes
	45	23.08.19	4.00 PM	592.0	24.7	0.124	5	0.620	0.650	0.179	4.50	38.7	137.7	16.6	59.0	0.5	1.4	3.6	yes	yes
	46	24.08.19	6.00 AM	606.0	25.3	0.18	2	0.360	0.700	0.104	4.53	31.5	133.1	12.6	53.0	0.4	1.2	4.2	yes	no
	47	25.08.19	11.30 PM	647.5	27.0	0.199	1	0.199	0.700	0.057	4.54	30.5	95.1	12.1	37.9	0.4	0.9	3.1	yes	no
	48	26.08.19	1.00 PM	661.0	27.5	0.233	1	0.233	0.650	0.067	4.53	35.9	83.4	15.4	35.8	0.5	0.8	2.3	yes	no

Supplementary Table S4 Single data obtained from the cultivation of *C. ljungdahlii* WT in nitrate-containing medium with H_2 and CO_2 using the self-built MBS (Reactor 5). Growth parameter: medium feed rate = 0.0986 mL min^{-1}; gas low rate = 30 mL min^{-1}, nitrate feed rate = 0.002 mM min^{-1}; CDW/L/OD_{600} [g] = 0.288 and total cultivation time = 661 h. The pH (6.0 – 4.5) was maintained with base but not with acid. Any negative production rate was set = 0. n.m. = not measured.

						Reactor 5 (nitrate)															
	sample	date	time	cultivation time [h]	cultivation time [d]	measured OD	DF	OD600nm	wet volume [L]	CDW_{total} [g]	pH	acetate measured [mM]	ethanol measured [mM]	acetate production rate [mmol-C L^{-1} d^{-1}]	ethanol production rate [mmol-C L^{-1} d^{-1}]	acetate production rate [g L^{-1} d^{-1}]	ethanol production rate [g L^{-1} d^{-1}]	ratio (ethanol/acetate)	nitrate	nitrite
Batch	0	29.07.19	7.45 PM	0.0	0.0	0	1	0	0.500	0.000	6.00	2.5	0	0.0	0	0	0	0	no	no
	1	29.07.19	8.00 PM	0.3	0.0	0.075	1	0.075	0.500	0.022	6.00	1.7	0	0.0	0	0	0	0	no	no
	2	30.07.19	10.45 AM	14.5	0.6	0.131	1	0.131	0.500	0.038	6.00	3.3	0	5.3	0	0.2	0	0	no	no
	3	30.07.19	4.00 AM	20.0	0.8	0.125	1	0.125	0.500	0.036	6.00	12.6	0	81.4	0	2.4	0	0	no	no
	4	31.07.19	8.30 AM	35.5	1.5	0.205	1	0.205	0.500	0.059	6.00	17.6	0	15.4	0	0.5	0	0	no	no
	5	31.07.19	4.00 PM	43.0	1.8	0.245	1	0.245	0.500	0.071	6.00	23.0	0	34.8	0	1.0	0	0	no	no
	6	01.08.19	9.00 AM	60.0	2.5	0.114	2	0.228	0.500	0.066	6.00	29.2	0	17.5	0	0.5	0	0	no	no
continuous, pH 6.0	7	01.08.19	4.30 PM	67.5	2.8	0.123	2	0.246	0.500	0.071	6.00	38.5	0	21.4	0	0.6	0	0	yes	no
	8	02.08.19	9.00 AM	84.0	3.5	0.177	2	0.354	0.550	0.102	6.00	44.3	0	22.4	0	0.7	0	0	yes	no
	9	02.08.19	3.30 PM	90.5	3.8	0.254	2	0.508	0.600	0.146	6.00	79.2	0	36.8	0	1.1	0	0	yes	no
	10	03.08.19	3.30 PM	114.5	4.8	0.151	5	0.755	0.650	0.218	6.00	119.8	0	51.4	0	1.5	0	0	no	no
	11	04.08.19	7.00 PM	140.0	5.8	0.191	5	0.955	0.600	0.275	6.00	139.7	2.4	64.9	1.1	1.9	0.0	0.0	no	no
	12	05.08.19	9.30 AM	154.5	6.4	0.209	5	1.045	0.600	0.301	6.00	144.5	2.9	67.1	1.4	2.0	0.0	0.0	no	no
	13	05.08.19	4.00 PM	161.0	6.7	0.211	5	1.055	0.650	0.304	6.00	146.5	3.3	62.8	1.4	1.9	0.0	0.0	no	no
	14	06.08.19	9.00 AM	178.0	7.4	0.185	5	0.925	0.650	0.267	6.00	161.5	3.5	69.2	1.5	2.1	0.0	0.0	no	no
	15	06.08.19	7.30 PM	188.5	7.9	0.217	5	1.085	0.650	0.313	6.00	168.6	4.4	72.3	1.9	2.2	0.0	0.0	no	no
	16	07.08.19	8.00 AM	201.0	8.4	0.243	5	1.215	0.600	0.350	6.00	175.3	6.2	81.5	2.9	2.4	0.1	0.0	no	no
continuous, pH 5.5	17	07.08.19	2.30 PM	207.5	8.6	0.25	5	1.250	0.600	0.360	5.81	167.5	7.0	77.8	3.3	2.3	0.1	0.0	no	no
	18	08.08.19	9.00 AM	226.0	9.4	0.242	5	1.210	0.625	0.349	5.50	167.5	21.8	74.7	9.7	2.2	0.2	0.1	no	no
	19	08.08.19	11.00 AM	228.0	9.5	0.245	5	1.225	0.625	0.353	5.50	n.m.	n.m.	n.m.	n.m.	n.m.	n.m.	n.m.	no	no
	20	08.08.19	2.30 PM	231.5	9.6	0.272	5	1.360	0.625	0.392	5.50	152.1	25.1	67.8	11.2	2.0	0.3	0.2	no	no
	21	09.08.19	9.00 AM	250.0	10.4	0.245	5	1.225	0.675	0.353	5.50	147.8	36.0	61.0	14.9	1.8	0.3	0.2	no	no
	22	09.08.19	4.30 PM	257.5	10.7	0.239	5	1.195	0.700	0.345	5.50	138.0	39.9	54.9	15.9	1.6	0.4	0.3	no	no
	23	10.08.19	9.30 AM	274.5	11.4	0.234	5	1.170	0.700	0.337	5.50	117.5	49.1	46.8	19.6	1.4	0.5	0.4	no	no
	24	11.08.19	8.30 PM	309.5	12.9	0.22	5	1.100	0.700	0.317	5.50	106.9	58.8	42.6	23.4	1.3	0.5	0.6	no	no
	25	12.08.19	7.30 AM	320.5	13.4	0.215	5	1.075	0.700	0.310	5.50	101.6	64.7	40.5	25.8	1.2	0.6	0.6	no	no
	26	12.08.19	4.00 PM	329.0	13.7	0.206	5	1.030	0.700	0.297	5.50	93.0	68.3	37.0	27.2	1.1	0.6	0.7	no	no
	27	13.08.19	7.00 AM	344.0	14.3	0.224	5	1.120	0.700	0.323	5.50	90.8	73.1	36.2	29.1	1.1	0.7	0.8	no	no
continuous, pH 5.0	28	13.08.19	3.30 PM	352.5	14.7	0.214	5	1.070	0.700	0.308	5.50	79.9	75.2	31.8	29.9	1.0	0.7	0.9	no	no
	29	14.08.19	8.30 AM	369.5	15.4	0.217	5	1.085	0.700	0.313	5.57	78.3	74.7	31.2	29.7	0.9	0.7	1.0	no	no
	30	14.08.19	4.00 PM	377.0	15.7	0.202	5	1.010	0.700	0.291	5.52	84.2	72.4	33.5	28.8	1.0	0.7	0.9	no	no
	31	15.08.19	11.00 AM	396.0	16.5	0.195	5	0.975	0.700	0.281	5.12	85.5	63.4	34.0	25.2	1.0	0.6	0.7	no	no
	32	15.08.19	4.00 PM	401.0	16.7	0.189	5	0.945	0.600	0.272	5.05	87.9	62.0	40.9	28.8	1.2	0.7	0.7	no	no
	33	16.08.19	2.00 PM	423.0	17.6	0.202	5	1.010	0.600	0.291	5.00	92.4	51.6	42.9	24.0	1.3	0.6	0.6	no	no
	34	17.08.19	2.00 PM	447.0	18.6	0.176	5	0.880	0.600	0.254	5.00	104.9	41.2	48.7	19.1	1.5	0.4	0.4	no	no
	35	18.08.19	5.00 PM	474.0	19.8	0.181	5	0.905	0.600	0.261	5.00	113.2	35.0	52.6	16.3	1.6	0.4	0.3	no	no
	36	19.08.19	9.00 AM	490.0	20.4	0.183	5	0.915	0.600	0.264	5.00	113.7	31.7	52.8	14.7	1.6	0.3	0.3	yes	yes
continuous, pH 4.5	37	19.08.19	4.30 PM	497.5	20.7	0.161	5	0.805	0.600	0.232	5.00	114.1	30.9	53.0	14.3	1.6	0.3	0.3	yes	yes
	38	20.08.19	9.00 AM	513.0	21.4	0.13	5	0.650	0.600	0.187	4.90	106.4	25.9	49.4	12.0	1.5	0.3	0.2	yes	no
	39	20.08.19	4.00 PM	521.0	21.7	0.118	5	0.590	0.600	0.170	4.90	90.3	24.1	42.0	11.2	1.3	0.3	0.3	yes	no
	40	21.08.19	9.30 AM	537.5	22.4	0.097	5	0.485	0.600	0.140	4.91	84.5	19.7	39.2	9.1	1.2	0.2	0.2	yes	no
	41	21.08.19	4.00 PM	544.0	22.7	0.074	5	0.370	0.600	0.107	4.92	67.8	18.0	31.5	8.4	0.9	0.2	0.3	yes	no
	42	22.08.19	9.30 AM	561.5	23.4	0.164	2	0.328	0.575	0.095	4.92	64.6	14.1	31.3	6.8	0.9	0.2	0.2	yes	no
	43	22.08.19	4.00 PM	568.0	23.7	0.166	2	0.332	0.575	0.096	4.93	53.9	13.3	26.1	6.5	0.8	0.1	0.2	yes	no
	44	23.08.19	9.30 AM	585.5	24.4	0.122	2	0.244	0.575	0.070	4.92	50.0	10.9	24.2	5.3	0.7	0.1	0.2	yes	no
	45	23.08.19	4.00 PM	592.0	24.7	0.225	1	0.225	0.575	0.065	4.50	42.8	9.9	20.7	4.8	0.6	0.1	0.2	yes	no
	46	24.08.19	6.00 AM	606.0	25.3	0.086	2	0.172	0.550	0.050	4.53	26.2	8.2	13.3	4.1	0.4	0.1	0.3	yes	no
	47	25.08.19	11.30 PM	647.5	27.0	0.154	1	0.154	0.525	0.044	4.54	21.8	4.7	11.6	2.5	0.3	0.1	0.2	yes	no
	48	26.08.19	1.00 PM	661.0	27.5	0.112	1	0.112	0.500	0.032	4.54	0.0	3.8	0.0	2.1	0.0	0.0	0.0	yes	no

Supplementary Table S5 Single data obtained from the cultivation of *C. ljungdahlii* WT in nitrate-containing medium with H_2 and CO_2 using the self-built MBS (Reactor 6). Growth parameter: medium feed rate = 0.0986 mL min^{-1}; gas low rate = 30 mL min^{-1}, nitrate feed rate = 0.002 mM min^{-1}; CDW/L/OD_{600} [g] = 0.288 and total cultivation time = 661 h. The pH (6.0 – 4.5) was maintained with base but not with acid. Any negative production rate was set = 0. n.m. = not measured.

						Reactor 6 (nitrate)														
	sample	date	time	cultivation time [h]	cultivation time [d]	measured OD	DF	OD600nm	wet volume [L]	CDW_{total} [g]	pH	acetate measured [mM]	ethanol measured [mM]	acetate production rate [mmol-C L^{-1} d^{-1}]	ethanol production rate [mmol-C L^{-1} d^{-1}]	acetate production rate [g L^{-1} d^{-1}]	ethanol production rate [g L^{-1} d^{-1}]	ratio (ethanol/acetate)	nitrate	nitrite
Batch	0	29.07.19	7.45 PM	0.0	0.0	0.000	1	0	0.500	0.000	6.00	0.0	0.0	0.0	0.0	0.0	0.0	0.0	no	no
	1	29.07.19	8.00 PM	0.3	0.0	0.076	1	0.076	0.500	0.022	6.00	1.9	0.0	0.0	0.0	10.7	0.0	0.0	no	no
	2	30.07.19	10.45 AM	14.5	0.6	0.113	1	0.113	0.500	0.033	6.00	1.7	0.0	0.0	0.0	0.0	0.0	0.0	no	no
	3	30.07.19	4.00 AM	20.0	0.8	0.124	1	0.124	0.500	0.036	6.00	3.2	0.0	13.4	0.0	0.4	0.0	0.0	no	no
	4	31.07.19	8.30 AM	35.5	1.5	0.263	1	0.263	0.500	0.076	6.00	16.7	0.0	41.8	0.0	1.3	0.0	0.0	no	no
	5	31.07.19	4.00 PM	43.0	1.8	0.325	1	0.325	0.500	0.094	6.00	28.6	0.0	76.5	0.0	2.3	0.0	0.0	no	no
	6	01.08.19	9.00 AM	60.0	2.5	0.289	2	0.578	0.500	0.167	6.00	61.9	1.9	93.8	5.5	2.8	0.3	0.0	no	no
continuous, pH 6.0	7	01.08.19	4.30 PM	67.5	2.8	0.360	2	0.720	0.500	0.208	6.00	81.5	1.7	45.4	0.9	1.4	0.0	0.0	no	no
	8	02.08.19	9.00 AM	84.0	3.5	0.475	2	0.950	0.500	0.274	6.00	104.8	1.6	58.4	0.9	1.8	0.0	0.0	no	no
	9	02.08.19	3.30 PM	90.5	3.8	0.214	5	1.070	0.500	0.308	6.00	114.3	1.8	63.7	1.0	1.9	0.0	0.0	no	no
	10	03.08.19	3.30 PM	114.5	4.8	0.229	5	1.145	0.500	0.330	6.00	146.3	3.5	81.6	2.0	2.4	0.0	0.0	no	no
	11	04.08.19	7.00 PM	140.0	5.8	0.230	5	1.150	0.500	0.332	6.00	169.9	7.5	94.7	4.2	2.8	0.1	0.0	no	no
	12	05.08.19	9.30 AM	154.5	6.4	0.240	5	1.200	0.500	0.346	6.00	175.6	10.0	97.9	5.6	2.9	0.1	0.1	no	no
	13	05.08.19	4.00 PM	161.0	6.7	0.229	5	1.145	0.500	0.330	6.00	170.0	10.6	94.8	5.9	2.8	0.1	0.1	no	no
	14	06.08.19	9.00 AM	178.0	7.4	0.219	5	1.095	0.500	0.316	6.00	176.0	13.0	98.1	7.3	2.9	0.2	0.1	no	no
	15	06.08.19	7.30 PM	188.5	7.9	0.268	5	1.340	0.500	0.386	6.00	190.9	14.2	106.4	7.9	3.2	0.2	0.1	no	no
	16	07.08.19	8.00 AM	201.0	8.4	0.242	5	1.210	0.500	0.349	6.00	194.2	16.3	108.3	9.1	3.3	0.2	0.1	no	no
continuous, pH 5.5	17	07.08.19	2.30 PM	207.5	8.6	0.266	5	1.330	0.500	0.383	5.79	198.4	16.7	110.6	9.3	3.3	0.2	0.1	no	no
	18	08.08.19	9.00 AM	226.0	9.4	0.246	5	1.230	0.500	0.355	5.50	176.8	32.1	98.5	17.9	3.0	0.4	0.2	no	no
	19	08.08.19	11.00 AM	228.0	9.5	0.244	5	1.220	0.500	0.352	5.50	n.m.	n.m.	n.m.	n.m.	n.m.	n.m.	n.m.	no	no
	20	08.08.19	2.30 PM	231.5	9.6	0.225	5	1.125	0.450	0.324	5.50	173.2	35.8	107.3	22.2	3.2	0.5	0.2	no	no
	21	09.08.19	9.00 AM	250.0	10.4	0.230	5	1.150	0.600	0.332	5.50	151.3	45.3	70.3	21.1	2.1	0.5	0.3	no	no
	22	09.08.19	4.30 PM	257.5	10.7	0.240	5	1.200	0.600	0.346	5.50	151.8	47.1	70.5	21.9	2.1	0.5	0.3	no	no
	23	10.08.19	9.30 AM	274.5	11.4	0.258	5	1.290	0.600	0.372	5.50	144.8	47.4	67.3	22.0	2.0	0.5	0.3	yes	yes
	24	11.08.19	8.30 PM	309.5	12.9	0.209	5	1.045	0.600	0.301	5.50	134.1	50.6	62.3	23.5	1.9	0.5	0.4	yes	yes
	25	12.08.19	7.30 AM	320.5	13.4	0.207	5	1.035	0.600	0.298	5.59	120.0	60.7	55.8	28.2	1.7	0.6	0.5	yes	yes
	26	12.08.19	4.00 PM	329.0	13.7	0.185	5	0.925	0.600	0.267	5.50	106.3	63.2	49.4	29.4	1.5	0.7	0.6	yes	yes
	27	13.08.19	7.00 AM	344.0	14.3	0.170	5	0.850	0.500	0.245	5.50	91.7	54.9	51.1	30.6	1.5	0.7	0.6	yes	yes
continuous, pH 5.0	28	13.08.19	3.30 PM	352.5	14.7	0.144	5	0.720	0.500	0.208	5.50	86.3	51.3	48.1	28.6	1.4	0.7	0.6	yes	yes
	29	14.08.19	8.30 AM	369.5	15.4	0.263	2	0.526	0.475	0.152	5.50	69.8	41.7	40.9	24.5	1.2	0.6	0.6	yes	yes
	30	14.08.19	4.00 PM	377.0	15.7	0.242	2	0.484	0.470	0.140	5.50	62.8	37.6	37.2	22.3	1.1	0.5	0.6	yes	yes
	31	15.08.19	11.00 AM	396.0	16.5	0.166	2	0.332	0.450	0.096	5.50	42.0	25.0	26.0	15.5	0.8	0.4	0.6	yes	yes
	32	15.08.19	4.00 PM	401.0	16.7	0.157	2	0.314	0.450	0.091	5.50	45.1	26.3	27.9	16.3	0.8	0.4	0.6	yes	no
	33	16.08.19	2.00 PM	423.0	17.6	0.113	2	0.226	0.450	0.065	5.50	31.3	17.8	19.4	11.0	0.6	0.3	0.6	yes	no
	34	17.08.19	2.00 PM	447.0	18.6	0.087	2	0.174	0.400	0.050	5.50	21.8	11.7	15.2	8.2	0.5	0.2	0.5	yes	no
	35	18.08.19	5.00 PM	474.0	19.8	0.119	1	0.119	0.475	0.034	5.50	15.1	7.8	8.9	4.6	0.3	0.1	0.5	yes	no
	36	19.08.19	9.00 AM	490.0	20.4	0.060	2	0.120	0.475	0.035	5.50	12.6	6.4	7.4	3.7	0.2	0.1	0.5	yes	no
continuous, pH 4.5	37	19.08.19	4.30 PM	497.5	20.7	0.111	1	0.111	0.475	0.032	5.50	11.0	6.0	6.5	3.5	0.2	0.1	0.5	yes	no
	38	20.08.19	9.00 AM	513.0	21.4	0.107	1	0.107	0.450	0.031	5.50	9.4	4.7	5.8	2.9	0.2	0.1	0.5	yes	no
	39	20.08.19	4.00 PM	521.0	21.7	0.100	1	0.100	0.450	0.029	5.50	8.7	4.3	5.4	2.7	0.2	0.1	0.5	yes	no
	40	21.08.19	9.30 AM	537.5	22.4	0.105	1	0.105	0.400	0.030	5.50	6.8	3.5	4.7	2.4	0.1	0.1	0.5	yes	no
	41	21.08.19	4.00 PM	544.0	22.7	0.082	1	0.082	0.400	0.024	5.50	6.4	3.3	4.4	2.3	0.1	0.1	0.5	yes	no
	42	22.08.19	9.30 AM	561.5	23.4	0.066	1	0.066	0.500	0.019	5.54	5.3	2.8	3.0	1.5	0.1	0.0	0.5	yes	no
	43	22.08.19	4.00 PM	568.0	23.7	0.069	1	0.069	0.500	0.020	5.53	5.0	2.6	2.8	1.4	0.1	0.0	0.5	yes	no
	44	23.08.19	9.30 AM	585.5	24.4	0.049	1	0.049	0.450	0.014	5.54	4.4	2.4	2.7	1.5	0.1	0.0	0.5	yes	no
	45	23.08.19	4.00 PM	592.0	24.7	0.033	1	0.033	0.400	0.010	4.50	4.3	2.4	3.0	1.6	0.1	0.0	0.6	yes	no
	46	24.08.19	6.00 AM	606.0	25.3	0.021	1	0.021	0.450	0.006	4.51	3.7	2.1	2.3	1.3	0.1	0.0	0.6	yes	no
	47	25.08.19	11.30 PM	647.5	27.0	0.062	1	0.062	0.375	0.018	4.52	3.3	1.9	2.5	1.4	0.1	0.0	0.6	yes	no
	48	26.08.19	1.00 PM	661.0	27.5	0.032	1	0.032	0.375	0.009	4.50	3.3	1.8	2.4	1.3	0.1	0.0	0.5	yes	no

Supplementary Table S6 Single data obtained from the cultivation of *C. ljungdahlii* WT in nitrate-containing medium with H_2 and CO_2 using the self-built MBS (Reactor 7). Growth parameter: medium feed rate = 0.186 mL min^{-1}; gas low rate = 30 mL min^{-1}, nitrate feed rate = 0.003 mM min^{-1}; CDW/L/OD_{600} [g] = 0.288 and total cultivation time = 672.5 h. The pH (6.0 – 4.5) was maintained with base but not with acid. Any negative production rate was set = 0. n.m. = not measured.

						Reactor 7 (nitrate)														
	sample	date	time	cultivation time [h]	cultivation time [d]	measured OD	DF	OD600nm	wet volume [L]	CDW_{total} [g]	pH	acetate measured [mM]	ethanol measured [mM]	acetate production rate [mmol-C L^{-1} d^{-1}]	ethanol production rate [mmol-C L^{-1} d^{-1}]	acetate production rate [g L^{-1} d^{-1}]	ethanol production rate [g L^{-1} d^{-1}]	ratio (ethanol/acetate)	nitrate	nitrite
Batch	0	06.02.20	3:30 PM	0.0	0.0	0.000	1	0.000	0.500	0.000	6.00	0.0	0.0	0.0	0.0	0.0	0.0	0.0	no	no
	1	06.02.20	4:45 PM	1.3	0.1	0.078	1	0.078	0.500	0.011	6.00	0.5	0.0	20.8	0.0	0.6	0.0	0.0	no	no
	2	07.02.20	9:00 AM	17.5	0.7	0.105	1	0.105	0.500	0.015	6.00	1.5	0.0	2.7	0.0	0.1	0.0	0.0	no	no
	3	07.02.20	5:00 PM	25.5	1.1	0.145	1	0.145	0.500	0.021	6.00	6.4	0.0	29.9	0.0	0.9	0.0	0.0	no	no
	4	08.02.20	11:30 AM	44.0	1.8	0.326	1	0.326	0.500	0.047	6.00	26.3	0.0	51.6	0.0	1.5	0.0	0.0	no	no
	5	09.02.20	1:00 PM	69.5	2.9	0.311	2	0.622	0.500	0.090	6.00	69.4	0.0	81.1	0.0	2.4	0.0	0.0	no	no
	6	09.02.20	5:15 PM	73.8	3.1	0.328	2	0.656	0.500	0.095	6.00	71.4	0.0	22.9	0.0	0.7	0.0	0.0	no	no
continuous, pH 6.0	7	10.02.20	1:30 PM	94.0	3.9	0.158	5	0.790	0.500	0.114	6.00	74.3	0.0	79.6	0.0	2.4	0.0	0.0	no	no
	8	10.02.20	5:30 PM	98.0	4.1	0.169	5	0.845	0.500	0.122	6.00	74.5	0.0	79.8	0.0	2.4	0.0	0.0	no	no
	9	11.02.20	10:00 AM	114.5	4.8	0.188	5	0.940	0.525	0.142	6.00	75.0	0.0	76.5	0.0	2.3	0.0	0.0	no	no
	10	11.02.20	5:00 PM	121.5	5.1	0.180	5	0.900	0.525	0.136	6.00	75.8	0.0	77.4	0.0	2.3	0.0	0.0	no	no
	11	12.02.20	10:30 AM	139.0	5.8	0.185	5	0.925	0.550	0.147	6.00	79.4	0.0	77.4	0.0	2.3	0.0	0.0	no	no
	12	12.02.20	5:45 PM	146.3	6.1	0.196	5	0.980	0.550	0.155	6.00	75.2	0.0	73.2	0.0	2.2	0.0	0.0	no	no
	13	13.02.20	9:45 AM	162.3	6.8	0.177	5	0.885	0.550	0.140	6.00	86.6	0.0	84.3	0.0	2.5	0.0	0.0	no	no
	14	13.02.20	4:00 PM	168.5	7.0	0.179	5	0.895	0.550	0.142	6.00	83.3	0.0	81.1	0.0	2.4	0.0	0.0	no	no
	15	14.02.20	9:00 AM	185.5	7.7	0.197	5	0.985	0.550	0.156	6.00	86.8	0.0	84.5	0.0	2.5	0.0	0.0	no	no
	16	14.02.20	6:00 PM	194.5	8.1	0.209	5	1.045	0.550	0.166	6.00	91.8	0.0	89.4	0.0	2.7	0.0	0.0	no	no
	17	15.02.20	5:00 PM	217.5	9.1	0.206	5	1.030	0.525	0.156	6.00	97.9	0.0	99.9	0.0	3.0	0.0	0.0	no	no
continuous, pH 5.5	18	16.02.20	12:00 PM	236.5	9.9	0.242	5	1.210	0.400	0.140	5.50	93.2	2.0	124.8	2.6	3.7	0.1	0.0	no	no
	19	17.02.20	9:00 AM	257.5	10.7	0.230	5	1.150	0.400	0.133	5.46	89.9	16.4	120.4	22.0	3.6	0.5	0.2	no	no
	20	17.02.20	5:00 PM	265.5	11.1	0.222	5	1.110	0.475	0.152	5.46	89.7	19.1	101.2	21.5	3.0	0.5	0.2	no	no
	21	18.02.20	9:15 AM	281.8	11.7	0.243	5	1.215	0.550	0.193	5.48	83.9	23.6	81.7	22.9	2.5	0.5	0.3	no	no
	22	18.02.20	5:00 PM	289.5	12.1	0.234	5	1.170	0.625	0.211	5.46	90.3	27.5	77.4	23.6	2.3	0.5	0.3	no	no
	23	19.02.20	8:30 AM	305.0	12.7	0.225	5	1.125	0.625	0.203	5.47	82.5	36.3	70.7	31.1	2.1	0.7	0.4	no	no
	24	19.02.20	5:00 PM	313.5	13.1	0.222	5	1.110	0.625	0.200	5.47	81.9	43.9	70.2	37.6	2.1	0.9	0.5	no	no
	25	20.02.20	9:00 AM	329.5	13.7	0.222	5	1.110	0.625	0.200	5.47	85.5	48.4	73.3	41.5	2.2	1.0	0.6	no	no
	26	20.02.20	4:30 PM	337.0	14.0	0.241	5	1.205	0.625	0.217	5.47	89.1	47.2	76.4	40.5	2.3	0.9	0.5	no	no
	27	21.02.20	10:00 AM	354.5	14.8	0.262	5	1.310	0.650	0.245	5.47	102.7	39.6	84.6	32.6	2.5	0.8	0.4	no	no
continuous, pH 5.0	28	21.02.20	6:45 PM	363.3	15.1	0.248	5	1.240	0.550	0.197	5.45	98.8	43.7	96.2	42.6	2.9	1.0	0.4	no	no
	29	22.02.20	5:30 PM	386.0	16.1	0.253	5	1.265	0.550	0.201	5.55	78.6	58.5	76.6	56.9	2.3	1.3	0.7	no	no
	30	23.02.20	8:45 PM	413.3	17.2	0.233	5	1.165	0.525	0.176	5.65	62.7	52.7	64.0	53.8	1.9	1.2	0.8	no	no
	31	24.02.20	9:00 AM	425.5	17.7	0.203	5	1.015	0.525	0.154	5.26	66.3	48.7	67.6	49.7	2.0	1.1	0.7	no	no
	32	24.02.20	5:00 PM	433.5	18.1	0.199	5	0.995	0.525	0.151	5.15	68.3	47.4	69.7	48.4	2.1	1.1	0.7	no	no
	33	25.02.20	9:00 AM	449.5	18.7	0.217	5	1.085	0.500	0.156	5.08	67.1	49.8	71.9	53.3	2.2	1.2	0.7	no	no
	34	25.02.20	5:30 PM	458.0	19.1	0.222	5	1.110	0.500	0.160	5.08	64.9	51.5	69.6	55.2	2.1	1.3	0.8	no	no
	35	26.02.20	8:15 AM	472.8	19.7	0.238	5	1.190	0.500	0.172	5.07	63.0	50.5	67.5	54.1	2.0	1.2	0.8	no	no
	36	26.02.20	4:45 PM	481.3	20.1	0.233	5	1.165	0.500	0.168	5.10	60.4	51.9	64.7	55.6	1.9	1.3	0.9	no	no
	37	27.02.20	9:15 AM	497.8	20.7	0.260	5	1.300	0.475	0.178	5.06	60.0	50.1	67.7	56.5	2.0	1.3	0.8	no	no
continuous, pH 4.5	38	27.02.20	5:00 PM	505.5	21.1	0.232	5	1.160	0.475	0.159	5.04	59.8	49.6	67.5	55.9	2.0	1.3	0.8	no	no
	39	28.02.20	9:15 AM	521.8	21.7	0.242	5	1.210	0.425	0.148	5.06	58.5	51.6	73.8	65.1	2.2	1.5	0.9	no	no
	40	28.02.20	5:00 PM	529.5	22.1	0.226	5	1.130	0.500	0.163	4.98	60.9	48.9	65.3	52.4	2.0	1.2	0.8	no	no
	41	29.02.20	11:30 AM	548.0	22.8	0.241	5	1.205	0.625	0.217	4.96	61.9	52.5	53.0	45.0	1.6	1.0	0.8	no	no
	42	01.03.20	12:30 PM	573.0	23.9	0.243	5	1.215	0.625	0.219	4.91	63.4	62.3	54.3	53.4	1.6	1.2	1.0	no	no
	43	02.03.20	1:30 PM	598.0	24.9	0.242	5	1.210	0.575	0.201	4.87	64.7	59.9	60.3	55.8	1.8	1.3	0.9	no	no
	44	02.03.20	5:00 PM	601.5	25.1	0.237	5	1.185	0.575	0.196	4.77	71.8	56.7	66.9	52.9	2.0	1.2	0.8	no	no
	45	03.03.20	9:45 AM	618.3	25.8	0.220	5	1.100	0.550	0.174	4.66	79.2	46.5	77.1	45.3	2.3	1.0	0.6	no	no
	46	03.03.20	4:30 PM	625.0	26.0	0.187	5	0.935	0.550	0.148	4.67	79.9	42.0	77.8	40.9	2.3	0.9	0.5	no	no
	47	04.03.20	8:30 AM	641.0	26.7	0.153	5	0.765	0.550	0.121	4.78	69.9	31.9	68.0	31.1	2.0	0.7	0.5	no	yes
	48	04.03.20	4:30 PM	649.0	27.0	0.129	5	0.645	0.550	0.102	4.84	61.3	27.5	59.7	26.8	1.8	0.6	0.4	yes	yes
	49	05.03.20	9:30 AM	666.0	27.8	0.107	5	0.535	0.525	0.081	4.89	44.9	19.5	45.8	19.9	1.4	0.5	0.4	yes	no
	50	05.03.20	4:00 PM	672.5	28.0	0.084	5	0.420	0.525	0.064	4.91	40.1	17.2	40.9	17.6	1.2	0.4	0.4	yes	no

Supplementary Table S7 Single data obtained from the cultivation of *C. ljungdahlii* WT in nitrate-containing medium with H_2 and CO_2 using the self-built MBS (Reactor 8). Growth parameter: medium feed rate = 0.186 mL min^{-1}; gas low rate = 30 mL min^{-1}, nitrate feed rate = 0.003 mM min^{-1}; CDW/L/OD_{600} [g] = 0.288 and total cultivation time = 672.5 h. The pH (6.0 – 4.5) was maintained with base but not with acid. Any negative production rate was set = 0. n.m. = not measured.

						Reactor 8 (nitrate)														
	sample	date	time	cultivation time [h]	cultivation time [d]	measured OD	DF	OD600nm	wet volume [L]	CDW_{total} [g]	pH	acetate measured [mM]	ethanol measured [mM]	acetate production rate [mmol-C $L^{-1}d^{-1}$]	ethanol production rate [mmol-C $L^{-1}d^{-1}$]	acetate production rate [g $L^{-1}d^{-1}$]	ethanol production rate [g $L^{-1}d^{-1}$]	ratio (ethanol/acetate)	nitrate	nitrite
Batch	0	06.02.20	3:30 PM	0.0	0.0	0.000	1	0.000	0.500	0.000	6.00	0.0	0.0	0.0	0.0	0.0	0.0	0.0	no	no
	1	06.02.20	4:45 PM	1.3	0.1	0.083	1	0.075	0.500	0.011	6.00	0.6	0.0	21.6	0.0	0.6	0.0	0.0	no	no
	2	07.02.20	9:00 AM	17.5	0.7	0.111	1	0.111	0.500	0.016	6.00	2.4	0.0	5.3	0.0	0.2	0.0	0.0	no	no
	3	07.02.20	5:00 PM	25.5	1.1	0.140	1	0.140	0.500	0.020	6.00	6.2	0.0	22.8	0.0	0.7	0.0	0.0	no	no
	4	08.02.20	11:30 AM	44.0	1.8	0.310	1	0.310	0.500	0.045	6.00	27.8	0.0	56.2	0.0	1.7	0.0	0.0	no	no
	5	09.02.20	1:00 PM	69.5	2.9	0.327	2	0.654	0.500	0.094	6.00	71.5	0.0	82.2	0.0	2.5	0.0	0.0	no	no
	6	09.02.20	5:15 PM	73.8	3.1	0.344	2	0.688	0.500	0.099	6.00	79.2	0.0	87.3	0.0	2.6	0.0	0.0	no	no
continuous, pH 6.0	7	10.02.20	1:30 PM	94.0	3.9	0.197	5	0.985	0.550	0.156	6.00	85.4	1.7	83.2	1.6	2.5	0.0	0.0	no	no
	8	10.02.20	5:30 PM	98.0	4.1	0.194	5	0.970	0.550	0.154	6.00	92.3	1.6	89.9	1.5	2.7	0.0	0.0	no	no
	9	11.02.20	10:00 AM	114.5	4.8	0.208	5	1.040	0.550	0.165	6.00	103.9	2.1	101.2	2.0	3.0	0.0	0.0	no	no
	10	11.02.20	5:00 PM	121.5	5.1	0.221	5	1.105	0.550	0.175	6.00	108.1	3.0	105.3	2.9	3.2	0.1	0.0	no	no
	11	12.02.20	10:30 AM	139.0	5.8	0.195	5	0.975	0.550	0.155	6.00	113.5	7.4	110.5	7.2	3.3	0.2	0.1	no	no
	12	12.02.20	5:45 PM	146.3	6.1	0.181	5	0.905	0.550	0.144	6.00	104.1	9.4	101.4	9.1	3.0	0.2	0.1	no	no
	13	13.02.20	9:45 AM	162.3	6.8	0.207	5	1.035	0.600	0.179	6.00	115.6	10.7	103.2	9.6	3.1	0.2	0.1	no	no
	14	13.02.20	4:00 PM	168.5	7.0	0.216	5	1.080	0.650	0.202	6.00	129.2	12.6	106.5	10.4	3.2	0.2	0.1	no	no
	15	14.02.20	9:00 AM	185.5	7.7	0.215	5	1.075	0.650	0.201	6.00	133.1	12.4	109.7	10.2	3.3	0.2	0.1	no	no
	16	14.02.20	6:00 PM	194.5	8.1	0.212	5	1.060	0.650	0.199	6.00	140.3	11.4	115.6	9.4	3.5	0.2	0.1	no	no
	17	15.02.20	5:00 PM	217.5	9.1	0.229	5	1.145	0.750	0.248	6.00	157.0	9.2	112.1	6.6	3.4	0.2	0.1	no	no
continuous, pH 5.5	18	16.02.20	12:00 PM	236.5	9.9	0.222	5	1.110	0.600	0.192	5.51	155.9	13.2	139.2	11.8	4.2	0.3	0.1	no	no
	19	17.02.20	9:00 AM	257.5	10.7	0.251	5	1.255	0.650	0.235	5.50	144.9	33.7	119.4	27.8	3.6	0.6	0.2	no	no
	20	17.02.20	5:00 PM	265.5	11.1	0.258	5	1.290	0.550	0.205	5.43	132.7	45.9	129.2	44.7	3.9	1.0	0.3	no	no
	21	18.02.20	9:15 AM	281.8	11.7	0.244	5	1.220	0.575	0.202	5.45	107.6	60.7	100.3	56.6	3.0	1.3	0.6	no	no
	22	18.02.20	5:00 PM	289.5	12.1	0.246	5	1.230	0.575	0.204	5.43	108.1	71.5	100.7	66.6	3.0	1.5	0.7	no	no
	23	19.02.20	8:30 AM	305.0	12.7	0.275	5	1.375	0.575	0.228	5.46	96.4	81.7	89.8	76.2	2.7	1.8	0.8	no	no
	24	19.02.20	5:00 PM	313.5	13.1	0.253	5	1.265	0.575	0.210	5.43	94.0	88.4	87.6	82.4	2.6	1.9	0.9	no	no
	25	20.02.20	9:00 AM	329.5	13.7	0.272	5	1.360	0.575	0.225	5.47	91.0	86.1	84.7	80.2	2.5	1.8	0.9	no	no
	26	20.02.20	4:30 PM	337.0	14.0	0.231	5	1.155	0.575	0.191	5.45	86.9	88.2	81.0	82.1	2.4	1.9	1.0	no	no
	27	21.02.20	10:00 AM	354.5	14.8	0.292	5	1.460	0.575	0.242	5.62	72.4	91.7	67.4	85.4	2.0	2.0	1.3	no	no
continuous, pH 5.0	28	21.02.20	6:45 PM	363.3	15.1	0.225	5	1.125	0.575	0.186	5.76	65.4	88.8	60.9	82.8	1.8	1.9	1.4	no	no
	29	22.02.20	5:30 PM	386.0	16.1	0.234	5	1.170	0.575	0.194	5.46	63.4	70.8	59.1	66.0	1.8	1.5	1.1	no	no
	30	23.02.20	8:45 PM	413.3	17.2	0.232	5	1.160	0.575	0.192	5.08	68.4	68.5	63.7	63.9	1.9	1.5	1.0	no	no
	31	24.02.20	9:00 AM	425.5	17.7	0.250	5	1.250	0.575	0.207	5.12	65.3	70.4	60.8	65.6	1.8	1.5	1.1	no	no
	32	24.02.20	5:00 PM	433.5	18.1	0.212	5	1.060	0.575	0.176	5.14	62.7	73.4	58.4	68.4	1.8	1.6	1.2	no	no
	33	25.02.20	9:00 AM	449.5	18.7	0.249	5	1.245	0.575	0.206	5.15	59.7	74.2	55.7	69.2	1.7	1.6	1.2	no	no
	34	25.02.20	5:30 PM	458.0	19.1	0.225	5	1.125	0.575	0.186	5.11	60.4	73.4	56.3	68.4	1.7	1.6	1.2	no	no
	35	26.02.20	8:15 AM	472.8	19.7	0.250	5	1.250	0.575	0.207	5.03	61.8	69.1	57.6	64.3	1.7	1.5	1.1	no	no
	36	26.02.20	4:45 PM	481.3	20.1	0.229	5	1.145	0.575	0.190	4.95	61.7	69.2	57.5	64.5	1.7	1.5	1.1	no	no
	37	27.02.20	9:15 AM	497.8	20.7	0.237	5	1.185	0.575	0.196	4.91	64.3	65.2	59.9	60.7	1.8	1.4	1.0	no	no
continuous, pH 4.5	38	27.02.20	5:00 PM	505.5	21.1	0.232	5	1.160	0.600	0.201	4.74	73.5	55.2	65.6	49.3	2.0	1.1	0.8	no	no
	39	28.02.20	9:15 AM	521.8	21.7	0.220	5	1.100	0.600	0.190	4.72	80.4	50.7	71.8	45.2	2.2	1.0	0.6	no	no
	40	28.02.20	5:00 PM	529.5	22.1	0.198	5	0.990	0.600	0.171	4.74	90.1	39.9	80.5	35.6	2.4	0.8	0.4	no	no
	41	29.02.20	11:30 AM	548.0	22.8	0.168	5	0.840	0.600	0.145	4.86	89.6	35.3	80.0	31.5	2.4	0.7	0.4	yes	yes
	42	01.03.20	12:30 PM	573.0	23.9	0.097	5	0.485	0.625	0.087	4.94	70.1	25.4	60.1	21.8	1.8	0.5	0.4	yes	no
	43	02.03.20	1:30 PM	598.0	24.9	0.194	2	0.388	0.625	0.070	5.01	47.0	16.0	40.3	13.7	1.2	0.3	0.3	yes	no
	44	02.03.20	5:00 PM	601.5	25.1	0.160	2	0.320	0.625	0.058	5.04	33.4	10.8	28.6	9.3	0.9	0.2	0.3	yes	no
	45	03.03.20	9:45 AM	618.3	25.8	0.138	2	0.276	0.625	0.050	5.09	30.2	9.5	25.9	8.2	0.8	0.2	0.3	yes	no
	46	03.03.20	4:30 PM	625.0	26.0	0.117	2	0.234	0.600	0.040	5.11	23.0	7.0	20.5	6.2	0.6	0.1	0.3	yes	no
	47	04.03.20	8:30 AM	641.0	26.7	0.103	2	0.206	0.600	0.036	5.13	20.5	6.2	18.3	5.5	0.5	0.1	0.3	yes	no
	48	04.03.20	4:30 PM	649.0	27.0	0.101	2	0.202	0.600	0.035	5.16	15.9	4.6	14.2	4.1	0.4	0.1	0.3	yes	no
	49	05.03.20	9:30 AM	666.0	27.8	0.078	2	0.156	0.600	0.027	5.27	14.0	4.0	12.5	3.5	0.4	0.1	0.3	yes	no
	50	05.03.20	4:00 PM	672.5	28.0	0.081	2	0.162	0.600	0.028	5.32	10.7	2.9	9.5	2.6	0.3	0.1	0.3	yes	no

Supplementary Table S8 Single data obtained from the cultivation of *C. ljungdahlii* WT in nitrate-containing medium with H_2 and CO_2 using the self-built MBS (Reactor 9). Growth parameter: medium feed rate = 0.186 mL min^{-1}; gas low rate = 30 mL min^{-1}, nitrate feed rate = 0.003 mM min^{-1}; CDW/L/OD_{600} [g] = 0.288 and total cultivation time = 672.5 h. The pH (6.0 – 4.5) was maintained with base and acid. Any negative production rate was set = 0. n.m. = not measured.

						Reactor 9 (nitrate)														
	sample	date	time	cultivation time [h]	cultivation time [d]	measured OD	DF	OD600nm	wet volume [L]	CDW_{total} [g]	pH	acetate measured [mM]	ethanol measured [mM]	acetate production rate [mmol-C $L^{-1}d^{-1}$]	ethanol production rate [mmol-C $L^{-1}d^{-1}$]	acetate production rate [g $L^{-1}d^{-1}$]	ethanol production rate [g $L^{-1}d^{-1}$]	ratio (ethanol/acetate)	nitrate	nitrite
Batch	0	06.02.20	3:30 PM	0.0	0.0	0.000	1	0.000	0.500	0.000	6.00	0.0	0.0	0.0	0.0	0.0	0.0	0.0	no	no
	1	06.02.20	4:45 PM	1.3	0.1	0.085	1	0.085	0.500	0.012	6.00	0.6	0.0	23.0	0.0	0.0	0.0	0.0	no	no
	2	07.02.20	9:00 AM	17.5	0.7	0.113	1	0.113	0.500	0.016	6.00	1.4	0.0	2.4	0.0	0.0	0.0	0.0	no	no
	3	07.02.20	5:00 PM	25.5	1.1	0.141	1	0.141	0.500	0.020	6.00	7.2	0.0	34.6	0.0	1.0	0.0	0.0	no	no
	4	08.02.20	11:30 AM	44.0	1.8	0.333	1	0.333	0.500	0.048	6.00	24.4	0.0	44.8	0.0	1.3	0.0	0.0	no	no
	5	09.02.20	1:00 PM	69.5	2.9	0.297	2	0.594	0.500	0.086	6.00	68.4	0.0	82.7	0.0	2.5	0.0	0.0	no	no
	6	09.02.20	5:15 PM	73.8	3.1	0.327	2	0.654	0.500	0.094	6.00	74.8	0.0	72.0	0.0	2.2	0.0	0.0	no	no
continuous, pH 6.0	7	10.02.20	1:30 PM	94.0	3.9	0.178	5	0.890	0.475	0.122	6.00	69.3	0.0	78.2	0.0	2.3	0.0	0.0	no	no
	8	10.02.20	5:30 PM	98.0	4.1	0.183	5	0.915	0.475	0.125	6.00	74.5	0.0	84.0	0.0	2.5	0.0	0.0	no	no
	9	11.02.20	10:00 AM	114.5	4.8	0.188	5	0.940	0.400	0.108	6.00	72.7	0.0	97.4	0.0	2.9	0.0	0.0	no	no
	10	11.02.20	5:00 PM	121.5	5.1	0.190	5	0.950	0.425	0.116	6.00	70.9	0.0	89.3	0.0	2.7	0.0	0.0	no	no
	11	12.02.20	10:30 AM	139.0	5.8	0.176	5	0.880	0.425	0.108	6.00	62.2	0.0	78.4	0.0	2.4	0.0	0.0	no	no
	12	12.02.20	5:45 PM	146.3	6.1	0.186	5	0.930	0.425	0.114	6.00	65.1	0.0	82.0	0.0	2.5	0.0	0.0	no	no
	13	13.02.20	9:45 AM	162.3	6.8	0.173	5	0.865	0.450	0.112	6.00	63.3	2.9	75.3	3.5	2.3	0.1	0.0	no	no
	14	13.02.20	4:00 PM	168.5	7.0	0.183	5	0.915	0.450	0.119	6.00	66.4	2.1	79.1	2.5	2.4	0.1	0.0	no	no
	15	14.02.20	9:00 AM	185.5	7.7	0.185	5	0.925	0.475	0.127	6.00	71.9	0.0	81.1	0.0	2.4	0.0	0.0	no	no
	16	14.02.20	6:00 PM	194.5	8.1	0.186	5	0.930	0.475	0.127	6.00	73.9	0.0	83.3	0.0	2.5	0.0	0.0	no	no
	17	15.02.20	5:00 PM	217.5	9.1	0.184	5	0.920	0.475	0.126	6.00	63.5	0.0	71.7	0.0	2.2	0.0	0.0	no	no
continuous, pH 5.5	18	16.02.20	12:00 PM	236.5	9.9	0.185	5	0.925	0.500	0.133	5.50	65.7	5.5	70.4	5.9	2.1	0.1	0.1	no	no
	19	17.02.20	9:00 AM	257.5	10.7	0.200	5	1.000	0.500	0.144	5.43	73.1	5.4	78.3	5.8	2.4	0.1	0.1	no	no
	20	17.02.20	5:00 PM	265.5	11.1	0.205	5	1.025	0.500	0.148	5.43	75.3	5.6	80.7	6.0	2.4	0.1	0.1	no	no
	21	18.02.20	9:15 AM	281.8	11.7	0.210	5	1.050	0.525	0.159	5.46	76.2	8.0	77.7	8.2	2.3	0.2	0.1	no	no
	22	18.02.20	5:00 PM	289.5	12.1	0.198	5	0.990	0.525	0.150	5.43	76.3	8.8	77.9	8.9	2.3	0.2	0.1	no	no
	23	19.02.20	8:30 AM	305.0	12.7	0.227	5	1.135	0.525	0.172	5.44	72.1	15.6	73.6	15.9	2.2	0.4	0.2	no	no
	24	19.02.20	5:00 PM	313.5	13.1	0.226	5	1.130	0.525	0.171	5.42	73.6	20.9	75.1	21.4	2.3	0.5	0.3	no	no
	25	20.02.20	9:00 AM	329.5	13.7	0.205	5	1.025	0.525	0.155	5.44	77.1	21.2	78.7	21.6	2.4	0.5	0.3	no	no
	26	20.02.20	4:30 PM	337.0	14.0	0.206	5	1.030	0.550	0.163	5.44	78.2	21.5	76.1	20.9	2.3	0.5	0.3	no	no
	27	21.02.20	10:00 AM	354.5	14.8	0.231	5	1.155	0.550	0.183	5.45	86.6	13.2	84.3	12.9	2.5	0.3	0.2	no	no
continuous, pH 5.0	28	21.02.20	6:45 PM	363.3	15.1	0.189	5	0.945	0.550	0.150	5.07	76.7	17.2	74.7	16.8	2.2	0.4	0.2	no	no
	29	22.02.20	5:30 PM	386.0	16.1	0.182	5	0.910	0.550	0.144	5.03	51.3	33.5	49.9	32.6	1.5	0.8	0.7	no	no
	30	23.02.20	8:45 PM	413.3	17.2	0.211	5	1.055	0.550	0.167	4.99	54.2	25.6	52.8	24.9	1.6	0.6	0.5	no	no
	31	24.02.20	9:00 AM	425.5	17.7	0.198	5	0.990	0.550	0.157	4.99	54.9	22.8	53.4	22.2	1.6	0.5	0.4	no	no
	32	24.02.20	5:00 PM	433.5	18.1	0.176	5	0.880	0.550	0.140	5.00	54.8	21.7	53.3	21.1	1.6	0.5	0.4	no	no
	33	25.02.20	9:00 AM	449.5	18.7	0.176	5	0.880	0.550	0.140	4.98	55.8	16.5	54.3	16.1	1.6	0.4	0.3	no	no
	34	25.02.20	5:30 PM	458.0	19.1	0.167	5	0.835	0.525	0.126	5.00	55.5	14.9	56.7	15.2	1.7	0.4	0.3	no	no
	35	26.02.20	8:15 AM	472.8	19.7	0.198	5	0.990	0.525	0.150	5.01	55.3	11.6	56.4	11.9	1.7	0.3	0.2	no	no
	36	26.02.20	4:45 PM	481.3	20.1	0.172	5	0.860	0.525	0.130	5.02	53.9	9.7	55.0	9.9	1.7	0.2	0.2	no	no
	37	27.02.20	9:15 AM	497.8	20.7	0.176	5	0.880	0.525	0.133	5.04	53.5	7.1	54.6	7.2	1.6	0.2	0.1	no	no
continuous, pH 4.5	38	27.02.20	5:00 PM	505.5	21.1	0.163	5	0.815	0.525	0.123	4.54	48.3	10.0	49.2	10.2	1.5	0.2	0.2	no	no
	39	28.02.20	9:15 AM	521.8	21.7	0.128	5	0.640	0.525	0.097	4.55	27.9	25.9	28.5	26.4	0.9	0.6	0.9	no	no
	40	28.02.20	5:00 PM	529.5	22.1	0.106	5	0.530	0.525	0.080	4.52	25.3	27.6	25.9	28.2	0.8	0.6	1.1	no	no
	41	29.02.20	11:30 AM	548.0	22.8	0.112	5	0.560	0.525	0.085	4.55	23.5	29.3	24.0	29.9	0.7	0.7	1.2	no	no
	42	01.03.20	12:30 PM	573.0	23.9	0.110	5	0.550	0.525	0.083	4.55	25.4	30.9	25.9	31.5	0.8	0.7	1.2	no	no
	43	02.03.20	1:30 PM	598.0	24.9	0.109	5	0.545	0.525	0.082	4.56	29.3	26.4	29.9	26.9	0.9	0.6	0.9	no	no
	44	02.03.20	5:00 PM	601.5	25.1	0.109	5	0.545	0.525	0.082	4.54	30.8	25.9	31.4	26.4	0.9	0.6	0.8	no	no
	45	03.03.20	9:45 AM	618.3	25.8	0.110	5	0.550	0.550	0.087	4.53	36.6	24.6	35.7	24.0	1.1	0.6	0.7	no	no
	46	03.03.20	4:30 PM	625.0	26.0	0.110	5	0.550	0.550	0.087	4.53	40.2	23.8	39.2	23.2	1.2	0.5	0.6	no	no
	47	04.03.20	8:30 AM	641.0	26.7	0.115	5	0.575	0.575	0.095	4.54	50.4	19.2	46.9	17.9	1.4	0.4	0.4	no	no
	48	04.03.20	4:30 PM	649.0	27.0	0.128	5	0.640	0.575	0.106	4.53	54.8	16.8	51.1	15.7	1.5	0.4	0.3	no	no
	49	05.03.20	9:30 AM	666.0	27.8	0.123	5	0.615	0.575	0.102	4.56	60.5	11.9	56.3	11.1	1.7	0.3	0.2	no	no
	50	05.03.20	4:00 PM	672.5	28.0	0.119	5	0.595	0.575	0.099	4.55	60.5	10.4	56.4	9.7	1.7	0.2	0.2	no	no

Supplementary Table S9 Single data obtained from the cultivation of *C. ljungdahlii* WT in nitrate-containing medium with H_2 and CO_2 using the self-built MBS (Reactor 10). Growth parameter: medium feed rate = 0.186 mL min^{-1}; gas low rate = 30 mL min^{-1}, nitrate feed rate = 0.003 mM min^{-1}; CDW/L/OD_{600} [g] = 0.288 and total cultivation time = 672.5 h. The pH (6.0 – 4.5) was maintained with base and acid. Any negative production rate was set = 0. n.m. = not measured.

						Reactor 10 (nitrate)														
	sample	date	time	cultivation time [h]	cultivation time [d]	measured OD	DF	OD600nm	wet volume [L]	CDW_{total} [g]	pH	acetate measured [mM]	ethanol measured [mM]	acetate production rate [mmol-C $L^{-1}d^{-1}$]	ethanol production rate [mmol-C $L^{-1}d^{-1}$]	acetate production rate [g $L^{-1}d^{-1}$]	ethanol production rate [g $L^{-1}d^{-1}$]	ratio (ethanol/acetate)	nitrate	nitrite
Batch	0	06.02.20	3:30 PM	0.0	0.0	0.000	1	0.000	0.500	0.000	6.00	0.0	0.0	0.0	0.0	0.0	0.0	0.0	no	no
	1	06.02.20	4:45 PM	1.3	0.1	0.072	1	0.075	0.500	0.011	6.00	0.5	0.0	0.0	0.0	0.5	0.0	0.0	no	no
	2	07.02.20	9:00 AM	17.5	0.7	0.104	1	0.104	0.500	0.015	6.00	1.3	0.0	0.0	0.0	0.0	0.0	0.0	no	no
	3	07.02.20	5:00 PM	25.5	1.1	0.136	1	0.136	0.500	0.020	6.00	6.1	0.0	28.6	0.0	0.9	0.0	0.0	no	no
	4	08.02.20	11:30 AM	44.0	1.8	0.301	1	0.301	0.500	0.043	6.00	24.4	0.0	47.5	0.0	1.4	0.0	0.0	no	no
	5	09.02.20	1:00 PM	69.5	2.9	0.303	2	0.606	0.500	0.087	6.00	69.6	0.0	85.1	0.0	2.6	0.0	0.0	no	no
	6	09.02.20	5:15 PM	73.8	3.1	0.327	2	0.654	0.500	0.094	6.00	77.3	0.0	86.6	0.0	2.6	0.0	0.0	no	no
continuous, pH 6.0	7	10.02.20	1:30 PM	94.0	3.9	0.156	5	0.780	0.575	0.129	6.00	74.8	0.0	69.7	0.0	2.1	0.0	0.0	no	no
	8	10.02.20	5:30 PM	98.0	4.1	0.163	5	0.815	0.575	0.135	6.00	74.5	0.0	69.4	0.0	2.1	0.0	0.0	no	no
	9	11.02.20	10:00 AM	114.5	4.8	0.171	5	0.855	0.550	0.136	6.00	72.9	0.0	71.0	0.0	2.1	0.0	0.0	no	no
	10	11.02.20	5:00 PM	121.5	5.1	0.174	5	0.870	0.550	0.138	6.00	72.6	0.0	70.7	0.0	2.1	0.0	0.0	no	no
	11	12.02.20	10:30 AM	139.0	5.8	0.177	5	0.885	0.550	0.140	6.00	71.6	0.0	69.8	0.0	2.1	0.0	0.0	no	no
	12	12.02.20	5:45 PM	146.3	6.1	0.187	5	0.935	0.550	0.148	6.00	71.1	0.0	69.2	0.0	2.1	0.0	0.0	no	no
	13	13.02.20	9:45 AM	162.3	6.8	0.173	5	0.865	0.575	0.143	6.00	69.2	0.0	64.4	0.0	1.9	0.0	0.0	no	no
	14	13.02.20	4:00 PM	168.5	7.0	0.183	5	0.915	0.575	0.152	6.00	76.2	0.0	71.0	0.0	2.1	0.0	0.0	no	no
	15	14.02.20	9:00 AM	185.5	7.7	0.192	5	0.960	0.575	0.159	6.00	86.2	0.0	80.3	0.0	2.4	0.0	0.0	no	no
	16	14.02.20	6:00 PM	194.5	8.1	0.191	5	0.955	0.600	0.165	6.00	90.3	0.0	80.6	0.0	2.4	0.0	0.0	no	no
	17	15.02.20	5:00 PM	217.5	9.1	0.216	5	1.080	0.675	0.210	6.00	93.7	12.9	74.3	10.2	2.2	0.2	0.1	no	no
continuous, pH 5.5	18	16.02.20	12:00 PM	236.5	9.9	0.235	5	1.175	0.600	0.203	5.50	106.2	14.6	94.8	13.1	2.8	0.3	0.1	no	no
	19	17.02.20	9:00 AM	257.5	10.7	0.207	5	1.035	0.700	0.209	5.49	112.4	9.4	86.0	7.2	2.6	0.2	0.1	no	no
	20	17.02.20	5:00 PM	265.5	11.1	0.206	5	1.030	0.575	0.171	5.48	108.1	10.9	100.7	10.2	3.0	0.2	0.1	no	no
	21	18.02.20	9:15 AM	281.8	11.7	0.207	5	1.035	0.575	0.172	5.47	85.8	11.0	79.9	10.3	2.4	0.2	0.1	no	no
	22	18.02.20	5:00 PM	289.5	12.1	0.203	5	1.015	0.575	0.168	5.47	94.6	15.1	88.1	14.1	2.6	0.3	0.2	no	no
	23	19.02.20	8:30 AM	305.0	12.7	0.208	5	1.040	0.600	0.180	5.45	87.6	20.2	78.2	18.1	2.3	0.4	0.2	no	no
	24	19.02.20	5:00 PM	313.5	13.1	0.201	5	1.005	0.600	0.174	5.47	86.6	25.1	77.3	22.4	2.3	0.5	0.3	no	no
	25	20.02.20	9:00 AM	329.5	13.7	0.184	5	0.920	0.600	0.159	5.50	89.7	20.2	80.1	18.0	2.4	0.4	0.2	no	no
	26	20.02.20	4:30 PM	337.0	14.0	0.191	5	0.955	0.600	0.165	5.45	90.2	20.8	80.5	18.5	2.4	0.4	0.2	no	no
	27	21.02.20	10:00 AM	354.5	14.8	0.219	5	1.095	0.675	0.213	5.47	95.7	15.3	76.0	12.2	2.3	0.3	0.2	no	no
continuous, pH 5.0	28	21.02.20	6:45 PM	363.3	15.1	0.174	5	0.870	0.550	0.138	5.02	81.7	25.2	79.6	24.6	2.4	0.6	0.3	no	no
	29	22.02.20	5:30 PM	386.0	16.1	0.197	5	0.985	0.600	0.170	4.98	67.8	42.1	60.5	37.6	1.8	0.9	0.6	no	no
	30	23.02.20	8:45 PM	413.3	17.2	0.241	5	1.205	0.700	0.243	4.98	90.7	29.9	69.4	22.9	2.1	0.5	0.3	no	no
	31	24.02.20	9:00 AM	425.5	17.7	0.223	5	1.115	0.800	0.257	4.99	102.7	22.7	68.8	15.2	2.1	0.3	0.2	no	no
	32	24.02.20	5:00 PM	433.5	18.1	0.221	5	1.105	0.600	0.191	4.98	105.5	21.3	94.2	19.0	2.8	0.4	0.2	no	no
	33	25.02.20	9:00 AM	449.5	18.7	0.214	5	1.070	0.625	0.193	4.98	111.4	9.3	95.5	7.9	2.9	0.2	0.1	no	no
	34	25.02.20	5:30 PM	458.0	19.1	0.200	5	1.000	0.650	0.187	4.95	109.0	6.8	89.8	5.6	2.7	0.1	0.1	no	no
	35	26.02.20	8:15 AM	472.8	19.7	0.229	5	1.145	0.650	0.215	4.99	112.9	4.9	93.0	4.0	2.8	0.1	0.0	no	no
	36	26.02.20	4:45 PM	481.3	20.1	0.219	5	1.095	0.700	0.221	4.97	114.5	3.4	87.6	2.6	2.6	0.1	0.0	no	no
	37	27.02.20	9:15 AM	497.8	20.7	0.220	5	1.100	0.600	0.190	4.97	109.6	3.0	97.8	2.7	2.9	0.1	0.0	no	no
continuous, pH 4.5	38	27.02.20	5:00 PM	505.5	21.1	0.187	5	0.935	0.600	0.162	4.52	101.6	6.3	90.7	5.6	2.7	0.1	0.1	no	no
	39	28.02.20	9:15 AM	521.8	21.7	0.192	5	0.960	0.650	0.180	4.46	90.6	18.1	74.7	14.9	2.2	0.3	0.2	no	no
	40	28.02.20	5:00 PM	529.5	22.1	0.200	5	1.000	0.650	0.187	4.46	93.6	16.9	77.1	14.0	2.3	0.3	0.2	no	no
	41	29.02.20	11:30 AM	548.0	22.8	0.197	5	0.985	0.725	0.206	4.50	100.7	13.2	74.4	9.8	2.2	0.2	0.1	no	no
	42	01.03.20	12:30 PM	573.0	23.9	0.193	5	0.965	0.575	0.160	4.45	101.0	16.0	94.1	14.9	2.8	0.3	0.2	no	no
	43	02.03.20	1:30 PM	598.0	24.9	0.187	5	0.935	0.575	0.155	4.54	90.5	22.5	84.3	21.0	2.5	0.5	0.2	no	no
	44	02.03.20	5:00 PM	601.5	25.1	0.153	5	0.765	0.575	0.127	4.53	74.1	33.4	69.0	31.1	2.1	0.7	0.5	no	no
	45	03.03.20	9:45 AM	618.3	25.8	0.135	5	0.675	0.600	0.117	4.52	55.7	42.7	49.7	38.1	1.5	0.9	0.8	no	no
	46	03.03.20	4:30 PM	625.0	26.0	0.141	5	0.705	0.600	0.122	4.49	55.4	41.5	49.5	37.0	1.5	0.9	0.7	no	no
	47	04.03.20	8:30 AM	641.0	26.7	0.155	5	0.775	0.625	0.140	4.48	65.7	31.5	56.3	27.0	1.7	0.6	0.5	no	no
	48	04.03.20	4:30 PM	649.0	27.0	0.160	5	0.800	0.625	0.144	4.48	70.4	27.4	60.3	23.5	1.8	0.5	0.4	no	no
	49	05.03.20	9:30 AM	666.0	27.8	0.163	5	0.815	0.625	0.147	4.47	79.4	20.1	68.0	17.3	2.0	0.4	0.3	no	no
	50	05.03.20	4:00 PM	672.5	28.0	0.173	5	0.865	0.625	0.156	4.46	81.2	18.0	69.6	15.4	2.1	0.4	0.2	no	no

Supplementary Table S10 CDW calculations for bioreactor cultures of *C. ljungdahlii* growing either with ammonium or with nitrate as N-source. A culture volume of 50 mL were collected from each bioreactor and harvest at 3492 rcf. The supernatant was discarded before drying the cell pellets at 65°C for 3 days.

	dry empty for 3 d at 65°C	dry with pellet for 3 d at 65°C	CDW [mg/50mL]	CDW [mg/L]	OD_{600} at sampling point	CDW [mg/L/OD_{600}]	CDW [mg/L/OD_{600}] (average)
Empty tube 1	14.167	14.166	1	-	-	-	
Empty tube 1	14.262	14.26	2	-	-	-	
Empty tube 1	14.325	14.323	2	-	-	-	
Bioreactor 1	14.275	14.286	11	220	0.885	248.59	
Bioreactor 2	14.521	14.53	9	180	0.815	220.86	**241.95 for ammonium bioreactors**
Bioreactor 3	14.243	14.253	10	200	0.78	256.41	
Bioreactor 4	14.157	14.167	10	200	0.615	325.20	
Bioreactor 5	14.365	14.384	19	380	1.225	310.20	**288.31 for nitrate bioreactors**
Bioreactor 6	14.39	14.404	14	280	1.22	229.51	

8.2. Supplementary information for Chapter 4

Supplementary Table S11-S17

Supplementary Figure S6-S12

8.2.1. Sequences, editing sites, and generated strains

Supplementary Table S11 ***Clostridium ljungdahlii*** **strains used.**

Strains	Description	References
DSM13528	*Clostridium ljungdahlii* type strain	DSM13528
QX3	DSM13528, *adhE1* Trp169*	This study
QX4	DSM13528, *adhE2* Gln33*	This study
QX5	DSM13528, *aor1* Gln267*	This study
QX6	DSM13528, *aor2* Gln267*	This study

Supplementary Table S12 Plasmids used in this study.

Name	Description	References
pANA1	p15A, *bla*, Φ3tI methyltransferase	(Richter *et al.*, 2016a)
pMTLdSpCas9	pMTL82254, P_{2tetO1}:*dcas9*	(Woolston *et al.*, 2018)
pTargetF	ColE1, *smR*	(Jiang *et al.*, 2015)
pScI_dCas9-CDA-UL	pSC101, *bla*, *dcas9*-PmCDA1-UGI-LVA	(Banno *et al.*, 2018)
pgRNA01	pTargetF, P_{J23119}:gRNA01	This study
pgRNA02	pgRNA01, P_{J23119}:gRNA02	This study
pgRNA05	pgRNA01, P_{J23119}:gRNA05	This study
pgRNA06	pgRNA01, P_{J23119}:gRNA06	This study
pgRNA07	pgRNA01, P_{J23119}:gRNA07	This study
pgRNA10	pgRNA01, P_{J23119}:gRNA10	This study
pgRNA11	pgRNA01, P_{J23119}:gRNA11	This study
pgRNA13	pgRNA01, P_{J23119}:gRNA13	This study
pgRNA14	pgRNA01, P_{J23119}:gRNA14	This study
pgRNA15	pgRNA01, P_{J23119}:gRNA15	This study
pgRNA19	pgRNA01, P_{J23119}:gRNA19	This study
pFX	pMTLdSpCas9, dcas9 fused with PmCDA-UGI-LVA tag	This study
pFX01	pFX, P_{J23119}:gRNA01	This study
pFX02	pFX, P_{J23119}:gRNA02	This study
pFX05	pFX, P_{J23119}:gRNA05	This study
pFX06	pFX, P_{J23119}:gRNA06	This study
pFX07	pFX, P_{J23119}:gRNA07	This study
pFX10	pFX, P_{J23119}:gRNA10	This study
pFX11	pFX, P_{J23119}:gRNA11	This study
pFX13	pFX, P_{J23119}:gRNA13	This study
pFX14	pFX, P_{J23119}:gRNA14	This study
pFX15	pFX, P_{J23119}:gRNA15	This study
pFX19	pFX, P_{J23119}:gRNA19	This study

Supplementary Table S13 Primers used for plasmid construction.

Primer	Sequence	Note
EBT-PFX-080	GATTTGAGTCAGCTAGGAGGTGACGGTGGAGGAGGTTCTGGAGG	pFX series
EBT-PFX-086	ATGCCTGGAGATCCTTACTCGAGTTATGCAACCAGTCCTAGCATCTTG	
EBT-PFX-081	CCTCCAGAACCTCCTCCACCGTCACCTCCTAGCTGACTCAAATC	
EBT-PFX-087	CAAGATGCTAGGACTGGTTGCATAACTCGAGTAAGGATCTCCAGGCAT	
EBT-PFX-088	GGCTCACCTTCGGGTGGGCCTTTCTGCGTTACCGCATATGCTGGATCCTT	
EBT-PFX-089	ACGTTGTAAAACGACGGCCAGTGCCGAGCTCTGCAGGTCGACTCTAGAGAAT	
EBT-PFX-090	TTACCTTTTCATTCCCTACAGTTTTAGAGCTAGAAATAGC	gRNA01
EBT-PFX-091	TGTAGGGAATGAAAAGGTAAGCTAGCATTATACCTAGGAC	
EBT-PFX-133	AAAAATTTGGAGTAAGGCAAGTTTTAGAGCTAGAAATAGC	gRNA02
EBT-PFX-134	TTGCCTTACTCCAAATTTTTGCTAGCATTATACCTAGGAC	
EBT-PFX-139	CAAATAGTAAAGACAGCTCCGTTTTAGAGCTAGAAATAGC	gRNA05
EBT-PFX-140	GGAGCTGTCTTTACTATTTGGCTAGCATTATACCTAGGAC	
EBT-PFX-141	AATTGATCACTATCTGGGCAGTTTTAGAGCTAGAAATAGC	gRNA06
EBT-PFX-142	TGCCCAGATAGTGATCAATTGCTAGCATTATACCTAGGAC	
EBT-PFX-143	TGAAATTGATGGAAAAAATTGTTTTAGAGCTAGAAATAGC	gRNA07
EBT-PFX-144	AATTTTTTCCATCAATTTCAGCTAGCATTATACCTAGGAC	
EBT-PFX-153	ATCCATCCTATAATTCCTTCGTTTTAGAGCTAGAAATAGC	gRNA10
EBT-PFX-154	GAAGGAATTATAGGATGGATGCTAGCATTATACCTAGGAC	
EBT-PFX-155	AACAAGTGGATGAAATTTTCGTTTTAGAGCTAGAAATAGC	gRNA11
EBT-PFX-156	GAAAATTTCATCCACTTGTTGCTAGCATTATACCTAGGAC	
EBT-PFX-178	GGTCAGGGAATGCCAACTTAGTTTTAGAGCTAGAAATAGC	gRNA13
EBT-PFX-179	TAAGTTGGCATTCCCTGACCGCTAGCATTATACCTAGGAC	
EBT-PFX-180	GATCAAGCAGATAAGATCAGGTTTTAGAGCTAGAAATAGC	gRNA14
EBT-PFX-181	CTGATCTTATCTGCTTGATCGCTAGCATTATACCTAGGAC	
EBT-PFX-182	TTCAAATAGTAAAGACAGCTCCGTTTTAGAGCTAGAAATAGC	gRNA15
EBT-PFX-183	GGAGCTGTCTTTACTATTTGAAGCTAGCATTATACCTAGGAC	
EBT-PFX-201	AATCAAGCAGATAAAATAAGGTTTTAGAGCTAGAAATAGC	gRNA19
EBT-PFX-202	CTTATTTTATCTGCTTGATTGCTAGCATTATACCTAGGAC	

Supplementary Table S14 Primers used for the verification of base editing.

Primer	Sequence	Note
EBT-PFX-131	AGGATAGGACATACCCTGTG	Verification of *pta* editing
EBT-PFX-132	CATCTACAGACATGCCTGTTC	
EBT-PFX-130	GGAGTAAGGCAAAGGAAGAC	Sequencing for *pta*
EBT-PFX-166	TCCCCAATTTAGCATACTAGGC	Verification of *adhE1* editing
EBT-PFX-167	CACATATGCCTCCAGTGCAT	
EBT-PFX-168	TTACTGACTGCTCTGAGGCA	Sequencing for *adhE1*
EBT-PFX-169	ATGCACTGGAGGCATATGTG	Verification of *adhE2* editing
EBT-PFX-170	GTGCAACTCCAAGACTACCAT	
EBT-PFX-171	AGGAGCACCAGCTTTAACTG	Sequencing for *adhE2*
EBT-PFX-163	TGAAGAAGCGCTTCAAGTTC	Verification of *aor1* editing
EBT-PFX-164	CTGCCTCTAATAGTGAATCTGC	
EBT-PFX-200	CGTTGGTGCAGTTATGGGAT	Sequencing for *aor1*
EBT-PFX-187	CTAAGGCAATGGGGATTGGA	Verification of *aor2* editing
EBT-PFX-188	AGTTTCCACCTCCTTAGGCTA	
EBT-PFX-189	GGGAGCAGAATTCAAAGCAG	Sequencing for *aor2*

Supplementary Table S15 All used gRNA and protospacer adjacent motifs (PAM) sequences.

gRNA	Targets[a]	Strand[b]	PAM	gRNA sequence
gRNA01	*pta*	N	AGG	TTACCTTTTCATTCCCTACA
gRNA02	*pta*	C	AGG	AAAAATTTGGAGTAAGGCAA
gRNA05	*pta*	C	AGG	CAAATAGTAAAGACAGCTCC
gRNA06	*pta*	N	TGG	AATTGATCACTATCTGGGCA
gRNA07	*pta*	C	TGG	TGAAATTGATGGAAAAAATT
gRNA10	*adhE1*	N	AGG	ATCCATCCTATAATTCCTTC
gRNA11	*adhE2*	C	AGG	AACAAGTGGATGAAATTTTC
gRNA13	*aor1*	C	TGG	GGTCAGGGAATGCCAACTTA
gRNA14	*aor2*	C	TGG	GATCAAGCAGATAAGATCAG
gRNA15	*pta*	C	AGG	TTCAAATAGTAAAGACAGCTCC
gRNA19	*aor1*	C	TGG	AATCAAGCAGATAAAATAAG

[a] *pta* (CLJU_c12770), *adhE1* (CLJU_c16510), *adhE2* (CLJU_c16520), *aor1* (CLJU_c20110), and *aor2* (CLJU_c20210).

[b] N indicates non-coding strand, and C indicates coding strand.

Supplementary Table S16 Summary of base editing in pta using gRNA01.

No.	Screened colonies	Edited colonies	Efficiency	Editing sites
1	8	8	100%	-16 (6); -16 and -17 (2)
2	8	4	50%	-16 (3); -16 and -17 (1)
3	16	9	56%	-16 (2); -16 and -17 (5); -16 and -11 (1)
4	11	4	36%	-16 (2); -16 and -17 (2)
5	2	2	100%	-16 and -17 (1); -2, -16 and -17 (1)
Total	45	27 (25)[b]	60% (55%)[c]	

[a] Negative numbers indicate the editing sites, and numbers in brackets indicate the number of colonies with the corresponding edit. Two colonies with mixed signals are included in the numbers here, but not in the numbers in the main text.

[b] Number in brackets indicates the edited colonies with pure signals.

[c] Number in brackets indicates the editing efficiency calculated with clean edited colonies only.

Supplementary Table S17 Summary of the *in-silico* evaluation of our base-editing tool.

Editing type	Editing window (-11 to -19)		Editing window (-16 to -19)	
	Screened colonies	Edited colonies	Efficiency	Editing sites
Missense mutation	190568	4171	98162	4159
Silent mutation	66545	4144	22393	3896
Nonsense mutation	12745	3404	6149	2657
Nonsense mutation (70%)[a]	-	3009	-	2203
Non-editable[b]	-	7	-	21

[a] Nonsense mutation (70%) indicates that a premature STOP codon can be installed within the first 70% of the coding sequence of a target gene.

[b] Details for non-editable genes can be found in *Dataset*.

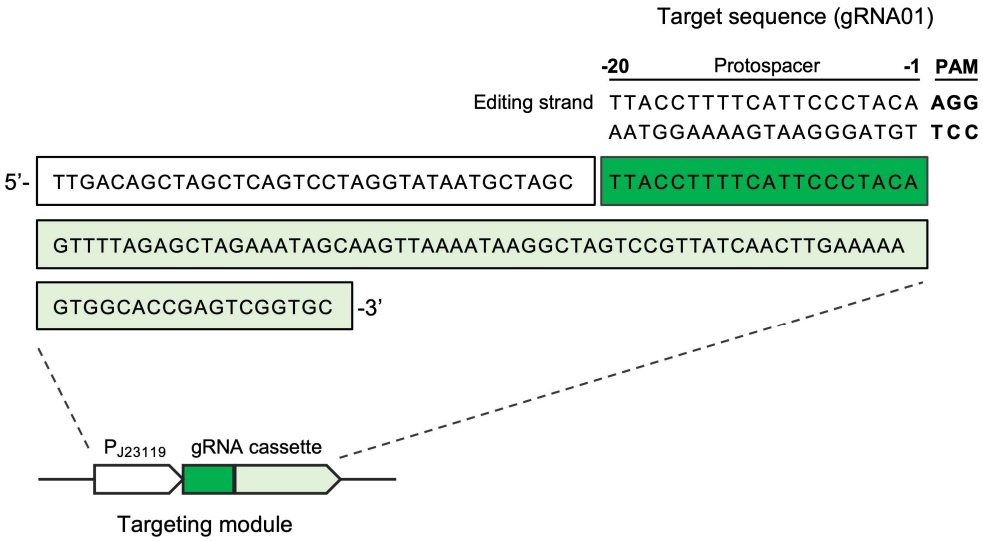

Supplementary Figure S6 **Scheme and sequence of gRNA cassette.** Taking gRNA01 as an example, the sequences of *P*$_{J23119}$ promoter (white), gRNA01 (green), and gRNA scaffold of dCas9 from *S. pyogenes* (light green) are shown. For each line, the sequence reads from left to right and does not indicate the structure. Both strands of the target sequence are displayed. The gRNA01 will bind the complimentary strand of the editing strand, and potentially edits the Cs on the editing strand within the editing window. The nucleotide directly adjacent to the protospacer adjacent motifs (PAM) is counted as position -1 and the starting position.

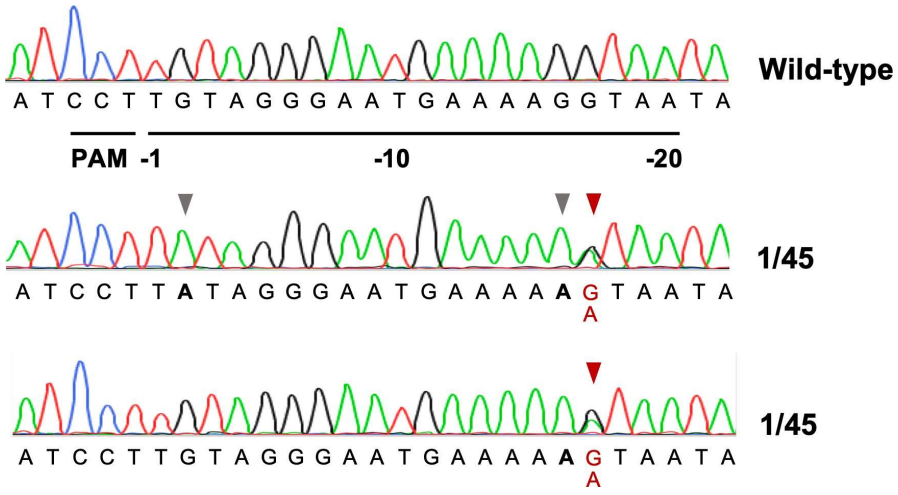

Supplementary Figure S7 **Mixed signals in the two colonies when editing *pta* using gRNA01.** Grey arrows indicate clean mutations, and red arrows indicate mixed signals of G and A. (PAM: protospacer adjacent motifs.)

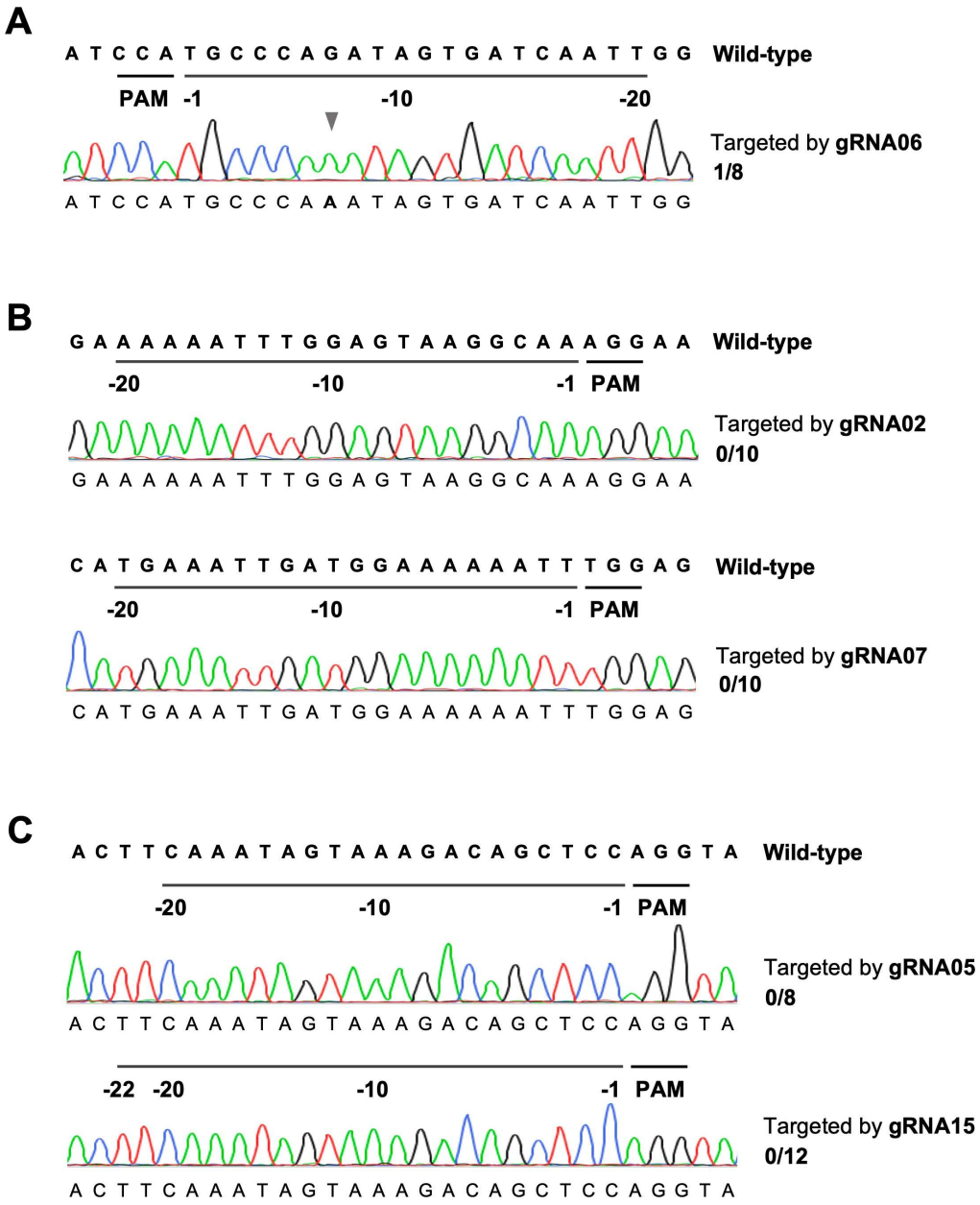

Supplementary Figure S8 Editing principles. (A) Base editing in *pta* with gRNA06. Grey arrow indicates successful editing. (B) Evaluation of base editing on target sequences without Cs using gRNA02 and gRNA07. (C) Base editing with different length of gRNAs (gRNA05 and gRNA15) for editing the C at position -20. (PAM: protospacer adjacent motifs.)

QX3 (10 transfers/ca. 66.2 generations)

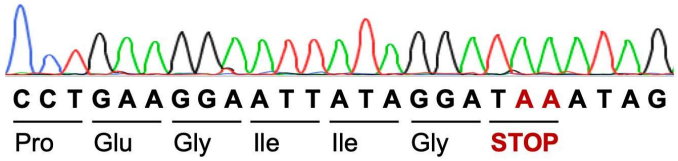

QX4 (10 transfers/ca. 66.1 generations)

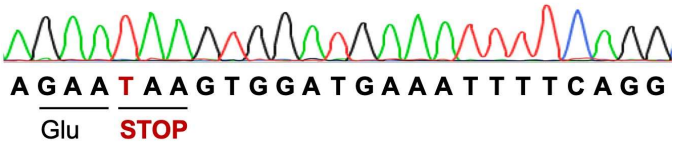

QX5 (10 transfers/ca. 65.9 generations)

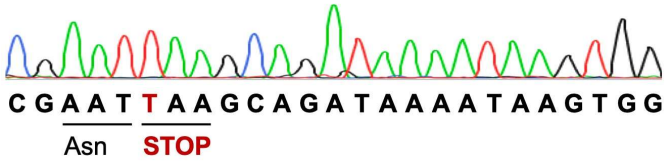

QX6 (10 transfers/ca. 66.5 generations)

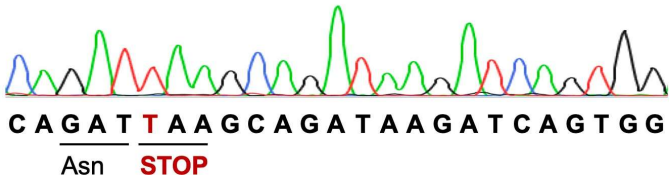

Supplementary Figure S9 **Stability test of four edited strains.** QX3, QX4, QX5, and QX6 were transferred 10 times in RCM and the single-nucleotide variations were sequenced to check stability. The sequencing results of the 10th transfer are shown.

8.2.2. Bottle experiments with base-edited strains

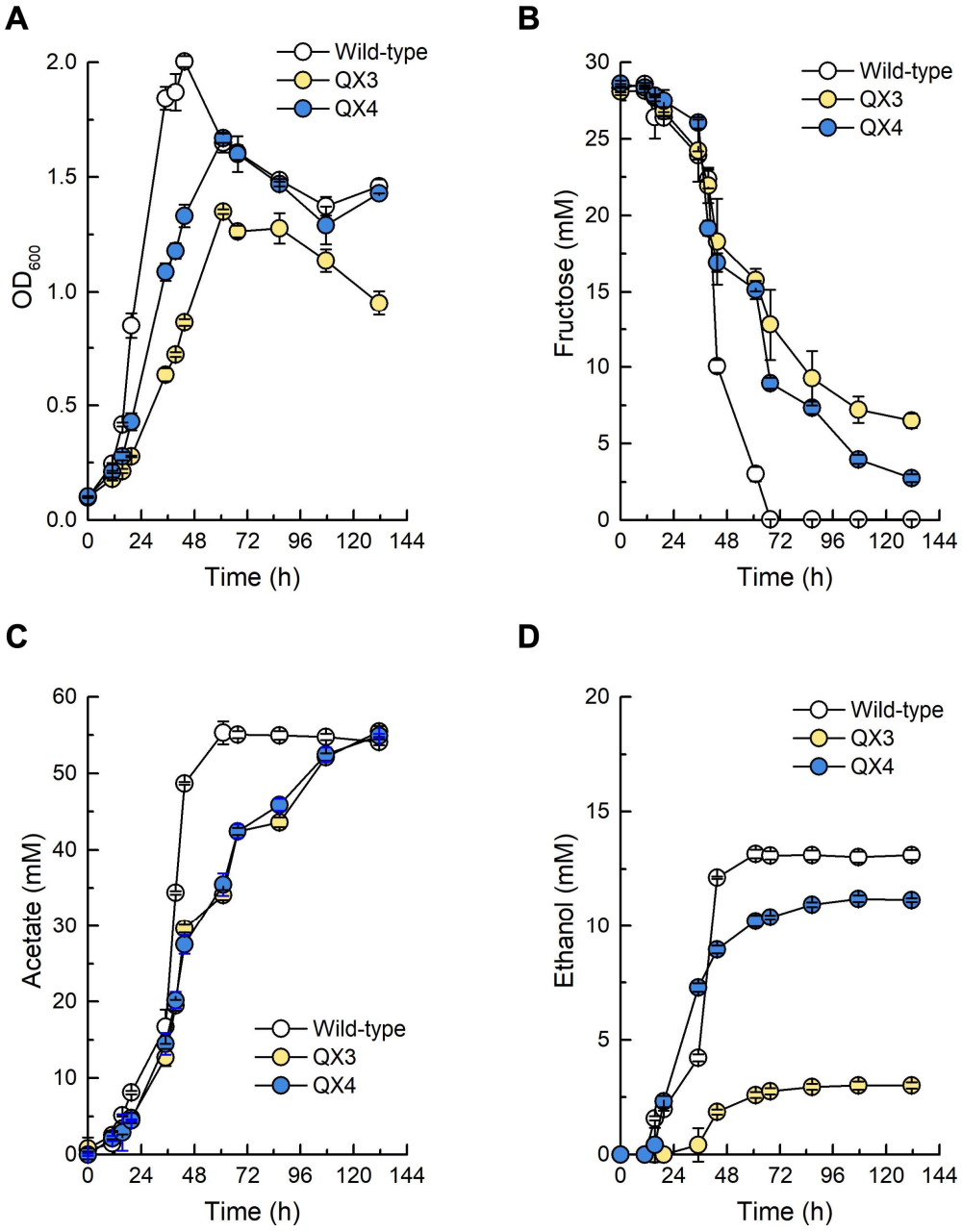

Supplementary Figure S10 Fermentation performances of wild-type, QX3 (*adhE1* Trp169*), and QX4 (*adhE2* Gln33*) under heterotrophic conditions with 5 g/L (27.8 mM) of fructose as the carbon source. (A) Growth, (B) concentration of fructose, (C) concentrations of acetate, and (D) concentration of ethanol in the culture during fermentation.

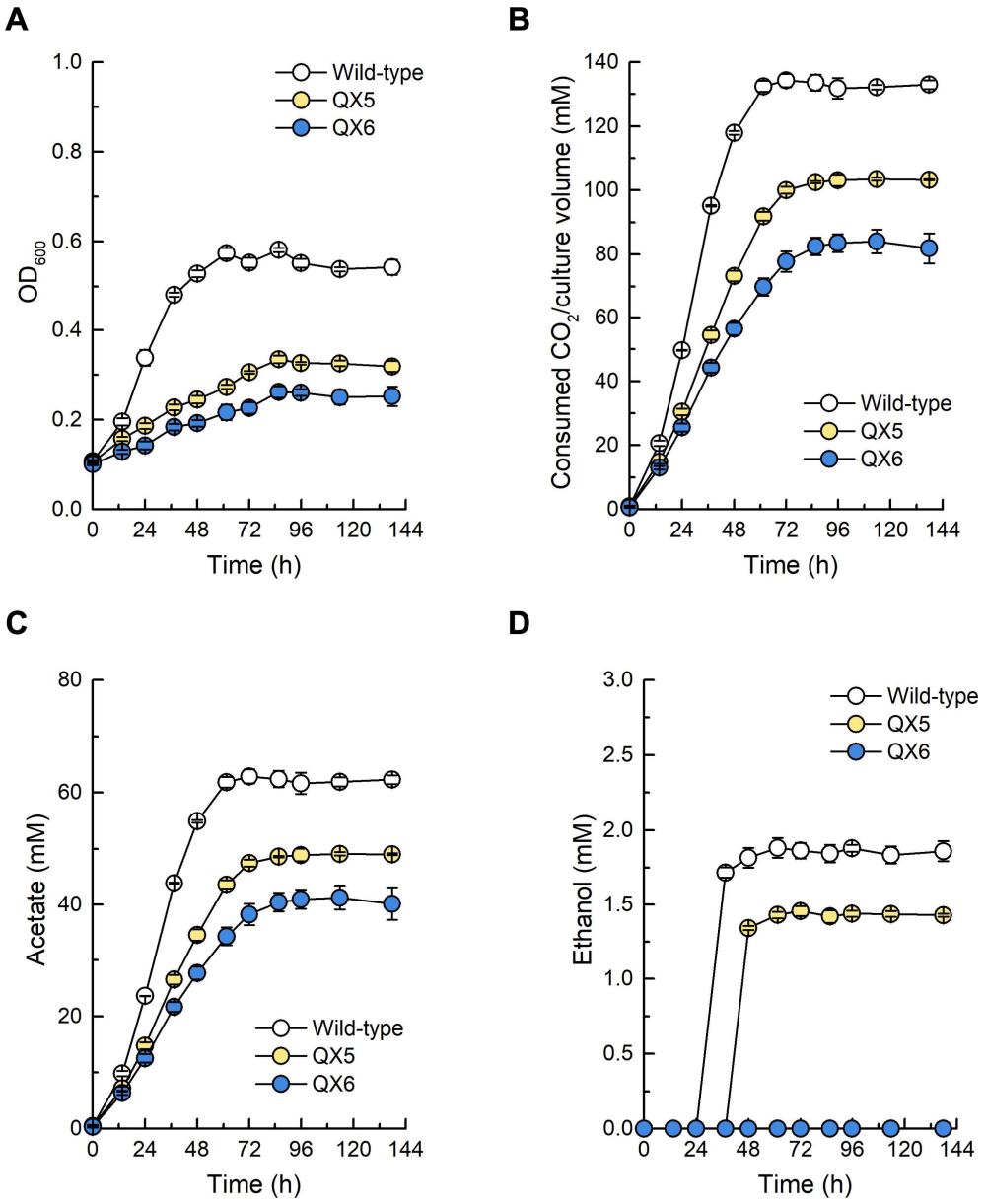

Supplementary Figure S11 Fermentation performance of wild-type, QX5 (*aor1* Gln267*), and QX6 (*aor2* Gln267*) under autotrophic conditions with a gas mixture (H_2/CO_2, 80/20 vol-%, 1.5 bar) as the substrate. (A) Growth, (B) consumed CO_2 per culture volume, (C) concentrations of acetate, and (D) concentration of ethanol in the culture during fermentation.

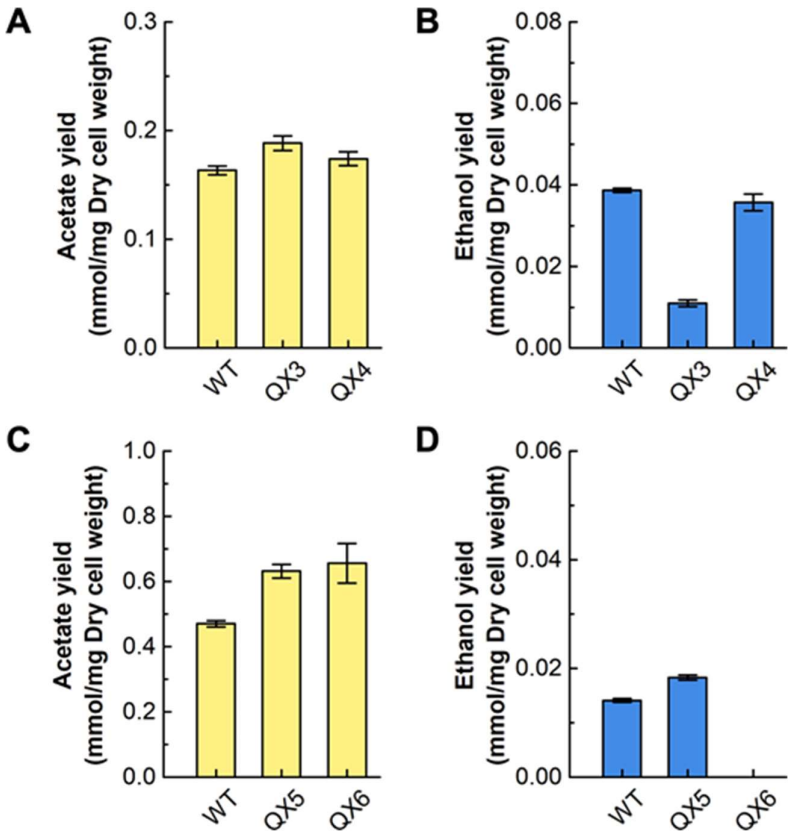

Supplementary Figure S12 Acetate and ethanol yields per dry cell weight. Acetate (A) and ethanol (B) yields of wild-type, QX3, and QX4 under heterotrophic conditions with 5 g/L (27.8 mM) of fructose as the carbon source. Acetate (C) and ethanol (D) yields of wild-type, QX5, and QX6 under autotrophic conditions with a gas mixture of H_2/CO_2 (80/20 vol-%, 1.5 bar) as the substrate. The fermentation experiments were conducted in triplicate (N=3), and the error bars indicate the standard de*via*tions.

8.3. Supplementary information for Chapter 5

Supplementary Text S1A-E

Supplementary Table S18-S23

Supplementary Figure S13-S19

8.3.1. Supplementary Text S1

8.3.2. Supplementary Text S1A - Implementing a CRISPR-Cas12a system for *C. ljungdahlii*

For *C. ljungdahlii*, the first CRISPR-based gene-deletion system was implemented with CRISPR-Cas9 (Huang *et al.*, 2016). Two years ago, a CRISPR-Cas12a system was successfully realized in *C. ljungdahlii* (Zhao *et al.*, 2019). Cas12a, also known as Cpf1, is an alternative Cas-type nuclease, which uses an AT-rich protospacer adjacent motif sequence instead of GC-rich protospacer adjacent motif sequences, which are preferred by Cas9. Since genomes of acetogens are in general AT rich (Drake *et al.*, 2008), the utilization of a CRISPR-Cas12a system offers more potential genome-editing sites compared to a CRISPR-Cas9 system. In addition, Cas12a cleaves the targeted DNA in a staggered pattern, which is postulated to increase the efficiency of DNA-repair mechanisms or might allow gene insertion through non-homologous end joining (Fagerlund *et al.*, 2015; Zetsche *et al.*, 2015; Bayat *et al.*, 2018).

We implemented a CRISPR-Cas12a system in the shuttle-vector system pMTL80000 (Heap *et al.*, 2009) (**Figure 16A**). We chose the constitutive thiolase promoter P_{thl} (Heap *et al.*, 2009) and the anhydrotetracycline-inducible promoter $P_{tetR\text{-}O1}$ (Dong *et al.*, 2012; Woolston *et al.*, 2018), to investigate whether the expression of the Cas12a-nuclease gene itself leads to poor transformation efficiency and genome edit rates as previously reported (Huang *et al.*, 2016). While cloning of the Cas12a gene was readily achieved in *E. coli*, we required several assembling attempts to form the final CRISPR-Cas12a plasmids, which contained the homology-directed repair arms and single guide RNAs. Once the plasmids were generated, we did not observe a noticeable difference between growth of the respective *E. coli* strain or an *E. coli* strain that harbors an empty pMTL plasmid. We also did not see any difference between recombinant *C. ljungdahlii* strains that harbor the control plasmids pMTL83152_Cas12a and pMTL83151_*tetR-O1*_Cas12a, which both lack homologous repair DNA and sgRNAs. However, transfer of the final CRISPR-Cas12a plasmids into *C. ljungdahlii* cells could only be achieved by using conjugation instead of electroporation. Overall, we found successful genome edited cells by using the plasmids pMTL83152_Cas12a-RNF, pMTL83152_Cas12a-rseC, and pMTL83152_Cas12a-nar. All CRISPR-Cas12a plasmids that harbored the $P_{tetR\text{-}O1}$ promoter instead of P_{thl} were successfully transferred into *C. ljungdahlii* cells, but genome edits were not detectable after induction with anhydrotetracycline and screening several colonies.

8.3.3. Supplementary Text S1B - Confirmation of strains

We purified gDNA from the generated strain *C. ljungdahlii* ΔRNF and used it for PCR analyses (***Material and Methods***). A *rnfCDGEAB* fragment could only be amplified when using gDNA from *C. ljungdahlii* WT but not with gDNA of the deletion strain (**Figure 16B**). In addition, the deletion strain showed the expected shortened fragment when using primers that bound outside of the RNF-gene cluster (**Figure 16B**). Sanger sequencing of this fragment confirmed the precise deletion of *rnfCDGEAB* from the genome. We performed similar PCR screening experiments with the *C. ljungdahlii* Δ*rseC* and Δ*nar* strain to confirm the genome edits (**Supplementary Figure S14**). After generating the *C. ljungdahlii* Δ*rseC* strain and verifying the successful genome edit, several transfers in non-selective RCM and a subsequent cultivation at 42°C for 72 h were required to cure the strain from the pMTL83152_Cas12a-rseC plasmid. The genome edit remained stable during this procedure. In contrast, the plasmid curing was achieved quickly for the *C. ljungdahlii* ΔRNF and Δ*nar* strains after several transfers in non-selective RCM and subsequent isolation of single colonies on non-selective RCM plates.

8.3.4. Supplementary Text S1C - Growth of *C. ljungdahlii* WT with nitrate or ammonium as nitrogen source

During autotrophy with ammonium, *C. ljungdahlii* WT showed a growth rate of 0.024±0.002 h^{-1}, reached its maximum OD_{600} at 0.56±0.01, and produced 59.5±1.8 mM acetate and 1.9±0.4 mM ethanol (**Table 9, Figure 17**). When using nitrate instead, the growth rate was 0.072±0.004 h^{-1} and the maximum OD_{600} increased to 1.00±0.06 (**Table 9, Figure 17A**). This is a significant increase of 198% ($P \leq 0.001$) and 79% ($P \leq 0.001$) in comparison to ammonium conditions, respectively. In contrast, the maximum acetate concentration decreased to 50.1±2.1 mM, which is a significant reduction of 16% ($P = 0.008$), and maximum ethanol concentrations increased to 8.0±1.6 mM corresponding to a significant increase of 327% ($P = 0.007$) when using nitrate as nitrogen source (**Table 9, Figure 17C, 17D**). Notably, the ethanol production of nitrate grown cells only started after all nitrate was consumed at a cultivation time of 47 h. During heterotrophy, we observed that *C. ljungdahlii* WT performed slightly better in ammonium-containing medium in terms of growth and production of acetate and ethanol (**Supplementary Table S18, Supplementary Figure S13**). With nitrate and fructose, the growth rate decreased by 7% ($P = 0.04$), maximum OD_{600} values dropped by 10% ($P = 0.03$), and maximum concentrations for acetate were significantly reduced by 17% ($P \leq 0.001$) and for ethanol by 53% ($P \leq 0.001$) in comparison to growth with fructose and ammonium (**Supplementary Table S18**). During autotrophy, we observed that the pH of the medium initially increased up to pH 7.31, before it decreased again until the end of the cultivation (**Figure 16B**). The pH of ammonium cultures only decreased during the cultivation. This pH effect was not observed during heterotrophy,

but the pH decreased slower for those cultures growing with nitrate (**Supplementary Figure S13B**). Notably, during heterotrophy, a halt in growth, pH decrease, and metabolic activity was observed after 55.5 h of cultivation when the fructose pool had been consumed completely (**Supplementary Figure S13**). In all our experiments, we found that a sufficient amount of nitrogen was supplied already by the yeast extract (1 g/L) that we had added, because further ammonium accumulated and was not consumed, even when only ammonium was provided as the nitrogen source. Similar observations were already reported by Emerson *et al.* (2019).

8.3.5. Supplementary Text S1D - The role of RseC genes in non-acetogens

The *rseC* gene was already described as an important factor in the regulation of the oxidative stress response in *E. coli*, which is mediated by SoxR and the *rsxABCDGE* genes that share homology to the *rnf* genes in *R. capsulatus* (Koo *et al.*, 2003). In *E. coli*, the *rseC* gene is organized in the *rseD-rpoE-rseABC* operon, but located separately from the *rsxABCDGE* genes (De Las Peñas *et al.*, 1997; Missiakas *et al.*, 1997; Koo *et al.*, 2003). The proteins that are encoded by the *rseD-rpoE-rseABC* operon integrate signals from the redox state of SoxR, which senses the cellular levels of the oxidants superoxide and nitric oxide, and which is reduced by the membrane-bound complex Rsx. Thus, it is assumed that electrons from NADH are channeled through the Rsx complex and are transferred onto SoxR directly or indirectly to regenerate a reduced state after oxidation by oxidants (Koo *et al.*, 2003; Biegel *et al.*, 2011). The proposed system would be similar to the electron translocation of the RNF complex (Biegel *et al.*, 2011). It is assumed that the RseC protein is responsible to regulate the expression of SoxR by repressing its own regulator gene *soxS* (Koo *et al.*, 2003). In *E. coli,* a Tn*10*-transposon insertion mutant of *rseC* showed increased expression levels of the gene *soxS* (Koo *et al.*, 2003). The level of *soxS* transcript was found to be responsible for the redox state of SoxR, and higher levels of *soxS* mRNA indicated higher oxidation rates of SoxR (Ding and Demple, 1997). Therefore, it is assumed that the function of RseC in *E. coli* is likely to keep the level of *soxS* transcript low, which then keeps SoxR in its reduced form (Koo *et al.*, 2003). However, whether RseC interacts or interferes either with the Rsx complex or *soxS* mRNA/SoxR is not understood, and neither is the function as transcription regulator (Koo *et al.*, 2003). Koo *et al.* (2003) reported that *rseC* of *E. coli* shares homology to the N-terminal half of the *rnfF* gene in *R. capsulatus*, and thus postulated a regulatory function of *rseC* in the nitrogen fixation. In our *in-silico* analysis, we found that *rnfF* and *rseC* in *R. capsulatus* are likely separated genes (**Figure 5**). This does not exclude the potential role of *rseC* in the nitrogen fixation, but it questions the homology between *rseC* and *rnf* genes. In addition, the *rnfF* gene is not part of the RNF complex gene cluster in genomes of acetogens.

8.3.6. Supplementary Text S1E - Regulation by RseC in *C. ljungdahlii*

We assume that the RseC protein most likely binds to the transcription start site, which is located upstream of the *rnfC* gene, because the entire RNF-gene cluster was downregulated during autotrophy and heterotrophy after 3 h of cultivation, (**Figure 19A**). Based on our qPCR results from the heterotrophic samples after 20 h of cultivation, it can be speculated that the second transcription start site, which is located upstream of *rnfE* (Al-Bassam *et al.*, 2018), might be a second binding site for the transcriptional regulation of RseC. We see an upregulation of the three genes *rnfE, rnfA,* and *rnfB* in these samples for the *rseC* deletion compared to the wild-type strain. Thus, we argue that RseC could act as a negative regulator to modulate RNF-gene cluster expression during heterotrophy by repressing the genes *rnfE, rnfA,* and *rnfB* (**Figure 19C**). The plasmid-based complementation of *rseC* in the *C. ljungdahlii* Δ*rseC* strain (and overexpression in the wild-type background) re-enabled growth with carbon dioxide and hydrogen, and reduced the *lag* phase during the transition from heterotrophy to autotrophy (**Table 10**, **Figure 19, Supplementary Figure S15**). This further argues for a function of RseC as a positive regulator of the RNF-gene cluster. In the RseC overproduction strain, the enhanced activation of gene expression could result in a further elevated level of RNF complex. The elevated level of RNF complex would lead to a higher oxidation rate of reduced ferredoxin. Thus, less or no reduced ferredoxin is available for the ferredoxin-dependent aldehyde oxidoreductase enzyme, which is the main contributor for the reduction of acetic acid to ethanol under autotrophic conditions in *C. ljungdahlii* (Liew *et al.*, 2017; Lo *et al.*, 2020). This would explain why ethanol production was abolished in *C. ljungdahlii* pMTL83152_*rseC* (**Supplementary Figure S15D**). However, heterotrophy was not negatively impacted in the *C. ljungdahlii* Δ*rseC* strain, and the RNF complex also plays a critical, yet not essential, role in re-fixation of carbon dioxide from glycolysis in acetogens. A downregulation of the RNF-gene cluster transcripts would contribute to reduce the energy cost that is required for the synthesis of RNF complex proteins. Also, a different subunit composition might be required during autotrophy and heterotrophy.

The RseC protein in *E. coli* seems to contain two transmembrane domains with the C-terminal end being located in the cytoplasm (Daley *et al.*, 2005). Thus, another possible function of RseC could be the modulation of protein-protein interactions with the RNF complex, because for all the RseC homologs that we investigated here, two transmembrane helices were predicted (**Supplementary Table S19**). For instance, RseC could stabilize the RNF complex in the membrane, which is required for the electron translocation mechanism or the interaction with other cytoplasmic proteins during autotrophy, but not during heterotrophy. This could explain why a lack of the RseC protein is not leading to the same reduced heterotrophy as observed for the *C. ljungdahlii* ΔRNF strain. Interestingly, we detected *rseC* genes only in those acetogens that contain an RNF complex (**Table 11**). In addition,

we found that the *rseC* gene was located directly upstream of the RNF complex genes only for those microbes, which possess an RNF complex that translocates protons (**Table 11**, **Figure 20**). The upregulation of the *rseC* gene in the *C. ljungdahlii* ΔRNF strain indicates that the *rseC* gene itself is also under further transcriptional control (**Figure 19B, 19D**). An upregulation of the *rseC* gene in all samples might indicate the effort of the cells to induce RNF-gene cluster expression further, which is apparently not possible in the *C. ljungdahlii* ΔRNF strain. Thus, potentially additional direct or indirect regulatory effects are mediated by RseC. This could be the regulation of further genes as a positive or negative regulator, which in turn could have an effect on the functionality of the RNF complex.

Supplementary Text S1F - Nitrate reduction in *C. ljungdahlii*

Recent studies have found that nitrate reduction in *C. ljungdahlii* is coupled to energy generation, and thus, is from a dissimilatory rather than from an assimilatory character (Emerson *et al.*, 2019; Klask *et al.*, 2020). Since the entire autotrophic metabolism and generation of ATP for cell division is based on RNF-complex activity in *C. ljungdahlii*, we assume that nitrate reduction and the RNF complex are closely connected. Our results indicate that the nitrate reduction resembles bacterial anaerobic nitrate respiration systems. However, *C. ljungdahlii* neither possesses genes for cytochromes nor for the biosynthesis of ubiquinone, which limits the generation of a chemiosmotic gradient to the RNF complex (Köpke *et al.*, 2010). The nitrate reductase in *C. ljungdahlii* is most likely located in the cytosol rather than associated with the membrane, as one would expect from dissimilatory nitrate reductases in bacteria (Zumft, 1997; Köpke *et al.*, 2010; Nagarajan *et al.*, 2013). This type of nitrate reduction was described as fermentative nitrate reduction and was already observed for other microbes, but is less understood than the assimilatory and dissimilatory nitrate reduction in the microbial world (Hall, 1973; Hasan and Hall, 1975; Seifritz *et al.*, 1993; Emerson *et al.*, 2019).

Supplementary Text S1G - Ethanol production in *C. ljungdahlii* Δ*nar*

In our batch experiments, *C. ljungdahlii* Δ*nar* reached a lower maximum OD_{600} compared to the wild type in nitrate-containing medium during both autotrophy and heterotrophy, which was expected, because nitrate reduction was completely abolished (**Figure 21A, 21F, Supplementary Figure S18A, S18F**). However, more unexpectedly, the fermentation product spectrum changed when compared to the wild type, especially with considerably increased maximum ethanol concentrations during heterotrophy (**Supplementary Figure S18D**). This was independent from the presence of ammonium or nitrate. Thus, the overall electron balance between fermentation products, besides the loss of nitrate reduction activity, is impacted by the deletion of the *nar* gene cluster. A possible explanation for increased ethanol production of the *C. ljungdahlii* Δ*nar* strain during heterotrophy could be that more reducing equivalents (*e.g.,* NADH, NADPH) are available for the alcohol dehydrogenases (ADHs),

which would be used to reduce nitrate in the wild type, and which predominantly catalyze the reduction of acetyl-CoA to ethanol during heterotrophy but not during autotrophy in *C. ljungdahlii* (Schuchmann and Müller, 2014; Richter *et al.*, 2016b; Liew *et al.*, 2017). Consequently, less acetate should be produced by the *C. ljungdahlii* Δ*nar* strain. Indeed, the *C. ljungdahlii* Δ*nar* strain produced only 66% ($P \leq 0.001$) of the acetate concentration that was measured for the wild type, when growing under heterotrophic conditions with nitrate, which is a significant reduction (**Supplementary Table S18, Supplementary Figure S13C, S18C**). Furthermore, this would argue for NADH or NADPH as the electron donor of the nitrate reductase. On the contrary, we observed increased ethanol concentrations also in the presence of ammonium instead of nitrate as nitrogen source. This might be due to an involvement of the nitrate reductase in other processes, but could also be due to genetic polar effects in the *nar* deletion strain. In addition, nitrate reduction could be regulated and controlled differently during autotrophy and heterotrophy.

8.3.7. Supplementary Tables

Supplementary Table S18. Performance of all tested *C. ljungdahlii* strains in heterotrophic batch cultivation experiments. Cultures were grown with fructose (5 g/L) in PETC medium, which contained either ammonium or nitrate as nitrogen source. All growth experiments were performed under anaerobic conditions. Data is given as mean values ± standard deviation from biological triplicates. WT, *C. ljungdahlii* wild type; ΔRNF, *C. ljungdahlii* with deleted *rnfCDGEAB* gene cluster; Δ*rseC*, *C. ljungdahlii* with deleted *rseC* gene; and Δ*nar, C. ljungdahlii* with deleted nitrate reductase gene cluster.

strain	nitrogen source	growth rate (μ in h)[a]	maximum OD_{600} value	maximum acetate concentration (mM)	maximum ethanol concentration (mM)
WT	ammonium	0.079±0.002	2.49±0.03	52.3±0.7	10.6±0.1
WT	nitrate	0.073±0.002	2.24±0.10	43.6±0.6	5.0±0.1
ΔRNF	ammonium	0.052±0.003	1.16±0.03	35.4±0.5	6.3±0.8
ΔRNF	nitrate	0.042±0.003	0.98±0.10	25.4±1.7	n.d.[b]
Δ*rseC*	ammonium	0.084±0.002	1.90±0.15	50.1±0.3	7.5±0.1
Δ*rseC*	nitrate	0.048±0.002	1.58±0.03	50.9±1.7	2.9±0.1
Δ*nar*	ammonium	0.071±0.002	2.35±0.04	51.9±0.9	15.3±0.1
Δ*nar*	nitrate	0.067±0.001	1.51±0.03	28.7±1.1	16.6±0.2

[a] μ values were calculated based on the individual OD_{600} values of each triplicate in the exponential growth phase.

[b] n.d., not detectable.

Supplementary Table S19 RseC peptide sequences and amount of predicted transmembrane helices. The type strains are listed in Table 11.

microbe	RseC peptide sequence	predicted transmembrane helices
C. ljungdahlii	MKRESEGIVIETSESIAKVRASRHGDCKSCGACPG DNAIVVDAKNPVGAKPGQHVVFEIKDANMLWAAFI VYILPLIGILIGALIGTWIGGKLGHSLREFQIGGG VLFFILSLIYIKIFDRSTSKNESKKPVITKILY	2
C. autoethanogenum	MKRESEGIVIETSESIAKVRASRHGDCKSCGACPG DNAIVVDAKNPVGAKPGQHVVFEIKDANMLWAAFI VYILPLIGILIGALIGTWIGGKLGHSLREFQIGGG VLFFILSLIYIKIFDRSTSKNESKKPVITKILY	2
C. carboxidovorans	MNRETEGIVIQIEGNIAKIKANRHGDCSNCGACPG DKAMVVDAINTIGAKPGQHVSFEIKEVNMLKAAFV VYILPLVSIFIGAVIGGFVAKKIAQDSVMCSVIGG IVLFILSIIYIKFFDKAANKDENMKPIITRILS	2
C. kluyveri	MKKESEGIVIETTEGFARVKASRHGDCKNCGACPG DNATVLDAKNPIGAKAGEHVILEMREQNMIRAAFV VYIMPIISIFLGVLVGTWIFNAVGYYEMAFKVVGG IVFFVISLVYIKVFDKATAKNDASKPVIKKVL	2
E. limosum	MKEIGIVEELKGKNAKVLIKRHAACGDCGACQVGK EKMTMEATARNAAGAQVGDTVSVEMEFANVIKATS IMYGIPLIAFVVGCAAGYFAAVALTLDLVLVPFFT GILLTVISYLVIRVFDKKGKFNSKYEPVITEIEAE AQELPPAGE	2
A. woodii	MKEIGTVKALKGKNAEIEIKRNTACGDCGACHVSK DQSVMLTTANNPIKAKIGETVEVEMEFANVFVAAF IMYGIPLVAFVLGSSGVYFLVGALNIGWDQVVSSF LAGICLTAVAYVVIRKLDRKGRFNSKYQPIVTAII EKKETIKTPMESRMGH	2
R. capsulatus	MTGCCDDGPATGPRDLRERLRVVAVRGESLVVAAD RASACAACAEAKGCGTRALMSMHRTDLMTIARPAG LIVAPGDEVEVAMSGNNLLAGAGLAYLLPALAFVV ALALASGAGLSDGGAALVGGVVLMFSFLPLVLLER RARLSRALQVLDVHPGHGR	2
E. coli	MIKEWATVVSWQNGQALVSCDVKASCSSCASRAGC GSRVLNKLGPQTTHTIVVPCDEPLVPGQKVELGIA EGSLLSSALLVYMSPLVGLFLIASLFQLLFASDVA ALCGAILGGIGGFLIARGYSRKFAARAEWQPIILS VALPPGLVRFETSSEDASQ	2

8.3.8. Supplementary Figures

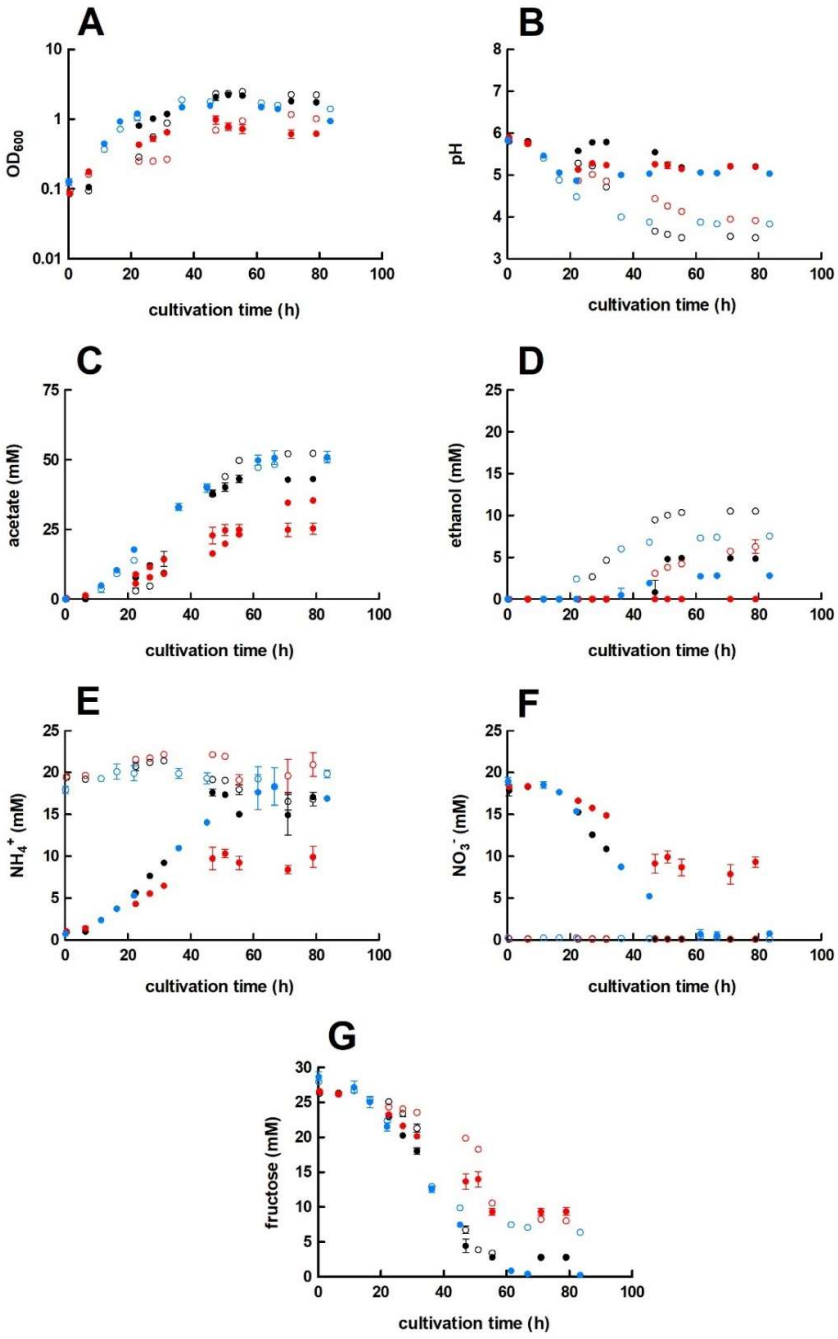

Supplementary Figure S13 Heterotrophic growth and metabolic products of *C. ljungdahlii* WT, ΔRNF, and Δ*rseC*. Cultures of *C. ljungdahlii* WT (●, ○), ΔRNF (●, ○), and Δ*rseC* (●, ○) were grown in 100 mL PETC medium in 240 mL bottles at 37°C. The headspace consisted of N_2 (100 vol-%). Fructose (5 g/L) was added as carbon source. The medium contained either 18.7 mM nitrate (NO_3^-) (filled circles) or 18.7 mM ammonium (NH_4^+) (open circles) as nitrogen source. The cultivation times were 79 h for the WT and ΔRNF strain, and 84 h for the Δ*rseC* strain. All cultures were grown in biological triplicates, data is given as mean values, with error bars indicating the standard deviation. **A**, growth; **B**, pH-behavior; **C**, acetate concentrations; **D**, ethanol concentration; **E**, ammonium concentration; and **F**, nitrate concentrations. WT, wild type; ΔRNF, RNF-gene cluster deletion; Δ*rseC*, *rseC* gene deletion.

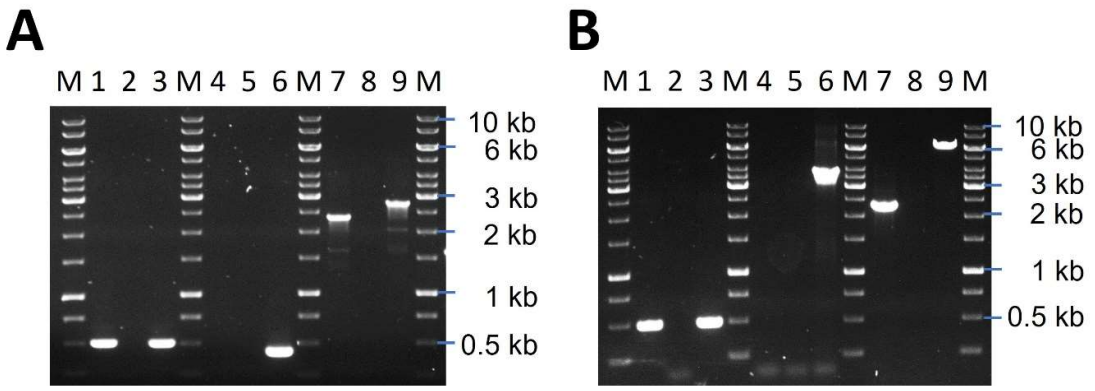

Supplementary Figure S14 CRISPR-Cas12a-mediated *rseC* gene and *nar* gene cluster deletion in *C. ljungdahlii*. A, verification of the *rseC* gene deletion. PCR-samples for the *fdhA* fragment (WT: 501 bp, deletion strain: 501 bp), *rseC* fragment (WT: 417 bp, deletion strain: no fragment), and for a fragment that was amplified with primers that bind 1104 bp upstream and 1208 bp downstream of the *rseC* gene locus (WT: 2755 bp, deletion strain: 2338 bp). DNA-template: gDNA of *C. ljungdahlii* Δ*rseC* (lane A1, A4, and A7); gDNA of *C. ljungdahlii* WT (lane A3, A6, and A9); and water (lane A2, A5, A8). **B**, verification of the *nar* gene cluster deletion PCR samples for the *fdhA* fragment (WT: 501 bp, deletion strain: 501 bp), *nar* fragment (WT: 3739 bp, deletion strain: no fragment), and for a fragment that was amplified with primers that bind 1137 bp upstream and 1110 bp downstream of the *nar* gene cluster locus (WT: 5986 bp, deletion strain: 2247 bp). DNA-template: gDNA of *C. ljungdahlii* Δ*nar* (lane B1, B4, and B7); gDNA of *C. ljungdahlii* WT (lane B3, B6, and B9); and water (lane B2, B5, B8). M: Generuler™ 1 kb.

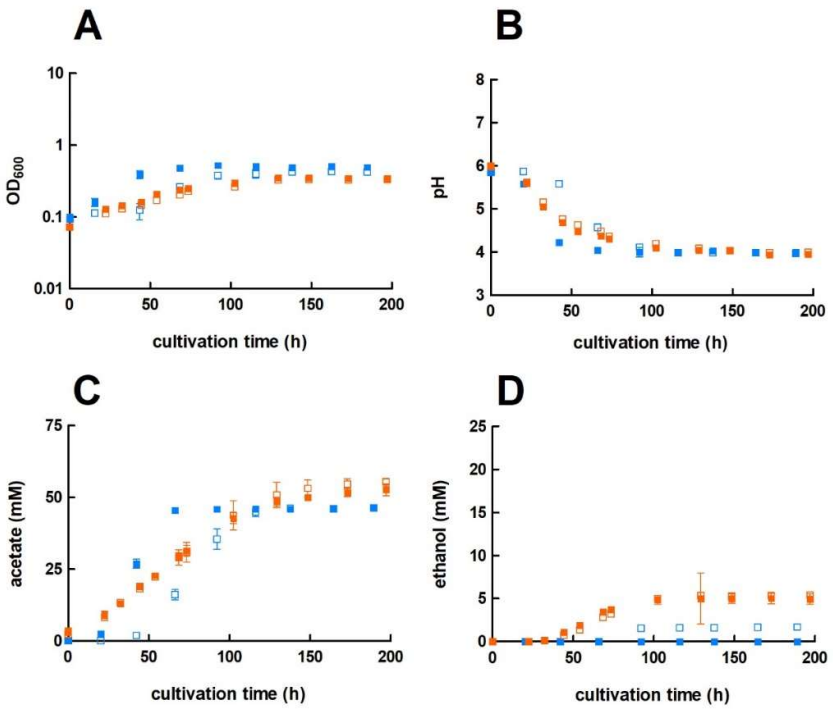

Supplementary Figure S15 Autotrophic growth and metabolic products of the overexpression strains *C. ljungdahlii* pMTL83151_P_{nat}_*rnfCDGEAB* and *C. ljungdahlii* pMTL83152_*rseC*. Cultures were grown in 100 mL PETC medium in 1 L bottles at 37°C and 150 rpm. The headspace consisted of H_2 and CO_2 (80/20 vol-%) and was set to 0.5 bar overpressure. For the strain *C. ljungdahlii* pMTL83151_P_{nat}_*rnfCDGEAB* and the control strain *C. ljungdahlii* pMTL83151 we refilled the headspace during this experiment with the same gas mixture to 0.5 bar overpressure at time points 44.5 h, 73.5 h, and 148.5 h. The medium contained 18.7 mM ammonium as nitrogen source. Thiamphenicol (5 µg/mL) was used for selection. All cultures were grown in biological triplicates, data is given as mean values, with error bars indicating the standard deviation. The cultivation time was 185 h and 197 h for *C. ljungdahlii* pMTL83151_P_{nat}_*rnfCDGEAB* and *C. ljungdahlii* pMTL83152_*rseC*, respectively. (■) *C. ljungdahlii* pMTL83151_P_{nat}_*rnfCDGEAB*; (□) *C. ljungdahlii* pMTL83151 (empty plasmid); (■) *C. ljungdahlii* pMTL83152_*rseC*; (□) *C. ljungdahlii* pMTL83152 (empty plasmid). **A**, growth; **B**, pH-behavior; **C**, acetate concentrations; and **D**, ethanol concentration. rpm, revolutions per minute; CO_2, carbon dioxide; and H_2, hydrogen.

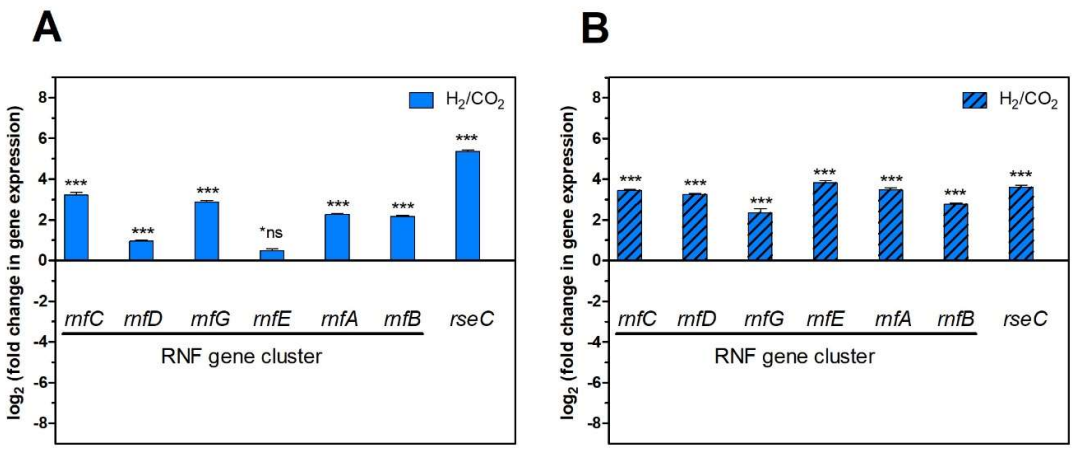

Supplementary Figure S16 Gene expression change of the *rnfCDGEAB* cluster genes and the *rseC* gene in the wild-type strain from heterotrophy to autotrophy. A, gene expression change after 3 h cultivation time; **B**, gene expression change after 20 h cultivation time. RNA samples were purified from cultures that were cultivated either autotrophically with hydrogen and carbon dioxide or heterotrophically with fructose. cDNA was synthesized from the purified RNA samples and used as template for qRT-PCR analyses. The *rho* gene was used as "housekeeping" gene. The fold change in gene expression was determined with the $2^{-\Delta\Delta CT}$ method (Livak and Schmittgen, 2001). ***, $P \leq 0.001$; and *ns, not significant ($P > 0.5$). We defined $\log_2$ (fc) ≤ -1 as downregulated genes and ≥ +1 as upregulated genes.

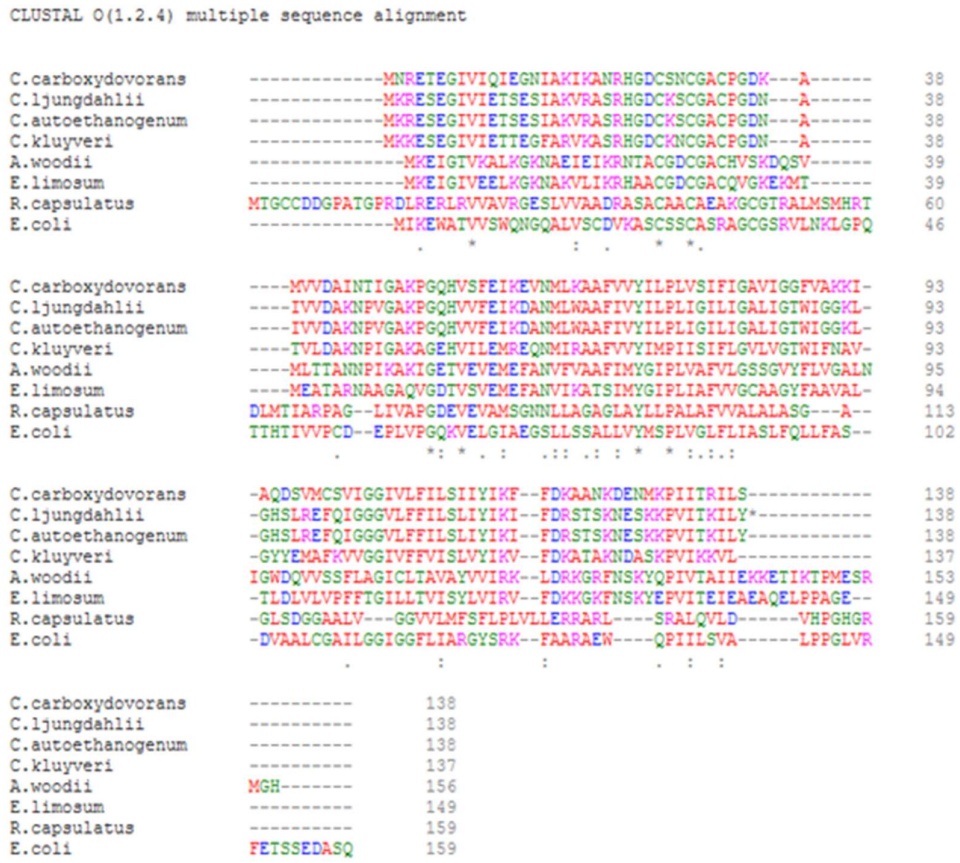

Supplementary Figure S17 Multiple sequence alignment of RseC amino-acid sequence using CLUSTAL Omega. The symbols indicate low similarity (.), high similarity (:), and identical amino acids (*) between the amino acid sequences. Similar colors indicate similar amino acids. The type strains were *C. ljungdahlii* DSM13528; *C. autoethanogenum* DSM10061; *C. carboxidovorans* P7; *C. kluyveri* DSM555; *E. limosum* ATCC8486; *A. woodii* DSM1030; *R. capsulatus* SB1003; and *E. coli* K-12. Clustal omega version 1.2.4. with default settings was used for the analysis (https://www.ebi.ac.uk/Tools/msa/clustalo/, 05/2021).

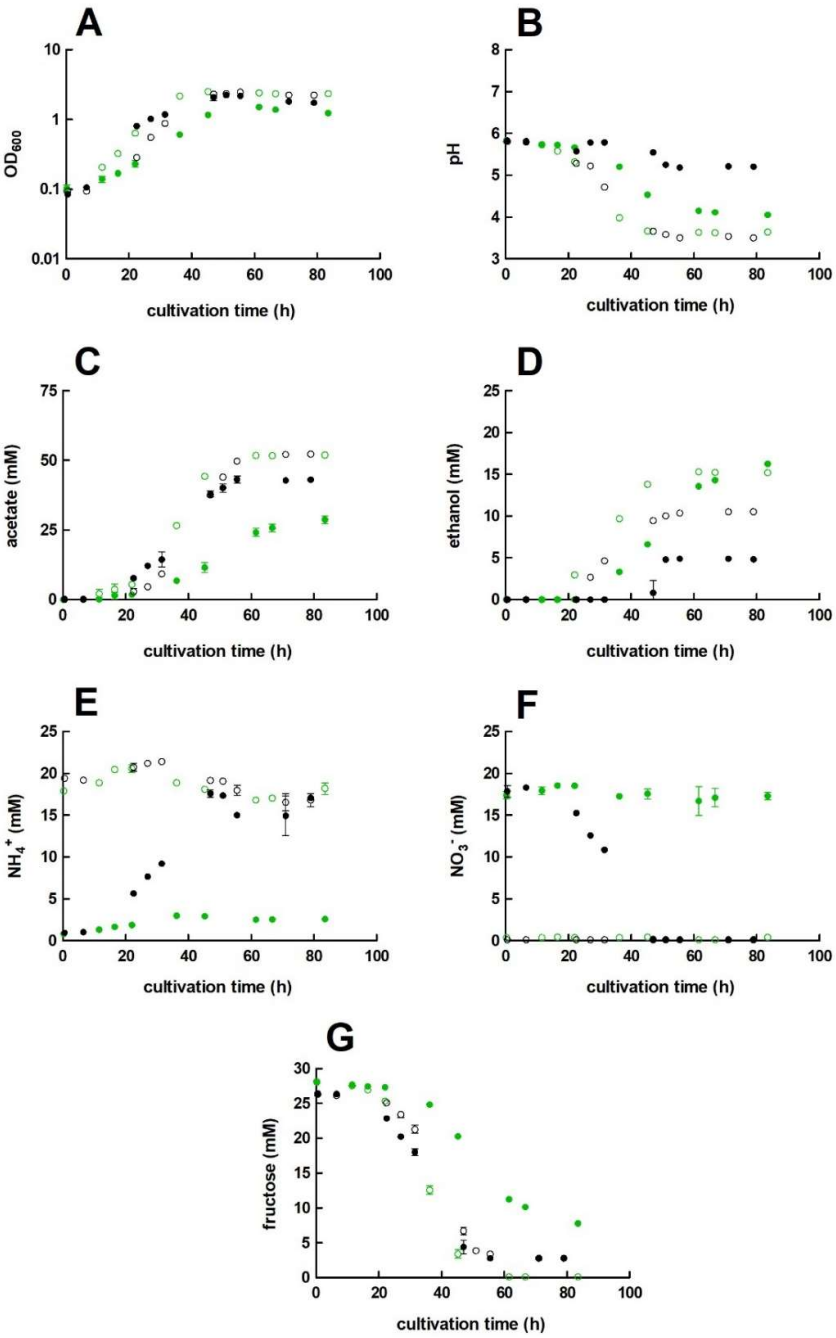

Supplementary Figure S18 Heterotrophic growth and metabolic products of *C. ljungdahlii* Δ*nar*. Cultures were grown in 100 mL PETC medium in 240 mL bottles at 37°C. Fructose (5 g/L) was added as carbon source. The headspace consisted of N_2 (100 vol-%). The medium contained either 18.7 mM nitrate (●) or 18.7 mM ammonium (○) as nitrogen source. All cultures were grown in biological triplicates, data is given as mean values, with error bars indicating the standard deviation. The cultivation times was 84 h. The *C. ljungdahlii* WT data (●, ○) from Supplementary Figure S1 is given for comparison. **A**, growth; **B**, pH-behavior; **C**, acetate concentrations; **D**, ethanol concentration; **E**, ammonium concentration; **F**, nitrate concentrations; and **G**, fructose concentrations. Δ*nar*, deletion of the nitrate reductase genes.

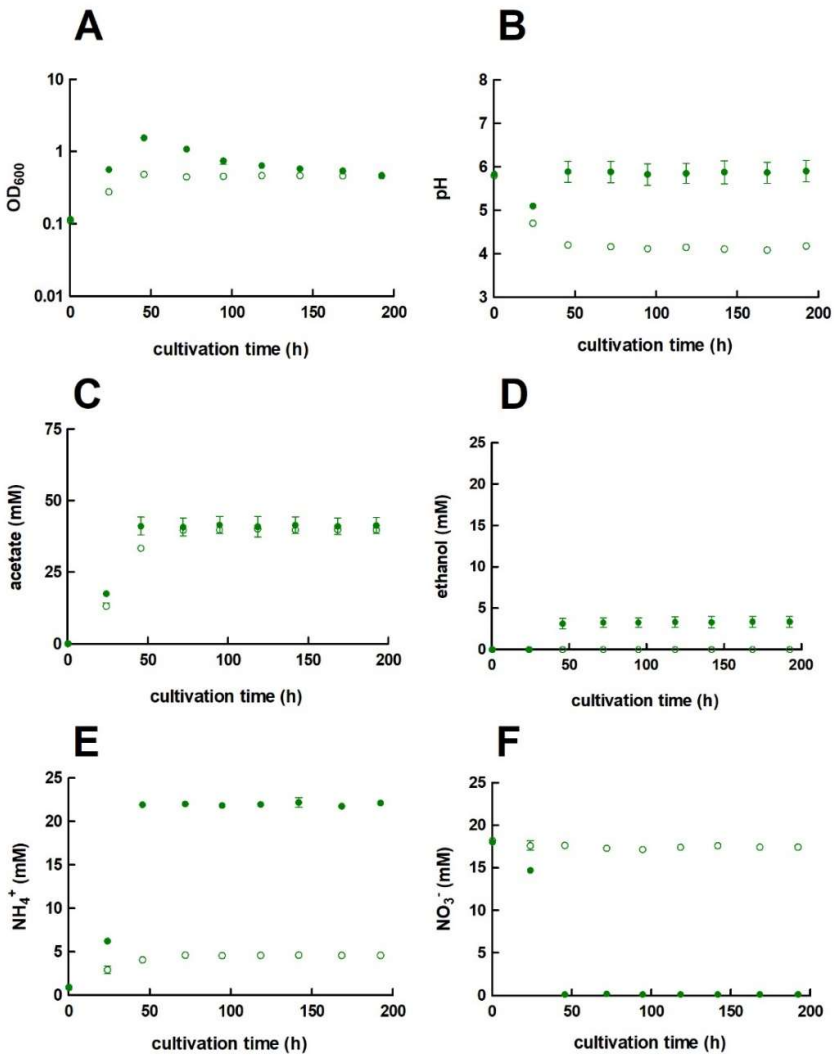

Supplementary Figure S19 Autotrophic growth and metabolic products of plasmid-based complemented strain *C. ljungdahlii* Δ*nar* pMTL83152_*nar*. Cultures were grown in 100 mL PETC medium in 1 L bottles at 37°C and 150 rpm. The headspace consisted of H_2 and CO_2 (80/20 vol-%) and was set to 0.5 bar overpressure. The medium contained 18.7 mM nitrate (NO_3^-) but no ammonium (NH_4^+) as nitrogen source. Thiamphenicol (5 µg/mL) was used for selection. All cultures were grown in biological triplicates, data is given as mean values, with error bars indicating the standard deviation. The cultivation times was 192.5 h. (●) *C. ljungdahlii* Δ*nar* pMTL83152_*nar*; (○) *C. ljungdahlii* Δ*nar* pMTL83152 (empty plasmid); **A**, growth, **B**, pH-behavior; **C**, acetate concentrations; **D**, ethanol concentration; **E**, ammonium concentration; and **F**, nitrate concentrations. Δ*nar*, gene deletion of the nitrate reductase genes; rpm, revolutions per minute; CO_2, carbon dioxide; and H_2, hydrogen.

8.4. Supplementary information for Chapter 6

Supplementary Table S20-S23

Supplementary Figure S20-S27

8.4.1. Strains, plasmids, and sequences

Supplementary Table S20 Primers used in this study.

Primer	Sequence (5'-> 3')	Function
Clj_cphA_fwd	GGATCCAGGAGGTTAAGAATGAGAAT AGATAATTTTAGAATTTTTCAGGGAAG	Amplification of *cphA* from the genome of *C. ljungdahlii* DSM13528
Clj_cphA_rv	CCATGGCTATATCATAGCTAGTGAATTT AAATTTGATTTTTC	Amplification of *cphA* from the genome of *C. ljungdahlii* DSM13528
An_cphA_fwd	GGATCCAGGAGGTTAAGAATGAGAAT CCTCAAGATCCAGACC	Amplification of *cphA* from the genome of *Anabaena* sp. PCC7120
An_cphA_rv	CCATGGCTACAGCAAAGTATTAATTAC AGAAGAAGATGC	Amplification of *cphA* from the genome of *Anabaena* sp. PCC7120
fdhA_fwd	AGCGTCTTTACGCATACTCTTTTTACGG	Amplification of a 501 bp fragment of the *fdhA* gene from the genome of *C. ljungdahlii* DSM13528
fdhA_rv	ATGAAAAGTATACTAACTACTTGTCC	Amplification of a 501 bp fragment of the fdhA gene from the genome of *C. ljungdahlii* DSM13528
tetR-O1_fwd	CCTGCAGGATAAAAAAATTGTAGATAA ATTTTATAAAATAG	Amplification of the promoter sequence for $P_{tetR-O1}$
tetR-O1_rv	GGATCCTATTTCAAATTCAAGTTTATCG CTCTAATGAAC	Amplification of the promoter sequence for $P_{tetR-O1}$
repH_643bp_rv	GCACTGTTATGCCTTTTGACTATCAC	Primer binding 643 bp upstream of *repH* located on pMTL83151 and pMTL83152, amplification of an insert in the MCS
tra_60bp_fw	CATGCGCTCCATCAAGAAGAG	Primer binding 60 bp downstream bp upstream of *traJ* located on pMTL83151 and pMTL83152, amplification of an insert in the MCS
seqP_clj_cphA1332bp_fwd	GCACCAGGTATTAGAATGCACC	Sanger sequencing of the $cphA_{Clj}$
seqP_clj_cphA_1451bp_rv	CCCGTAACTGAAACTACAGGTATTG	Sanger sequencing of the $cphA_{Clj}$
seqP_clj_cphA2049bp_fwd	GAAAATGCTATGGCTGCTTGTGC	Sanger sequencing of the $cphA_{Clj}$
seqP_clj_cphA2222bp_rv	CCTTCTATATTGTGTCCATAATCTA AAACTACTT	Sanger sequencing of the $cphA_{Clj}$
seq_cphAAn_1223fwd	CCCGTAACTGAAACTACAGGTATTG	Sanger sequencing of the $cphA_{An}$
seq_clj_cphA150bp_fwd	GAGTTAAATGAACACAGGTGTGG	Sanger sequencing of the $cphA_{An}$
seq_clj_cpha700bp_rv	CAATTCCGCCTTCTGCTACG	Sanger sequencing of the $cphA_{An}$
seq_clj_cphA1332bp_fwd	GCACCAGGTATTAGAATGCACC	Sanger sequencing of the $cphA_{An}$
seq_clj_cphA2049bp_fwd	GAAAATGCTATGGCTGCTTGTGC	Sanger sequencing of the $cphA_{An}$
seq_clj_cphA2222bp_rv	CCTTCTATATTGTGTCCATAATCTAAAA CTACTT	Sanger sequencing of the $cphA_{An}$
seqP_ tetR-O1_500bp_fw	CAGCTTTCCCCTTCTAAAGGGC	Sanger sequencing of the promoter sequence for $P_{tetR-O1}$
seqP_ tetR-O1_545bp_rw	GATAGGCACCATACTCACTTTTGC	Sanger sequencing of the promoter sequence for $P_{tetR-O1}$

Supplementary Table S21 Plasmids used in this study.

Plasmid	Function	Source
pMTL83152	Shuttle-vector with constitutive promoter P_{thl}	Heap et al. 2009
pMTL83151_$P_{tetR-O1}$	Shuttle-vector with inducible promoter system $P_{tetR-O1}$	This study
pMTL83152_*cphA*$_{Clj}$	Constitutive expression of *cphA* from *C. ljungdahlii*	This study
pMTL83152_*cphA*$_{An.}$	Constitutive expression of *cphA* from *Anabaena* sp.	This study
pMTL83151_$P_{tetR-O1}$_*cphA*$_{Clj}$	Inducible expression of *cphA* from *C. ljungdahlii*	This study
pMTL83151_$P_{tetR-O1}$_*cphA*$_{An.}$	Inducible expression of *cphA* from *Anabaena* sp.	This study

Supplementary Table S22 Used strains in this study.

Name	Phenotype	Source
E. coli TOP10	normal	Invitrogen
E. coli pMTL83152	normal	This study
E. coli pMTL83152_*cphA*$_{Clj}$	normal	This study
E. coli pMTL83152_*cphA*$_{An.}$	Opaque colour, slower growth	This study
E. coli pMTL83151_$P_{tetR-O1}$	normal	This study
E. coli pMTL83151_$P_{tetR-O1}$_*cphA*$_{Clj}$	normal	This study
E. coli pMTL83151_$P_{tetR-O1}$_*cphA*$_{An.}$	normal	This study
C. ljungdahlii	normal	DSM13528
C. ljungdahlii pMTL83152	normal	This study
C. ljungdahlii pMTL83152_*cphA*$_{Clj}$	normal	This study
C. ljungdahlii pMTL83152_*cphA*$_{An.}$	normal	This study
C. ljungdahlii pMTL83151_$P_{tetR-O1}$_*cphA*$_{Clj}$	normal	This study
C. ljungdahlii pMTL83151_$P_{tetR-O1}$_*cphA*$_{An.}$	normal	This study

Supplementary Table S23 CGP calibration curve for NMR analyses. Purified CGP was used and diluted with TSP. The subsequent NMR analyses are then used to calculate back the concentration of CGP in relation to the integrated TSP peak area. The NMR analyses was performed as described before (Erickson *et al.*, 2001).

Original CGP concentration [mg/mL]	CGP conc after dilution with TSP/D_2O [mg/mL]	CGP δCH_2 peak area in relation to TSP peak area [mg/mL]
10	7.917	9.74
5	3.56265	4.57
0.25	0.197925	0.27
0.05	0.039585	0.0545

8.4.2. Electron microscopy of *C. ljungdahlii*

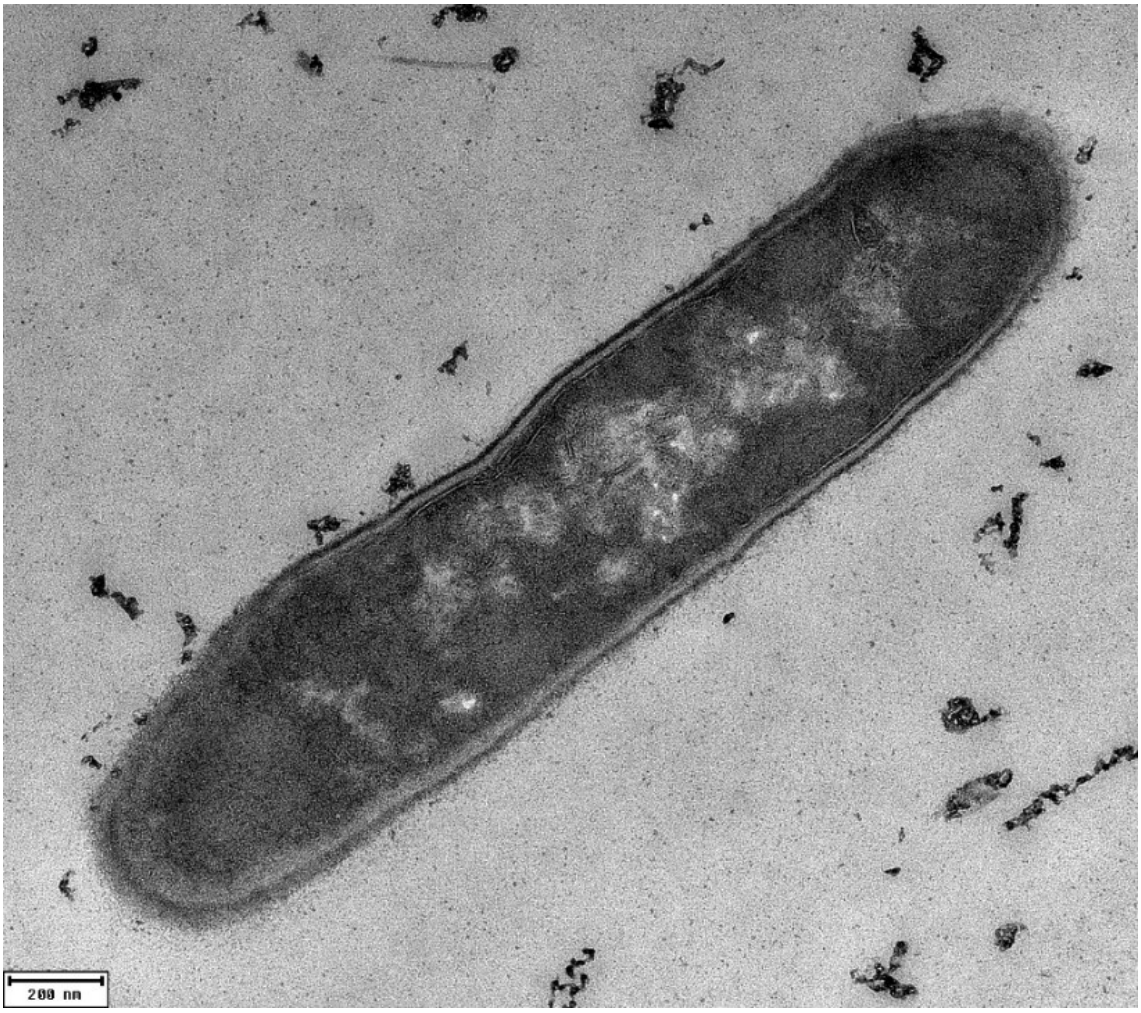

Supplementary Figure S20. Transmission electron microscopic picture of *C. ljungdahlii* pMTL83152_*cpha*$_{An.}$ growing with fructose in nitrate containing medium. *C. ljungdahlii* pMTL83152_*cphA*$_{An.}$ was cultivated for 48 h in PETC medium until early exponential growth phase and directly used for the sample preparation (Material and Methods). Cells of *C. ljungdahlii* pMTL83152_*cphA*$_{Clj}$ and *C. ljungdahlii* pMTL83152 were also tested but are not shown here. None of the analyzed cells showed intracellular cell inclusions, which could indicate the accumulation of CGP.

8.4.3. Control PCRs to verify strain purity during the bioreactor experiment

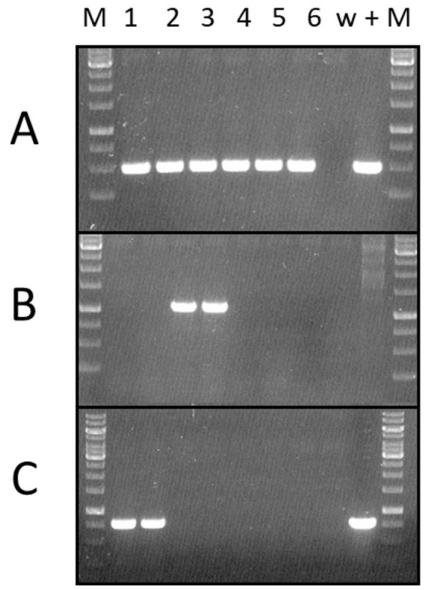

Supplementary Figure S21 Control PCR to verify the purity of the recombinant *C. ljungdahlii* strains cultivated in the bioreactors. A, PCR with FdhA primers (501 bp fragment for all clostridial DNA); B, PCR with primers specifically binding in the *cphA* sequence of *Anabeana* sp.; and C, PCR with primers specifically binding in the *cphA* sequence of *C. ljungdahlii*. W, water; +, gDNA of *C. ljungdahlii* WT, and M, marker GeneRuler 1 kb.

8.4.4. CGP extraction and biochemical analyses of bioreactor samples

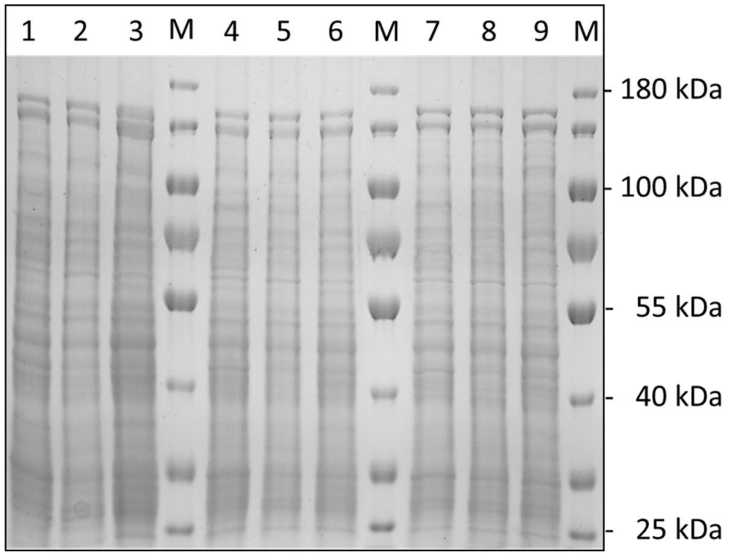

Supplementary Figure S22 SDS-PAGE of *C. ljungdahlii* cell samples after multiple lysis steps through bead beating and ultra-sonification. Samples were loaded in the order *C. ljungdahlii* pMTL83152, *C. ljungdahlii* pMTL83152_$cphA_{Clj}$, and *C. ljungdahlii* pMTL83152_$cphA_{An.}$ (from left to right). 1-3, resuspended pellet after 1x lysis; 4-6, resuspended pellet after 1x lysis; and 7-9, resuspended pellet after 3x lysis. M, PageRuler™ Pre-stained Protein Ladder. The gel was stained with InstantBlue™ for 30-40 min and washed with deionized water before imaging.

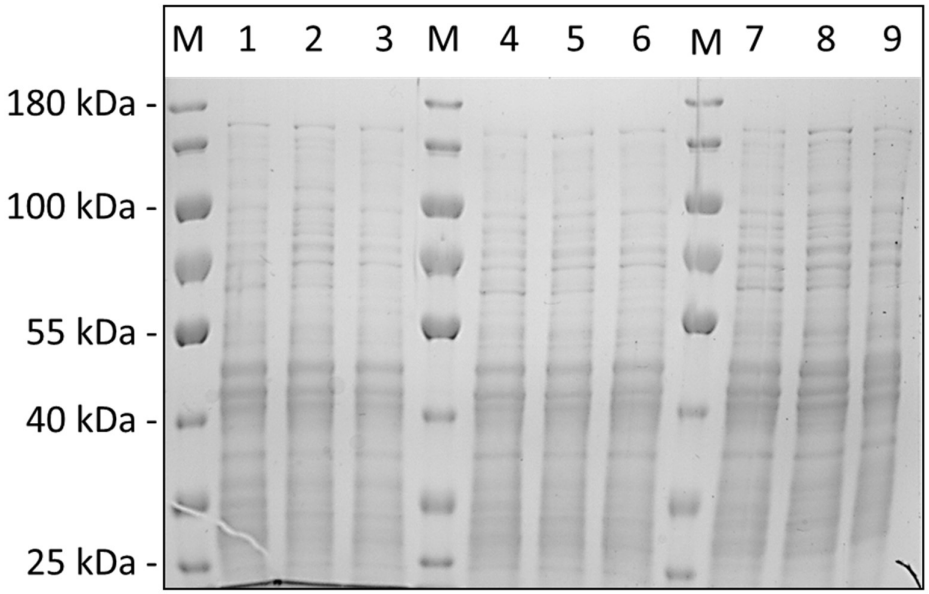

Supplementary Figure S23 SDS-PAGE of *C. ljungdahlii* **cell samples after multiple lysis and acid and neutralization treatment.** Samples were loaded in the order *C. ljungdahlii* pMTL83152, *C. ljungdahlii* pMTL83152_*cphA*$_{Clj}$, and *C. ljungdahlii* pMTL83152_*cphA*$_{An.}$ (from left to right). 1-3, resuspended pellet after 1x lysis and acid/neutralization treatment; 4-6, resuspended pellet after 2x lysis and acid/neutralization treatment; and 7-9, resuspended pellet after 3x lysis and acid/neutralization treatment. M, PageRuler™ Prestained Protein Ladder. The gel was stained with InstantBlue™ for 30-40 min and washed with deionized water before imaging.

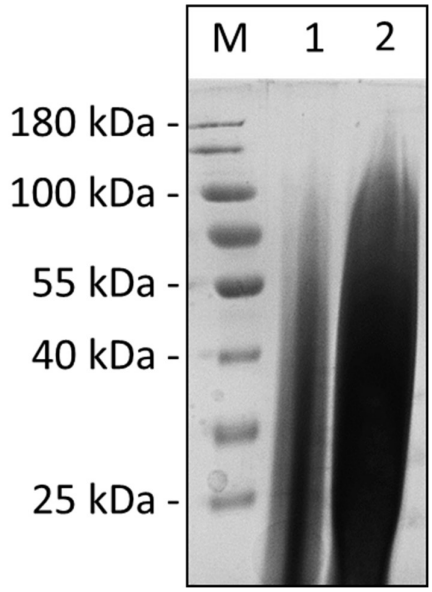

Supplementary Figure S24 SDS-PAGE of purified CGP isolated from cyanobacteria (kind gift from the Forchhammer lab). 1, 5 mg/mL sample; and 2, 10 mg/mL sample. M, PageRuler™ Pre-stained Protein Ladder. The gel was stained with InstantBlue™ for 30-40 min and washed with deionized water before imaging.

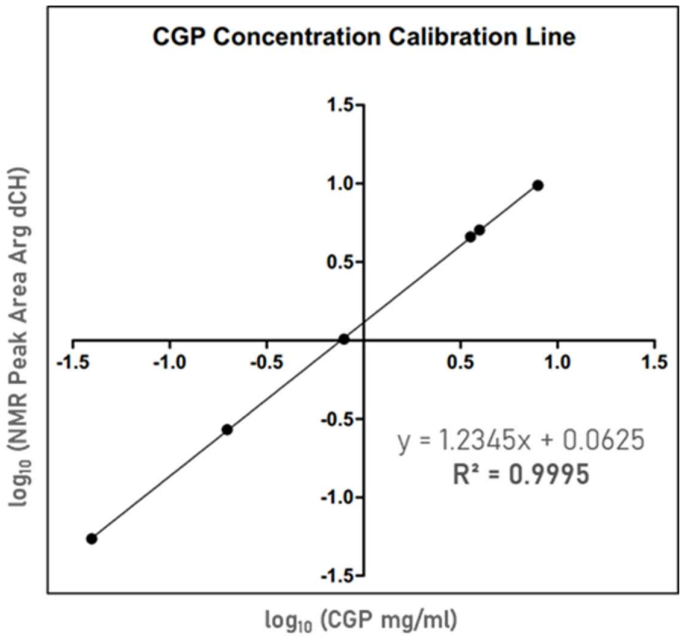

Supplementary Figure S25 CGP calibration curved derived from NMR analyses with TSP as standard. Purified CGP was used and diluted with TSP in the concentrations 0.05, 0.25, 5, and 10 mg/ml. The NMR analyses was performed as described before (Erickson *et al.*, 2001).

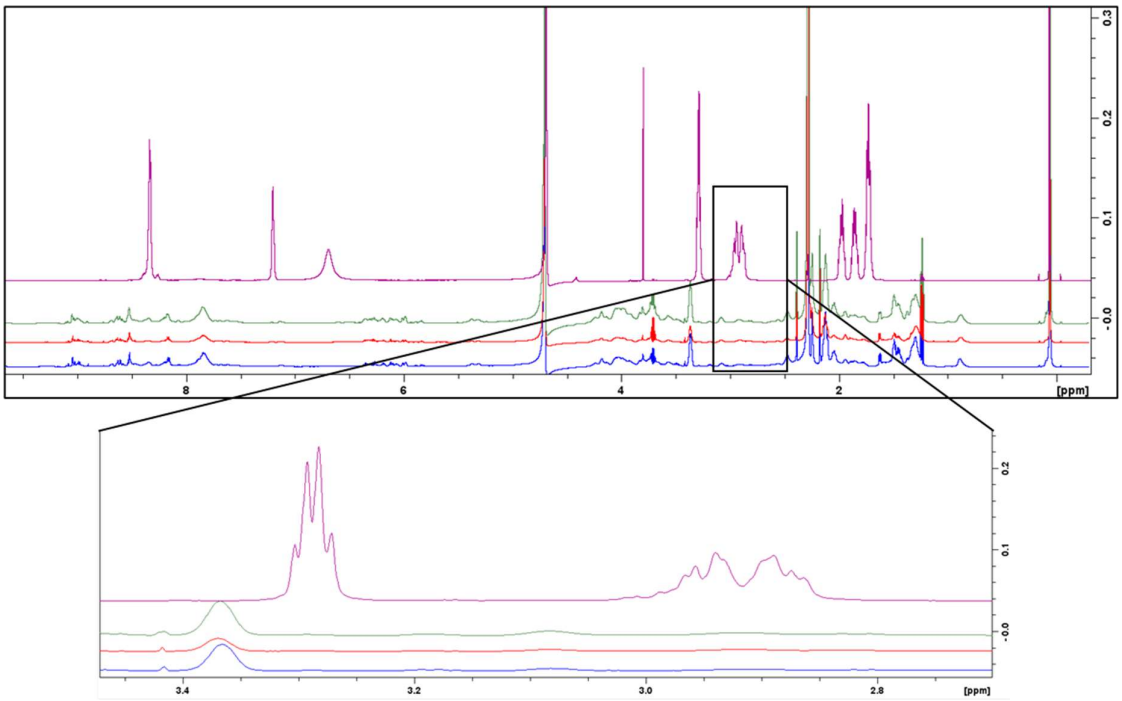

Supplementary Figure S26 NMR spectrum for water soluble CGP samples extracted from recombinant *E. coli* and *C. ljungdahlii* cells. Only the CGP sample extracted from *E. coli* pMTL83152_*cphA*$_{An.}$ showed the typical NMR peaks for CGP. Since the NMR method showed high accuracy even for low concentrations of CGP, it is likely that the clostridial strains did not accumulated CGP under the tested conditions. CGP extraction samples: *C. ljungdahlii* pMTL83152_*cphA*$_{Clj}$ (green); *C. ljungdahlii* pMTL83152_*cphA*$_{An.}$ (red); *C. ljungdahlii* pMTL83152 (control) (blue); and 10 mg/ml purified CGP sample from cyanobacteria (purple). The NMR analyses was performed as described before (Erickson *et al.*, 2001).

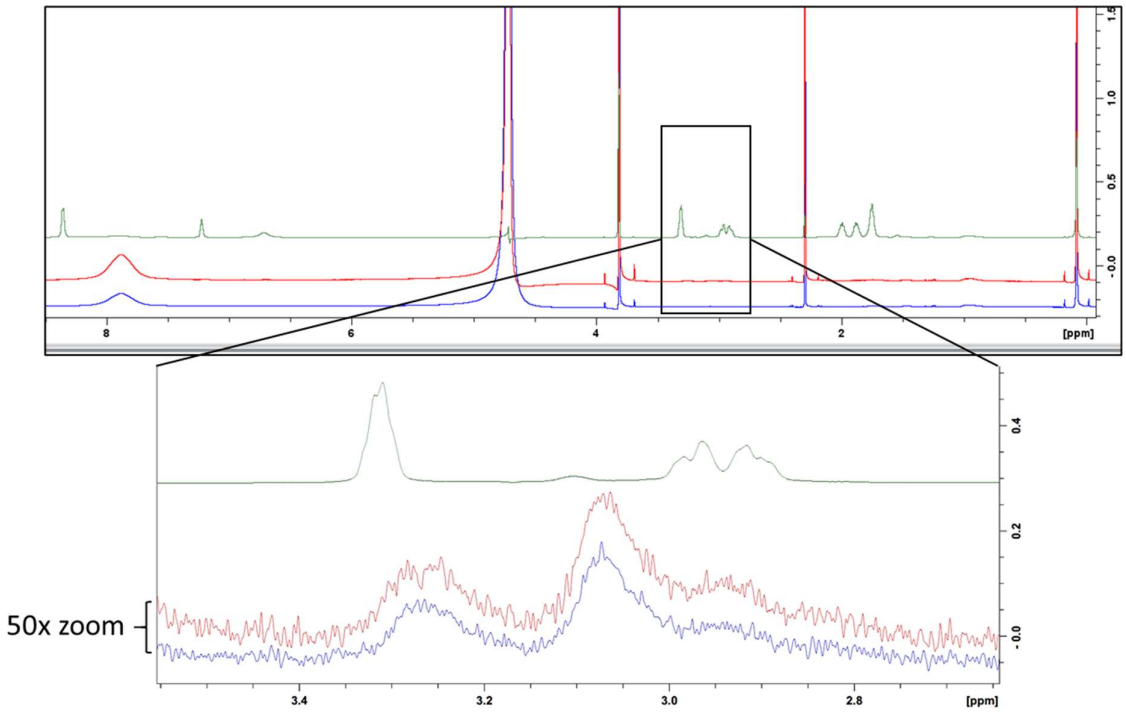

Supplementary Figure S27 NMR spectrum for water insoluble CGP samples extracted from recombinant *E. coli* and *C. ljungdahlii* cells. Only the CGP sample extracted from *E. coli* pMTL83152_*cphA*$_{An.}$ showed the typical NMR peaks for CGP. Since the NMR method showed high accuracy even for low concentrations of CGP, it is likely that the *C. ljungdahlii* strains did not accumulate CGP under the tested conditions. CGP extraction samples: *E. coli* pMTL83152_*cphA*$_{An.}$ (green); *C. ljungdahlii* pMTL83152_*cphA*$_{An.}$ (red); and *C. ljungdahlii* pMTL83152 (control) (blue). A sample of *C. ljungdahlii* pMTL83152_*cphA*$_{Clj}$ was not measured, due to a failure during preparation. The CGP extracted from cyanobacteria is water soluble and was not used here. The NMR analysis was performed as described before (Erickson *et al.*, 2001).

LITERATURE

Aboulmagd, E., Oppermann-Sanio, F.B., and Steinbüchel, A. (2000). Molecular characterization of the cyanophycin synthetase from *Synechocystis* sp. strain PCC6308. *Archives of microbiology* 174(5)**,** 297-306. doi: 10.1007/s002030000206.

Aboulmagd, E., Voss, I., Oppermann-Sanio, F.B., and Steinbüchel, A. (2001). Heterologous expression of cyanophycin synthetase and cyanophycin synthesis in the industrial relevant bacteria *Corynebacterium glutamicum* and *Ralstonia eutropha* and in *Pseudomonas putida*. *Biomacromolecules* 2(4)**,** 1338-1342. doi: 10.1021/bm010075a.

Abrini, J., Naveau, H., and Nyns, E.J. (1994). *Clostridium autoethanogenum*, Sp-Nov, an anaerobic bacterium that produces ethanol from carbon monoxide. *Archives of Microbiology* 161(4)**,** 345-351. doi: 10.1007/Bf00303591.

Abubackar, H.N., Veiga, M.C., and Kennes, C. (2011). Biological conversion of carbon monoxide: rich syngas or waste gases to bioethanol. *Biofuels, Bioproducts & Biorefining* 5(1)**,** 93-114. doi: 10.1002/bbb.256.

Abubackar, H.N., Veiga, M.C., and Kennes, C. (2015). Carbon monoxide fermentation to ethanol by *Clostridium autoethanogenum* in a bioreactor with no accumulation of acetic acid. *Bioresource Technology* 186**,** 122-127. doi: 10.1016/j.biortech.2015.02.113.

Al-Bassam, M.M., Kim, J.N., Zaramela, L.S., Kellman, B.P., Zuniga, C., Wozniak, J.M.*, et al.* (2018). Optimization of carbon and energy utilization through differential translational efficiency. *Nature Communications* 9(1)**,** 4474. doi: 10.1038/s41467-018-06993-6.

Al-Hinai, M.A., Fast, A.G., and Papoutsakis, E.T. (2012). A novel system for efficient isolation of double-crossover allelic exchange mutants in *Clostridium* enabling markerless chromosomal gene deletions and DNA integration. *Applied and Environmental Microbiology***,** 02214-02212. doi: 10.1128/AEM.02214-12

Al Rowaihi, I.S., Kick, B., Grötzinger, S.W., Burger, C., Karan, R., Weuster-Botz, D.*, et al.* (2018). A two-stage biological gas to liquid transfer process to convert carbon dioxide into bioplastic. *Bioresource Technology Reports* 1**,** 61-68. doi: 10.1016/j.biteb.2018.02.007.

Anzalone, A.V., Randolph, P.B., Davis, J.R., Sousa, A.A., Koblan, L.W., Levy, J.M.*, et al.* (2019). Search-and-replace genome editing without double-strand breaks or donor DNA. *Nature* 576(7785)**,** 149-157. doi: 10.1038/s41586-019-1711-4.

Arai, T., and Kino, K. (2008). A cyanophycin synthetase from *Thermosynechococcus elongatus* BP-1 catalyzes primer-independent cyanophycin synthesis. *Applied Microbiology and Biotechnology* 81(1)**,** 69-78. doi: 10.1007/s00253-008-1623-y.

Asimakopoulos, K., Gavala, H.N., and Skiadas, I.V. (2018). Reactor systems for syngas fermentation processes: A review. *Chemical Engineering Journal* 348**,** 732-744. doi: 10.1016/j.cej.2018.05.003.

Backiel, J., Juarez, O., Zagorevski, D.V., Wang, Z., Nilges, M.J., and Barquera, B. (2008). Covalent binding of flavins to RnfG and RnfD in the Rnf complex from *Vibrio cholerae*. *Biochemistry* 47(43)**,** 11273-11284. doi: 10.1021/bi800920j.

Banerjee, A., Leang, C., Ueki, T., Nevin, K.P., and Lovley, D.R. (2014). Lactose-inducible system for metabolic engineering of *Clostridium ljungdahlii*. *Applied and Environmental Microbiology* 80(8)**,** 2410-2416. doi: 10.1128/AEM.03666-13.

Banno, S., Nishida, K., Arazoe, T., Mitsunobu, H., and Kondo, A. (2018). Deaminase-mediated multiplex genome editing in *Escherichia coli*. *Nature Microbiology* 3(4)**,** 423-429. doi: 10.1038/s41564-017-0102-6.

Bayat, H., Modarressi, M.H., and Rahimpour, A. (2018). The conspicuity of CRISPR-Cpf1 system as a significant breakthrough in genome editing. *Current Microbiology* 75(1)**,** 107-115. doi: 10.1007/s00284-017-1406-8.

Beck, B.J., Connolly, L.E., De Las Peñas, A., and Downs, D.M. (1997). Evidence that *rseC*, a gene in the *rpoE* cluster, has a role in thiamine synthesis in *Salmonella typhimurium*. *Journal of Bacteriology* 179(20)**,** 6504-6508. doi: 0021-9193/97/$04.00+0.

Beck, M.H., Flaiz, M., Bengelsdorf, F.R., and Dürre, P. (2020). Induced heterologous expression of the arginine deiminase pathway promotes growth advantages in the strict anaerobe *Acetobacterium woodii*. *Applied Microbiology and Biotechnology* 104(2)**,** 687-699. doi: 10.1007/s00253-019-10248-9.

Bengelsdorf, F.R., and Dürre, P. (2017). Gas fermentation for commodity chemicals and fuels. *Microbial biotechnology* 10(5)**,** 1167-1170. doi: 10.1111/1751-7915.12763.

Bengelsdorf, F.R., Poehlein, A., Linder, S., Erz, C., Hummel, T., Hoffmeister, S*., et al.* (2016). Industrial acetogenic biocatalysts: A comparative metabolic and genomic analysis. *Frontiers in Microbioly* 7(1036)**,** 1-15. doi: 10.3389/fmicb.2016.01036.

Bengelsdorf, F.R., Straub, M., and Dürre, P. (2013). Bacterial synthesis gas (syngas) fermentation. *Environmental Technology* 34(13-16)**,** 1639-1651. doi: 10.1080/09593330.2013.827747.

Benito-Vaquerizo, S., Diender, M., Olm, I.P., Dos Santos, V.A.M., Schaap, P.J., Sousa, D.Z*., et al.* (2020). Modeling a co-culture of *Clostridium autoethanogenum* and *Clostridium kluyveri* to increase syngas conversion to medium-chain fatty-acids. *Computational and Structural Biotechnology Journal* 18**,** 3255-3266. doi: 10.1016/j.csbj.2020.10.003.

Berg, H., Ziegler, K., Piotukh, K., Baier, K., Lockau, W., and Volkmer-Engert, R. (2000). Biosynthesis of the cyanobacterial reserve polymer multi-L-arginyl-poly-L-aspartic acid (cyanophycin) mechanism of the cyanophycin synthetase reaction studied with synthetic primers. *European Journal of Biochemistry* 267(17)**,** 5561-5570. doi: 10.1046/j.1432-1327.2000.01622.x

Bertsch, J., and Müller, V. (2015). Bioenergetic constraints for conversion of syngas to biofuels in acetogenic bacteria. *Biotechnology for Biofuels* 8**,** 210. doi: 10.1186/s13068-015-0393-x.

Biegel, E., and Müller, V. (2010). Bacterial Na^+-translocating ferredoxin:NAD^+ oxidoreductase. *Proceedings of the National Academy of Sciences of the United States of America* 107(42)**,** 18138-18142. doi: 10.1073/pnas.1010318107.

Biegel, E., Schmidt, S., Gonzalez, J.M., and Müller, V. (2011). Biochemistry, evolution and physiological function of the Rnf complex, a novel ion-motive electron transport complex in prokaryotes. *Cellular and Molecular Life Sciences* 68(4)**,** 613-634. doi: 10.1007/s00018-010-0555-8.

Biegel, E., Schmidt, S., and Müller, V. (2009). Genetic, immunological and biochemical evidence for a Rnf complex in the acetogen *Acetobacterium woodii*. *Environmental Microbiology* 11(6)**,** 1438-1443. doi: 10.1111/j.1462-2920.2009.01871.x.

Biswas, R., Zheng, T., Olson, D.G., Lynd, L.R., and Guss, A.M. (2015). Elimination of hydrogenase active site assembly blocks H_2 production and increases ethanol yield in *Clostridium thermocellum*. *Biotechnology for Biofuels* 8(1)**,** 20. doi: 10.1186/s13068-015-0204-4.

Blaut, M., and Gottschalk, G. (1984). Protonmotive force-driven synthesis of ATP during methane formation from molecular hydrogen and formaldehyde or carbon dioxide in *Methanosarcina barkeri*. *FEMS Microbiology Letters* 24(1)**,** 103-107. doi: 10.1111/j.1574-6968.1984.tb01253.x.

Boiangiu, C.D., Jayamani, E., Brügel, D., Herrmann, G., Kim, J., Forzi, L*., et al.* (2005). Sodium ion pumps and hydrogen production in glutamate fermenting anaerobic bacteria. *Journal of Molecular Microbiology and Biotechnology* 10(2-4)**,** 105-119. doi: 10.1159/000091558

Borrero-de Acuña, J.M., Timmis, K., Jahn, M., and Jahn, D. (2017). Protein complex formation during denitrification by *Pseudomonas aeruginosa*. *Microbial Biotechnology* 10(6)**,** 1523-1534. doi: 10.1111/1751-7915.12851.

Boucher, J.C., Schurr, M.J., Yu, H., Rowen, D.W., and Deretic, V. (1997). *Pseudomonas aeruginosa* in cystic fibrosis: role of *mucC* in the regulation of alginate production and stress sensitivity. *Microbiology* 143(11)**,** 3473-3480. doi: 10.1099/00221287-143-11-3473.

Bowien, B., and Kusian, B. (2002). Genetics and control of CO_2 assimilation in the chemoautotroph *Ralstonia eutropha*. *Archives of Microbiology* 178(2)**,** 85-93. doi: 10.1007/s00203-002-0441-3.

Brown, S.D., Nagaraju, S., Utturkar, S., De Tissera, S., Segovia, S., Mitchell, W.*, et al.* (2014). Comparison of single-molecule sequencing and hybrid approaches for finishing the genome of *Clostridium autoethanogenum* and analysis of CRISPR systems in industrial relevant Clostridia. *Biotechnology for Biofuels* 7(40)**,** 1-18. doi: 10.1186/1754-6834-7-40.

Brüggemann, H., Bäumer, S., Fricke, W.F., Wiezer, A., Liesegang, H., Decker, I.*, et al.* (2003). The genome sequence of *Clostridium tetani*, the causative agent of tetanus disease. *Proceedings of the National Academy of Sciences of the United States of America* 100(3)**,** 1316-1321. doi: 10.1073/pnas.0335853100.

Buckel, W., and Thauer, R.K. (2013). Energy conservation *via* electron bifurcating ferredoxin reduction and proton/Na^+ translocating ferredoxin oxidation. *Biochimica et Biophysica Acta* 1827(2)**,** 94-113. doi: 10.1016/j.bbabio.2012.07.002.

Buckel, W., and Thauer, R.K. (2018). Flavin-based electron bifurcation, ferredoxin, flavodoxin, and anaerobic respiration with protons (Ech) or NAD^+ (Rnf) as electron acceptors: A historical review. *Frontiers in Microbiology* 9**,** 401. doi: 10.3389/fmicb.2018.00401.

Campbell, B.J., Smith, J.L., Hanson, T.E., Klotz, M.G., Stein, L.Y., Lee, C.K.*, et al.* (2009). Adaptations to submarine hydrothermal environments exemplified by the genome of *Nautilia profundicola*. *PLOS Genetics* 5(2)**,** e1000362. doi: 10.1371/journal.pgen.1000362.

Caskey, W.H., and Tiedje, J.M. (1980). The reduction of nitrate to ammonium by a *Clostridium* sp. isolated from soil. *Journal of General Microbiology* 119(1)**,** 217-223. doi: 10.1099/00221287-119-1-217.

Chen, W., Zhang, Y., Zhang, Y., Pi, Y., Gu, T., Song, L.*, et al.* (2018). CRISPR/Cas9-based genome editing in *Pseudomonas aeruginosa* and cytidine deaminase-mediated base editing in *Pseudomonas* species. *IScience: Cell Press* 6**,** 222-231. doi: 10.1016/ j.isci.2018.07.024.

Cui, Y., Yang, K.-L., and Zhou, K. (2020). Using co-culture to functionalize *Clostridium* fermentation. *Trends in Biotechnology*.

Curatti, L., Brown, C.S., Ludden, P.W., and Rubio, L.M. (2005). Genes required for rapid expression of nitrogenase activity in *Azotobacter vinelandii*. *Proceedings of the National Academy of Sciences of the United States of America* 102(18)**,** 6291-6296. doi: 10.1073/pnas.0501216102.

Daley, D.O., Rapp, M., Granseth, E., Melén, K., Drew, D., and Von Heijne, G. (2005). Global topology analysis of the *Escherichia coli* inner membrane proteome. *Science* 308(5726)**,** 1321-1323. doi: 10.1126/science.1109730.

De Las Peñas, A., Connolly, L., and Gross, C.A. (1997). The σ^E-mediated response to extracytoplasmic stress in *Escherichia coli* is transduced by RseA and RseB, two negative regulators of σ^E. *Molecular Microbiology* 24(2)**,** 373-385. doi: 10.1046/j.1365-2958.1997.3611718.x

Diender, M., Stams, A.J., and Sousa, D.Z. (2016). Production of medium-chain fatty acids and higher alcohols by a synthetic co-culture grown on carbon monoxide or syngas. *Biotechnology for Biofuels* 9(1)**,** 82.

Diner, B.A., Fan, J., Scotcher, M.C., Wells, D.H., and Whited, G.M. (2018). Synthesis of heterologous mevalonic acid pathway enzymes in *Clostridium ljungdahlii* for the conversion of fructose and of syngas to mevalonate and Isoprene. *Applied and Environmental Microbiology* 84(1). doi: 10.1128/AEM.01723-17.

Ding, D., Chen, K., Chen, Y., Li, H., and Xie, K. (2018). Engineering introns to express RNA guides for Cas9- and Cpf1-mediated multiplex genome editing. *Molecular Plant*. doi: 10.1016/j.molp.2018.02.005.

Ding, H., and Demple, B. (1997). *In vivo* kinetics of a redox-regulated transcriptional switch. *Proceedings of the National Academy of Sciences of the United States of America* 94(16)**,** 8445-8449. doi: 10.1073/pnas.94.16.8445.

Dominguez, A.A., Lim, W.A., and Qi, L.S. (2016). Beyond editing: repurposing CRISPR–Cas9 for precision genome regulation and interrogation. *Nature Reviews Molecular Cell Biology* 17(1)**,** 5.

Dong, H., Tao, W., Zhang, Y., and Li, Y. (2012). Development of an anhydrotetracycline-inducible gene expression system for solvent-producing *Clostridium acetobutylicum*: A useful tool for strain engineering. *Metabolic Engineering* 14(1)**,** 59-67. doi: 10.1016/j.ymben.2011.10.004.

Doudna, J.A., and Charpentier, E. (2014). The new frontier of genome engineering with CRISPR-Cas9. *Science* 346(6213)**,** 1258096.

Drake, H.L., Gossner, A.S., and Daniel, S.L. (2008). Old acetogens, new light. *Annals of the New York Academy of Sciences* 1125**,** 100-128. doi: 10.1196/annals.1419.016.

Dürre, P. (2017). Gas fermentation - A biotechnological solution for today's challenges. *Microbial Biotechnology* 10(1)**,** 14-16. doi: 10.1111/1751-7915.12431.

Dürre, P., and Andreesen, J.R. (1983). Purine and glycine metabolism by purinolytic clostridia. *Journal of Bacteriology* 154(1)**,** 192-199.

Elbahloul, Y., Krehenbrink, M., Reichelt, R., and Steinbüchel, A. (2005). Physiological conditions conducive to high cyanophycin content in biomass of *Acinetobacter calcoaceticus* strain ADP1. *Applied and Environmental Microbiology* 71(2)**,** 858-866.

Emerson, D.F., Woolston, B.M., Liu, N., Donnelly, M., Currie, D.H., and Stephanopoulos, G. (2019). Enhancing hydrogen-dependent growth of and carbon dioxide fixation by *Clostridium ljungdahlii* through nitrate supplementation. *Biotechnology and Bioengineering* 116(2)**,** 294-306. doi: 10.1002/bit.26847.

Enríquez, J.A. (2016). Supramolecular organization of respiratory complexes. *Annual Review of Physiology* 78**,** 533-561.

Erickson, N.A., Kolodny, N.H., and Allen, M.M. (2001). A rapid and sensitive method for the analysis of cyanophycin. *Biochimica et Biophysica Acta* 1526(1)**,** 5-9.

Fackler, N., Heffernan, J., Juminaga, A., Doser, D., Nagaraju, S., Gonzalez-Garcia, R.A*., et al.* (2021). Transcriptional control of *Clostridium autoethanogenum* using CRISPRi. *Synthetic Biology* 6(1)**,** ysab008.

Fagerlund, R.D., Staals, R.H., and Fineran, P.C. (2015). The Cpf1 CRISPR-Cas protein expands genome-editing tools. *Genome Biology* 16**,** 251. doi: 10.1186/s13059-015-0824-9.

Fast, A.G., and Papoutsakis, E.T. (2012). Stoichiometric and energetic analyses of non-photosynthetic CO_2-fixation pathways to support synthetic biology strategies for production of fuels and chemicals. *Current Opinion in Chemical Engineering* 1(4)**,** 380-395. doi: 10.1016/j.coche.2012.07.005.

Flaiz, M., Ludwig, G., Bengelsdorf, F.R., and Dürre, P. (2021). Production of the biocommodities butanol and acetone from methanol with fluorescent FAST-tagged proteins using metabolically engineered strains of *Eubacterium limosum*. *Biotechnology for Biofuels* 14(1)**,** 1-20.

Fröstl, J.M., Seifritz, C., and Drake, H.L. (1996). Effect of nitrate on the autotrophic metabolism of the acetogens *Clostridium thermoautotrophicum* and *Clostridium thermoaceticum*. *Journal of Bacteriology* 178(15)**,** 4597-4603.

Fuchs, G. (2011). Alternative pathways of carbon dioxide fixation: insights into the early evolution of life? *Annual Review of Microbiology* 65**,** 631-658.

Füser, G., and Steinbüchel, A. (2007). Analysis of genome sequences for genes of cyanophycin metabolism: identifying putative cyanophycin metabolizing prokaryotes. *Macromolecular Bioscience* 7(3)**,** 278-296.

Gaudelli, N.M., Komor, A.C., Rees, H.A., Packer, M.S., Badran, A.H., Bryson, D.I*., et al.* (2017). Programmable base editing of A•T to G•C in genomic DNA without DNA cleavage. *Nature* 551(7681)**,** 464-471.

Girbal, L., Mortier-Barrière, I., Raynaud, F., Rouanet, C., Croux, C., and Soucaille, P. (2003). Development of a sensitive gene expression reporter system and an inducible promoter-repressor system for *Clostridium acetobutylicum*. *Applied and Environmental Microbiology* 69(8)**,** 4985-4988.

Gu, T., Zhao, S., Pi, Y., Chen, W., Chen, C., Liu, Q*., et al.* (2018). Highly efficient base editing in *Staphylococcus aureus* using an engineered CRISPR RNA-guided cytidine deaminase. *Chemical Science* 9(12)**,** 3248-3253.

Hai, T., Oppermann-Sanio, F.B., and Steinbüchel, A. (2002). Molecular characterization of a thermostable cyanophycin synthetase from the thermophilic cyanobacterium *Synechococcus* sp. strain MA19 and in vitro synthesis of cyanophycin and related polyamides. *Applied and Environmental Microbiology* 68(1)**,** 93.

Hall, J.B. (1971). Evolution of the prokaryotes. *Journal of Theoretical Biology* 30(3)**,** 429-454.

Hall, J.B. (1973). The occurrence of nitrate on the early earth and its role in the evolution of the prokaryotes. *Space Life Science* 4(1)**,** 204-213. doi: 10.1007/BF02626353.

Hartman, A.H., Liu, H., and Melville, S.B. (2011). Construction and characterization of a lactose-inducible promoter system for controlled gene expression in *Clostridium perfringens*. *Applied and Environmental Microbiology* 77(2)**,** 471-478. doi: 10.1128/AEM.01536-10.

Hasan, M., and Hall, J.B. (1977). Dissimilatory nitrate reduction in *Clostridium tertium*. *Zeitschrift für allgemeine Mikrobiologie* 17(7)**,** 501-506.

Hasan, S.M., and Hall, J.B. (1975). The physiological function of nitrate reduction in *Clostridium perfringens*. *Journal of General Microbiology* 87(1)**,** 120-128. doi: 10.1099/00221287-87-1-120.

Heap, J.T., Kuehne, S.A., Ehsaan, M., Cartman, S.T., Cooksley, C.M., Scott, J.C*., et al.* (2010). The ClosTron: mutagenesis in *Clostridium* refined and streamlined. *Journal of Microbiological Methods* 80(1)**,** 49-55.

Heap, J.T., Pennington, O.J., Cartman, S.T., Carter, G.P., and Minton, N.P. (2007). The ClosTron: a universal gene knock-out system for the genus *Clostridium*. *Journal of Microbiological Methods* 70(3)**,** 452-464.

Heap, J.T., Pennington, O.J., Cartman, S.T., and Minton, N.P. (2009). A modular system for *Clostridium* shuttle plasmids. *Journal of Microbiological Methods* 78(1)**,** 79-85. doi: 10.1016/j.mimet.2009.05.004.

Held, C.M. (2013). *Funktionelle Genomanalyse von Clostridium ljungdahlii.* Technische Universität München.

Henstra, A.M., Sipma, J., Rinzema, A., and Stams, A.J. (2007). Microbiology of synthesis gas fermentation for biofuel production. *Current Opinion in Biotechnology* 18(3)**,** 200-206.

Hess, V., Gallegos, R., Jones, J.A., Barquera, B., Malamy, M.H., and Müller, V. (2016). Occurrence of ferredoxin:NAD^+ oxidoreductase activity and its ion specificity in several Gram-positive and Gram-negative bacteria. *PeerJ* 4**,** e1515. doi: 10.7717/peerj.1515.

Hess, V., Poehlein, A., Weghoff, M.C., Daniel, R., and Müller, V. (2014). A genome-guided analysis of energy conservation in the thermophilic, cytochrome-free acetogenic bacterium *Thermoanaerobacter kivui*. *BMC Genomics* 15**,** 1139. doi: 10.1186/1471-2164-15-1139.

Hess, V., Schuchmann, K., and Müller, V. (2013). The ferredoxin:NAD^+ oxidoreductase (Rnf) from the acetogen Acetobacterium woodii requires Na^+ and is reversibly coupled to the membrane potential. *Journal of Biological Chemistry* 288(44)**,** 31496-31502. doi: 10.1074/jbc.M113.510255.

Hille, F., Richter, H., Wong, S.P., Bratovič, M., Ressel, S., and Charpentier, E. (2018). The biology of CRISPR-Cas: backward and forward. *Cell* 172(6)**,** 1239-1259.

Hoffmeister, S., Gerdom, M., Bengelsdorf, F.R., Linder, S., Flüchter, S., Öztürk, H*., et al.* (2016). Acetone production with metabolically engineered strains of *Acetobacterium woodii*. *Metabolic Engineering* 36**,** 37-47.

Hong, W., Zhang, J., Cui, G., Wang, L., and Wang, Y. (2018). Multiplexed CRISPR-Cpf1-mediated genome editing in *Clostridium difficile* toward the understanding of pathogenesis of *C. difficile* infection. *ACS Synthetic Biology* 7(6)**,** 1588-1600.

Hreha, T.N., Mezic, K.G., Herce, H.D., Duffy, E.B., Bourges, A., Pryshchep, S.*, et al.* (2015). Complete topology of the RNF complex from *Vibrio cholerae*. *Biochemistry* 54(15)**,** 2443-2455. doi: 10.1021/acs.biochem.5b00020.

Hu, J.H., Miller, S.M., Geurts, M.H., Tang, W., Chen, L., Sun, N.*, et al.* (2018). Evolved Cas9 variants with broad PAM compatibility and high DNA specificity. *Nature* 556(7699)**,** 57-63.

Hu, P., Chakraborty, S., Kumar, A., Woolston, B., Liu, H., Emerson, D.*, et al.* (2016). Integrated bioprocess for conversion of gaseous substrates to liquids. *Proceedings of the National Academy of Sciences* 113(14)**,** 3773-3778.

Huang, H., Chai, C., Li, N., Rowe, P., Minton, N.P., Yang, S.*, et al.* (2016). CRISPR/Cas9-based efficient genome editing in *Clostridium ljungdahlii*, an autotrophic gas-fermenting bacterium. *ACS Synthetic Biology* 5(12)**,** 1355-1361. doi: 10.1021/acssynbio.6b00044.

Huang, H., Chai, C., Yang, S., Jiang, W., and Gu, Y. (2019). Phage serine integrase-mediated genome engineering for efficient expression of chemical biosynthetic pathway in gas-fermenting *Clostridium ljungdahlii*. *Metabolic Engineering* 52**,** 293-302.

Huhnke, R.L., Lewis, R.S., and Tanner, R.S. (2010). *Isolation and characterization of novel clostridial species*. Patent No. 7,704, 723 B2 United States of America.

Humphreys, C.M., and Minton, N.P. (2018). Advances in metabolic engineering in the microbial production of fuels and chemicals from C1 gas. *Current Opinion in Biotechnology* 50**,** 174-181. doi: 10.1016/j.copbio.2017.12.023.

IEA (2021). "Global Energy Review 2021 ". (Paris: International Energy Agency).

Ishimoto, M., and Egami, F. (1959). "Meaning of nitrate and sulphate reduction in the process of metabolic evolution," in *The Origin of Life on the Earth*. Elsevier), 555-561.

Jiang, Y., Chen, B., Duan, C., Sun, B., Yang, J., and Yang, S. (2015). Multigene editing in the *Escherichia coli* genome *via* the CRISPR-Cas9 system. *Applied and Environmental Microbiology* 81(7)**,** 2506-2514.

Jiang, Y., Qian, F., Yang, J., Liu, Y., Dong, F., Xu, C.*, et al.* (2017). CRISPR-Cpf1 assisted genome editing of *Corynebacterium glutamicum*. *Nature Communications* 8**,** 15179. doi: 10.1038/ncomms15179.

Jinek, M., Chylinski, K., Fonfara, I., Hauer, M., Doudna, J.A., and Charpentier, E. (2012). A programmable dual-RNA–guided DNA endonuclease in adaptive bacterial immunity. *Science***,** 1225829.

Jouanneau, Y., Jeong, H.S., Hugo, N., Meyer, C., and Willison, J.C. (1998). Overexpression in *Escherichia coli* of the *rnf* genes from *Rhodobacter capsulatus* characterization of two membrane-bound iron-sulfur proteins. *European Journal of Biochemistry* 251(1-2)**,** 54-64.

Katsyv, A., and Müller, V. (2020). Overcoming energetic barriers in acetogenic C1 conversion. *Frontiers in Bioengineering and Biotechnology* 8. doi: 10.3389/fbioe.2020.621166

Kim, J., Hetzel, M., Boiangiu, C.D., and Buckel, W. (2004). Dehydration of (R)-2-hydroxyacyl-CoA to enoyl-CoA in the fermentation of alpha-amino acids by anaerobic bacteria. *FEMS Microbiology Reviews* 28(4)**,** 455-468. doi: 10.1016/j.femsre.2004.03.001.

Klask, C.M., Kliem-Kuster, N., Molitor, B., and Angenent, L.T. (2020). Nitrate feed improves growth and ethanol production of *Clostridium ljungdahlii* with CO_2 and H_2, but results in stochastic inhibition events. *Frontiers in Microbiology* 11**,** 724. doi: 10.3389/fmicb.2020.00724.

Klueglein, N., Zeitvogel, F., Stierhof, Y.-D., Floetenmeyer, M., Konhauser, K.O., Kappler, A.*, et al.* (2014). Potential role of nitrite for abiotic Fe(II) oxidation and cell encrustation during nitrate reduction by denitrifying bacteria. *Applied and Environmental Microbiology* 80(3)**,** 1051-1061. doi: 10.1128/AEM.03277-13.

Knott, G.J., and Doudna, J.A. (2018). CRISPR-Cas guides the future of genetic engineering. *Science* 361(6405)**,** 866-869.

Komor, A.C., Kim, Y.B., Packer, M.S., Zuris, J.A., and Liu, D.R. (2016). Programmable editing of a target base in genomic DNA without double-stranded DNA cleavage. *Nature* 533(7603)**,** 420-424.

Koo, M.S., Lee, J.H., Rah, S.Y., Yeo, W.S., Lee, J.W., Lee, K.L*., et al.* (2003). A reducing system of the superoxide sensor SoxR in *Escherichia coli*. *The EMBO Journal* 22(11)**,** 2614-2622. doi: 10.1093/emboj/cdg252

Koonin, E.V., and Makarova, K.S. (2019). Origins and evolution of CRISPR-Cas systems. *Philosophical Transactions of the Royal Society B* 374(1772)**,** 20180087.

Koonin, E.V., Makarova, K.S., and Zhang, F. (2017). Diversity, classification and evolution of CRISPR-Cas systems. *Current Opinion in Microbiology* 37**,** 67-78.

Köpke, M., Held, C., Hujer, S., Liesegang, H., Wiezer, A., Wollherr, A*., et al.* (2010). *Clostridium ljungdahlii* represents a microbial production platform based on syngas. *Proceedings of the National Academy of Sciences of the United States of America* 107(29)**,** 13087-13092. doi: 10.1073/pnas.1004716107.

Köpke, M., and Liew, F. (2012). *Production of butanol from carbon monoxide by a recombinant microorganism*. Patent No. WO2012053905A1. New Zealand: World Intellectual Property Organization.

Köpke, M., Simpson, S.D., Liew, F., and Chen, W. (2016). *Fermentation process for producing isopropanol using a recombinant microorganism*. Patent No. US9365868B2. United States: U.S. Patent and Trademark Office.

Kuhns, M., Trifunović, D., Huber, H., and Müller, V. (2020). The Rnf complex is a Na^+ coupled respiratory enzyme in a fermenting bacterium, *Thermotoga maritima*. *Communications Biology* 3(1)**,** 1-10.

Kumagai, H., Fujiwara, T., Matsubara, H., and Saeki, K. (1997). Membrane localization, topology, and mutual stabilization of the *rnfABC* gene products in *Rhodobacter capsulatus* and implications for a new family of energy-coupling NADH oxidoreductases. *Biochemistry* 36(18)**,** 5509-5521. doi: 10.1021/bi970014q.

Kuscu, C., Parlak, M., Tufan, T., Yang, J., Szlachta, K., Wei, X*., et al.* (2017). CRISPR-STOP: gene silencing through base-editing-induced nonsense mutations. *Nature Methods* 14(7)**,** 710-712.

Kusian, B., and Bowien, B. (1997). Organization and regulation of *cbb* CO_2 assimilation genes in autotrophic bacteria. *FEMS Microbiology Reviews* 21(2)**,** 135-155.

Larson, M.H., Gilbert, L.A., Wang, X., Lim, W.A., Weissman, J.S., and Qi, L.S. (2013). CRISPR interference (CRISPRi) for sequence-specific control of gene expression. *Nature Protocols* 8(11)**,** 2180.

Latif, H., Zeidan, A.A., Nielsen, A.T., and Zengler, K. (2014). Trash to treasure: Production of biofuels and commodity chemicals via syngas fermenting microorganisms. *Current Opinion in Biotechnology* 27**,** 79-87. doi: 10.1016/j.copbio.2013.12.001.

Leang, C., Ueki, T., Nevin, K.P., and Lovley, D.R. (2013). A genetic system for *Clostridium ljungdahlii*: A chassis for autotrophic production of biocommodities and a model homoacetogen. *Applied and Environmental Microbiology* 79(4)**,** 1102-1109. doi: 10.1128/AEM.02891-12.

Li, Q., Seys, F.M., Minton, N.P., Yang, J., Jiang, Y., Jiang, W*., et al.* (2019). CRISPR–$Cas9^{D10A}$ nickase-assisted base editing in the solvent producer *Clostridium beijerinckii*. *Biotechnology and Bioengineering* 116(6)**,** 1475-1483.

Li, X., Wang, Y., Liu, Y., Yang, B., Wang, X., Wei, J*., et al.* (2018). Base editing with a Cpf1–cytidine deaminase fusion. *Nature Biotechnology* 36(4)**,** 324.

Liew, F., Henstra, A.M., Köpke, M., Winzer, K., Simpson, S.D., and Minton, N.P. (2017). Metabolic engineering of *Clostridium autoethanogenum* for selective alcohol production. *Metabolic Engineering* 40**,** 104-114. doi: 10.1016/j.ymben.2017.01.007.

Liew, F., Köpke, M., and Simpson, S. (2013). "Gas Fermentation for Commercial Biofuels Production," in *Liquid, Gaseous and Solid Biofuels - Conversion Techniques*.).

Liew, F., Martin, M.E., Tappel, R.C., Heijstra, B.D., Mihalcea, C., and Köpke, M. (2016). Gas fermentation- A flexible platform for commercial scale production of low-carbon-fuels and chemicals from waste and renewable feedstocks. *Frontiers in Microbiology* 7**,** 694.

Lino, C.A., Harper, J.C., Carney, J.P., and Timlin, J.A. (2018). Delivering CRISPR: A review of the challenges and approaches. *Drug Delivery* 25(1)**,** 1234-1257.

Liu, H., Ray, W.K., Helm, R.F., Popham, D.L., and Melville, S.B. (2016). Analysis of the spore membrane proteome in *Clostridium perfringens* implicates cyanophycin in spore assembly. *Journal of Bacteriology* 198(12)**,** 1773-1782.

Liu, J., Tan, Y., Yang, X., Chen, X., and Li, F. (2013). Evaluation of *Clostridium ljungdahlii* DSM 13528 reference genes in gene expression studies by qRT-PCR. *Journal of Bioscience and Bioengineering* 116(4)**,** 460-464. doi: 10.1016/j.jbiosc.2013.04.011.

Livak, K.J., and Schmittgen, T.D. (2001). Analysis of relative gene expression data using real-time quantitative PCR and the $2^{-\Delta\Delta CT}$ method. *Methods* 25(4)**,** 402-408. doi: 10.1006/meth.2001.1262.

Ljungdahl, L.G. (2009). A life with acetogens, thermophiles, and cellulolytic anaerobes. *Annual Review of Microbiology* 63**,** 1-25. doi: 10.1146/annurev.micro.091208.073617

Ljungdhal, L.G. (1986). The autotrophic pathway of acetate synthesis in acetogenic bacteria. *Annual Reviews in Microbiology* 40(1)**,** 415-450. doi: 10.1146/annurev.mi.40.100186.002215.

Lo, J., Humphreys, J.R., Jack, J., Urban, C., Magnusson, L., Xiong, W.*, et al.* (2020). The metabolism of *Clostridium ljungdahlii* in phosphotransacetylase negative strains and development of an ethanologenic strain. *Frontiers in Bioengineering and Biotechnology* 8. doi: 10.3389/fbioe.2020.560726

Lo, J., Olson, D.G., Murphy, S.J., Tian, L., Hon, S., Lanahan, A.*, et al.* (2017). Engineering electron metabolism to increase ethanol production in *Clostridium thermocellum*. *Metabolic Engineering* 39**,** 71-79. doi: 10.1016/j.ymben.2016.10.018.

Madigan, M.T., Martinko, J., Dunlap, P., and Clark, D. (2009). "Brock-Biology of Microorganisms. 12th International Edition". Pearson Benjamin Cummings, San Francisco, CA94111).

Makarova, K.S., Haft, D.H., Barrangou, R., Brouns, S.J., Charpentier, E., Horvath, P.*, et al.* (2011). Evolution and classification of the CRISPR–Cas systems. *Nature Reviews Microbiology* 9(6)**,** 467-477.

Makarova, K.S., Wolf, Y.I., Alkhnbashi, O.S., Costa, F., Shah, S.A., Saunders, S.J.*, et al.* (2015). An updated evolutionary classification of CRISPR–Cas systems. *Nature Reviews Microbiology* 13(11)**,** 722-736.

Martin, M.E., Richter, H., Saha, S., and Angenent, L.T. (2016). Traits of selected *Clostridium* strains for syngas fermentation to ethanol. *Biotechnology and Bioengineering* 113(3)**,** 531-539. doi: 10.1002/bit.25827.

Martin, W.F., Sousa, F.L., and Lane, N. (2014). Energy at life's origin. *Science* 344(6188)**,** 1092-1093.

Martinez-Salazar, J.M., Moreno, S., Najera, R., Boucher, J.C., Espín, G., Soberon-Chavez, G.*, et al.* (1996). Characterization of the genes coding for the putative sigma factor AlgU and its regulators MucA, MucB, MucC, and MucD in *Azotobacter vinelandii* and evaluation of their roles in alginate biosynthesis. *Journal of Bacteriology* 178(7)**,** 1800-1808. doi: 10.1128/jb.178.7.1800-1808.1996.

Messineo, L. (1966). Modification of the Sakaguchi reaction: Spectrophotometric determination of arginine in proteins without previous hydrolysis. *Archives of Biochemistry and Biophysics* 117(3)**,** 534-540.

Mishra, A., Ntihuga, J.N., Molitor, B., and Angenent, L.T. (2020). Power-to-Protein: Carbon fixation with renewable electric power to feed the world. *Joule* 4(6)**,** 1142-1147.

Missiakas, D., Mayer, M.P., Lemaire, M., Georgopoulos, C., and Raina, S. (1997). Modulation of the *Escherichia coli* σ^E (RpoE) heat-shock transcription-factor activity by the RseA, RseB and RseC proteins. *Molecular Microbiology* 24(2)**,** 355-371. doi: 10.1046/j.1365-2958.1997.3601713.x.

Mock, J., Zheng, Y., Müller, A.P., Ly, S., Tran, L., Segovia, S.*, et al.* (2015). Energy conservation associated with ethanol formation from H_2 and CO_2 in *Clostridium autoethanogenum* involving electron bifurcation. *Journal of Bacteriology* 197(18)**,** 2965-2980. doi: 10.1128/JB.00399-15.

Mohammadi, M., Mohamed, A.R., Najafpour, G., Younesi, H., and Uzir, M.H. (2016). *Clostridium ljungdahlii* for production of biofuel from synthesis gas. *Energy Sources, Part A: Recovery, Utilization, and Environmental Effects* 38(3)**,** 427-434. doi: 10.1080/15567036.2012.729254.

Mohammadi, M., Najafpour, G.D., Younesi, H., Lahijani, P., Uzir, M.H., and Mohamed, A.R. (2011). Bioconversion of synthesis gas to second generation biofuels: A review. *Renew Sust Energ Rev* 15(9)**,** 4255-4273. doi: 10.1016/j.rser.2011.07.124.

Mohammadi, M., Younesi, H., Najafpour, G., and Mohamed, A.R. (2012). Sustainable ethanol fermentation from synthesis gas by *Clostridium ljungdahlii* in a continuous stirred tank bioreactor. *Journal of Chemical Technology and Biotechnology* 87(6)**,** 837-843. doi: 10.1002/jctb.3712.

Molitor, B., Kirchner, K., Henrich, A.W., Schmitz, S., and Rosenbaum, M.A. (2016a). Expanding the molecular toolkit for the homoacetogen *Clostridium ljungdahlii*. *Scientific Reports* 6**,** 31518. doi: 10.1038/srep31518.

Molitor, B., Marcellin, E., and Angenent, L.T. (2017). Overcoming the energetic limitations of syngas fermentation. *Current Opinion in Chemical Biology* 41**,** 84-92. doi: 10.1016/j.cbpa.2017.10.003.

Molitor, B., Mishra, A., and Angenent, L.T. (2019). Power-to-protein: converting renewable electric power and carbon dioxide into single cell protein with a two-stage bioprocess. *Energy & Environmental Science*.

Molitor, B., Richter, H., Martin, M.E., Jensen, R.O., Juminaga, A., Mihalcea, C*., et al.* (2016b). Carbon recovery by fermentation of CO-rich off gases - Turning steel mills into biorefineries. *Bioresource Technology* 215**,** 386-396. doi: 10.1016/j.biortech.2016.03.094.

Molla, K.A., and Yang, Y. (2019). CRISPR/Cas-mediated base editing: technical considerations and practical applications. *Trends in Biotechnology* 37(10)**,** 1121-1142.

Moreno-Vivián, C., Cabello, P., Martínez-Luque, M., Blasco, R., and Castillo, F. (1999). Prokaryotic nitrate reduction: molecular properties and functional distinction among bacterial nitrate reductases. *Journal of Bacteriology* 181(21)**,** 6573-6584.

Müller, V. (2019). New horizons in acetogenic conversion of one-carbon substrates and biological hydrogen storage. *Trends in Biotechnology* 37(12)**,** 1344-1354.

Müller, V., Imkamp, F., Biegel, E., Schmidt, S., and Dilling, S. (2008). Discovery of a ferredoxin:NAD^+-oxidoreductase (Rnf) in *Acetobacterium woodii*: a novel potential coupling site in acetogens. *Annals of the New York Academy of Sciences* 1125**,** 137-146. doi: 10.1196/annals.1419.011.

Nagarajan, H., Sahin, M., Nogales, J., Latif, H., Lovley, D.R., Ebrahim, A*., et al.* (2013). Characterizing acetogenic metabolism using a genome-scale metabolic reconstruction of *Clostridium ljungdahlii*. *Microbial Cell Factories* 12(13)**,** 118. doi: 10.1186/1475-2859-12-118.

Nagaraju, S., Davies, N.K., Walker, D.J., Kopke, M., and Simpson, S.D. (2016a). Genome editing of Clostridium autoethanogenum using CRISPR/Cas9. *Biotechnol Biofuels* 9**,** 219. doi: 10.1186/s13068-016-0638-3.

Nagaraju, S., Davies, N.K., Walker, D.J., Köpke, M., and Simpson, S.D. (2016b). Genome editing of *Clostridium autoethanogenum* using CRISPR/Cas9. *Biotechnology for Biofuels* 9**,** 219. doi: 10.1186/s13068-016-0638-3.

Nakade, S., Yamamoto, T., and Sakuma, T. (2017). Cas9, Cpf1 and C2c1/2/3 - What's next? *Bioengineered* 8(3)**,** 265-273. doi: 10.1080/21655979.2017.1282018.

Nangle, S.N., Sakimoto, K.K., Silver, P.A., and Nocera, D.G. (2017). Biological-inorganic hybrid systems as a generalized platform for chemical production. *Current Opinion in Chemical Biology* 41**,** 107-113.

Nevin, K.P., Hensley, S.A., Franks, A.E., Summers, Z.M., Ou, J., Woodard, T.L*., et al.* (2011). Electrosynthesis of organic compounds from carbon dioxide is catalyzed by a diversity of acetogenic microorganisms. *Applied and Environmental Microbiology* 77(9)**,** 2882-2886.

Nishida, K., Arazoe, T., Yachie, N., Banno, S., Kakimoto, M., Tabata, M*., et al.* (2016). Targeted nucleotide editing using hybrid prokaryotic and vertebrate adaptive immune systems. *Science* 353(6305).

Orosz, A., Boros, I., and Venetianer, P. (1991). Analysis of the complex transcription termination region of the *Escherichia coli rrn B* gene. *European Journal of Biochemistry* 201(3)**,** 653-659. doi: 10.1111/j.1432-1033.1991.tb16326.x.

Phillips, J.R., Atiyeh, H.K., Tanner, R.S., Torres, J.R., Saxena, J., Wilkins, M.R.*, et al.* (2015). Butanol and hexanol production in *Clostridium carboxidivorans* syngas fermentation: medium development and culture techniques. *Bioresource Technology* 190**,** 114-121.

Phillips, J.R., Huhnke, R.L., and Atiyeh, H.K. (2017). Syngas fermentation: A microbial conversion process of gaseous substrates to various products. *Fermentation* 3(2)**,** 1-28. doi: 10.3390/fermentation3020028.

Pickar-Oliver, A., and Gersbach, C.A. (2019). The next generation of CRISPR–Cas technologies and applications. *Nature Reviews Molecular Cell Biology* 20(8)**,** 490-507.

Pierce, E., Xie, G., Barabote, R.D., Saunders, E., Han, C.S., Detter, J.C.*, et al.* (2008). The complete genome sequence of *Moorella thermoacetica* (f. *Clostridium thermoaceticum*). *Environmental microbiology* 10(10)**,** 2550-2573. doi: 10.1111/j.1462-2920.2008.01679.x.

Poehlein, A., Schmidt, S., Kaster, A.K., Goenrich, M., Vollmers, J., Thurmer, A.*, et al.* (2012). An ancient pathway combining carbon dioxide fixation with the generation and utilization of a sodium ion gradient for ATP synthesis. *PLOS One* 7(3)**,** e33439. doi: 10.1371/journal.pone.0033439.

Porras, C.A., and Bai, Y. (2015). Respiratory supercomplexes: plasticity and implications. *Frontiers in Bioscience* 20**,** 621.

Ragsdale, S.W., and Pierce, E. (2008). Acetogenesis and the Wood-Ljungdahl pathway of CO_2 fixation. *Biochimica et Biophysica Acta* 1784(12)**,** 1873-1898. doi: 10.1016/j.bbapap.2008.08.012.

Rees, H.A., and Liu, D.R. (2018). Base editing: precision chemistry on the genome and transcriptome of living cells. *Nature Reviews Genetics* 19(12)**,** 770-788.

Richter, H., Martin, M.E., and Angenent, L.T. (2013). A two-stage continuous fermentation system for conversion of syngas into ethanol. *Energies* 6(8)**,** 3987-4000. doi: 10.3390/en6083987.

Richter, H., Molitor, B., Diender, M., Sousa, D.Z., and Angenent, L.T. (2016a). A narrow pH range supports butanol, hexanol, and octanol production from syngas in a continuous co-culture of *Clostridium ljungdahlii* and *Clostridium kluyveri* with in-line product extraction. *Frontiers in Microbiology* 7**,** 1773. doi: 10.3389/fmicb.2016.01773.

Richter, H., Molitor, B., Wei, H., Chen, W., Aristilde, L., and Angenent, L.T. (2016b). Ethanol production in syngas-fermenting *Clostridium ljungdahlii* is controlled by thermodynamics rather than by enzyme expression. *Energy & Environmental Science* 9(7)**,** 2392-2399. doi: 10.1039/c6ee01108j.

Roberts, R.J., Carneiro, M.O., and Schatz, M.C. (2013). The advantages of SMRT sequencing. *Genome Biology* 14(6)**,** 405.

Sambrook, J., Fritsch, E.F., and Maniatis, T. (1989). *Molecular cloning: A laboratory manual.* Cold Spring Harbor Laboratory Press.

Sambrook, J., and Russell, D.W. (2006a). Preparation and transformation of competent *Escherichia coli* using calcium chloride. *Cold Spring Harbor Protocols* 2006(1).

Sambrook, J., and Russell, D.W. (2006b). SDS-polyacrylamide gel electrophoresis of proteins. *Cold Spring Harbor Protocols* 2006(4)**,** pdb. prot4540.

Sander, J.D., and Joung, J.K. (2014). CRISPR-Cas systems for editing, regulating and targeting genomes. *Nature Biotechnology* 32(4)**,** 347.

Scheffers, D.-J., and Pinho, M.G. (2005). Bacterial cell wall synthesis: New insights from localization studies. *Microbiology and Molecular Biology Reviews* 69(4)**,** 585-607.

Schmehl, M., Jahn, A., Meyer zu Vilsendorf, A., Hennecke, S., Masepohl, B., Schuppler, M.*, et al.* (1993). Identification of a new class of nitrogen fixation genes in *Rhodobacter capsulatus*: A putative membrane complex involved in electron transport to nitrogenase. *Molecular Genetics and Genomics* 241(5-6)**,** 602-615. doi: 10.1007/BF00279903.

Schoelmerich, M.C., Katsyv, A., Sung, W., Mijic, V., Wiechmann, A., Kottenhahn, P.*, et al.* (2018). Regulation of lactate metabolism in the acetogenic bacterium *Acetobacterium woodii*. *Environmental Microbiology* 20(12)**,** 4587-4595.

Schoelmerich, M.C., and Müller, V. (2019). Energy conservation by a hydrogenase-dependent chemiosmotic mechanism in an ancient metabolic pathway. *Proceedings of the National Academy of Sciences* 116(13)**,** 6329-6334.

Schoelmerich, M.C., and Müller, V. (2020). Energy-converting hydrogenases: The link between H_2 metabolism and energy conservation. *Cellular and Molecular Life Sciences* 77(8)**,** 1461-1481. doi: 10.1007/s00018-019-03329-5.

Schuchmann, K., and Müller, V. (2014). Autotrophy at the thermodynamic limit of life: a model for energy conservation in acetogenic bacteria. *Nature Reviews Microbiology* 12(12)**,** 809-821. doi: 10.1038/nrmicro3365.

Schunder, E., Rydzewski, K., Grunow, R., and Heuner, K. (2013). First indication for a functional CRISPR/Cas system in *Francisella tularensis*. *International Journal of Medical Microbiology* 303(2)**,** 51-60.

Seedorf, H., Fricke, W.F., Veith, B., Brüggemann, H., Liesegang, H., Strittmatter, A.*, et al.* (2008). The genome of *Clostridium kluyveri*, a strict anaerobe with unique metabolic features. *Proceedings of the National Academy of Sciences of the United States of America* 105(6)**,** 2128-2133.

Seifritz, C., Daniel, S.L., Gossner, A., and Drake, H.L. (1993). Nitrate as a preferred electron sink for the acetogen *Clostridium thermoaceticum*. *Journal of Bacteriology* 175(24)**,** 8008-8013. doi: 10.1128/jb.175.24.8008-8013.1993.

Selle, K., and Barrangou, R. (2015). Harnessing CRISPR–Cas systems for bacterial genome editing. *Trends in Microbiology* 23(4)**,** 225-232.

Shin, J., Kang, S., Song, Y., Jin, S., Lee, J.S., Lee, J.-K.*, et al.* (2019). Genome engineering of *Eubacterium limosum* using expanded genetic tools and the CRISPR-Cas9 system. *ACS Synthetic Biology* 8(9)**,** 2059-2068.

Simon, R.D., and Weathers, P. (1976). Determination of the structure of the novel polypeptide containing aspartic acid and arginine which is found in cyanobacteria. *Biochimica et Biophysica Acta (BBA)-Protein Structure* 420(1)**,** 165-176.

Simpson, S., Allen, W.E., Cornado, R.J., and Molloy, S. (2016). *Gas fermentation for the production of protein or feed*. Patent No. WO2016187494A1.

Song, Y., Lee, J.S., Shin, J., Lee, G.M., Jin, S., Kang, S.*, et al.* (2020). Functional cooperation of the glycine synthase-reductase and Wood–Ljungdahl pathways for autotrophic growth of *Clostridium drakei*. *Proceedings of the National Academy of Sciences of the United States of America* 117(13)**,** 7516-7523. doi: 10.1073/pnas.1912289117.

Sternberg, S.H., and Doudna, J.A. (2015). Expanding the biologist's toolkit with CRISPR-Cas9. *Molecular Cell* 58(4)**,** 568-574.

Streett, H.E., Kalis, K.M., and Papoutsakis, E.T. (2019). A strongly fluorescing anaerobic reporter and protein-tagging system for *Clostridium* organisms based on the fluorescence-activating and absorption-shifting tag protein (FAST). *Applied and Environmental Microbiology* 85(14)**,** e00622-00619. doi: 10.1128/AEM.00622-19.

Stubbe, J., Tian, J., He, A., Sinskey, A.J., Lawrence, A.G., and Liu, P. (2005). Nontemplate-dependent polymerization processes: polyhydroxyalkanoate synthases as a paradigm. *Annual Review of Biochemistry* 74**,** 433-480.

Suharti, S., Wang, M., de Vries, S., and Ferry, J.G. (2014). Characterization of the RnfB and RnfG subunits of the Rnf complex from the archaeon *Methanosarcina acetivorans*. *PLOS One* 9(5)**,** e97966. doi: 10.1371/journal.pone.0097966.

Sutton, D., Kelleher, B., and Ross, J.R. (2001). Review of literature on catalysts for biomass gasification. *Fuel Processing Technology* 73(3)**,** 155-173.

Takahashi, H., Taniguchi, S., and Egami, F. (2012). Inorganic nitrogen compounds: distribution and metabolism. *Comparative Biochemistry V5: A Comprehensive Treatise***,** 91.

Takors, R., Kopf, M., Mampel, J., Bluemke, W., Blombach, B., Eikmanns, B.*, et al.* (2018). Using gas mixtures of CO, CO_2 and H_2 as microbial substrates: the do's and don'ts of successful technology transfer from laboratory to production scale. *Microbial Biotechnology* 11(4)**,** 606-625. doi: 10.1111/1751-7915.13270.

Tan, J., Zhang, F., Karcher, D., and Bock, R. (2019). Engineering of high-precision base editors for site-specific single nucleotide replacement. *Nature Communications* 10(1)**,** 1-10.

Tan, Y., Liu, J., Chen, X., Zheng, H., and Li, F. (2013). RNA-seq-based comparative transcriptome analysis of the syngas-utilizing bacterium *Clostridium ljungdahlii* DSM 13528 grown autotrophically and heterotrophically. *Molecular BioSystems* 9(11)**,** 2775-2784. doi: 10.1039/c3mb70232d.

Tanner, R., and Laopaiboon, R. (1997). Metabolism of *Clostridium ljungdahlii*, an acetogen in the clostridial RNA homology group I. *Biofactors* 6**,** 59.

Tanner, R.S., Miller, L.M., and Yang, D. (1993). *Clostridium ljungdahlii* sp. nov., an acetogenic species in clostridial rRNA homology group I. *International Journal of Systematic and Evolutionary Microbiology* 43(2)**,** 232-236. doi: 10.1099/00207713-43-2-232.

Thauer, R.K., Jungermann, K., and Decker, K. (1977). Energy conservation in chemotrophic anaerobic bacteria. *Bacteriological Reviews* 41(1)**,** 100.

Tong, Y., Whitford, C.M., Robertsen, H.L., Blin, K., Jørgensen, T.S., Klitgaard, A.K.*, et al.* (2019). Highly efficient DSB-free base editing for streptomycetes with CRISPR-BEST. *Proceedings of the National Academy of Sciences of the United States of America* 116(41)**,** 20366-20375.

Tremblay, P.L., Zhang, T., Dar, S.A., Leang, C., and Lovley, D.R. (2012). The Rnf complex of *Clostridium ljungdahlii* is a proton-translocating ferredoxin:NAD^+ oxidoreductase essential for autotrophic growth. *MBio* 4(1)**,** e00406-00412. doi: 10.1128/mBio.00406-12.

Ueki, T., Nevin, K.P., Woodard, T.L., and Lovley, D.R. (2014). Converting carbon dioxide to butyrate with an engineered strain of *Clostridium ljungdahlii*. *MBio* 5(5)**,** 1-10. doi: 10.1128/mBio.01636-14.

Ungerer, J., and Pakrasi, H.B. (2016). Cpf1 is a versatile tool for CRISPR genome editing across diverse species of cyanobacteria. *Scientific Reports* 6**,** 39681. doi: 10.1038/srep39681.

Valgepea, K., Loi, K.Q., Behrendorff, J.B., Lemgruber, R.S.P., Plan, M., Hodson, M.P.*, et al.* (2017). Arginine deiminase pathway provides ATP and boosts growth of the gas-fermenting acetogen *Clostridium autoethanogenum*. *Metabolic Engineering* 41**,** 202-211. doi: 10.1016/j.ymben.2017.04.007.

Vento, J.M., Crook, N., and Beisel, C.L. (2019). Barriers to genome editing with CRISPR in bacteria. *Journal of Industrial Microbiology and Biotechnology* 46(9-10)**,** 1327-1341.

Verwaal, R., Buiting-Wiessenhaan, N., Dalhuijsen, S., and Roubos, J.A. (2018). CRISPR/Cpf1 enables fast and simple genome editing of *Saccharomyces cerevisiae*. *Yeast* 35(2)**,** 201-211. doi: 10.1002/yea.3278.

Vestergaard, G., Garrett, R.A., and Shah, S.A. (2014). CRISPR adaptive immune systems of Archaea. *RNA Biology* 11(2)**,** 156-167.

Walker, D.J.F., and Köpke, M. (2015). *Method of producing a recombinant microorganism*. Patent No. US20150211022 A1.

Wang, S., Huang, H., Moll, J., and Thauer, R.K. (2010). $NADP^+$ reduction with reduced ferredoxin and $NADP^+$ reduction with NADH are coupled via an electron-bifurcating enzyme complex in *Clostridium kluyveri*. *Journal of Bacteriology* 192(19)**,** 5115-5123.

Wang, Y., Wang, S., Chen, W., Song, L., Zhang, Y., Shen, Z.*, et al.* (2018). CRISPR-Cas9 and CRISPR-assisted cytidine deaminase enable precise and efficient genome editing in *Klebsiella pneumoniae*. *Applied and Environmental Microbiology* 84(23).

Watzer, B., Engelbrecht, A., Hauf, W., Stahl, M., Maldener, I., and Forchhammer, K. (2015). Metabolic pathway engineering using the central signal processor P_{II}. *Microbial Cell Factories* 14(1)**,** 1-12.

Watzer, B., and Forchhammer, K. (2018). Cyanophycin: A nitrogen-rich reserve polymer. *Cyanobacteria***,** 85.

Westphal, L., Wiechmann, A., Baker, J., Minton, N.P., and Muller, V. (2018). The Rnf complex is an energy-coupled transhydrogenase essential to reversibly link cellular NADH and ferredoxin pools in the acetogen *Acetobacterium woodii*. *Journal of Bacteriology* 200(21)**,** e00357-00318. doi: 10.1128/JB.00357-18.

Wood, H.G. (1991). Life with CO or CO_2 and H_2 as a source of carbon and energy. *The FASEB Journal* 5(2)**,** 156-163. doi: 10.1096/fasebj.5.2.1900793.

Wood, H.G., Ragsdale, S.W., and Pezacka, E. (1986). The acetyl-CoA pathway of autotrophic growth. *FEMS Microbiology Reviews* 2(4)**,** 345-362. doi: 10.1016/0378-1097(86)90022-4.

Woolston, B.M., Emerson, D.F., Currie, D.H., and Stephanopoulos, G. (2018). Rediverting carbon flux in *Clostridium ljungdahlii* using CRISPR Interference (CRISPRi). *Metabolic Engineering*. doi: 10.1016/j.ymben.2018.06.006.

Xia, P.F., Casini, I., Schulz, S., Klask, C.M., Angenent, L.T., and Molitor, B. (2020). Reprogramming acetogenic bacteria with CRISPR-targeted base editing *via* deamination. *ACS Synthetic Biology* 9(8)**,** 2162-2171. doi: 10.1021/acssynbio.0c00226.

Xia, P.F., Ling, H., Foo, J.L., and Chang, M.W. (2019). Synthetic biology toolkits for metabolic engineering of cyanobacteria. *Biotechnology Journal* 14(6)**,** 1800496.

Xu, T., Li, Y., Shi, Z., Hemme, C.L., Li, Y., Zhu, Y.*, et al.* (2015). Efficient genome editing in *Clostridium cellulolyticum via* CRISPR-Cas9 nickase. *Applied and Environmental Microbiology* 81(13)**,** 4423-4431. doi: 10.1128/AEM.00873-15.

Yagi, T. (1993). The bacterial energy-transducing NADH-quinone oxidoreductases. *Biochimica et Biophysica Acta (BBA)-Bioenergetics* 1141(1)**,** 1-17.

Yagi, T., Yano, T., and Matsuno-Yagi, A. (1993). Characteristics of the energy-transducing NADH-quinone oxidoreductase of *Paracoccus denitrificans* as revealed by biochemical, biophysical, and molecular biological approaches. *Journal of Bioenergetics and Biomembranes* 25(4)**,** 339-345.

Yamano, T., Nishimasu, H., Zetsche, B., Hirano, H., Slaymaker, I.M., Li, Y.*, et al.* (2016). Crystal structure of Cpf1 in complex with guide RNA and target DNA. *Cell* 165(4)**,** 949-962. doi: 10.1016/j.cell.2016.04.003.

Younesi, H., Najafpour, G., and Mohamed, A.R. (2005). Ethanol and acetate production from synthesis gas *via* fermentation processes using anaerobic bacterium, *Clostridium ljungdahlii*. *Biochemical Engineering Journal* 27(2)**,** 110-119. doi: 10.1016/j.bej.2005.08.015.

Yura, T., and Nakahigashi, K. (1999). Regulation of the heat-shock response. *Current Opinion in Microbiology* 2(2)**,** 153-158. doi: 10.1016/S1369-5274(99)80027-7.

Zetsche, B., Gootenberg, J.S., Abudayyeh, O.O., Slaymaker, I.M., Makarova, K.S., Essletzbichler, P.*, et al.* (2015). Cpf1 is a single RNA-guided endonuclease of a class 2 CRISPR-Cas system. *Cell* 163(3)**,** 759-771. doi: 10.1016/j.cell.2015.09.038.

Zetsche, B., Heidenreich, M., Mohanraju, P., Fedorova, I., Kneppers, J., DeGennaro, E.M.*, et al.* (2017). Multiplex gene editing by CRISPR-Cpf1 using a single crRNA array. *Nature Biotechnology* 35(1)**,** 31-34. doi: 10.1038/nbt.3737.

Zhang, J., Hong, W., Zong, W., Wang, P., and Wang, Y. (2018a). Markerless genome editing in *Clostridium beijerinckii* using the CRISPR-Cpf1 system. *Journal of Biotechnology* 284**,** 27-30.

Zhang, J., Zong, W., Hong, W., Zhang, Z.-T., and Wang, Y. (2018b). Exploiting endogenous CRISPR-Cas system for multiplex genome editing in *Clostridium tyrobutyricum* and engineer the strain for high-level butanol production. *Metabolic Engineering* 47**,** 49-59.

Zhao, R., Liu, Y., Zhang, H., Chai, C., Wang, J., Jiang, W.*, et al.* (2019). CRISPR-Cas12a-mediated gene deletion and regulation in *Clostridium ljungdahlii* and its application in carbon flux redirection in synthesis gas fermentation. *ACS Synthetic Biology* 8(10)**,** 2270-2279. doi: 10.1021/acssynbio.9b00033.

Ziegler, K., Diener, A., Herpin, C., Richter, R., Deutzmann, R., and Lockau, W. (1998). Molecular characterization of cyanophycin synthetase, the enzyme catalyzing the biosynthesis of the

cyanobacterial reserve material multi-L-arginyl-poly-L-aspartate (cyanophycin). *European Journal of Biochemistry* 254(1)**,** 154-159.

Zumft, W.G. (1997). Cell biology and molecular basis of denitrification. *Microbiology and Molecular Biology Reviews* 61(4)**,** 533-616. doi: 10.1128/mmbr.61.4.533-616.1997.

Zuo, E., Sun, Y., Yuan, T., He, B., Zhou, C., Ying, W.*, et al.* (2020). A rationally engineered cytosine base editor retains high on-target activity while reducing both DNA and RNA off-target effects. *Nature Methods***,** 1-5.